

NASA Contractor Report 172367

EFFECT OF THICKNESS ON FATIGUE CRACK
PROPAGATION IN 7475-T731 ALUMINUM
ALLOY SHEET

R. A. Daiuto and B. M. Hillberry

PURDUE UNIVERSITY
School of Mechanical Engineering
W. Lafayette, Indiana 47907

Grant NAG1-231
June 1984



National Aeronautics and
Space Administration

Langley Research Center
Hampton, Virginia 23665

EFFECT OF THICKNESS ON FATIGUE CRACK PROPAGATION
IN 7475-T731 ALUMINUM ALLOY SHEET*

R. A. Daiuto**
Graduate Research Assistant

and

B. M. Hillberry
Professor

School of Mechanical Engineering
Purdue University
W. Lafayette, Indiana 47907

Grant No. NAG-1-231
National Aeronautics and Space Administration
Langley Research Center
Hampton, Virginia 23665

* This report is essentially R. A. Daiuto's M.S. thesis.

** Currently Associate Engineer, Allison Gas Turbine Division,
General Motors Corporation, Indianapolis, IN.

TABLE OF CONTENTS

	Page
NOMENCLATURE	iv
ABSTRACT	vii
CHAPTER	
1. INTRODUCTION	1
2. LITERATURE REVIEW	4
Constant Amplitude Loading	5
No Thickness Effect	5
Increased Growth Rate With Decreasing Thickness	9
Increased Growth Rate With Increasing Thickness	12
Variable Amplitude Loading	16
3. TEST PROGRAM	24
Development of Constant Amplitude Tests	24
Development of Single-Peak Overload Tests	27
4. APPARATUS AND PROCEDURE	37
5. DATA REDUCTION	41
Constant Amplitude Loading Tests	41
Single-Peak Overload Tests	41
6. TEST RESULTS	44
Constant Amplitude Loading Tests	44
Single-Peak Overload Tests	48

7. ANALYSIS OF RESULTS	56
Constant Amplitude Loading Tests	56
Crack Closure	57
Tests at R=0.05	63
Tests at R=0.75	66
Fracture Mode Transition	66
Strain Energy Density Analysis	66
Tests at R=0.05	74
Tests at R=0.75	75
Strain Energy Release Rate Analysis	78
Tests at R=0.05	82
Tests at R=0.75	85
Microscopic Behavior	85
Plane Strain Region	87
Mixed Mode Region	87
Plane Stress Region	90
Single-Peak Overload Tests	93
Macroscopic Behavior	93
Tests at R=0.05	94
Tests at R=0.70	101
Comparison of Tests at R=0.05 and R=0.70 ...	107
Microscopic Behavior	107
Test at R=0.05	114
Test at R=0.70	114
8. DISCUSSION OF RESULTS AND CONCLUSIONS	120
Thickness Effects Under Constant Amplitude Loading	120
Thickness Effects Following a Single-Peak Overload	124
LIST OF REFERENCES	131
APPENDICES	
Appendix A	136
Appendix B	152
Appendix C	159
Appendix D	172
Appendix E	177
Appendix F	190
Appendix G	197

NOMENCLATURE

A	cross sectional area of specimen
a	crack length
a_{ol}	overload affected zone size
b	constant
c	constant
$\frac{da}{dN}$	fatigue crack growth rate
$\left. \frac{da}{dN} \right _{min}$	minimum fatigue crack propagation rate.
$\left. \frac{da}{dN} \right _{ol}$	pre-overload fatigue crack propagation rate.
E	modulus of elasticity
G	strain energy release rate
G_{max}	maximum strain energy release rate
G_{min}	minimum strain energy release rate
G_{ϵ}	strain energy release rate in plane strain
$(G_{\epsilon})_{0^{\circ}}$	strain energy release rate in plane strain for a crack at an angle of 0° to a plane perpendicular to the plane of the specimen
$(G_{\epsilon})_{45^{\circ}}$	strain energy release rate in plane strain for a crack at an angle of 45° to a plane perpendicular to the plane of the specimen
G_{σ}	strain energy release rate in plane stress
$(G_{\sigma})_{0^{\circ}}$	strain energy release rate in plane stress for a crack at an angle of 0° to a plane perpendicular to the plane of the specimen

$(G)_{\sigma 45^\circ}$	strain energy release rate in plane stress for a crack at an angle of 45° to a plane perpendicular to the plane of the specimen
H(T)	constraint parameter
K_I	mode I stress intensity factor
K_{II}	mode II stress intensity factor
K_{III}	mode III stress intensity factor
K_{max}	maximum stress intensity factor
K_{min}	minimum stress intensity factor
K_{ol}	overload stress intensity factor
K_{op}	stress intensity factor at crack opening
ΔK	stress intensity factor range
ΔK_{eff}	effective stress intensity factor range
ΔKP	stress intensity factor range at first slope transition of crack growth rate data
ΔKPP	stress intensity factor range at second slope transition of growth rate data
m	constant
N	number of cycles
N_D	number of delay cycles
a	constant
P	applied load
P_{max}	maximum applied load
P_{min}	minimum applied load
P_{ol}	applied overload
ΔP	cyclic load range
Q_{ol}	overload ratio, K_{ol}/K_{max}
R	stress ratio, K_{min}/K_{max}

R_{ol}	overload stress ratio, K_{min}/K_{ol}
$r_{y\epsilon}$	plane strain plastic zone radius
$r_{y\epsilon ol}$	overload plane strain plastic zone radius
$r_{y\sigma}$	plane stress plastic zone radius
$r_{y\sigma ol}$	overload plane stress plastic zone radius
$\Delta r_{y\epsilon}$	cyclic plane strain plastic zone radius
$\Delta r_{y\sigma}$	cyclic plane stress plastic zone radius
S	strain energy density
S_{max}	maximum strain energy density
S_{min}	minimum strain energy density
ΔS	strain energy density range
ΔS_{ϵ}	strain energy density range in plane strain
ΔS_{σ}	strain energy density range in plane stress
T	thickness parameter, r_{σ} / t
t	specimen thickness
α	the angle between the crack surface and the plane of the specimen
ϵ	strain
π	ratio of circumference to diameter of a circle
σ	stress
σ_{ys}	yield stress
θ	the angle between the crack surface and a plane perpendicular to the plane of the specimen
ν	Poisson's ratio

ABSTRACT

Tests were conducted on three thicknesses of 7475-T731 aluminum alloy sheet to investigate the effect of thickness on fatigue crack propagation under constant amplitude loading conditions and on retardation following a single-peak overload.

Constant amplitude loading tests were performed at stress ratios of 0.05 and 0.75 to obtain data for conditions with crack closure and without crack closure, respectively. At both stress ratios a thickness effect was clearly evident, with thicker specimens exhibiting higher growth rates in the mixed mode region. The effect of thickness for a stress ratio of 0.05 corresponded well with the fracture mode transitions observed on the specimens. A model based on the strain energy release rate which accounted for the fracture mode transition was found to correlate the thickness effects well. The specimens tested at the stress ratio of 0.75 did not make the transition from tensile mode to shear mode, indicating that another mechanism besides crack closure or fracture mode transition was active.

Single-peak overload tests were conducted at baseline stress ratios of 0.05 and 0.70 to determine the effect of thickness on retardation for conditions with crack closure and without crack closure. At both stress ratios a thickness effect on retardation was observed. The tests at a stress ratio of 0.05 showed a consistent thickness effect, with thicker specimens exhibiting less retardation. The tests at the stress ratio of 0.70, in which no crack closure occurred following overload, did not show a consistent effect of thickness on retardation. The characteristics of the retardation were different from those observed at the stress ratio of 0.05, and were consistent with those which would be expected if crack tip blunting were the retardation mechanism.

CHAPTER 1 - INTRODUCTION

Fatigue crack propagation has been shown to be primarily a function of the stress intensity factor, which represents the magnitude of the stress field at the crack tip. The stress intensity factor is an important design parameter, because a plot of crack growth rate versus the stress intensity factor range characterizes the material's resistance to crack growth.

Although the stress intensity factor range primarily controls crack growth rate, other factors such as stress ratio, environment, frequency, and load interactions also affect crack growth rate. These other "effects" arise due to the inability of the stress intensity factor to account for these factors. For example, the stress ratio effect can be attributed to crack closure caused by the plasticity developed at the crack tip. The stress intensity factor is a linear elastic parameter, and hence cannot account for the effects of plasticity at the crack tip. The result is a stress ratio effect when crack growth rate is correlated with the stress intensity factor range, and therefore the stress ratio is another parameter which must

be considered when applying the da/dN versus ΔK curve to design.

Another factor which may affect fatigue crack propagation and retardation for similar reasons is the specimen thickness. Under constant amplitude loading conditions, the thickness effect would be expected to be caused by a plane strain to plane stress transition. Since plastic zones are larger in plane stress than plane strain under the same stress intensity conditions, greater crack closure and therefore a lower effective stress intensity range would exist in plane stress, resulting in lower crack growth rates in plane stress. Hence, two growth rate curves would be expected to exist, one for plane strain and one for plane stress. As a crack propagates under increasing ΔK conditions, the stress state may vary from plane strain to plane stress, resulting in a transition of growth rate from the plane strain curve to the plane stress curve. A crack grown in a thicker specimen under identical ΔK conditions will begin the transition to the plane stress curve at a higher level of ΔK and growth rate, resulting in higher crack growth rates in the thicker specimen within the transition region.

The difference in plastic zone size between plane strain and plane stress would also be expected to cause a thickness effect on retardation. An overload of a certain

stress intensity magnitude which is applied to two different thickness specimens may produce a state of plane stress in the thin specimen, and a state of plane strain in the thicker specimen. The larger plastic zone due to an overload applied to the thinner specimen would result in greater crack closure, and hence greater retardation than in the thicker specimen.

The above discussion presents a means by which thickness may be expected to affect fatigue crack propagation rate. It was the purpose of this investigation to study the effect of thickness on crack growth rate under constant amplitude loading and on retardation following an overload.

CHAPTER 2 - LITERATURE SEARCH

The FCP rate in a material is primarily a function of the stress intensity factor range, however there are other factors which affect da/dn also. These other factors arise primarily because of the assumptions involved in the definition of the stress intensity factor, specifically the assumption of a perfectly elastic material. In reality, a zone of plastically deformed material exists at the crack tip, and the effects due to the presence of this plastic zone can not be taken into account by the stress intensity factor, thus resulting in other factors affecting crack growth rate.

One effect resulting from the inability of the stress intensity factor to account for the presence of the plastic zone is the thickness effect. Despite the large amount of literature on FCP, surprisingly little is concerned with the thickness effect. That which does exist however can be generally separated into two areas: 1) thickness effects under constant amplitude loading; 2) thickness effects under variable amplitude loading.

Constant Amplitude Loading

The investigations which have been made on thickness effects in constant amplitude loading provide little engineering guidance as to what the effect is, let alone what exactly the cause for this effect is, if it does in fact exist. The results of these investigations are contradictory and fall into three categories: 1) no effect of thickness; 2) increased growth rate in thinner specimens; 3) decreased growth rate in thinner specimens. Theoretical and empirical analyses have been done which support all three results, such that much uncertainty remains concerning the thickness effect. A review of these investigations is therefore provided according to the conclusions drawn in order to specify exactly what is known and what remains to be determined about the thickness effect.

No Thickness Effect

Probably the first systematic investigation of thickness effects was done by Frost and Denton [1] in 1960. The tests were performed under constant amplitude conditions on mild steel center-cracked specimens in thicknesses of 0.128, 0.3, and 1.0 inches. It was found that for similar nominal stresses and crack lengths, there were no consistent changes in crack growth characteristics with thickness. In all cases initial crack growth occurred on a plane through the thickness at 90° to the

plane of the specimen. For the 1.0 inch specimen subsequent growth occurred on this plane. For the 0.128 and 0.3 inch thick specimens subsequent growth occurred on planes through the thickness at angles of 45° and 90° to the plane of the specimen, respectively. Thus, one further implication was that crack growth was the same in the tensile mode as in the shear mode, that is, FCP rate was independent of stress state.

Hertzberg and Paris [2] in 1965 investigated FCP behavior in 2024-T3 aluminum sheets of thicknesses of 0.064, 0.094, and 0.126 inches. They observed the change in the fatigue fracture mode from 90° to 45° to the plane of the specimen. They found that the points of fracture mode transition were related to the stress intensity factor and its effect on the plastic zone size. A constant plastic zone size to thickness ratio, $\frac{r_y \sigma}{t} = T$, herein referred to as the thickness parameter, was observed at the transition points in all three investigations, with the crack lengths at transition increasing as the thickness increased. Consequently, the thicker specimens remained on the 90° plane over a longer crack length than the thinner specimens. Furthermore, the use of electron fractography to study the crack surface showed that the morphology in the macroscopically flat region was considerably different than the shear mode region, thus indicating differences in the fatigue micromechanisms between

plane strain and plane stress. It was therefore anticipated that any effects of thickness on FCP rate would be delineated at the points of transition. Any difference in FCP rates between plane strain and plane stress would be revealed because the transition occurred at longer crack lengths as thickness increased so that a change in growth rate towards the growth rate in plane stress would be seen to occur at progressively higher ΔK values as thickness increased. The test results indicated that FCP rates correlated with ΔK were the same in all thicknesses. In addition, FCP growth rates were also determined from fatigue striation spacings on the crack surface and the growth rates were again found to be independent of sheet thickness. These results therefore implied that there is no difference in growth rate between plane strain and plane stress, due to either the fatigue micromechanism or the crack surface geometry.

Griffiths and Richards [3] investigated the influence of thickness on FCP rates in a low alloy steel weld metal both above and below general yield. During the tests variation of the stress state from plane strain to plane stress was indicated by the variation of the crack surface from 90° plane to the 45° plane. Etchings of the specimens revealed that the plane stress plastic zone was considerably larger than in plane strain. The test results indicated that there was no significant effect of

thickness on the FCP rates on tests conducted below general yield. However, unlike Hertzberg and Paris, it was established through examination with a scanning electron microscope that fatigue cracks propagated by the same fatigue micromechanism (ductile striation) on both the 90° and 45° planes. They concluded that when FCP occurred by the ductile striation mechanism where conditions were such that K_{\max} was less than $0.8K_c$, no thickness effects will be present. For tests above general yield, effects of thickness on FCP rate were observed. Specifically, thinner specimens exhibited higher crack growth rates than thicker ones. This was attributed to the thinner specimens having a lower general yield stress due to less constraint than the thicker specimens. As a consequence, the crack tip displacements and strain energy density at the crack tip are larger in thin specimens, which results in higher FCP rates in the thin specimens at conditions above general yield.

Tests conducted by Hahn et al. [4] gave results very similar to Griffith and Richards in Fe-3Si steel. There was an absence of a thickness effect observed for crack propagation from plane strain to plane stress. In particular, no changes in the slope of the da/dN versus ΔK curve occurred with the development of shear lips. It was established that the micromechanism of fatigue was always by ductile striation formation, both on the flat and the

slant portions of the crack surface.

Two investigations by Clark [5,6] on thickness effects using a wide spectrum of aluminum and steel alloys concluded that no effects of thickness on FCP rate existed. In all tests the reported data covered a range which included both plane strain and plane stress conditions, and still no differences in FCP rate could be distinguished, thus lending further evidence of no difference in growth rates between plane strain and plane stress.

There have been other studies [7,8] which have obtained results similar to those just described. That is, given crack growth over a range from plane strain to plane stress, no influences of thickness on FCP rate were detected.

Increased Growth Rate With Decreasing Thickness

Theoretical investigations of the effect thickness on FCP have generally concluded that FCP rate should be greater in plane stress than in plane strain. Most theories predict a relationship between the plastic zone size and the growth rate. Through theoretical considerations (i.e. application of a yield criterion to the stress field at the crack tip) it was shown that the plastic zone size in plane stress is significantly larger than in plane strain. Owing to the larger plastic zone in plane stress,

the crack tip displacement and the strain energy density were shown to be larger in plane stress, thus a higher growth rate expectation in plane stress.

Liu [9] also suggested that the effects of thickness on FCP rate should be based on his deductions about the effects of stress state on FCP. It was pointed out that the state of stress in the vicinity of the crack front changes from plane stress on the surface to plane strain at the interior, resulting in a large plastic zone on the surface tapering down in size towards the interior. As a crack propagates under constant amplitude loading beginning in a nominally plane strain state, the surface plastic zone gradually increases in size. When the surface plastic zone size reaches some fraction of the specimen thickness, nominal plane strain conditions no longer exist and the growth rate becomes affected. Specifically, the presence of greater plasticity increases the growth rate, and as the nominal stress state approaches plane stress the growth rate increases more due to the increased crack tip displacement at the crack tip. Since transition should occur at constant plastic zone size to thickness ratios, thicker specimens will spend more time in plane strain resulting in longer life for increased thickness specimens.

Test results of an investigation by Wilhem [10] support the hypotheses of Liu. In tests on different thicknesses of 7075-T6 aluminum sheet, it was found that the beginning of shear lip development was independent of thickness, i.e. it occurred at a constant plastic zone size to thickness ratio. Corresponding to this development of shear lips was a marked increase in growth rate, in agreement with Liu. Furthermore, this increase in growth rate was also confirmed by investigations of the crack surface. Electron fractographs in the tensile mode zone showed the usual fatigue striation microtopography. Near the point of transition where shear lips began developing, there was a rapid 3-fold increase in the fatigue striation spacing, thus giving further credence to the macroscopically observed increase in crack growth with increasing shear lip development.

Jack and Price [11] investigated the effects of thickness on mild steel specimens in thicknesses ranging from 0.05 to 0.9 inches, and found that growth rates definitely increased with decreasing thickness. Again, macroscopic appearance of the crack surfaces exhibited the flat region which eventually disappeared as the shear lips developed to eventually cover the whole crack surface. The beginning of shear lip development was observed to occur at longer crack lengths as thickness increased, and that it occurred at a constant plastic zone size to

thickness ratio in all thicknesses. The fatigue lives of the specimens increased with increasing specimen thickness, which was attributed to the longer time spent by the thicker specimens in plane strain. Although no change in growth rate could be correlated with the transition point as Wilhem did, it was concluded that growth rate in plane strain was slower than in plane stress.

Other investigators [12,13] have obtained similar results. In all cases the same macroscopic crack surface features were made, with shear lip development occurring at longer crack lengths with increasing specimen thicknesses. Although a change in growth rate at transition was not always observed, the fatigue lives of the thicker specimens were always longer owing to the greater time spent in plane strain, leading to the conclusion that FCP rate is faster in plane stress than plane strain.

Increased Growth Rate With Increasing Thickness

Broek and Schijve [14] investigated the effects of thickness in four different thicknesses of 2024-T3 Alclad sheet. Their results showed distinctly that fatigue crack propagation rates increased with increasing specimen thickness, as indicated by comparison of the crack length versus cycles data. The fatigue fracture surface exhibited the usual flat tensile mode at shorter crack lengths with gradual shear lip development which eventually

covered the entire surface to form a 45° angle with the specimen surface. Analysis of the data revealed that the crack length at the beginning of shear lip development increased with increasing specimen thickness and that FCP rate here increased with increasing thickness. Comparison of the fatigue lives after transition showed small, unsystematical differences between the thicknesses as opposed to the significant, systematic differences before transition. Differences in the lives of different thickness specimens was therefore attributed to the change in the fracture mode, which was intimated to be governed by the change in the state of stress at the crack tip. That is, the shear lip development was produced by the increasing plastic zone in the plane stress area on the surface. The change from approximately plane stress on the surface to approximately plane strain at the interior of the sheet will occur over a distance along the crack front which is independent of specimen thickness. Thus, for a given crack length and stress amplitude, the central part of the crack front where plane strain exists will be greater for thicker sheets. Since the lives of the thicker specimens were shorter than the thinner ones, it was concluded that plane strain induces higher FCP rates than plane stress.

Swanson et al.[15] observed different behavior than did Broek and Schijve on 7079-T6 aluminum, but which led to the same conclusion that FCP rates are higher under

plane strain conditions. The same tensile mode to shear mode transition was observed, however the crack length and stress intensity at the beginning of shear lip development was found to be independent of specimen thickness, contrary to the findings of Broek and Schijve. It was also noted that a drop in FCP rate occurred at the point of shear lip development. The FCP rate would then continue to increase as shear lips continued to develop, but at a lower rate. The crack length and stress intensity at which complete transition to 45° plane did, however, vary with thickness. It was observed that generally thinner specimens made this transition at shorter crack lengths and lower crack growth rates. So thinner specimens exhibited longer lives by virtue of the fact that more time was spent in crack propagation on 45° plane. Although these observations differ from those of Broek and Schijve, the same conclusion that shear mode is inherently more resistant to crack propagation than tensile mode.

Heiser and Mortimer [16] conducted tests on 4340 steel under constant amplitude loading, and found that thicker specimens exhibited higher FCP rates than thinner specimens. The change of fracture mode transition from the tensile mode to shear mode was attributed to the variation of stress state from plane strain to plane stress. It was observed that the transition from tensile to shear mode occurred at increasingly longer crack lengths as the

thickness increased, with the thickest specimen remaining in the tensile mode up to fracture. Examination of the surfaces revealed that the microscopic fracture modes did not differ with thickness. Therefore, the conclusion was reached that the thickness effect was really a plastic zone effect as a result of the variation in the stress state, with plane strain promoting higher FCP rates.

McGowan and Liu [17] illustrated that FCP rates were greater in plane strain than in plane stress, and that this difference was the reason for the existence of the thickness effect observed. Their FCP data indicated that in two regions of the graph, the FCP rates were independent of thickness but that in between these two regions, differences in FCP rates between the thicknesses became apparent. They hypothesized that the two regions where growth rate was independent of thickness were the regions where all thicknesses were in plane strain and plane stress, respectively. Between these two regions was where the transition from plane strain to plane stress was taking place. Since the greater constraint in thicker specimens would inhibit transition until greater ΔK values than the thinner specimens, this phenomenon would be delineated as difference in growth rates between the thicknesses in this mixed mode region. Therefore, the difference in growth rates between plane strain and plane stress could be the reason for the thickness effect. To confirm these

hypotheses, the data for all three thicknesses were correlated with the ΔK_{eff} , which was assumed to be a linear combination of ΔK_{eff} in plane strain [18] and the ΔK_{eff} in plane stress [19], with both ΔK_{eff} being weighted with a constraint parameter which accounted for the variation in constraint at the crack tip in the mixed mode region. The resulting correlation with ΔK_{eff} collapsed the three growth rate curves to one line, thus showing that the difference in crack closure between plane strain and plane stress was the cause for the thickness effects observed.

In summary, this review revealed that the effect of thickness on fatigue crack propagation under constant amplitude loading has not yet been fully determined. However, any thickness effects would be expected to be attributed to a change in crack closure or crack slant associated with the transition from plane strain to plane stress. Only one investigation [17] has clearly delineated a thickness effect, and determined that it was due to the difference in crack closure between plane strain and plane stress.

Variable Amplitude Loading

The effects of thickness on fatigue crack propagation under variable amplitude loading is more firmly established in the literature than under constant amplitude

loading, at least qualitatively. However, the mechanism through which the thickness effect is manifested, let alone the mechanism of load interactions in general, are still not fully understood.

One of the first indications that thickness may effect the amount of retardation after an overload occurred was when Wei and Shin [20] observed that the reinitiation of fatigue crack growth following an overload proceeded from the mid-thickness of a specimen. Since the state of stress at the crack tip can vary from plane strain at the center to plane stress at the surface, their observation suggested that retardation is dependent on the state of stress, and therefore would be affected by the specimen thickness. A subsequent series of tests on three thicknesses of 7075-T6 aluminum alloy indicated a significant effect of thickness on the retardation, with a higher number of delay cycles being exhibited in the thinner specimens. Furthermore, the amount of crack length necessary to reestablish the equilibrium FCP rate was much greater in the thinner specimens. This result indicated that the zone affected by the overload is related to the overload plastic zone size, which was greater in the thinner specimens due to the lesser through the thickness constraint.

Chanani [21] conducted single peak overload tests on different thickness specimens using four different high strength aluminum alloys. The results showed that for all overload ratios tested, the number of delay cycles decreased with increasing thickness. Furthermore, at a given overload ratio, the number of delay cycles decreased as the baseline stress intensity increased, even though the affected crack length increased. This was attributed to the higher crack growth rate prior to overload, thus permitting the crack to pass through the overload affected zone in relatively fewer cycles. Chanani indicated that the observed thickness effect on the number of delay cycles at a given K level was probably due to the larger plastic zone sizes formed in the thinner specimens due to the smaller constraint. The variation in the N_D between thicknesses for a particular alloy as compared to the variation for other alloys was significant. In fact, a 2024-T8 alloy showed only a small variation in delay as a result of thickness effects. Chanani noted however, that it had a completely different cyclic hardening exponent than the other alloys, probably as a consequence of the nature of its precipitates, therefore pointing out the possible importance of microstructure on delay behavior. Finally, fractographic inspection of the crack surface revealed that before overload the surfaces were covered with fatigue striations. In the overload affected zone,

there existed a smooth topography with evidence of abrasion, thus supporting the idea that crack closure is, at least in part, the cause for retardation.

Mills and Hertzberg [22] conducted tests on various thicknesses of 2024-T3 aluminum alloy in order to evaluate the possibility that retardation was due to a favorable residual compressive stress at the crack tip after a high load excursion. Several important features of retardation were drawn from the results of their tests. For a given overload ratio and baseline stress intensity factor range, the number of delay cycles increased and the minimum FCP rate following the overload decreased with decreasing sheet thickness. Fractographic examination of the fracture surfaces revealed that abrasion, indicative of crack closure, reached a maximum at some distance from the point of overload application, and then gradually decreased beyond this point of maximum abrasion. This observation was consistent with crack closure arguments, in which the minimum growth rate after overload would be attained as the crack grew into the overload plastic zone, followed by a gradual increase in growth rate as the crack grew out of the overload plastic zone. Furthermore, the thickest specimen showed very little evidence of abrasion, while the intermediate thickness showed a cleavage like appearance coupled with abrasion, with the amount of abrasion increasing near the surfaces. Mills and Hertzberg believed that

these phenomena were direct consequences of the variation of the size of the plastic zone through the thickness due to the variation of constraint. The larger plastic zone sizes in the thinner specimens resulted in the greater amount of delay. Furthermore, the increased abrasion in the thinner specimens illustrated that crack closure is a major cause of the retardation and is probably a manifestation of the variation of plastic zone sizes due to the variation of stress state through the thickness.

A more detailed analysis of data on thickness effects on delayed retardation by Wei et al.[23] provided further insight into the characteristics of delay in 2219-T851 aluminum alloy. The number of delay cycles was seen to increase with decreasing specimen thickness at a given overload ratio and baseline stress intensity. Delay occurred within the plastic zone formed by the overload, and within this zone the FCP response included an abrupt increase in growth to a value greater than the steady state rate, a rapid decrease to a minimum value over some distance from the point of the overload, and subsequent gradual increase in FCP rate back to the steady state value. The abrupt increase in growth rate after the overload occurred over a crack length approximately equal to the size of the cyclic plastic zone size of the baseline stress intensity. The retardation itself was found to occur over a crack length corresponding to the size of the

plane stress plastic zone size of the overload in the thinner specimens, while the zone of retardation decreased with increasing thickness towards a size corresponding to the plane strain plastic zone size. This investigation showed that the retardation could be correlated with the different plastic zone sizes involved, and furthermore illustrated the three-dimensional nature of retardation due to the variation of stress state through the specimen thickness, as evidenced by the smaller overload affected zones in the thicker specimens. Wei et al. did not go so far as to say that crack closure was the cause of the retardation, but rather found that a model using a residual compressive stress at the crack tip was useful in describing the retardation effects.

Matsuoka and Tanaka [24] performed single peak overload tests on different thickness specimens of A5083 and HT80 steel to determine the effects of the variation in plastic zone size through the thickness, i.e. to examine the difference in delay behavior between the interior plane strain region, and the surface plane stress region. First, overload tests were run on all thickness specimens with a specific overload ratio and baseline stress intensity. It was found that for a particular alloy, the delay increased with decreasing specimen thickness, and the aluminum alloy exhibited more pronounced delay behavior than the steel. These tests were then repeated, except

that after the overload was applied, the surfaces were machined off to remove the surface plastic zones. Cycling was then continued on these specimens at the original baseline stress intensity until fracture to observe the resulting delay behavior. For the aluminum, machining away the surface layers resulted in a drastic decrease in retardation, and a reduced overload affected zone. However, for the HT80 steel the surface removal caused either no change or even a slight increase in the retardation. Although the results of the tests on the aluminum alloy may have indicated less delay in plane strain due to smaller plastic zone and reduced closure, the result for the the steel specimens indicated that a major contribution to the retardation effect is not necessarily due to the crack closure phenomenon.

Sharpe et al. [25] provided further evidence that perhaps crack closure may not be the only mechanism involved in retardation phenomenon. Overload tests on 2024-T851 specimens in thicknesses varying from 0.64cm to 2.54 cm were conducted with different amounts of hold time at zero load after overload, varying from 3 min. to 24 hrs. Results showed that the delay observed tended to decrease slightly for increasing hold times. However, the measurement of the crack closure using an interferometric displacement technique indicated that the crack closure in the overload affected zone tended to decrease with

increasing hold time, and with a 24 hour hold time the crack closure was virtually the same in the overload affected zone as in the pre-overload region. Since there was almost as much delay in the specimen with the 24 hour hold time as in any other specimen, it was evident that the closure concept did not completely account for retardation, at least in this alloy. Also observed in the results was that there was no significant difference in the delay behavior between the various thicknesses. However, it was noted that in all thicknesses the conditions for plane strain were always met, even due to the overload. Since no deviation from plane strain occurred, the fact that all thicknesses exhibited about the same amount of delay agrees with the theory that variation in closure with stress state is the reason for the thickness effect in delayed retardation.

In summary, the most significant point revealed by this review was that variation of crack closure with the stress state at overload plays an important part in the effects of thickness on retardation. When crack closure was the primary cause of retardation, retardation increased with decreasing thickness due to greater closure caused by the larger plastic zones in the thinner specimens due to less through the thickness constraint. However, crack closure alone may not totally account for the amount of retardation observed.

CHAPTER 3 - TEST PROGRAM

The primary purpose of this investigation was to define the effect which specimen thickness has on FCP under constant amplitude loading and on retardation following an overload. Ultimately, insight into the mechanism(s) causing the thickness effects was to be provided through analysis of test results. Therefore, the following test program was developed to meet these objectives.

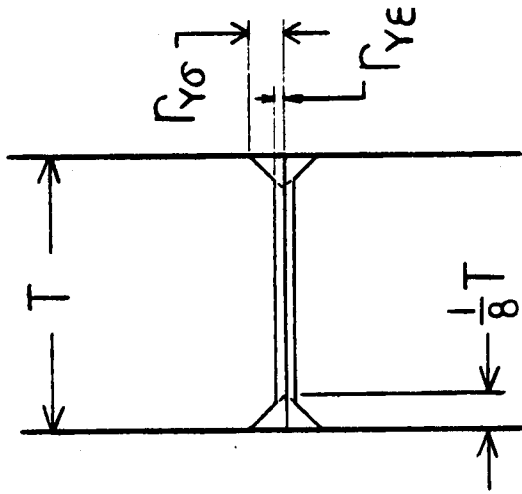
Development of Constant Amplitude Tests

The literature review revealed that the effects of thickness on FCP under constant amplitude loading have not yet been defined. However, it is expected that any thickness effects would be attributed to the change in crack closure and crack slant associated with the transition from plane strain to plane stress. Therefore, the constant amplitude test program was developed assuming that variation of stress state at the crack tip is paramount in delineating any thickness effects in the crack growth rate data. The main idea behind the test program was to propagate cracks from plane strain to plane stress in three

specimen thicknesses. Any differences in growth rate due to the stress state transition would then become evident in the final da/dN versus ΔK curves.

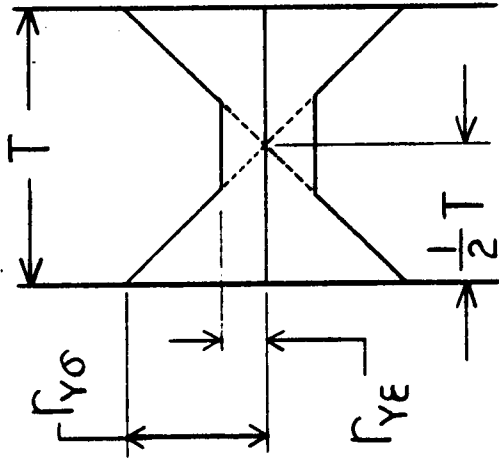
It was necessary to use two specimens for each thickness in order to obtain continuous FCP rate data from plane strain to plane stress. One specimen was used to obtain data in the plane strain and mixed mode regions, and the second specimen was used to obtain data in the mixed mode and plane stress regions. The data from the two specimens was to overlap in the mixed mode region. One advantage of this was that it precluded any crack length effects, since data in plane strain would be obtained at approximately the same crack lengths as data in plane stress. The criterion used to define plane strain and plane stress was based on the model illustrated in Figure 3.1.

Since McGowan and Liu [17] found crack closure variation with stress state to be the cause of thickness effects in their data, the tests were conducted under conditions of crack closure and conditions of no crack closure. This was achieved by conducting the tests at two stress ratios, 0.05 and 0.75. The tests at $R=0.05$ provided data under which crack closure occurred, while the tests at $R=0.75$ provided data under which no crack closure occurred. The choice of $R=0.75$ was based on results of



PLANE STRAIN

$$\frac{r_{Y\sigma}}{T} \leq .125$$



PLANE STRESS

$$\frac{r_{YE}}{T} \geq .5$$

Figure 3.1 Model used to define plane strain and plane stress.

Newman, which showed that for conditions of plane stress, no crack closure occurred for stress ratios greater than $R=0.70$. Therefore, any thickness effects present in data at $R=0.75$ would indicate another mechanism besides crack closure effects must be active in the thickness effect. The actual Test Programs for both stress ratios are shown in Tables 3.1 and 3.2.

Three supplementary tests were conducted at $R=0.75$. These were found to be necessary because the original tests did not provide data at high enough values of ΔK to show crack growth rate in plane stress. Thus, these tests were conducted at high ΔK values on each thickness to extend the da/dN versus ΔK curves as far out as possible into the plane stress region. These tests are shown in Table 3.3.

Development of Single-Peak Overload Tests

Studies in the past [21,22] have shown that when crack closure was the primary retardation mechanism, retardation increased with decreasing specimen thickness. This has been attributed to the larger plastic zone developed in the thinner specimens due to lower through the thickness constraint. The larger plastic zone results in more crack closure, and hence greater retardation.

Table 3.1 Constant amplitude loading test program at R=0.05.

TEST NO.	THICKNESS (in.)	CRACK LENGTH (in.)	P _{max} (kip)	ΔP (kip)	K _{max} (ksi√in)	ΔK (ksi√in)
1	0.08	0.35 2.00	3.09 3.09	2.94 2.94	6.98 24.00	6.63 22.80
2	0.08	0.35 2.00	5.79 5.79	5.50 5.50	13.09 45.00	12.44 42.75
3	0.17	0.35 2.00	6.56 6.56	6.23 6.23	6.98 24.00	6.63 22.80
4	0.17	0.35 2.00	12.31 12.31	11.69 11.69	13.09 45.00	12.44 42.75
5	0.248	0.35 2.00	9.56 9.56	9.08 9.08	6.98 24.00	6.63 22.80
6	0.248	0.35 2.00	17.95 17.95	17.05 17.05	13.09 45.00	12.44 42.75

Table 3.2 Constant amplitude loading test program at R=0.75.

TEST NO.	THICKNESS (in.)	CRACK LENGTH (in.)	P _{max} (kip)	ΔP (kip)	K _{max} (ksi√in)	ΔK (ksi√in)
7	0.08	0.35 2.00	4.43 4.43	1.11 1.11	10.00 34.38	2.50 8.60
8	0.08	0.35 2.00	6.05 6.05	1.51 1.51	13.67 47.00	3.42 11.75
9	0.17	0.35 2.00	9.40 9.40	2.35 2.35	10.00 34.38	2.50 8.60
10	0.17	0.35 2.00	12.86 12.86	3.22 3.22	13.67 47.00	3.42 11.75
11	0.248	0.35 2.00	13.72 13.72	3.43 3.43	10.00 34.38	2.50 8.60
12	0.248	0.35 2.00	18.76 18.76	4.69 4.69	13.67 47.00	3.42 11.75

Table 3.3 Supplementary constant amplitude tests at R=0.75.

TEST NO.	THICKNESS (in.)	CRACK LENGTH (in.)	P _{max} (kip)	ΔP (kip)	K _{max} (ksi√in)	ΔK (ksi√in)
8s	0.08	1.13	7.21	1.80	31.94	7.98
		2.00	7.21	1.80	56.00	14.00
10s	0.17	1.13	15.31	3.83	31.94	7.98
		2.00	15.31	3.83	56.00	14.00
12s	0.248	0.35	19.00	4.75	31.66	7.92
		2.00	19.00	4.75	58.83	14.71

A test program was developed to evaluate the above hypothesis. Single-peak overload tests with an overload ratio ($Q_{ol} = \frac{K_{ol}}{K_{max}}$) of 1.8 were to be conducted on specimens of three thicknesses. In each thickness, the crack was grown under constant amplitude loading conditions to some specific crack length. At this point, a single-peak overload was to be applied, after which cycling was continued under the same loading conditions. The loading and crack length at which the overload was to be applied were chosen such that the stress intensity factor at overload, K_{ol} , and the ΔK at overload, were the same in all three thicknesses. The magnitude of K_{ol} was chosen such that different stress states existed at the crack tip in each thickness. Subsequent differences in retardation characteristics could then be attributed directly to the differences in stress states between the thicknesses.

Since the degree of crack closure has been shown to play a significant part in the thickness effect on retardation, tests were to be done at two stress ratios, one at which crack closure occurred after overload, and the other for which no crack closure occurred after overload. The stress ratios chosen to achieve this were $R=0.05$ and $R=0.75$, respectively.

All tests at a stress ratio of 0.75 exhibited complete crack arrest, resulting in no retardation data.

Therefore, tests were conducted to determine at what values of R , Q_{ol} and K_{ol} that overload tests could be conducted while still maintaining the conditions of no crack closure after the application of the overload. The test programs for both stress ratios are shown in Tables 3.4 and 3.5.

Himmelein and Hillberry [26] developed a delay/arrest boundary by performing overload tests at various combinations of Q_{ol} and R_{ol} , where R_{ol} is $\frac{K_{min}}{K_{ol}}$. A similar procedure was used in this investigation, except K_{ol} was kept the same in all cases in order to maintain a constant stress state during overload application. The procedure consisted of growing a crack under constant amplitude loading at a specific R value to a certain crack length. At this point, an overload was applied to produce a specific K_{ol} , and then the cycling was continued at the same R . If no observable crack growth occurred after 10^4 cycles, complete arrest was assumed, and the loads were raised such that R_{ol} remained constant, but Q_{ol} increased. Q_{ol} was raised in specific increments at a constant R_{ol} until crack growth occurred within 10^4 cycles of overload application. The crack was then grown out of the overload affected zone, and the procedure was repeated at another R_{ol} value. Repeating this procedure produced a delay/arrest boundary on a Q_{ol} versus R_{ol} graph for a

Table 3.4 Single-peak overload test program at R=0.05 and $G_{ol} = 1.80$.

TEST NO.	THICKNESS			CRACK LENGTH			FATIGUE CYCLE						OVERLOAD	
	(in)	(in)	(in)	(in)	(in)	(in)	P_{max} (kip)	ΔP (kip)	K_{max} (ksi \sqrt{in})	ΔK (ksi \sqrt{in})	P_{ol} (kip)	K_{ol} (ksi \sqrt{in})		
13	0.08	0.08	0.35	0.35	0.35	0.35	3.37	3.20	7.62	7.24	6.07	24.75		
							3.37	3.20	13.75	13.06				
							3.37	3.20	26.18	24.87				
14	0.08	0.08	0.35	1.40	2.00	2.00	5.55	5.27	12.53	11.90	9.98	52.20		
							5.55	5.27	29.00	27.55				
							5.55	5.27	43.12	40.96				
15	0.17	0.17	0.35	1.00	2.00	2.00	7.16	6.80	7.62	7.24	12.89	24.75		
							7.16	6.80	13.75	13.06				
							7.16	6.80	26.18	24.87				
16	0.17	0.17	0.35	1.50	2.00	2.00	11.08	10.53	11.78	11.19	20.00	52.20		
							11.08	10.53	29.00	27.55				
							11.08	10.53	40.51	38.48				
17	0.248	0.248	0.35	1.00	2.00	2.00	10.45	9.93	7.62	7.24	18.81	24.75		
							10.45	9.93	13.75	13.06				
							10.45	9.93	26.18	24.87				
18	0.248	0.248	0.35	1.40	2.00	2.00	17.20	16.34	12.53	11.90	30.94	52.20		
							17.20	16.34	29.00	27.55				
							17.20	16.34	43.12	40.96				

Table 3.5 Single-peak overload test program at R=0.75 and $Q_{o1}=1.60$.

TEST NO.	THICKNESS (in)	CRACK LENGTH (in)	FATIGUE CYCLE						OVERLOAD	
			P_{max} (kip)	ΔP (kip)	K_{max} (ksi \sqrt{in})	ΔK (ksi \sqrt{in})	P_{o1} (kip)	K_{o1} (ksi \sqrt{in})		
19	0.08	0.80	2.79	0.70	9.91	2.48	5.03	24.75		
			2.79	0.70	13.75	3.44				
			2.79	0.70	21.71	5.43				
20	0.08	0.35	5.55	1.39	12.53	3.13	9.98	52.20		
			5.55	1.39	29.00	7.25				
			5.55	1.39	43.12	10.78				
21	0.17	0.80	5.94	1.49	9.91	2.48	10.69	24.75		
			5.94	1.49	13.75	3.44				
			5.94	1.49	21.71	5.43				
22	0.17	0.35	11.08	2.77	11.78	2.95	20.00	52.20		
			11.08	2.77	29.00	7.25				
			11.08	2.77	40.51	10.13				
23	0.248	0.80	8.66	2.17	9.91	2.48	15.59	24.75		
			8.66	2.17	13.75	3.44				
			8.66	2.17	21.71	5.43				
24	0.248	0.35	17.20	4.30	12.53	3.13	30.94	52.20		
			17.20	4.30	29.00	7.25				
			17.20	4.30	43.12	10.78				

specific overload stress state. This was done for two overload stress states, plane stress and mixed mode. Based on these delay/arrest experiments, six more tests were run at a stress ratio of 0.70 and an overload ratio of 1.5, where it was known crack arrest would not occur. These loading parameters were also chosen because no crack closure would occur after the overload was applied. Specifically, Reuping [27] has shown that for plane stress

$$K_{op} = C K_{ol} \quad 0.4 < C < 0.5$$

Therefore, after overload application in plane stress

$$\Delta K_{eff} = K_{max} - 0.45 (1.5K_{max}) = 0.325K_{max} > \Delta K$$

and therefore there is no crack closure. Furthermore, it has been shown that no crack closure occurs under constant amplitude loading for stress ratios of 0.7 or greater. Therefore, in none of these tests should crack closure occur, and retardation can not be attributed to the crack closure mechanism. The test program for these six tests are shown in Table 3.6.

Table 3.6 Single-peak overload test program at $R=0.70$ and $Q_{ol}=1.50$.

TEST NO.	THICKNESS (in)	CRACK LENGTH (in)	FATIGUE CYCLE						OVERLOAD	
			P_{max} (kip)	ΔP (kip)	K_{max} (ksi \sqrt{in})	ΔK (ksi \sqrt{in})	P_{ol} (kip)	K_{ol} (ksi \sqrt{in})		
25	0.08	0.35	4.83	1.45	10.98	3.29	7.23	24.75		
		0.75	4.83	1.45	16.50	4.95				
		1.14	4.83	1.45	21.56	6.47				
26	0.08	1.26	3.81	1.14	18.29	5.49	5.71	35.00		
		1.65	3.81	1.14	23.33	7.00				
		2.05	3.81	1.14	30.69	9.21				
27	0.17	0.35	10.27	3.08	10.98	3.29	15.40	24.75		
		0.75	10.27	3.08	16.50	4.95				
		1.14	10.27	3.08	21.56	6.47				
28	0.17	1.26	8.10	2.43	18.29	5.49	12.15	35.00		
		1.50	8.10	2.43	23.33	7.00				
		2.00	8.10	2.43	30.69	9.21				
29	0.248	0.59	12.55	3.77	12.08	3.02	18.82	24.75		
		1.00	12.55	3.77	16.50	4.125				
		1.38	12.55	3.77	20.89	5.22				
30	0.248	1.26	11.82	3.55	18.29	5.49	17.73	35.00		
		1.65	11.82	3.55	23.33	7.00				
		2.00	11.82	3.55	30.69	9.21				

CHAPTER 4 - APPARATUS AND PROCEDURE

The material tested was 7475-T731 aluminum alloy sheet, which was donated by the Aluminum Company of America, and all the material was from a single heat. The relevant mechanical properties of this material as determined by the Alcoa Laboratories [28] are shown in Table 4.1.

Center cracked panel type specimens, in thicknesses of 0.08, 0.17 and 0.248 inches were used in this investigation. The dimensions of the specimen are shown in Figure 4.1. The starter notches were 0.01x 0.2 inches in size and were produced through the electrical discharge machining process. The initiation of the fatigue crack was done in accordance with the load reduction procedure recommended by ASTM Standard E647 [29]. The tests were conducted on a MTS 20-kip closed-loop electrohydraulic fatigue machine.

The fatigue cracks were observed using a 150X bifocal microscope, which was mounted on a horizontal traverse. A digital resolver with a resolution of 1 micron was used to monitor the distance traveled by the microscope on the horizontal traverse. Crack lengths were measured from the

Table 4.1 Mechanical properties of the specimen material.

7475-T731 Aluminum Alloy	
Yield Strength (ksi)	57
Ultimate Strength (ksi)	68
Elongation (percent)	10
Elastic Modulus (ksi)	10.3
Shear Modulus (ksi)	3.9

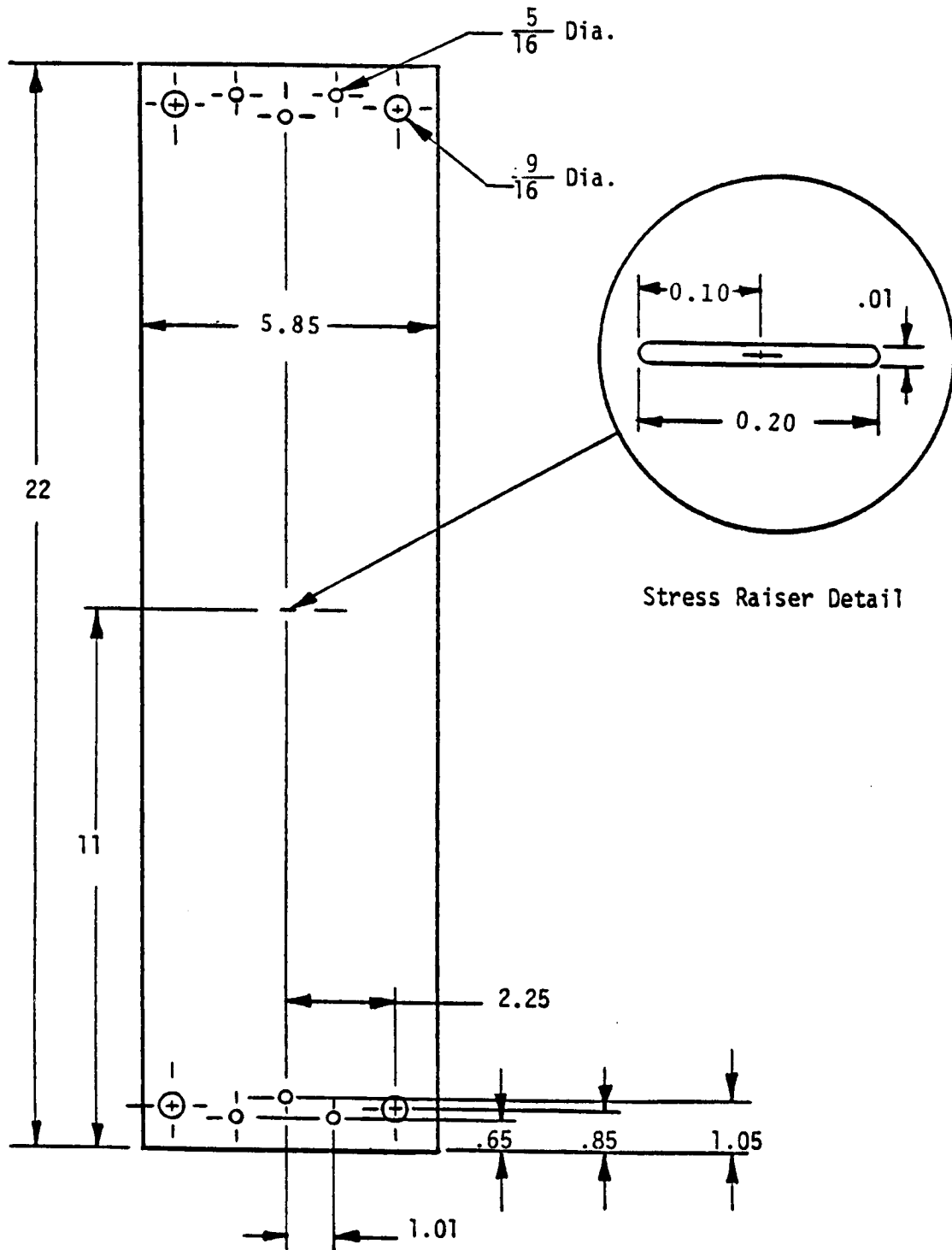


Figure 4.1 Fatigue Test Specimen [38].

specimen centerline by moving the microscope a set distance ahead of the crack tip. When the crack tip reached the cross-hair of the microscope, the crack length and number of cycles data were recorded. A cycle counter and the digital resolver were directly connected to a remotely actuated printer, which allowed the crack length and cycles data to be recorded simultaneously without stopping the test. Data were recorded every 0.2 mm in the constant amplitude tests. Data were recorded every 0.2 mm in the constant amplitude portion of the overload tests, and every 0.02 mm after the overload was applied. A strobe light synchronized with the loading cycle was used to illuminate the cracked portion of the specimen.

Since the effects of thickness were being investigated, an effort was made to eliminate other variables which affect FCP. The environment was held constant from test to test by running the tests in dry air at a relatively constant temperature. Silica gel, which served as a dessicant, was placed behind the crack to absorb moisture in the air. The mid-section of the specimen was sealed in clear polyurethane to minimize the amount of air passing through the crack. The laboratory in which the testing took place was air-conditioned, and the temperatures were in the range of 65^o to 72^o for all tests. The test frequencies were either 10 Hz. or 20 Hz., depending on the expected crack growth rate.

CHAPTER 5 - DATA REDUCTION

Constant Amplitude Loading Tests

The crack length versus number of cycles data were differentiated using a seven point incremental polynomial method to obtain the crack growth rate, as recommended by ASTM E647 [29].

Single-Peak Overload Tests

The number of delay cycles and the size of the overload affected zone, defined in Figure 5.1, for the R=0.05 tests were determined by numerically differentiating the crack length versus cycles data using the same technique described above. The number of delay cycles was defined as the number of cycles it took for the growth rate to reach the FCP rate just prior to overload application. The overload affected zone was the corresponding increment of crack growth over which the retardation took place.

The number of delay cycles and the size of the overload plastic zone for the R=0.70 tests were determined graphically from large plots of the crack length versus cycles data. This could not be done numerically as in the

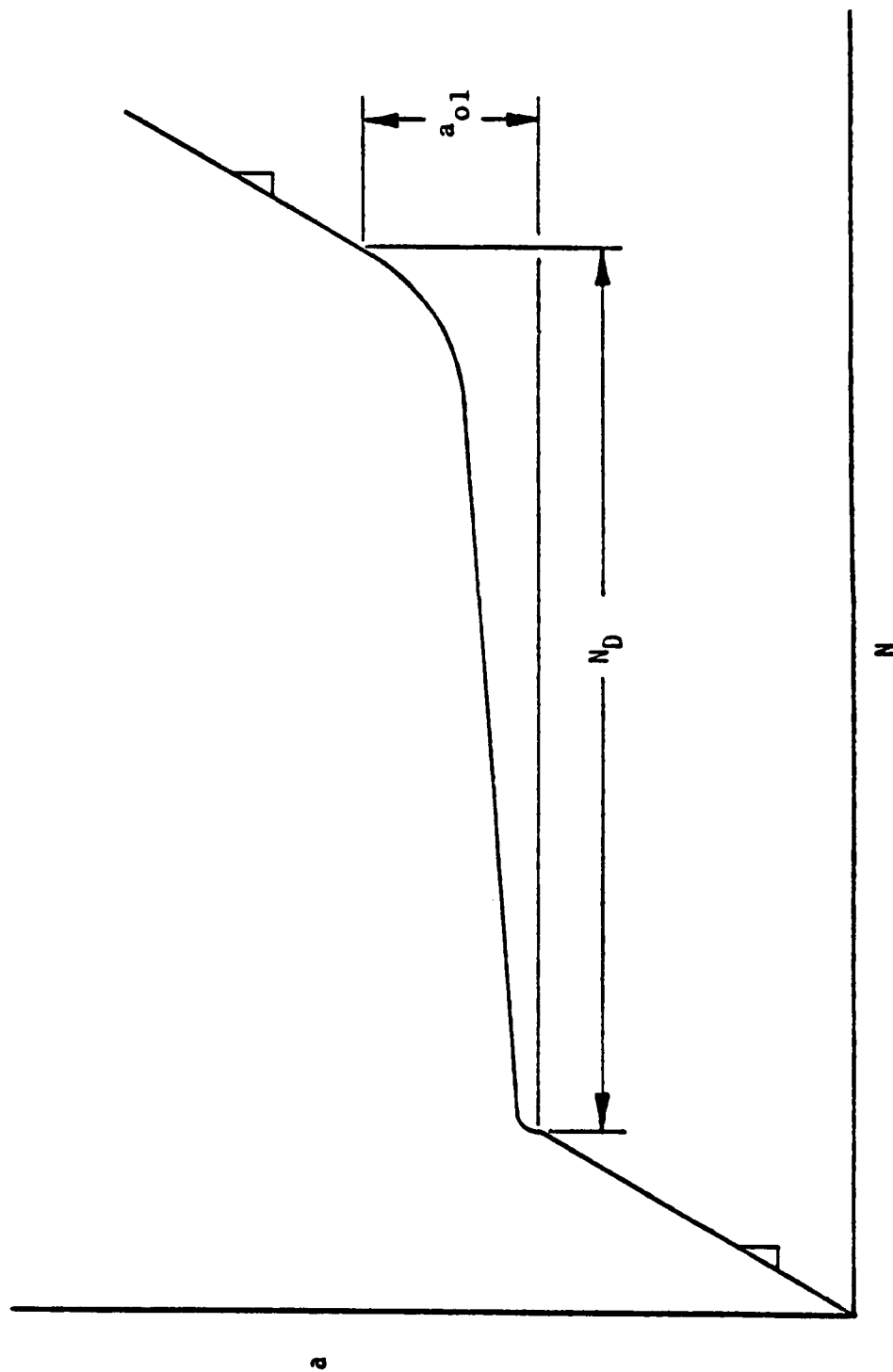


Figure 5.1 Typical a versus N Curve Defining Delay Terms [38].

case of the $R=0.05$ tests because the end of retardation was unclear due to a tendency of the data to oscillate about the pre-overload growth rate. The delay cycles and the overload affected zone were determined by constructing two parallel lines, the first tangent to the a versus N curves at the point of overload application and the second one tangent to the a versus N curve after the point of overload application. The number of delay cycles occurring between the points of tangency was taken as the number of delay cycles, while the increment of crack growth between the points of tangency was taken as the overload affected zone.

CHAPTER 6 - TEST RESULTS

Constant Amplitude Loading Tests

The data acquired from the tests was in the form of crack length versus cycles. To delineate any effects due to thickness on the fatigue crack propagation rate, this data was differentiated using a seven point second order incremental polynomial method and plotted versus the mode I stress intensity factor range ΔK_I . Comparison of the growth rate curves for the different thicknesses tested would reveal any effects of thickness on FCP rate which exists.

Figures A.1 through A.15 in Appendix A show the crack growth rate curves of individual tests on all three thickness specimens at stress ratios of 0.05 and 0.75. In order to obtain growth rate data over a large enough range of ΔK such that both the plane strain and plane stress regions were encompassed, it was necessary to use two specimens for each thickness at both stress ratios. These tests were designed to overlap in the expected mixed mode region to provide a check on the consistency and validity of the data in this region where the transition was

expected to occur. Figures B.1 through B.6 in Appendix B show the growth rate data of corresponding tests for each thickness. The data overlaps very well in the mixed mode region for all thicknesses tested and at both stress ratios, thus confirming the validity and reliability of the data.

Figures 6.1 and 6.2 show the comparison of the FCP rates between the three thicknesses investigated at stress ratios of 0.05 and 0.75, respectively. These graphs clearly show an effect of thickness on the FCP rates in this material at both stress ratios. In both cases, the growth rate is independent of thickness at low ΔK values, with the curves being generally straight. As the ΔK increases, the slopes of the growth rate curves change rather abruptly, with the curves of the thicker specimens changing slope at increasingly higher values of ΔK . After the slope of each curve has changed, they continue to parallel each other, with the thicker specimens clearly exhibiting the higher growth rates. As higher values of ΔK are reached, the slopes of the curves show a tendency to change back to the slope prior to the initial transition. Again, the thicker the specimen, the higher the ΔK at which the change in slope occurs. After the second slope change, the FCP rates once again become independent of thickness, with the curves essentially coincident after the second slope transition.

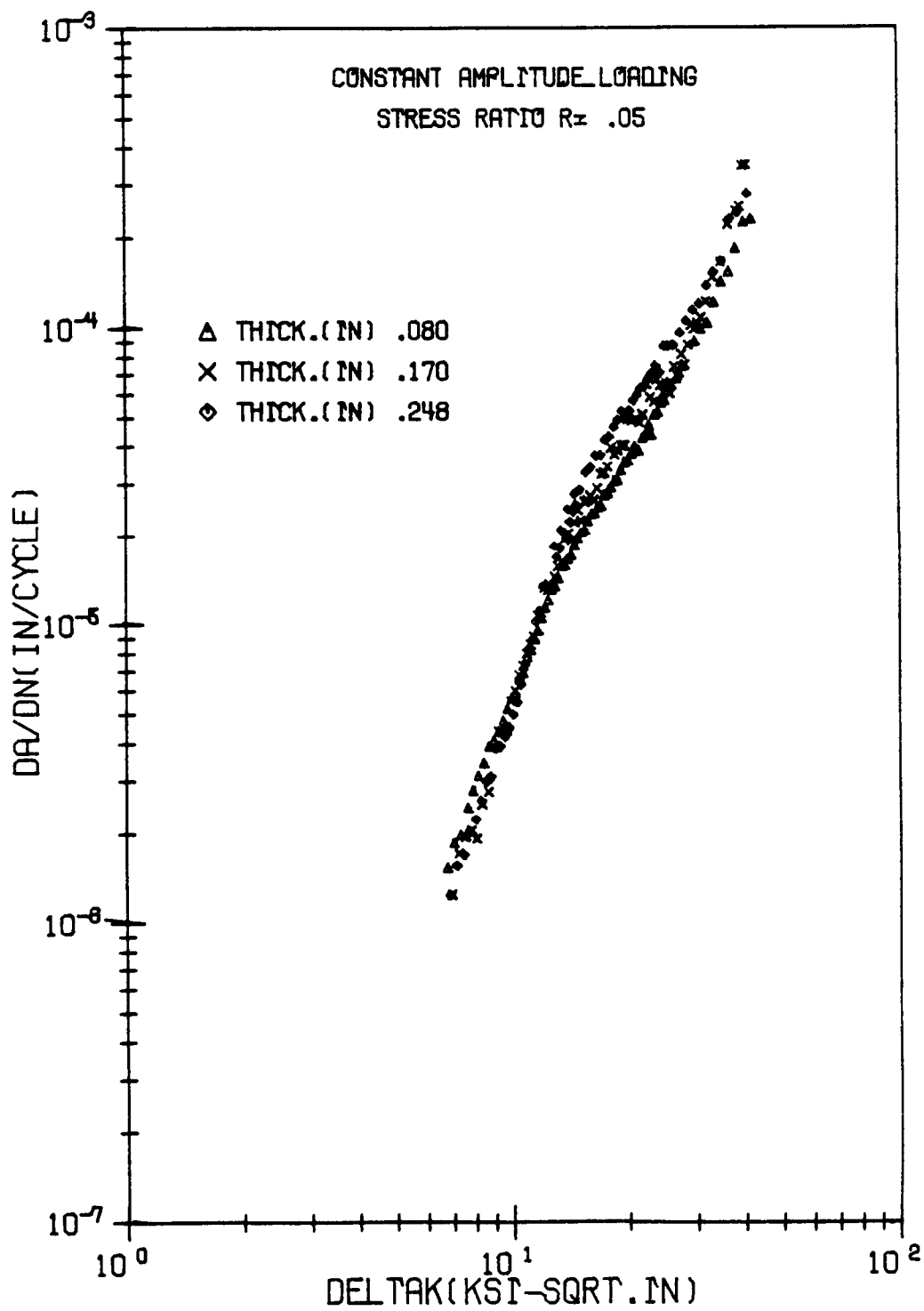


Figure 6.1 Results of constant amplitude loading tests at $R=0.05$.

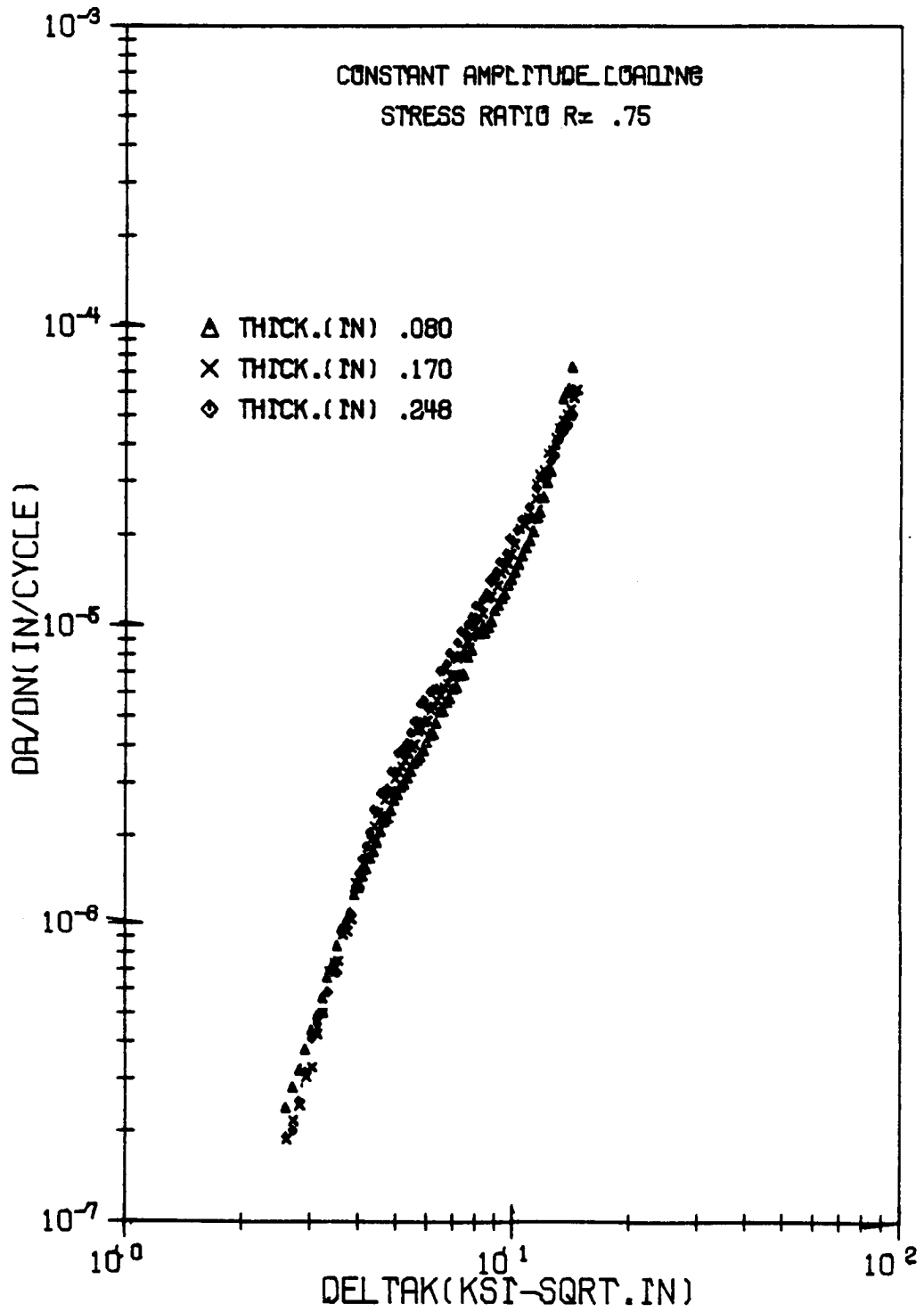


Figure 6.2 Results of constant amplitude loading tests at $R=0.75$.

Single-Peak Overload Tests

The data acquired from the tests was in the form of crack length versus number of cycles. To determine any effects which thickness had on retardation, the data was differentiated using either a seven point incremental polynomial method or a graphical method, as described in Chapter 5. Comparison of the number of delay cycles and overload affected zones between thicknesses would reveal any effect of thickness on the retardation.

Figures C.1 through C.12 in Appendix C show the plots of the crack length versus number of delay cycles for all the overload tests, with the exception of the $R=0.75$ tests which experienced complete crack arrest. These plots clearly show the retardation after overload application in each test, as indicated by the flat spot in the curves. As a comparison of the total fatigue lives of the specimens after overload, the a versus N data for all three thicknesses were plotted on one graph for each set of tests. These graphs are shown in Figures D.1 through D.12 in Appendix D.

Graphs of the differentiated a versus N data for each test are presented in Figures E.1 through E.12 in Appendix E. These graphs illustrate the sudden drop in growth rate experienced after the overload, with the growth rate reaching a minimum after propagating a certain

crack length, and then a gradual increase in FCP rate back to the pre-overload FCP rate.

Tables 6.1 and 6.2 give the numerical values of the retardation characteristics of each set of tests. They present the number of delay cycles, the overload affected zone, the minimum FCP rate after overload, and the increment of crack growth after overload at which the minimum growth rate occurred, all of which are defined in Figure 6.3. Included are the theoretical values of the plastic zone size at overload and the cyclic plastic zone size (based on the Irwin plastic zone model) for each test.

Delay/Arrest Boundary Tests

The results of the tests to determine the delay/arrest boundary are presented in Figures 6.4 and 6.5. The lines represent the boundary between conditions under which arrest occurred and conditions under which delay occurred. Figure 6.4 represents the boundary for conditions of plane stress during overload, and Figure 6.5 represents the boundary for a state of mixed mode during overload. There is a difference between the two boundaries, with arrest occurring at higher overload ratios in mixed mode than plane stress for a given overload stress ratio, except at high overload stress ratios. This is as expected, since if crack closure is the primary retardation mechanism, the greater closure present when plane

Table 6.1 Results of the single-peak overload tests at $R=0.05$ and $\theta_{01}=1.80$.

TEST NO.	$r_{y\sigma}$ (in.)	r_{ye} (in.)	a_{min} (in.)	a_{01} (in.)	$\frac{da}{dn}/min$ (in/cyc) $\times 10^{-6}$	$\frac{da}{dn}/01$ (in/cyc) $\times 10^{-5}$	N_D (cycles)
13	0.06	0.02	0.010	0.070	2.70	1.57	8650.
14	0.27	0.09	0.044	0.300	6.40	7.67	14000.
15	0.06	0.02	0.009	0.030	2.85	1.33	6500.
16	0.27	0.09	0.032	0.197	8.60	9.40	5900.
17	0.06	0.02	0.012	0.030	4.01	1.47	5100.
18	0.27	0.09	0.040	0.179	9.21	6.88	6100.

Table 6.2 Results of the single-peak overload tests at $R=0.70$ and $Q_{01}=1.50$.

TEST NO.	$r_{y\sigma}$ (in.)	$r_{y\epsilon}$ (in.)	a_{min} (in.)	a_{01} (in.)	$\frac{da}{dn}/min$ (in/cyc) $\times 10^{-7}$	$\frac{da}{dn}/01$ (in/cyc) $\times 10^{-6}$	N_D (cycles)
25	0.06	0.02	0.010	0.010	1.70	2.03	33000.
26	0.12	0.04	0.002	0.005	1.20	5.30	37000.
27	0.06	0.02	0.001	0.004	3.30	2.50	19000.
28	0.12	0.04	0.003	0.005	3.10	6.04	20000.
29	0.06	0.02	0.002	0.004	1.50	1.90	23000.
30	0.12	0.04	0.003	0.005	2.21	5.82	23000.

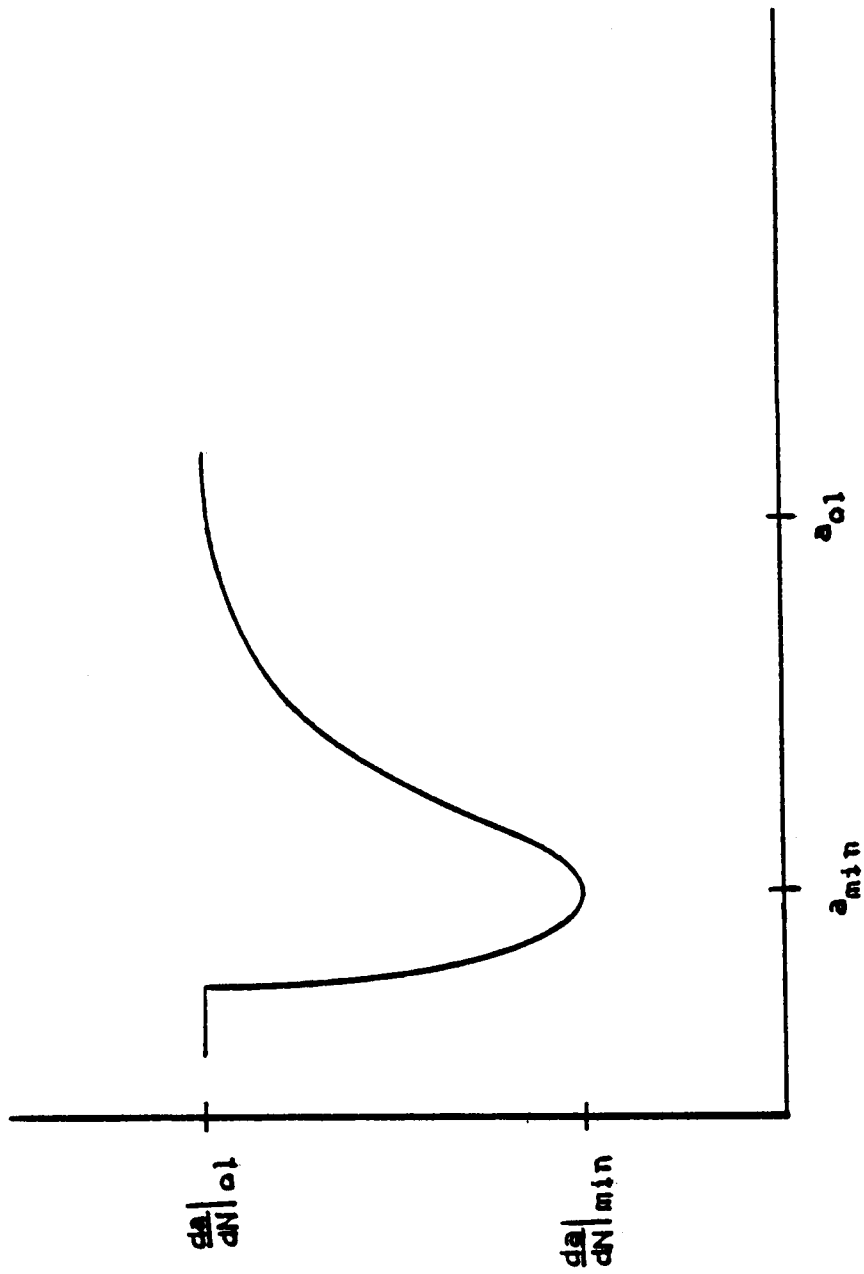


Figure 6.3 Definition of terms associated with delayed retardation.

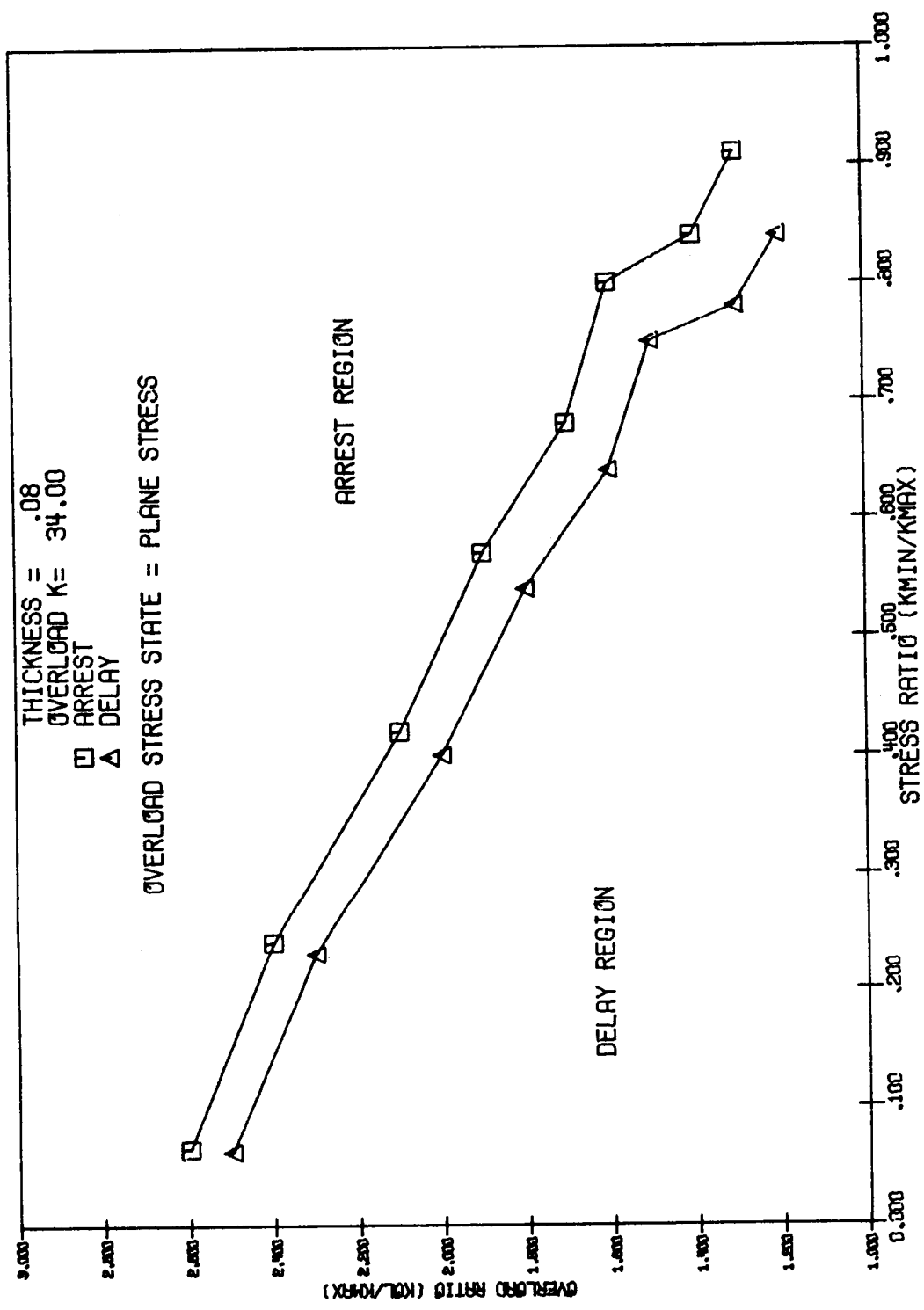


Figure 6.4 Delay/Arrest boundary for plane stress.

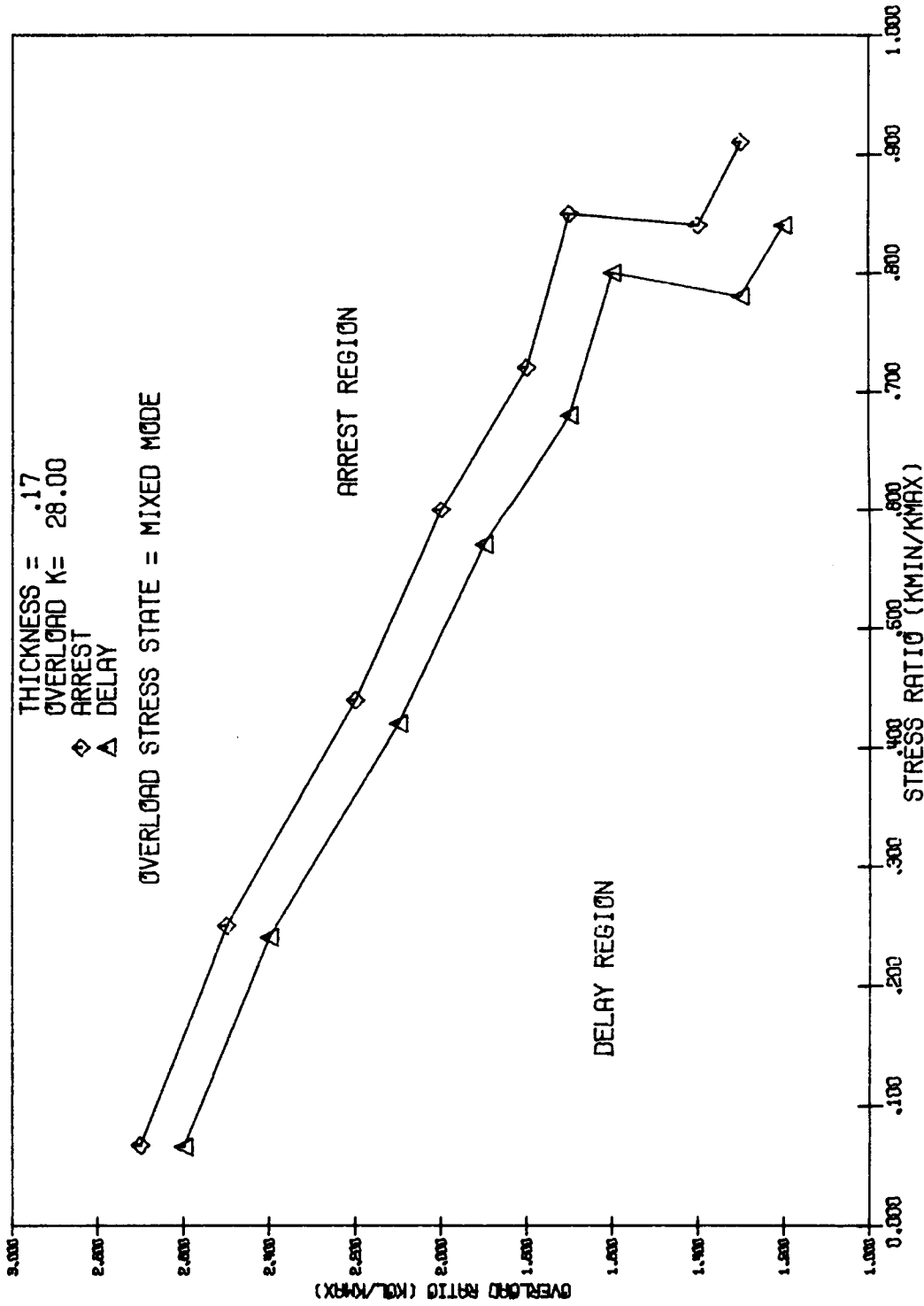


Figure 6.5 Delay/Arrest boundary for mixed mode.

stress is present at overload would result in a lower boundary relative to the boundary formed when mixed mode is present at overload.

Between stress ratios of 0.75 and 0.85, the boundaries coincide, suggesting that at high levels of R, stress state may no longer have as much affect on the delay/arrest boundary. This may further imply that this is because crack closure is no longer the primary retardation mechanism at these high overload stress ratio levels, but rather another mechanism which is not as sensitive to stress state may be active. This possibility will be discussed further in Chapter 8.

CHAPTER 7 - ANALYSIS OF RESULTS

Constant Amplitude Loading Tests

The test results revealed that thickness did affect FCP rate under constant amplitude loading conditions at both $R=0.05$ and $R=0.75$. The nature of the effect was qualitatively similar at both stress ratios. The nature of the thickness effect was also similar to that observed by McGowan and Liu [17], who found that this effect could be explained by the differences in crack closure occurring in each thickness in the mixed mode region as a result of the transition from plane strain to plane stress. Therefore, the analysis used by McGowan and Liu was attempted on this data to determine if difference in crack closure with thickness could adequately explain the observed thickness effects.

Another feature associated with the transition from plane strain to plane stress is the slanting of the crack surface from 0° to 45° with the plane of the specimen. This slanting induces both mode I and mode III crack surface displacements at the crack tip, although the growth rate is routinely correlated with ΔK_I . Models based on

strain energy density and strain energy release rate were developed to account for the slanting of the crack, and were applied to the data to determine if this may be a cause for the observed thickness effects.

Crack Closure

McGowan and Liu [17] demonstrated that the thickness effect present in data they obtained on IN-100 steel may have been due to crack closure variation with stress state. Crack closure occurs as a result of permanent tensile strains left in the wake of an advancing crack front. The result of crack closure is a lower ΔP at the crack tip than is applied externally, because the crack opens at some load $P_{op} > P_{min}$, resulting in a lower than expected FCP rate. The growth rate can be expressed as a function of the effective stress intensity factor range,

$$\frac{da}{dN} = f(\Delta K_{eff})$$

where

$$\Delta K_{eff} = K_{max} (1 - C)$$

and C is an empirically determined function of stress ratio which represents the ratio of the opening stress intensity K_{op} to the maximum stress intensity K_{max} .

The degree or magnitude of crack closure at a given R is dependent upon the magnitude of permanent tensile deformation (i.e. the size of the plastic zone). Under

plane strain conditions, crack closure is less than in plane stress owing to the relative size of the plastic zones [29]. Consequently, the crack growth rate would be expected to be a function of the stress state,

$$\frac{da}{dN_{\epsilon}} = f((\Delta K_{\text{eff}})_{\epsilon})$$

$$\frac{da}{dN_{\sigma}} = f((\Delta K_{\text{eff}})_{\sigma})$$

In a specimen under constant amplitude loading conditions, a crack may be grown from a state of plane strain to a state of plane stress. As the crack grows out of plane strain, the plane stress plastic zones on the free surfaces occupy an increasingly larger fraction of the specimen thickness, resulting in a variation of plastic zone size through the specimen thickness. Since crack closure is dependent on the stress state, the FCP rate under such a mixed mode condition would be different (in fact lower) than under nominally plane strain conditions. In a thicker specimen under the same stress intensity factor range conditions, this transition to mixed mode would occur at a higher ΔK due to its greater thickness, and therefore would exhibit higher growth rates in the mixed mode region than would the thinner specimen. The resulting crack growth rate curves for three different thickness would be as shown in Figure 7.1.

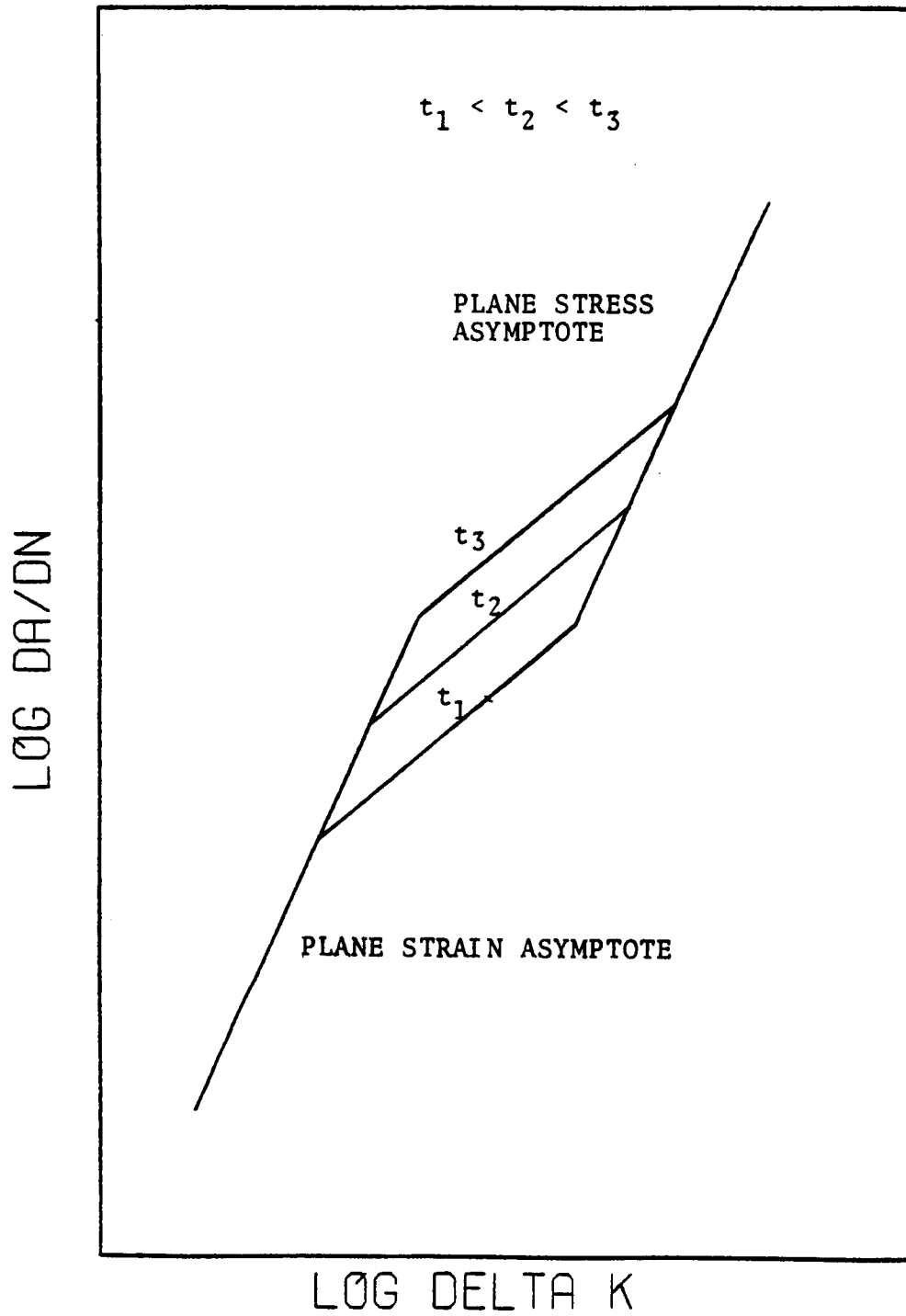


Figure 7.1 Expected effect of thickness on fatigue crack propagation rate.

The model developed by McGowan and Liu essentially used the ΔK_{eff} in plane strain and the ΔK_{eff} in plane stress, and combined them to describe the FCP rates in the mixed mode regions as dictated by the data. In the plane strain region, ΔK_{eff} is given by

$$(\Delta K_{\text{eff}})_{\epsilon} = K_{\text{max}} (1 - C_{\epsilon})$$

and in the plane stress region

$$(\Delta K_{\text{eff}})_{\sigma} = K_{\text{max}} (1 - C_{\sigma})$$

where C_{ϵ} is the ratio $K_{\text{op}} / K_{\text{max}}$ under plane strain conditions and C_{σ} is the ratio $K_{\text{op}} / K_{\text{max}}$ under plane stress conditions. C_{σ} was taken as

$$C_{\sigma} = 0.438 + 0.0947e^{1.78R}$$

as proposed by Elber[5], and C_{ϵ} was taken as

$$C_{\epsilon} = -1.857 + 2.016e^{0.35R}$$

which was estimated from data from Sharpe et al. [18]. In the mixed mode region, the ΔK_{eff} is found by using a linear combination of $(\Delta K_{\text{eff}})_{\epsilon}$ and $(\Delta K_{\text{eff}})_{\sigma}$,

$$\Delta K_{\text{eff}} = HK (1 - C_{\sigma}) + (1 - H)K (1 - C_{\epsilon})$$

where $H = H(T)$. The function $H(T)$ is the constraint parameter which describes the continuous change in constraint at the crack tip as dictated by the data. It is found through the following argument: for any given thickness the da/dN versus ΔK curve forms a shape between two asymptotes. The left asymptote represents plane

strain behavior and the right plane stress behavior. The transition between the two asymptotes depends on the thickness, and thinner specimens make the transition at a smaller ΔK value. At a given rate of da/dN the three ΔK values, ΔK_{ϵ} , ΔK_{σ} and ΔK_H , as shown in Figure 7.2, will all give the same ΔK_{eff} such that

$$\begin{aligned}\Delta K_{eff} &= 0.9 \Delta K_{\epsilon} (1 - C_{\epsilon}) \\ \Delta K_{eff} &= H \Delta K_H (1 - C_{\sigma}) + 0.9 (1 - H) \Delta K_H (1 - C_{\epsilon}) \\ \Delta K_{eff} &= \Delta K_{\sigma} (1 - C_{\sigma})\end{aligned}$$

The resulting expression for H is then

$$H = \frac{\Delta K_{\sigma} (\Delta K_H - \Delta K_{\epsilon})}{\Delta K_H (\Delta K_{\sigma} - \Delta K_{\epsilon})}$$

The constraint parameter $H(T)$ is then obtained by plotting H versus T for different da/dN values within the mixed mode region. The $0.9 (\Delta K_{eff})_{\epsilon}$ term was placed in there to correct for the variation of K due to crack front curvature.

Upon applying this model to data from three thicknesses of IN-100, McGowan found $H(T)$ to be

$$\begin{aligned}H &= 0. & 0 < T < 0.14 \\ H &= \left(\frac{T - 0.14}{0.26} \right)^{0.70} & 0.14 < T < 0.40 \\ H &= 1 & T > 0.40\end{aligned}$$

One important point from this is that all three thicknesses were found to make the transitions at the same ratios of plastic zone size to thickness, that is, equal

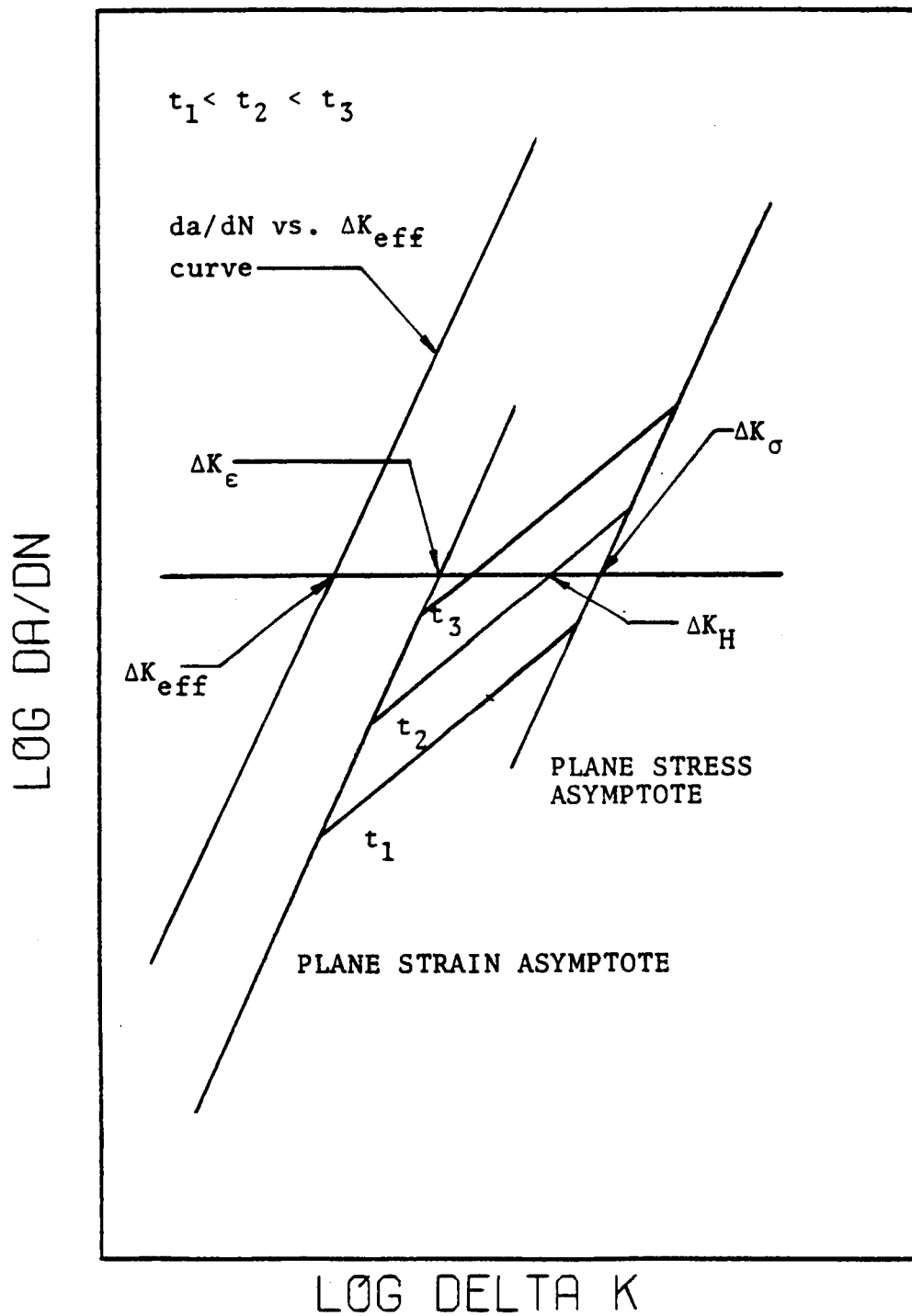


Figure 7.2 Definition of terms in crack closure analysis used by McGowan [30].

values of T . When their data was correlated using this model, the FCP data for all thicknesses collapsed to one straight line.

Tests at $R=0.05$

The primary problem encountered in applying this analysis to the test data was that a single $H(T)$ function could not be obtained for all three thicknesses. The reason was that the transitions on the da/dN versus ΔK curve did not occur at constant values of the ratio of plastic zone size to thickness ratios, T . In fact, Figures F1 through F3 in Appendix F illustrate how the transitions in the actual data compare with the theoretical predictions based on stress state transition. As can be seen, the transitions in the data do not correspond with the predicted transitions. Figure 7.3 illustrates how this ratio, as calculated from the points of the actual slope change on the $\frac{da}{dN}$ versus ΔK curves, varied between the thicknesses for both points of transition. T tends to decrease with increasing thickness for both transition points, with the value for the 0.248 inch specimen being about half the value for the 0.08 inch thick specimen. This variation resulted in a large difference in the constraint parameter $H(T)$ between the thicknesses, as illustrated in Figure 7.4. Due to this difference in the constraint parameters between thicknesses, this analysis

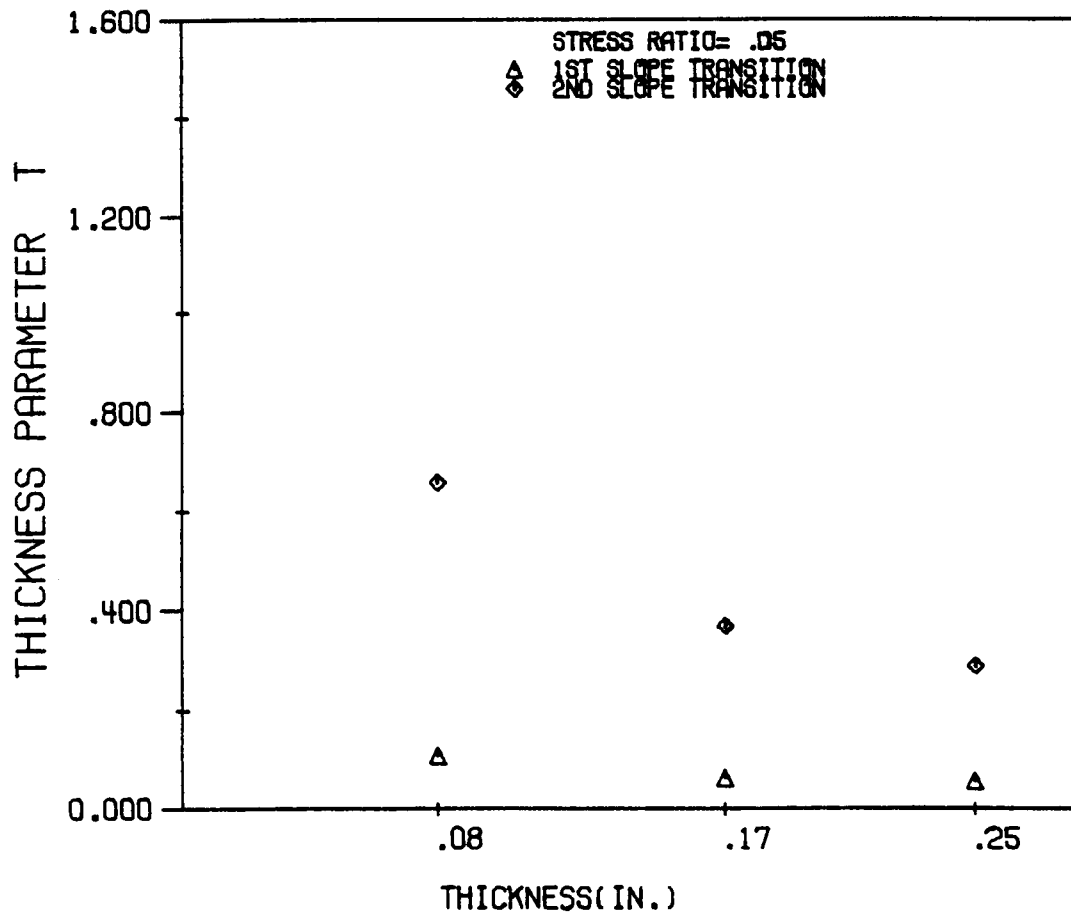


Figure 7.3 Variation of thickness parameter at slope transitions of the actual data with specimen thickness for tests at $R=0.05$.

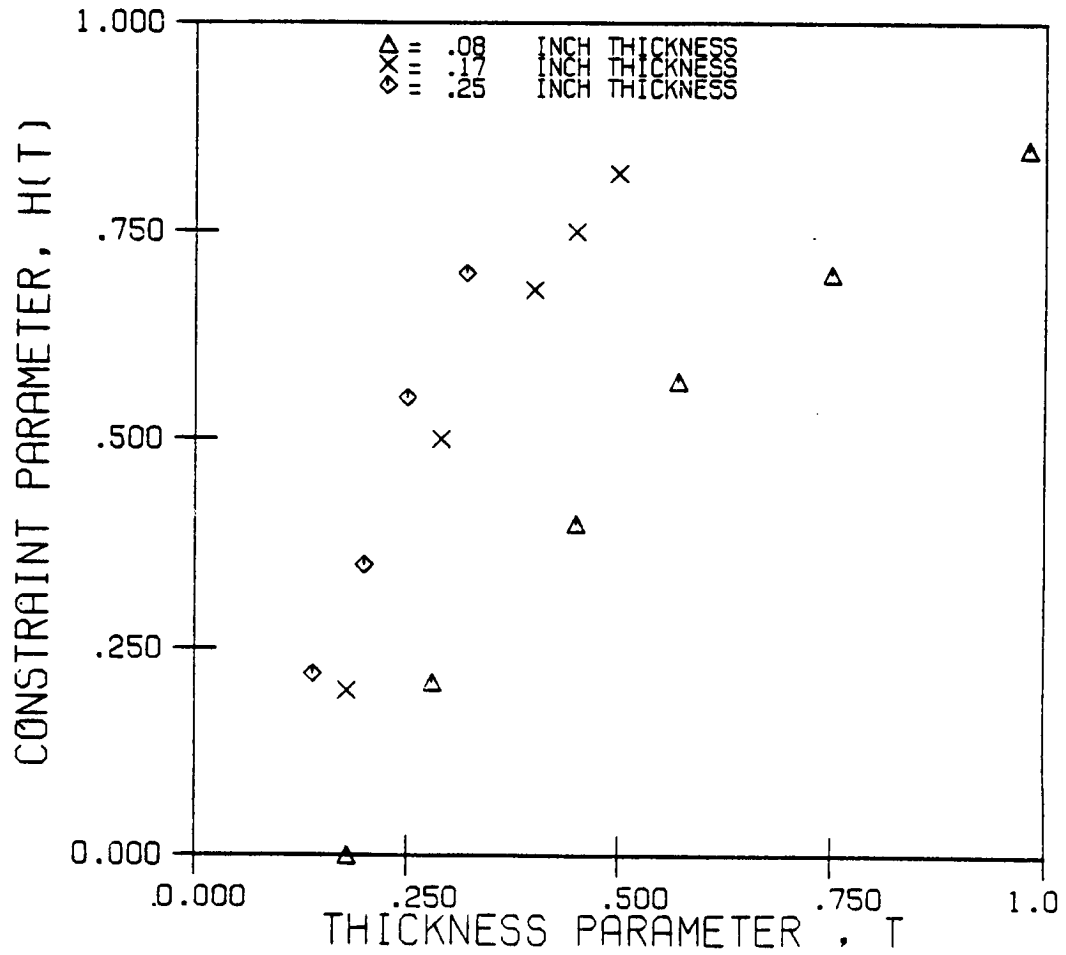


Figure 7.4 Constraint parameter of each thickness for tests at $R=0.05$.

could not be applied to these data.

Tests at R=0.75

The tests at R=0.75 were not expected to have crack closure occur, and therefore this analysis would not apply. However, it would not apply anyway, because the slope transitions of the data did not occur at constant values of T, the ratio of plastic zone size to specimen thickness, as shown in Figure 7.5. Furthermore, the slope transitions of the data did not correspond with the theoretical predictions, shown in Figures F4 through F6 in Appendix F.

Despite the absence of crack closure in these tests, the data still exhibit an effect of thickness, which suggests that another mechanism(s) was active.

Fracture Mode Transition

Strain Energy Density Analysis

A feature which has commonly been associated with the transition from plane strain to plane stress is the transition from tensile mode to shear mode, as shown in Figure 7.6. During this transition, the plane of the crack changes from a 0° angle to a 45° angle with the plane of the specimen. Once the crack plane has varied from 0° , it is no longer strictly a mode I crack, i.e. a combination

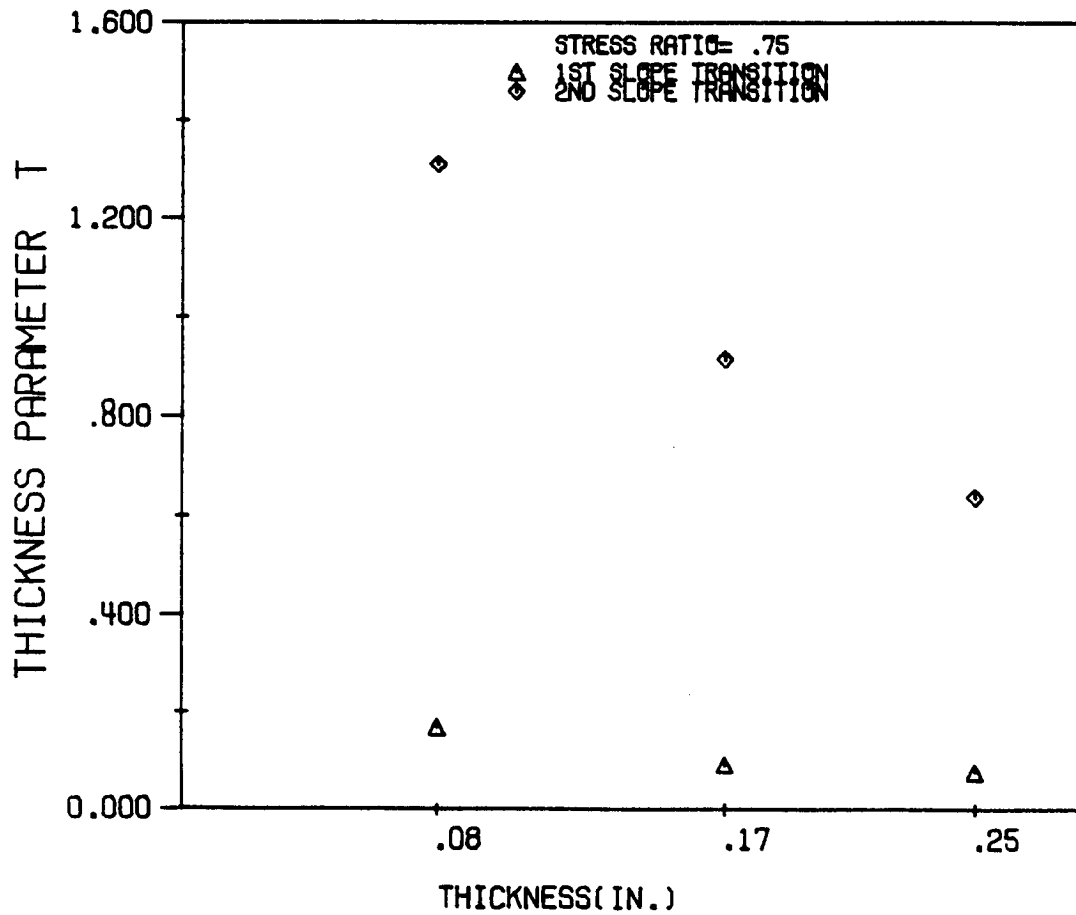


Figure 7.5 Variation of thickness parameter at slope transitions of the actual data with specimen thickness for tests at $R=0.75$.

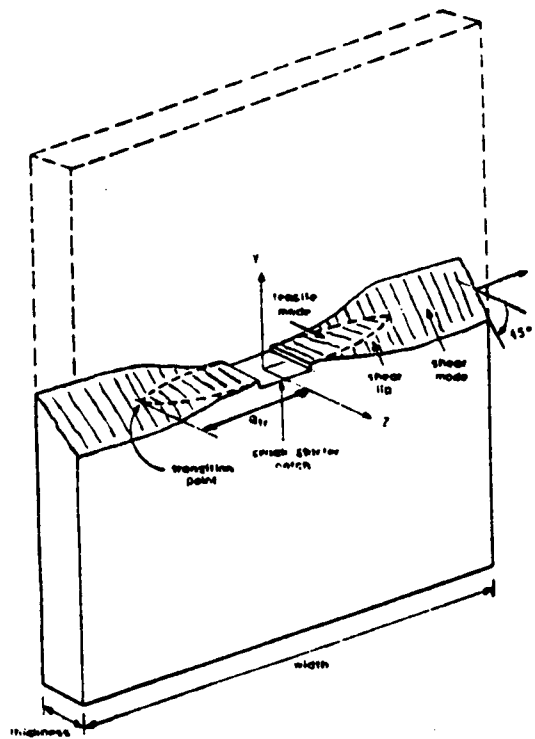


Figure 7.6 Typical shear lips in a center-cracked panel type fatigue specimen.

of mode I and mode III crack tip displacements are present. In correlating FCP data, the slant of the crack as conditions of plane stress are approached is routinely ignored, with the resulting FCP data being correlated with ΔK_I . It has been shown experimentally in this investigation that initiation and termination of shear lip development occurs at longer crack lengths for increasing specimen thickness. Consequently, if crack growth rate is different for a slanted crack than a flat crack under the same R and ΔK_I conditions, then one would expect differences in FCP rates between specimen thicknesses to be delineated in plots of da/dN versus ΔK_I .

To properly correlate the data, a parameter which fully describes the conditions at the crack tip must be used. Since for a slanted crack mode I and mode III exist simultaneously, K_I can not fully describe conditions at the crack tip. Rather, mode I and mode III must be combined in some appropriate manner to account for both modes of crack tip displacement.

The strain energy density factor, S [30], combines K_I , K_{II} and K_{III} to characterize the strain energy density at the tip of a crack under combined mode loading. This theory states that fracture occurs when the strain energy density in a continuum element ahead of the crack reaches some critical value S_c . Furthermore, under combined

loading the crack will not continue to grow in the same plane. The S criterion asserts that the crack will propagate in the direction along which S is a minimum.

The strain energy density in an incremental volume element is given by

$$dW/dV = \frac{1}{2} \sigma_{ij} \epsilon_{ij} \quad i, j=1, 2, 3$$

Substitution of the crack tip singular terms of stresses and strains leads to

$$dW/dV = (a_{11}K_I^2 + 2a_{12}K_I K_2 + a_{22}K_2^2 + a_{33}K_3^2) \frac{1}{r} = \frac{S}{r}$$

The coefficients are [31]

$$a_{11} = \frac{1}{8\mu} ((\kappa - 1))$$

$$a_{12} = 0$$

$$a_{22} = \frac{1}{4\mu}$$

$$a_{33} = \frac{1}{4\mu}$$

where $\kappa = 3 - 4\nu$ for plane strain and $\frac{3-\nu}{1+\nu}$ for plane stress, and μ is the shear modulus of elasticity.

For a crack slanted through the thickness of a center-cracked specimen, the minimum strain energy density is given by

$$S_{\min} = \frac{(\kappa - 1)}{8\nu} \sigma^2 a \sin^4 \alpha + \frac{(\sigma^2 a \sin^2 \alpha \cos^2 \alpha)}{4\nu}$$

where K_I and K_{III} were given as [45]

$$K_I = \sigma \sqrt{a} \sin^2 \alpha$$

$$K_{III} = \sigma \sqrt{a} \sin \alpha \cos \alpha$$

and α is the crack slant angle shown in Figure 7.7.

The strain energy density criterion can be extended to fatigue crack propagation by using the strain energy density range [31], ΔS , to correlate growth rates, where

$$\Delta S_{\min} = S_{\max}^{\min} - S_{\min}^{\min}$$

Using this relation, the strain energy density range can be written

$$\Delta S = \frac{\kappa - 1}{8\nu} (K_{I_{\max}}^2 - K_{I_{\min}}^2) + \frac{1}{4\nu} (K_{III_{\max}}^2 - K_{III_{\min}}^2) \quad (7.1)$$

This equation for the strain energy density range provided the basis for the development of a model to correlate the crack growth rate data. In developing the strain energy density model, three distinct regions were assumed: 1) the tensile mode region, the part of the da/dN versus ΔK_I curve before the first change in slope occurred; 2) the mixed mode region, the part of the curve between the first and second change in slope; 3) the shear mode region, the part of the curve after the second change in slope.

In the tensile mode region, the crack surfaces are macroscopically flat. Therefore, no mode III effects are present, and the strain energy density range is given by

$$\Delta S_{\epsilon} = \frac{\kappa - 1}{8\nu} (K_{I_{\max}}^2 - K_{I_{\min}}^2)$$

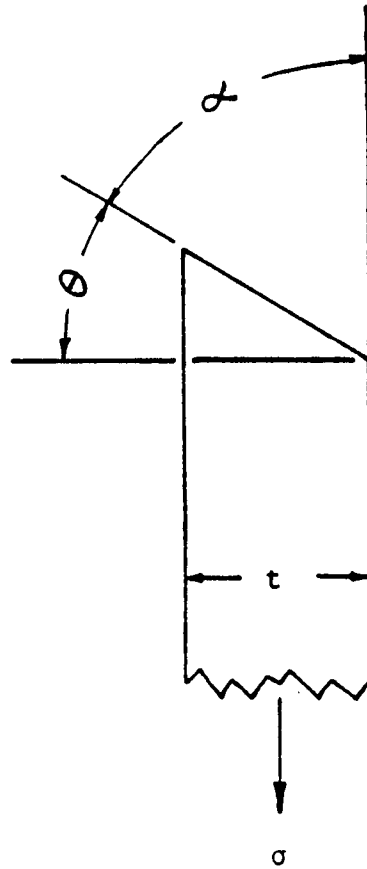


Figure 7.7 Definition of the crack slant angles.

In the mixed mode region, two things occur. The first consideration was the gradual transition from plane strain to plane stress. To accommodate this, ΔS was considered to be a linear combination of ΔS in plane strain (ΔS_{ϵ}) and ΔS in plane stress (ΔS_{σ}), with both terms weighted according to what percentage of the way between plane strain and plane stress the crack was. Since the stress state is generally dependent on the size of the plastic zone relative to the sheet thickness, and r_y is proportional to ΔK^2 , then the weighting factor was defined as

$$X = \frac{\Delta K^2 - \Delta K_P^2}{\Delta K_{PP}^2 - \Delta K_P^2}$$

where ΔK_P and ΔK_{PP} were the ΔK^s at transition from tensile mode, and to shear mode, respectively. The second consideration was the slanting of the crack from 0° to 45° in the mixed mode region. To account for this, the ΔS which incorporates both K_I and K_{III} , where the crack angle α was assumed to vary between 0° and 45° as did the stress state, i.e. α varied as $\alpha = (0^\circ - 45^\circ) X$ in the mixed mode region. Consequently, in the mixed mode region, ΔS was assumed to be given by

$$\Delta S = X(\Delta S_{\sigma}) + (1 - X)\Delta S_{\epsilon}$$

where ΔS_{ϵ} and ΔS_{σ} are given by equation (8.1)

In the shear mode region, the crack was assumed to be at a 45° angle. Therefore, from equation (7.1), ΔS was taken to be

$$\Delta S = \frac{\kappa - 1}{8\nu} (K_{I_{\max}}^2 - K_{I_{\min}}^2) + \frac{1}{4\nu} (K_{III_{\max}}^2 - K_{III_{\min}}^2)$$

where $\kappa = \frac{3-\nu}{1+\nu}$. It should be noted that correction factors for finite specimen width were applied to K_I and K_{III} . These correction factors were taken from Tada et al. [33] for a center-cracked panel assuming remotely applied loads. This model can be used to correlate the crack growth rate data as follows; by differentiating the a versus N data, the growth rate is known at any crack length. From examination of the fracture surface, the crack slant angle can be determined at any crack length, and hence ΔK_I , ΔK_{III} and ΔS can be determined at any crack length. The growth rate can then be correlated with ΔS .

Tests at $R=0.05$. The fatigue fracture surfaces of the specimens at $R=0.05$ showed the transition from tensile mode to shear mode. The crack lengths at which shear lips began to develop and where shear lips became fully developed were measured directly from the specimen fracture surfaces of the $R=0.05$ specimens. It was noticed that crack lengths at the beginning and end of shear lip development were longer in the thicker specimens. With these crack lengths, the ΔK at these points were calculated using the known loading, and compared with the ΔK at

the transitions on the da/dN versus ΔK curves, as shown in Figures G.1 through G.6 in Appendix G. The comparison is fairly good, indicating that the transitions observed on the da/dN versus ΔK curves of the $R=0.05$ data may be a result of the slanting of the crack through the specimen thickness. The strain energy density model was then used to correlate these data. The resulting correlation of $\frac{da}{dN}$ versus ΔS is shown in Figure 7.8. An effect of thickness is still clearly present in this correlation, with the difference lying mainly in the mixed mode region, similar to the original correlations with ΔK_I .

Tests at $R=0.75$. The fatigue fracture surfaces of the specimens at $R=0.75$ did not show a complete transition from tensile mode to shear mode. The crack lengths at which shear lip development began were measured directly from the specimen fracture surfaces. The values of ΔK at these points were used to calculate the thickness parameter, T , at these points. The comparison of the T values at which the tensile mode ended shows that it is not constant, with decreasing values with increasing thickness. Comparison of the T values from the da/dN versus ΔK curves, shown in Figure 7.9, shows that there is no correlation between crack slant and the transition of the FCP rate curves. The values of T at the end of tensile mode are much greater than the first slope transition on the FCP rate curve, and no transition to shear mode occurred.

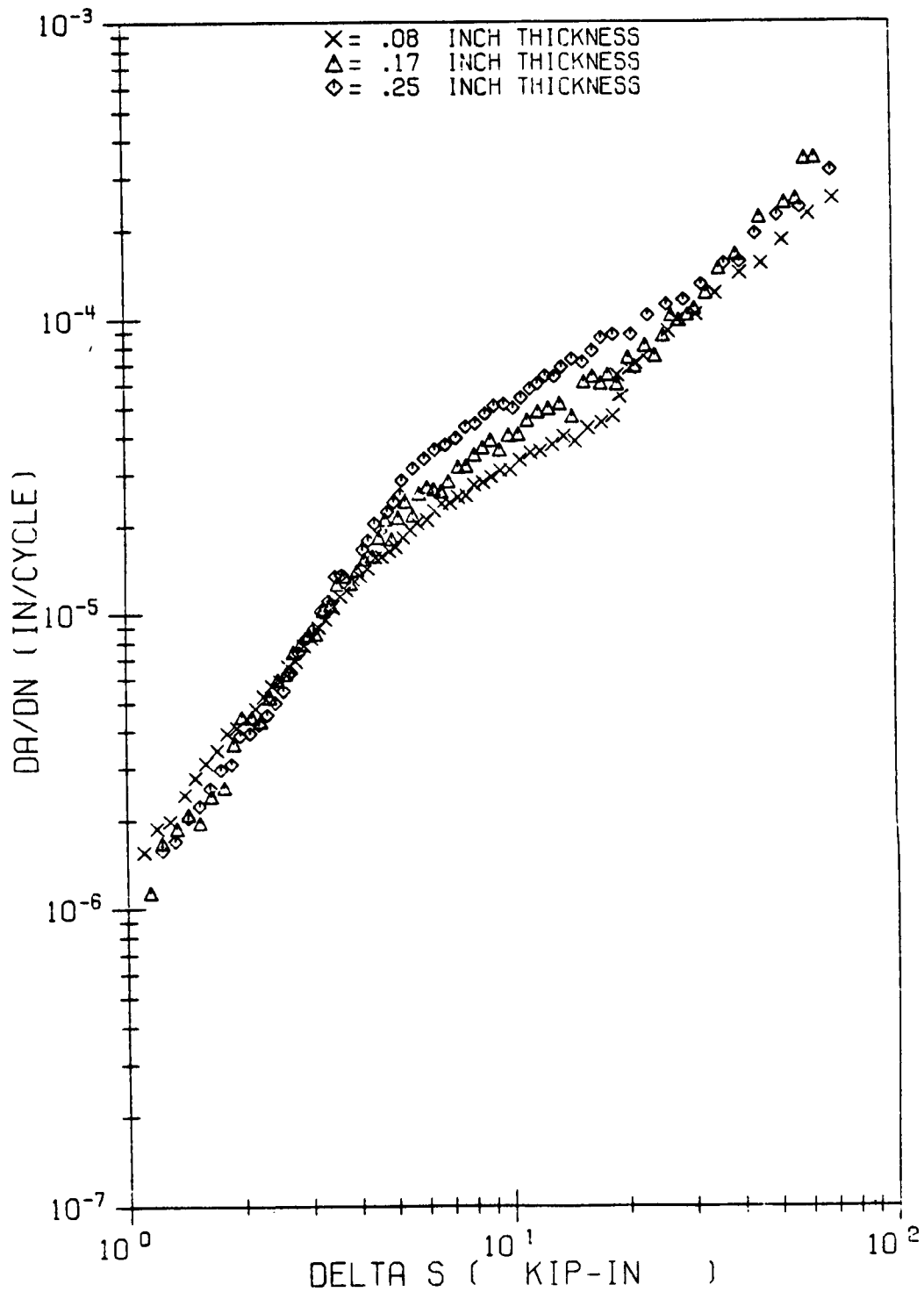


Figure 7.8 Correlation of the data at R=0.05 using the the strain energy density factor range.

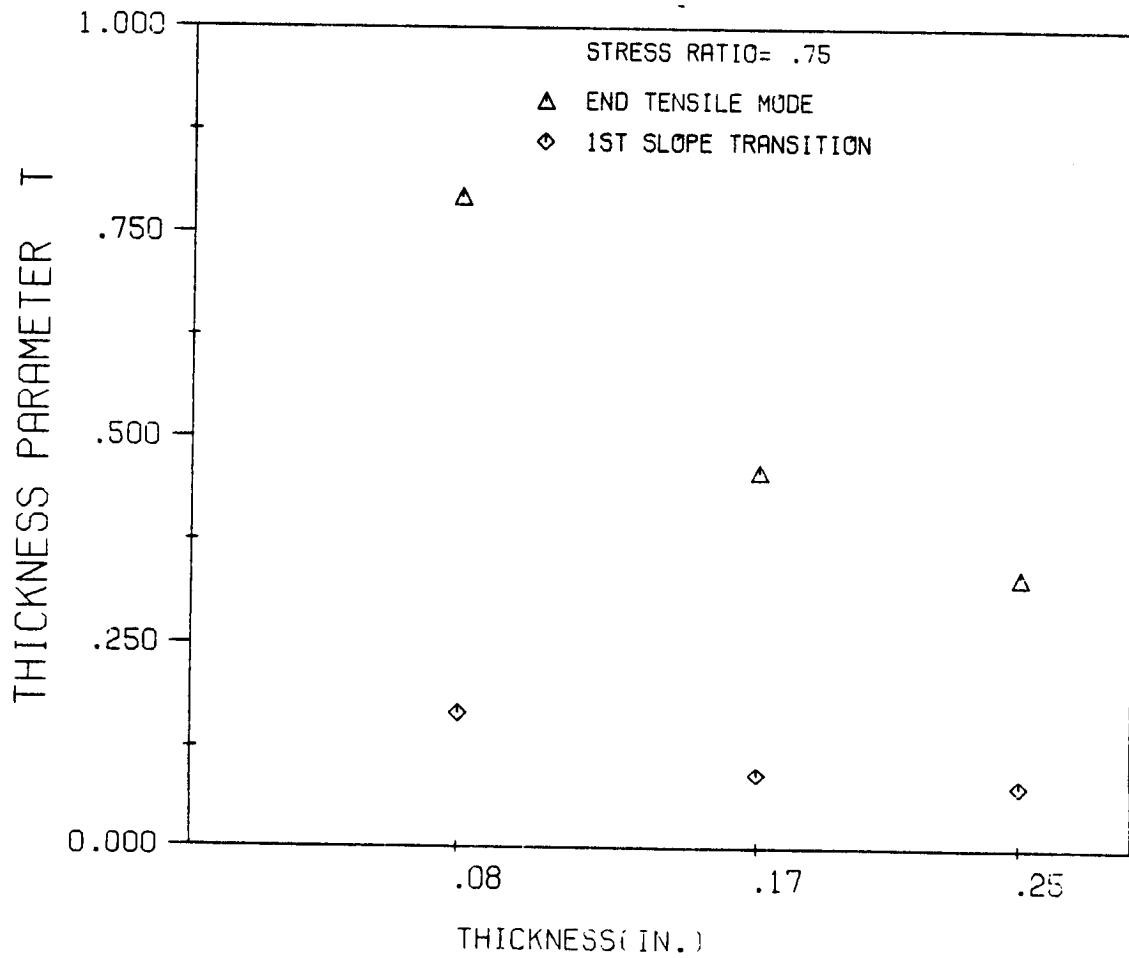


Figure 7.9 Thickness parameter at the end of tensile mode for all thicknesses tested at $R=0.75$ compared to thickness parameter at first slope transition of the actual data.

Apparently, the crack slant, as well as crack closure, had no part in the effects of thickness in the R=0.75 data.

Strain Energy Release Rate Analysis

The results of the strain energy density analysis seem to imply that compensation for the existence of the mode III component of crack tip displacement through the use of a more "appropriate" parameter to correlate the data is not the answer for the thickness effect. The thickness effects in this correlation with ΔS were more extreme than those present in the original correlation with ΔK_I . Apparently, the mode III component does not contribute to crack advance as much as would be indicated by the magnitude of the ΔK_{III} .

The effects which crack slant has on FCP rate were further investigated by employing a model based on the strain energy release rate, G . Unlike the stress intensity factor, it is an energy based parameter which represents the amount of energy available for crack extension per incremental crack extension. For a Mode I crack, the strain energy release rate is

$$G_{0^0} = \frac{1}{2} \frac{P^2}{t} \frac{\partial C}{\partial a}$$

where C is the specimen compliance, P is the applied load, a is the crack length, and t is the specimen thickness. The subscript 0^0 indicates that this is for a mode I

crack, expressing the fact that it is a flat crack.

In obtaining an expression for G for a slanted crack, it was assumed that only the component of the external applied load normal to the crack surface contributed to crack extension. This was done for two reasons. First, the results of the strain energy density analysis suggested that the magnitude of the mode III component of S was not really representative of the amount which mode III contributes to crack advance. Second, a search of the literature revealed that it has been found that FCP rates under mode III loading exhibit FCP rates which are 10 to 50 times smaller than under mode I loading under the same crack opening displacement conditions [34]. Consequently, the contribution to FCP by mode III is actually smaller than would be indicated by the magnitude of the ΔK_{III} , perhaps due to crack surface rubbing and friction. This hypothesis is supported by work done by Tschegg et al. [35], in which they found that due to rubbing, friction and interlocking between the fracture surfaces, and that mode III FCP showed no unique dependence on ΔK_{III} . Furthermore, the FCP rates were found to increase with increasing crack length under constant ΔK_{III} . Therefore, due to those interference effects, perhaps the magnitude of ΔK_{III} is not a good indication of how much mode III contributes to FCP. Since it has been shown that mode III crack growth rate is at least an order of magnitude slower than

mode I, it was totally neglected in this model. Therefore, the strain energy release rate on a crack slanted at an angle θ , as shown in Figure 7.7, was assumed to be given by

$$G_{\theta} = \frac{1}{2} \frac{(P \cos \theta)^2}{\frac{t}{\cos \theta}} \frac{\partial C}{\partial a}$$

Notice that the thickness is divided by $\cos \theta$. This takes into account the increased amount of surface area produced per incremental crack extension. Assuming that $\frac{\partial C}{\partial a}$ is the same for a slant crack and a flat crack in the same state of stress, the ratio of the strain energy release rate for a flat crack to that for a crack slanted at 45° to the specimen thickness is

$$\frac{G_0}{G_{\theta}} = \frac{1}{\cos^3 \theta}$$

The relation between the strain energy release rates in plane strain and plane stress for a mode I crack is

$$(G_{\epsilon})_0 = (1 - \nu^2) (G_{\sigma})_0$$

This same relation was assumed to be true for slanted cracks, that is,

$$(G_{\epsilon})_{\theta} = (1 - \nu^2) (G_{\sigma})_{\theta}$$

Thus the relation between G for a mode I crack in plane strain to G for a 45° crack in plane stress is

$$(G_{\sigma})_{45} = \frac{\cos^3 45^{\circ}}{(1 - \nu^2)} (G_{\epsilon})_0 \quad (7.2)$$

where

$$(G_{\epsilon})_0 = \frac{(1 - \nu^2)}{E} K_I^2 \quad (7.3)$$

For cyclic loading, the strain energy release rate range was used to correlate the data, and is defined as

$$\Delta G = G_{\max} - G_{\min} = \frac{(1 - \nu^2)}{E} (1 - R^2) K_{I_{\max}}^2$$

Therefore, for cyclic loading, the strain energy release rate range for equations (7.2) and (7.3) are

$$(\Delta G_{\sigma})_{45} = \frac{\cos^3 45^\circ}{(1 - \nu^2)} (\Delta G_{\epsilon})_0 \quad (7.4)$$

where

$$(\Delta G_{\epsilon})_0 = \frac{(1 - \nu^2)}{E} (1 - R^2) K_{I_{\max}}^2 \quad (7.5)$$

Equations (7.4) and (7.5) were used to correlate the data in the shear mode and the tensile mode regions, respectively. In the mixed mode region, ΔG was assumed to vary linearly with crack length (which is proportional to ΔK^2), such that

$$\Delta G = (1 - (1 - F)X) (\Delta G_{\epsilon})_0$$

where

$$F = \frac{\cos^3(45^\circ)}{(1 - \nu^2)}$$

$$X = \frac{(\Delta K^2 - \Delta KP^2)}{(\Delta KPP^2 - \Delta KP^2)}$$

ΔKP and ΔKPP are the stress intensity factor ranges at

which the first and second changes in slope of the da/dN versus ΔK_I curve for the given specimen thickness, respectively.

Tests at R=0.05. Applying the above model to the test results, the FCP rate data for the R=0.05 tests was correlated with the mode I strain energy release rate range, as shown in Figure 7.10. A successful correlation of the data for thickness effect would be expected to collapse the curves of all three thicknesses to one straight line. In contrast to the initial da/dN versus ΔK data, these curves show no indication of thickness effect on FCP rate, because the curves of all three thicknesses fall on a single line.

The use of the linear interpolation of the strain energy release rate in the mixed mode region gave a correlation which showed no indication of a thickness effect. However, it was desired to determine whether the assumption of a linear variation of ΔG in the mixed mode region actually agreed with the actual variation of crack angle in the mixed mode region on the specimen fatigue fracture surfaces. Therefore, the results of this correlation were used to work backwards to see how the crack angle would have been forced to vary had the model been used directly to correlate the data in the mixed mode region, and the same results were to be obtained. The model states that

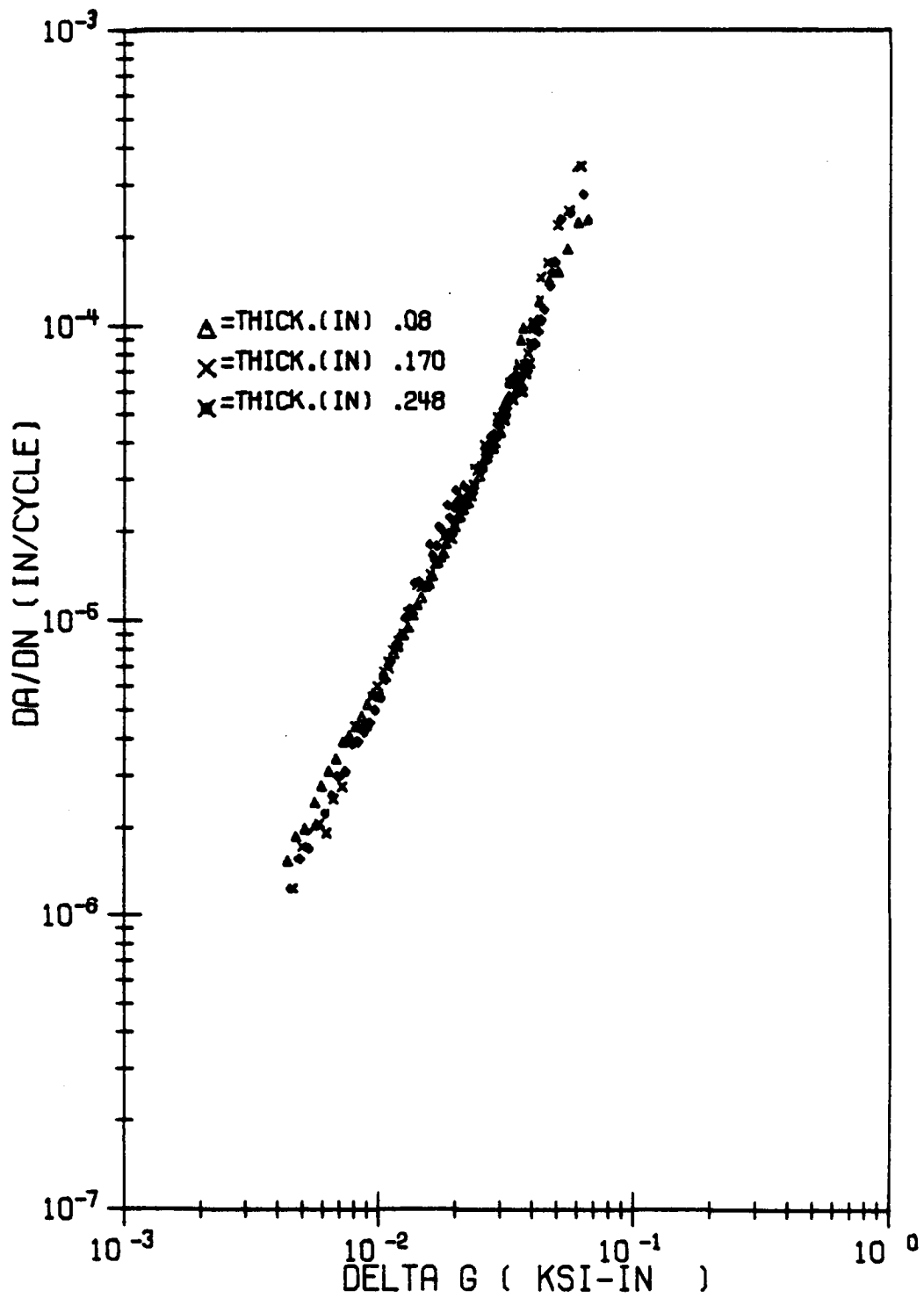


Figure 7.10 Correlation of the data at R=0.05 using the strain energy release rate model.

the relation between a flat and a slant crack is

$$\Delta G_{\theta} = \Delta G_0 \cos^3 \theta$$

and the relation between the strain energy release rates for cracks at the same angle, but in plane strain and plane stress is

$$\Delta G_{\epsilon} = (1 - \nu^2) G_{\sigma}$$

Consequently, in the mixed mode region, the strain energy release rate range is given by

$$\Delta G = \frac{\cos^3 \theta}{1 - (1 - (1 - \nu^2))X} (G_{\epsilon})_0 \quad (7.6)$$

where

$$X = \frac{\Delta K^2 - \Delta K P^2}{\Delta K P P^2 - \Delta K P^2}$$

The term $(1 - \nu^2)$ is present due to accounting for the state of stress. Since it is close to 1, this term was varied from 1 to $(1 - \nu^2)$ linearly with ΔK^2 in the mixed mode region to approximately account for stress state variation.

Using equation (7.6), ΔG in the mixed mode region as correlated by the linear interpolation method was used to calculate what the crack angle needed to be in the model if the same ΔG were to be obtained. These results were then plotted against a normalized ΔK^2 (because the plastic zone size is linear in ΔK^2).

This necessary variation of θ with ΔK^2 if the model were to work in the mixed mode region was then compared to the actual variation of the crack angle with ΔK^2 . The actual variation of θ in the mixed mode region was plotted with a normalized ΔK^2 , and plotted with the needed variation, shown in Figure 7.11. It can be seen that the curves are fairly close to each other, and that the shape of the curves are similar. This graph shows that the crack angle develops in a non-linear fashion, which differs from the linear variation which would be expected, since the ratio r_y/t determines stress state, and r_y varies linearly with ΔK^2 . This therefore indicates that the correlation using the linear interpolation method does have some physical justification.

Tests at $R=0.75$. As mentioned previously, the specimens of these tests did not exhibit a transition from tensile mode to shear mode. The strain energy release rate model, therefore, could not be applied to these data. The implications of this on the results of the analysis of the $R=0.05$ data will be discussed in Chapter 8.

Microscopic Behavior

Specimens tested at both stress ratios were examined using a scanning electron microscope. For specimens tested at each stress ratio, three regions were examined: 1) plane strain region; 2) mixed mode region 3) plane stress

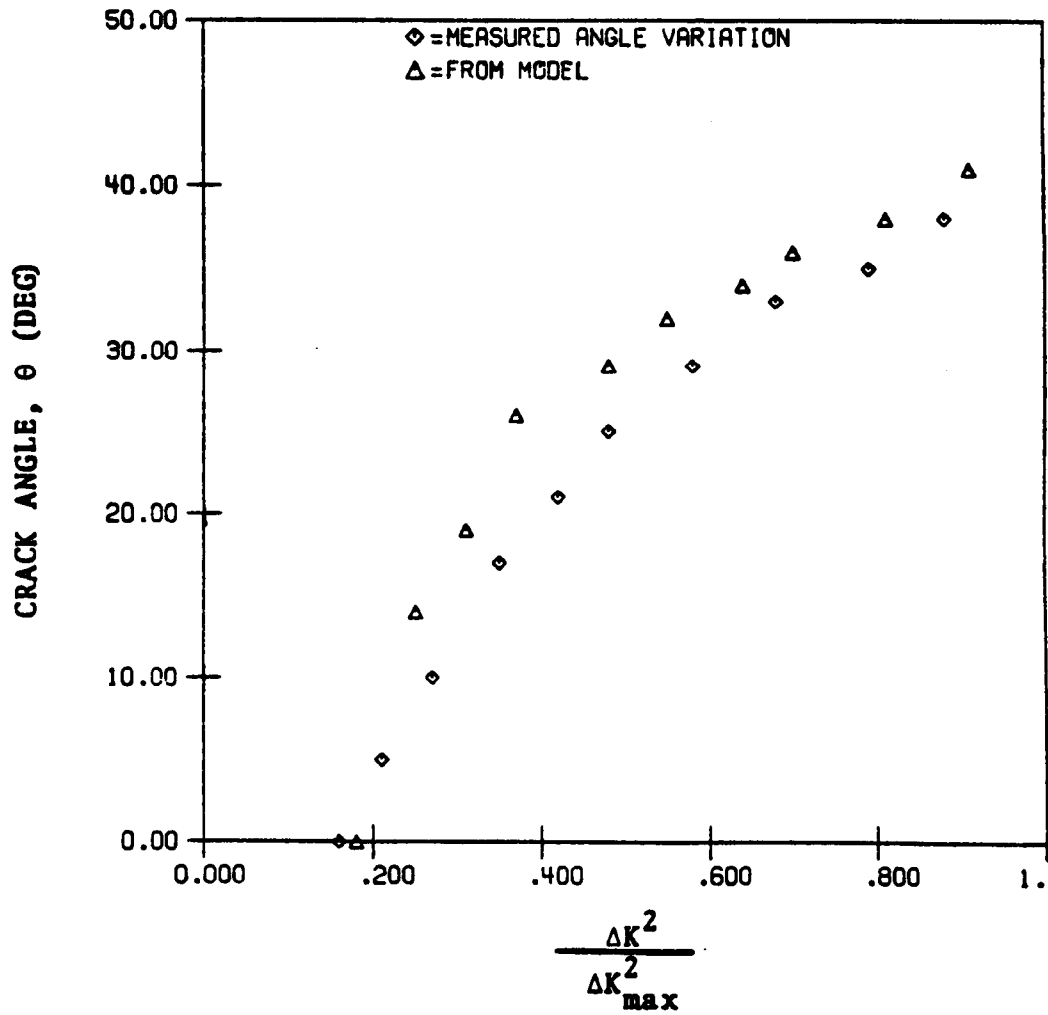


Figure 7.11 Actual crack angle variation compared to that assumed in the strain energy release rate model.

region. Comparison of the topographical features in these areas provided evidence of crack closure occurring in the tests at $R=0.05$, and of no crack closure occurring in the tests at $R=0.75$.

Plane Strain Regions

The plane strain region of a specimen tested at $R=0.05$ is shown in the upper fractograph of Figure 7.12. Fatigue striations were found, and a small dispersion of particles was on the surface. A composition analysis of these particles revealed that they were likely pieces of the fracture surface which had been rubbed off by abrasion, which may be evidence of crack closure occurring in this region.

The plane strain region of a specimen tested at $R=0.75$ is shown in the lower fractograph of Figure 7.12. The striations were much sharper and more clearly defined than those at the low stress ratio, and there were no particles on the surface.

Mixed Mode Region

Figure 7.13 shows the mixed mode region of a specimen tested at $R=0.05$. The top fractograph shows that striations were present, although they appeared somewhat flat and rubbed out. A greater dispersion of particles were present on this surface than in the plane strain region,

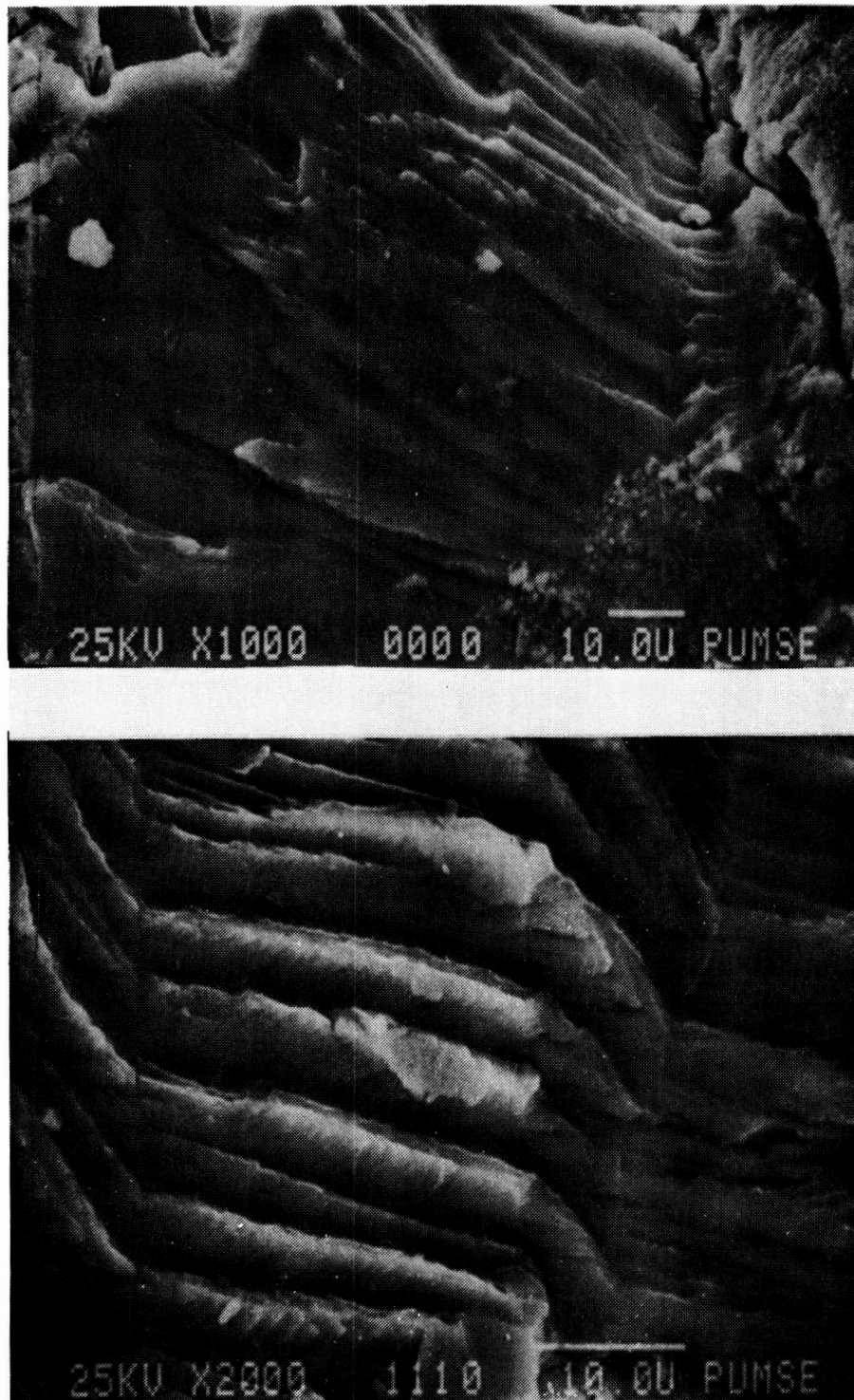


Figure 7.12 The plane strain region of a 0.17 inch specimen tested at $R=0.05$ (upper photo), and the plane strain region of a 0.17 inch specimen tested at $R=0.75$.

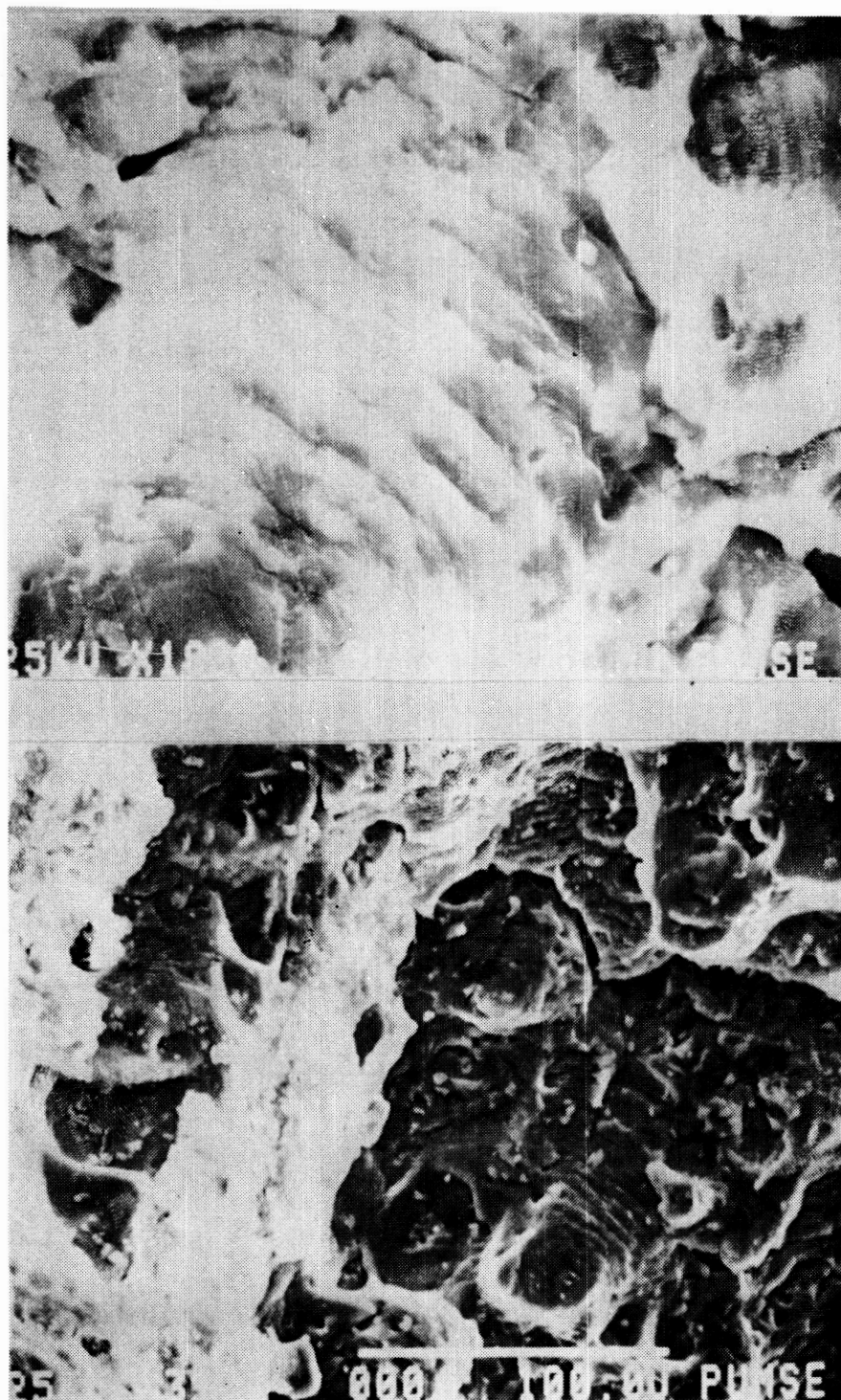


Figure 7.13 The mixed mode region of a 0.25 inch specimen tested at $R=0.05$ (both photos).

as seen in the lower fractograph of Figure 7.13. This indicates greater crack closure occurred in the mixed mode region than in the plane strain region.

Figure 7.14 shows the mixed mode region of a specimen tested at $R=0.75$. Fatigue striations were clearly defined, and no particles were present on the surface. In contrast to the low stress ratio, it appears crack closure did not occur here, as well as in the plane strain region of the $R=0.75$ tests.

Plane Stress Region

The plane stress region of a specimen tested at $R=0.05$ is shown in the upper fractograph of Figure 7.15. The surface appeared abraded, and a large dispersion of particles was present on the surface, which is evidence that crack closure occurred in this region.

The lower fractograph shows the plane stress region of a specimen tested at $R=0.75$. Fatigue striations were clearly defined, and still no particles were present on the surface. Apparently, no crack closure occurred in this region, as was the case in the plane strain and mixed mode regions of specimens tested at this stress ratio.

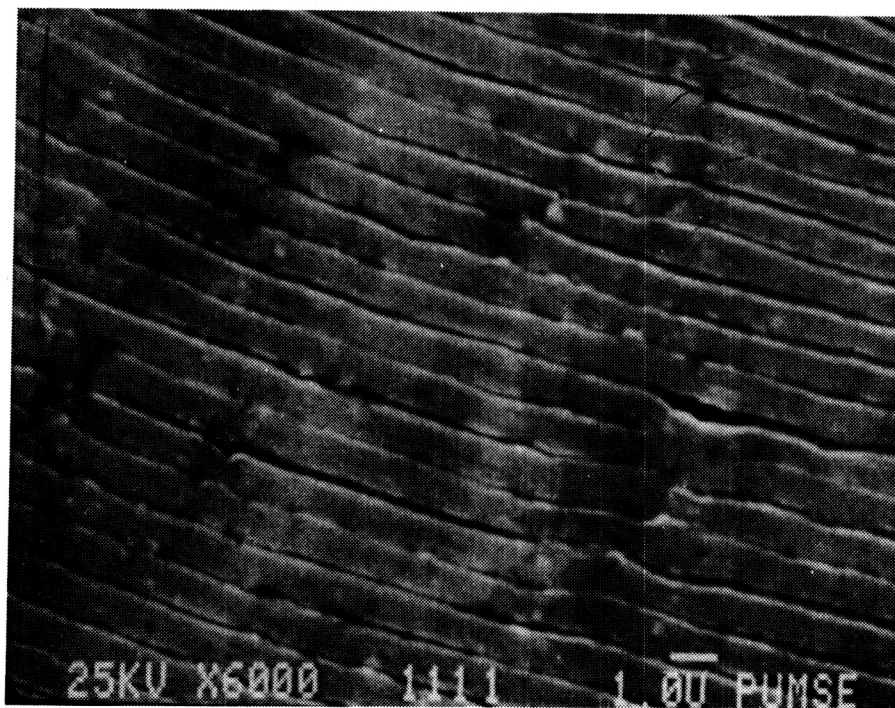


Figure 7.14 The mixed mode region of a 0.25 inch specimen tested at R=0.75.

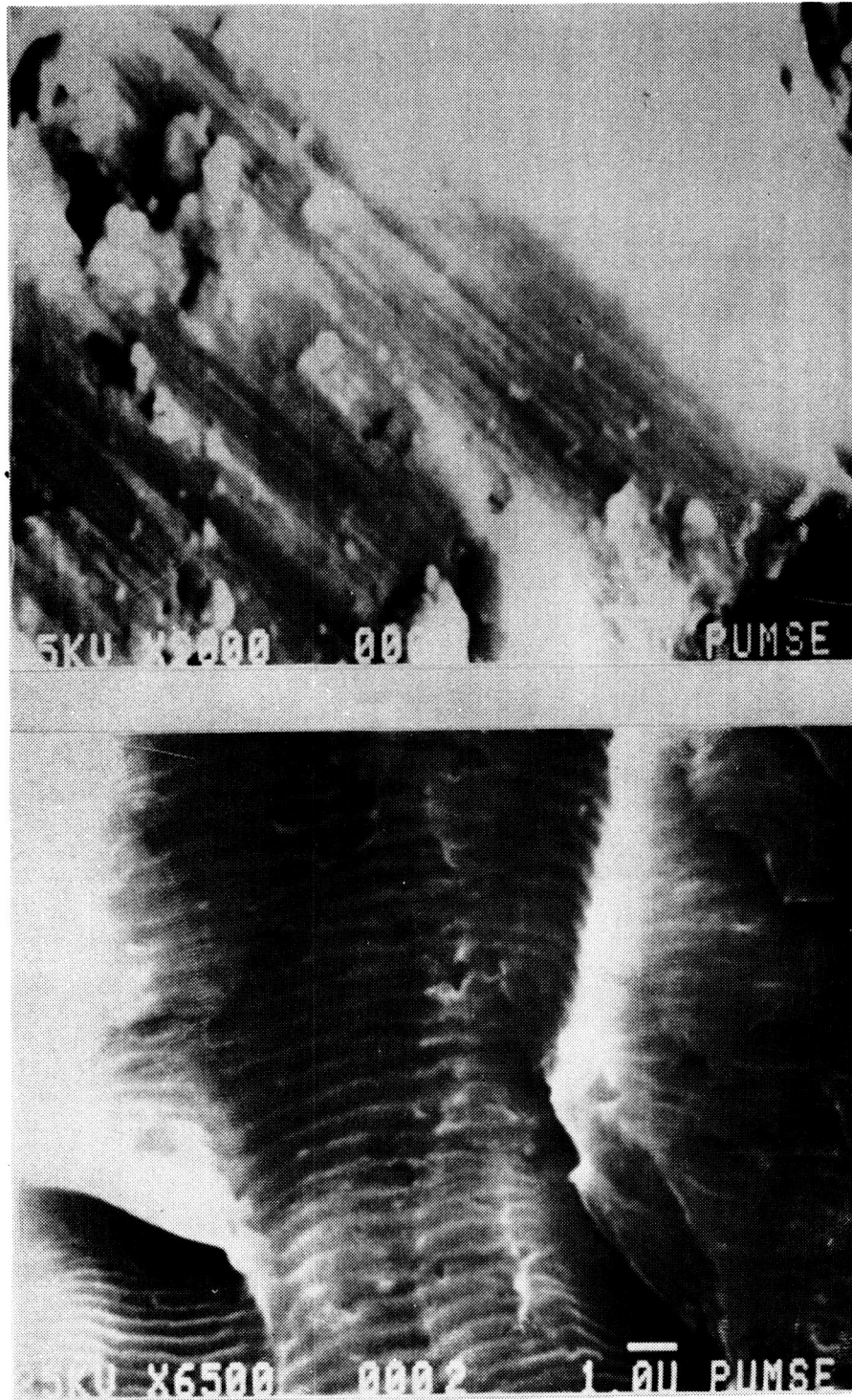


Figure 7.15 The plane stress region of a 0.25 inch specimen tested at $R=0.05$ (upper photo), and the plane stress region of a 0.25 inch specimen tested at $R=0.75$.

Single-Peak Overload Tests

Macroscopic Behavior

Investigations in the past generally confirm that a consistent effect of thickness on retardation following an overload exists, with less retardation occurring in thicker specimens. Several of these investigations [22,23] identified crack closure as the principle retardation mechanism, and the resulting thickness effect on retardation was explained by a difference in crack closure occurring in each thickness after the overload. The variation in crack closure with thickness following an overload was attributed to the difference in stress state at overload caused by the through the thickness constraint developed at the crack tip. Furthermore, when crack closure was identified as the principle retardation mechanism, not only did the number of delay cycles show a consistent variation with thickness, but other parameters associated with the retardation showed a consistent variation with thickness also. Specifically, these other parameters were the overload affected zone size, a_{o1} , the minimum growth rate attained after overload, $(da/dN)_{min}$, and the distance beyond the point of overload at which $(da/dN)_{min}$ occurred, a_{min} . Following an overload, these parameters were found to vary as follows for increasing specimen thickness:

1. the overload affected zone, a_{ol} , decreased
2. the minimum growth rate attained, $(da/dN)_{min}$, increased
3. the distance beyond overload at which $(da/dN)_{min}$ occurred, a_{min} , remained relatively invariant

Therefore, the above parameters obtained from the overload tests of this investigation were examined to identify the retardation mechanisms involved and explain the resulting variation of retardation with thickness.

Tests at $R=0.05$

Two sets of tests were conducted under this condition, one with $K_{ol}=24.75$ and the other with $K_{ol}=52.20$. For both sets of tests, the parameters discussed previously showed similar variations with thickness. The overload affected zone decreased with increasing thickness. The size of a_{ol} compared well with the size of the overload plastic zones, lying between the values of the calculated plane stress and plane strain plastic zone sizes, in agreement with Mills et al.[21]. The magnitude of a_{min} was affectively independent of thickness, and was between the calculated values of the plane stress and plane strain cyclic plastic zone sizes, in agreement with Wei et al.[22]. The variation of a_{ol} and a_{min} with thickness for both test sets are shown in Figure 7.16. The minimum

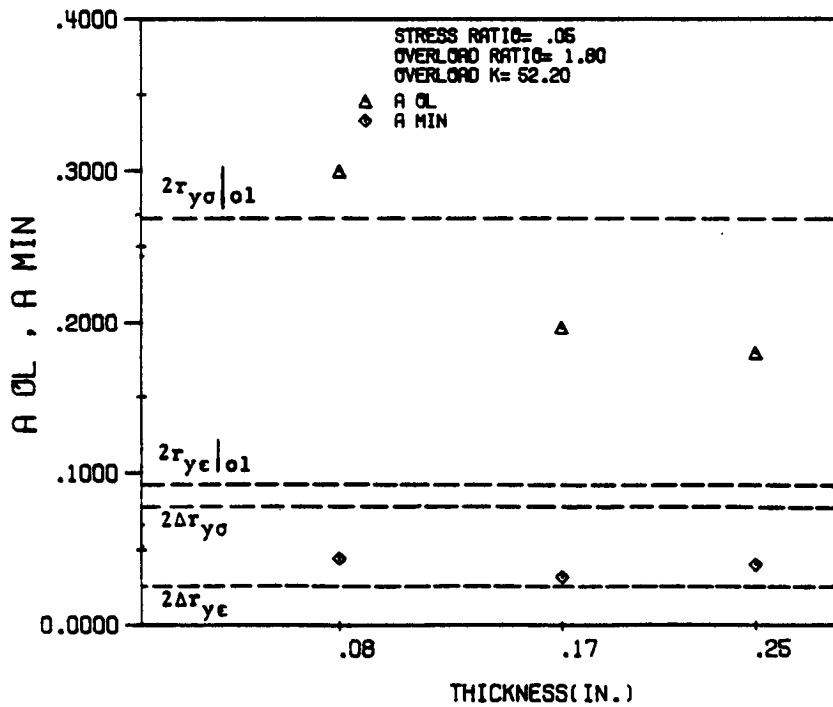
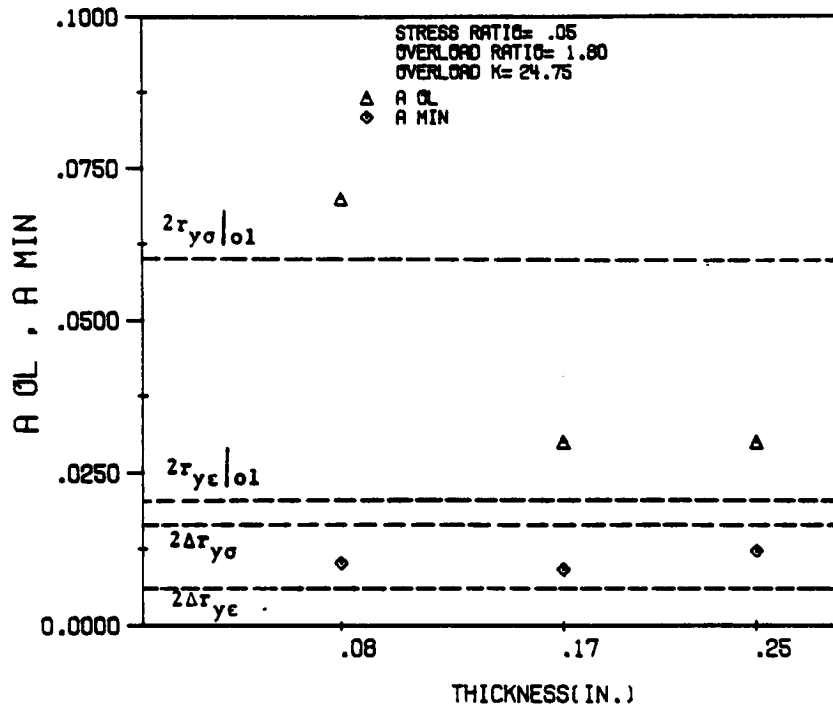


Figure 7.16 Variation of a_{ol} and a_{min} with thickness for both test sets at $R=0.05$.

growth attained following the overload showed a consistent increase with thickness for both test sets, as shown in Figure 7.17.

Figure 7.18 illustrates the variation in delay cycles for both sets of tests. The tests at $K_{O1}=24.75$ showed a consistent decrease in delay cycles with increasing thickness, as expected from the behavior of the parameters mentioned previously. The tests at $K_{O1}=52.20$ did not show this trend, with the delay cycles in the test on the 0.17 inch specimen being slightly less than in the test on the 0.248 inch specimen, contrary to what would be expected. This may be explained by the fact that the overload was applied at 1.5 inches in the 0.17 inch specimen, as opposed to 1.4 inches in the 0.08 and 0.248 inch specimens. At longer crack lengths, the stress intensity factor increases more rapidly per increment of crack extension than at shorter crack lengths. This would account for the shorter life after overload in the 0.17 inch specimen, and may explain the fewer number of delay cycles.

All tests showed delayed retardation, that is, a gradual decrease in FCP rate to some minimum value, and then a gradual rise to the pre-overload growth rate. This can be seen in Figures 7.19 and 7.20, and also illustrates the relative variation of a_{O1} , a_{min} , and $(da/dN)_{min}$ with thickness.

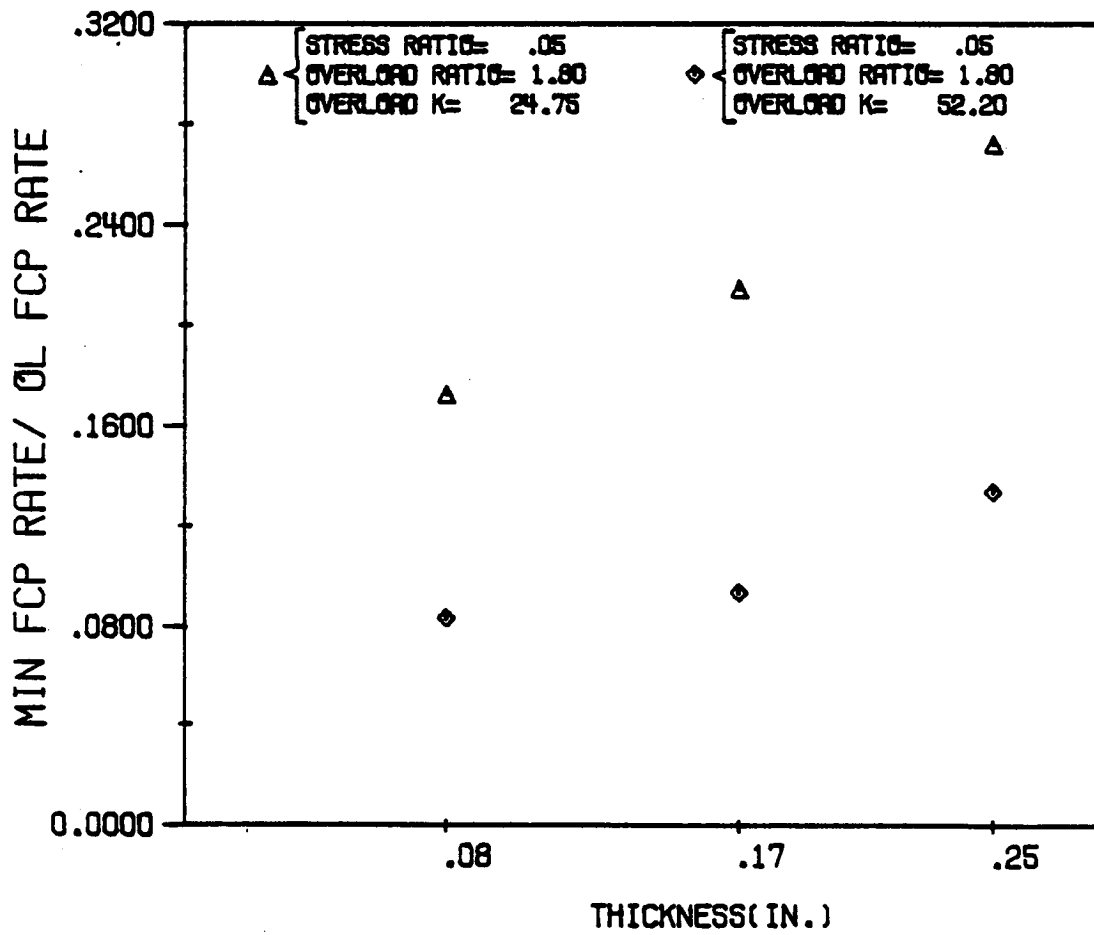


Figure 7.17 Variation of ratio of da/dN_{min} to da/dN_{ol} with thickness for both test sets at $R=0.05$.

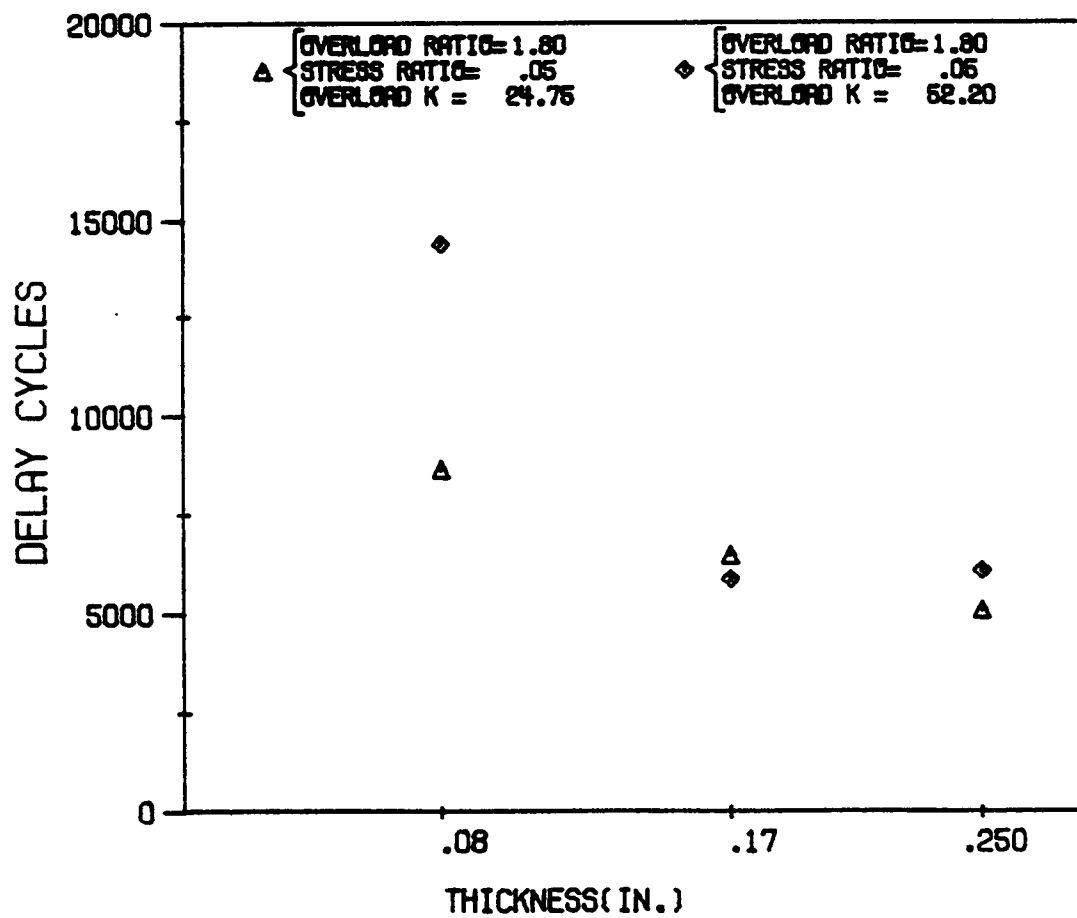


Figure 7.18 Variation of delay cycles with thickness for both test sets at R=0.05.

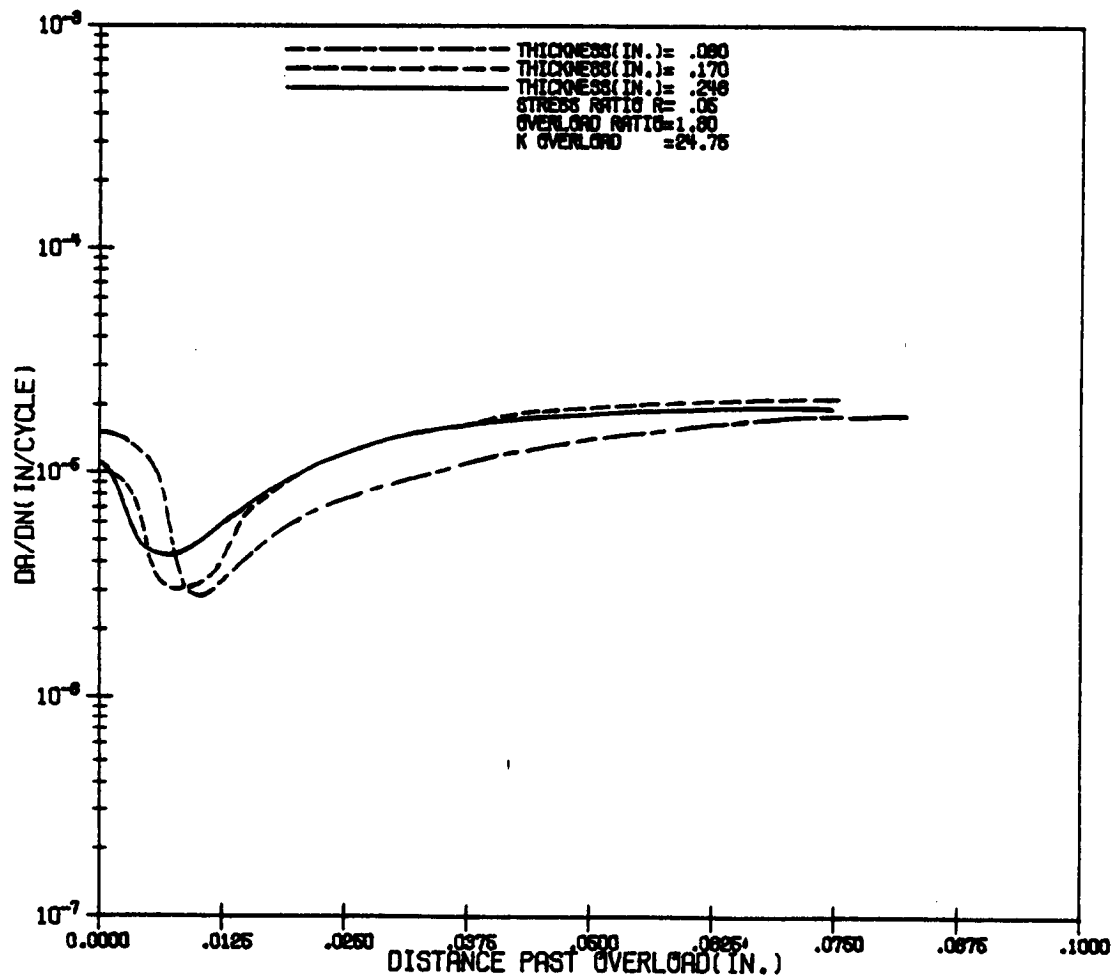


Figure 7.19 Variation of FCP rate after overload for tests at $R=0.05$, $K_{O1}=24.75$.

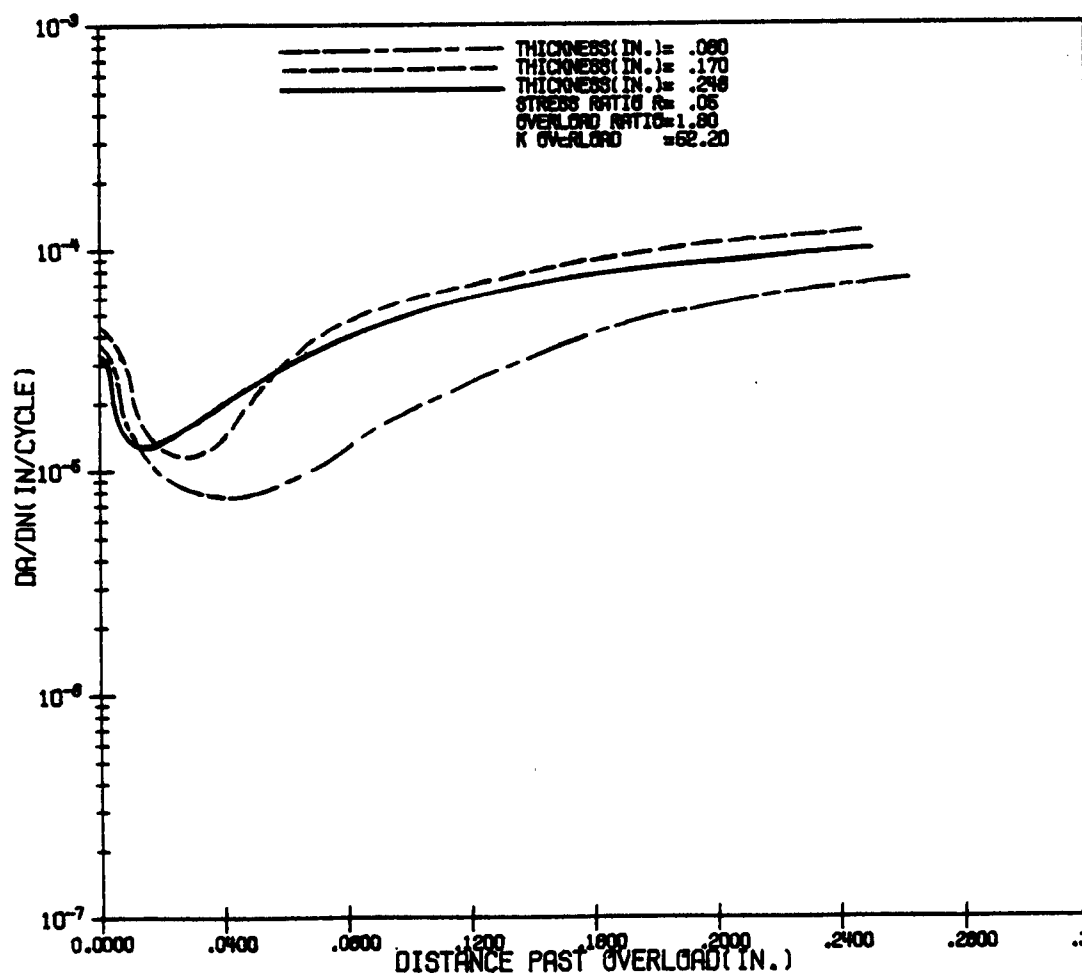


Figure 7.20 Variation of FCP rate after overload for tests at $R=0.70$, $K_{ol}=52.20$.

Tests at $R=0.70$

Two sets of tests were conducted under these conditions, one with $K_{ol}=24.75$ and the other with $K_{ol}=35.00$. For both sets of tests, the retardation parameters showed similar variation with thickness. The overload affected zone did not show a consistent variation with thickness, and the sizes of the overload affected zones were much smaller than the calculated plane stress and plane strain plastic zone sizes. The overload affected zones were approximately the same size between the two test sets, despite the difference in the applied overload K , as shown in Figure 7.21. Neither test set showed a consistent variation of minimum growth rate with thickness, as illustrated in Figure 7.22.

Figure 7.23 illustrates the variation in the number of delay cycles with thickness for both test sets. Although neither set itself showed a consistent variation with thickness, both showed a similar variation, with the thinnest specimen exhibiting the greatest delay and the 0.17 inch specimen the least.

It did not appear that delayed retardation occurred in any of the tests, as shown in Figures 7.24 and 7.25. In all tests, there was a sudden drop in growth rate to a minimum value. The subsequent increase in growth rate also occurred over a very small distance.

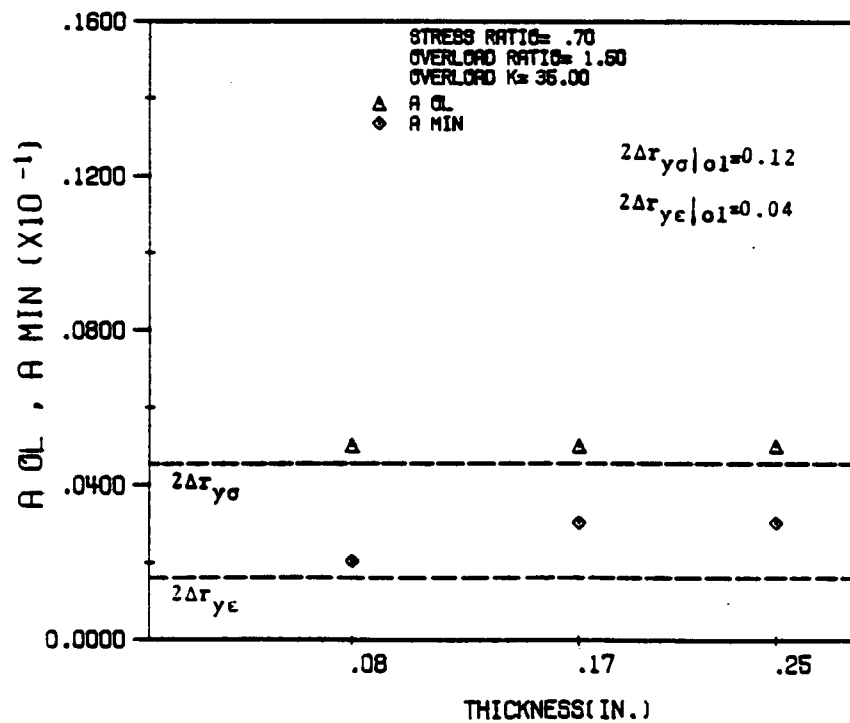
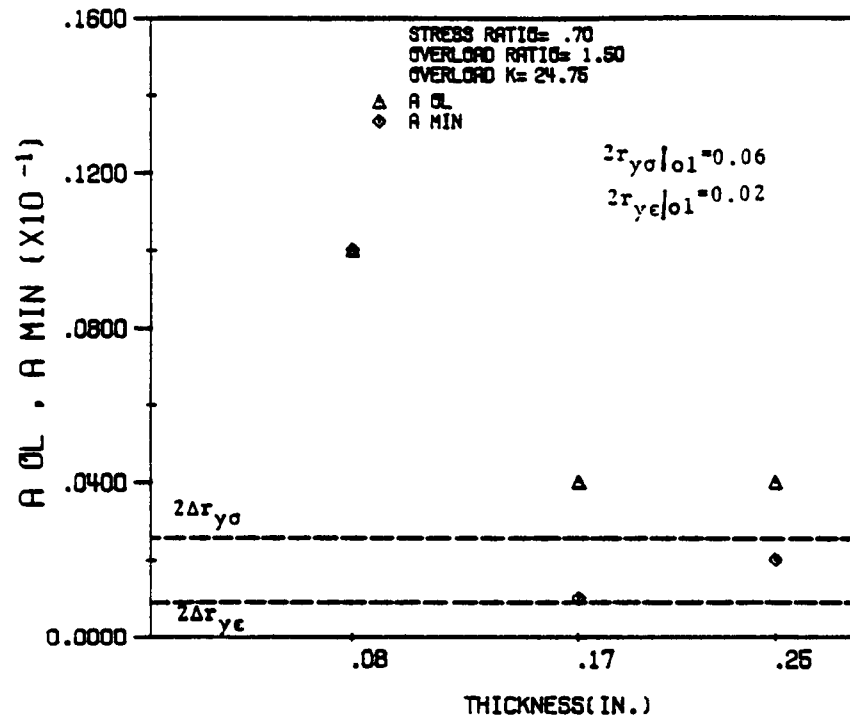


Figure 7.21 Variation of a_{ol} and a_{min} with thickness for both test sets at $R=0.70$.

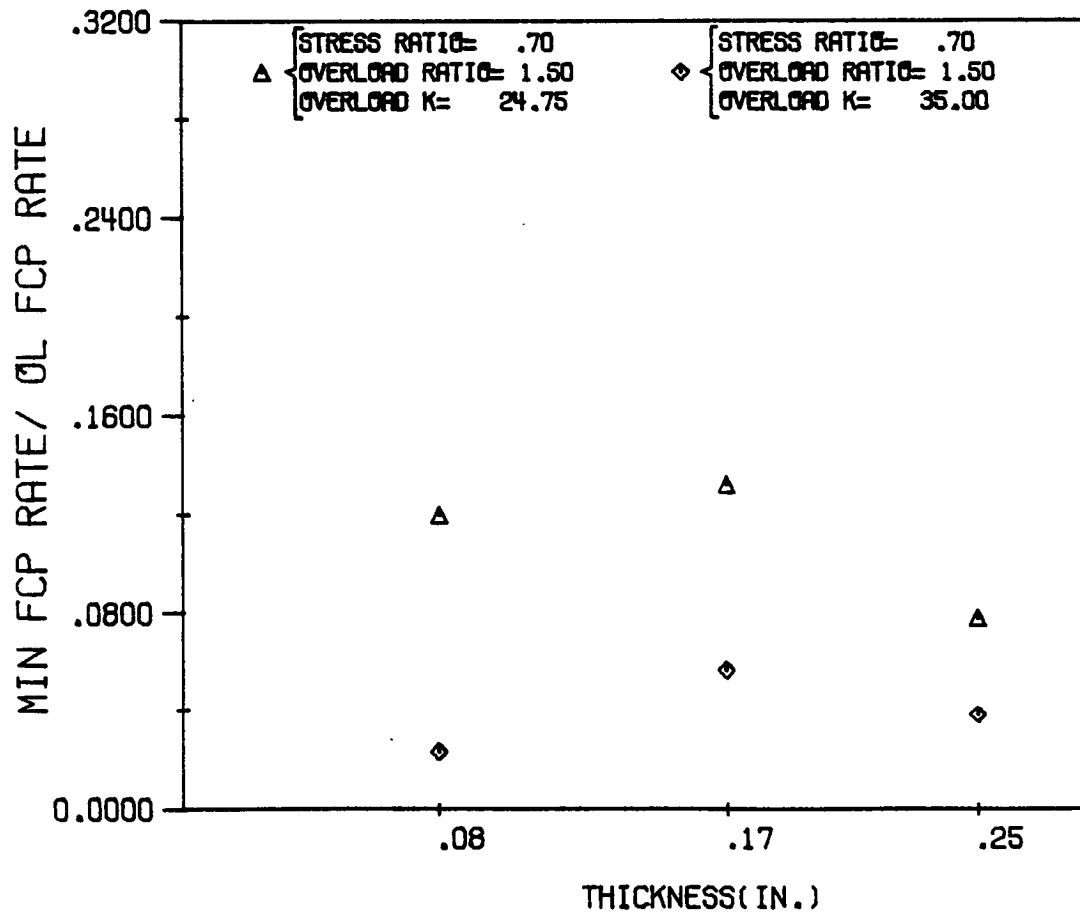


Figure 7.22 Variation of ratio of da/dN_{min} to da/dN_{ol} with thickness for both test sets at $R=0.70$.

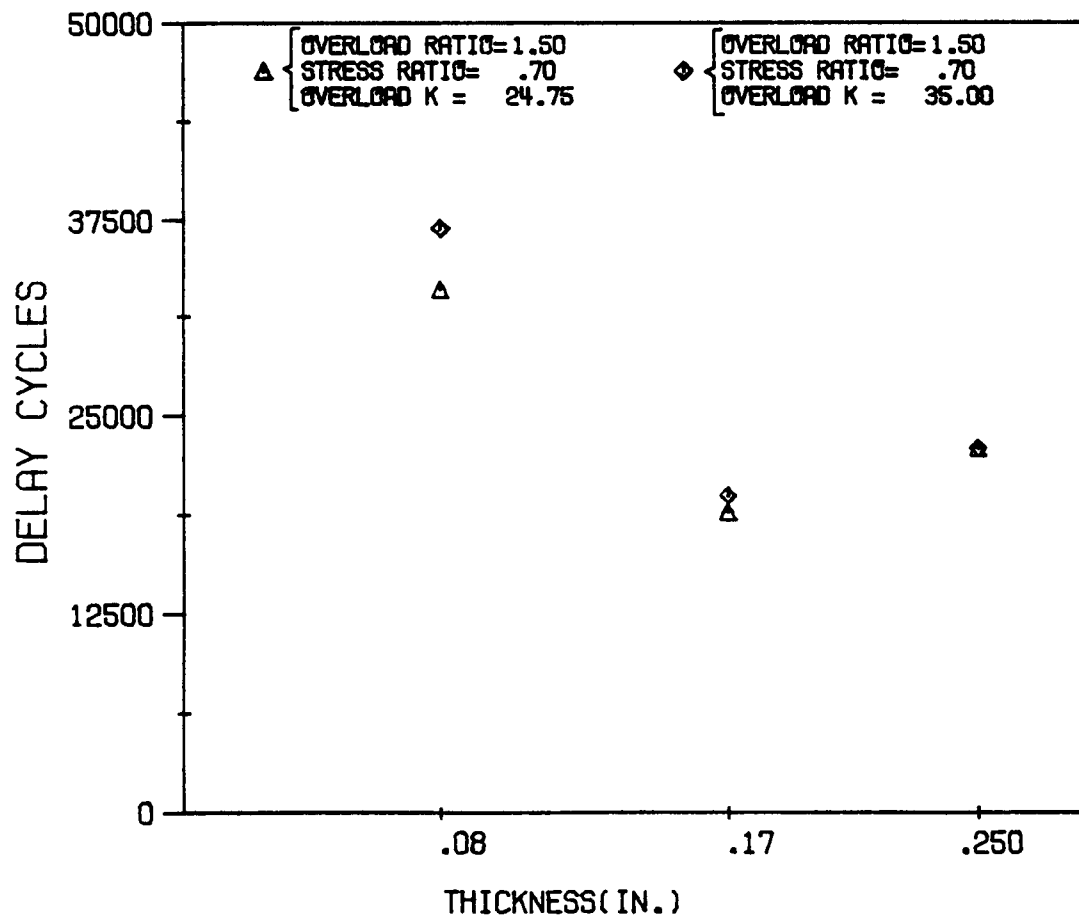


Figure 7.23 Variation of delay cycles with thickness for both test sets at $R=0.70$.

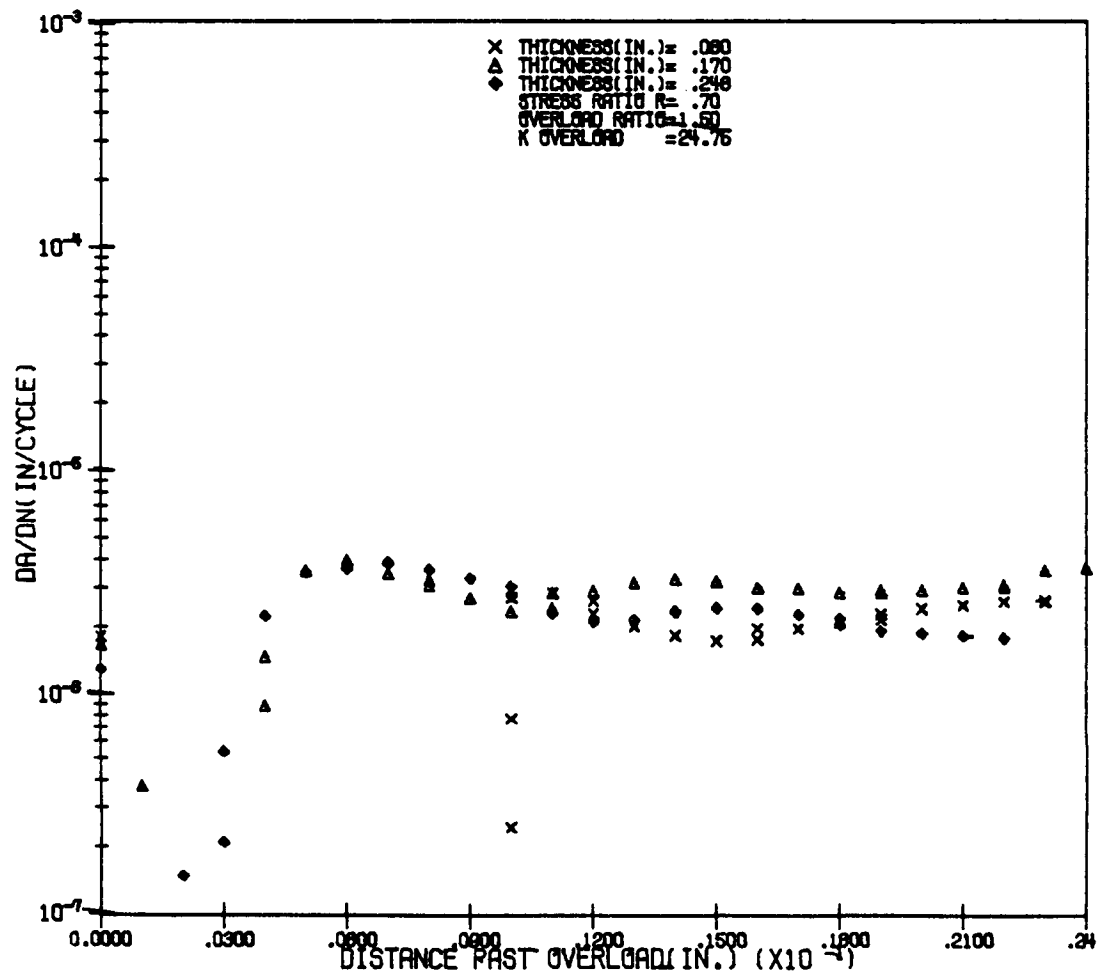


Figure 7.24 Variation of FCP rate after overload for tests at $R=0.70$, $K_{ol}=24.75$.

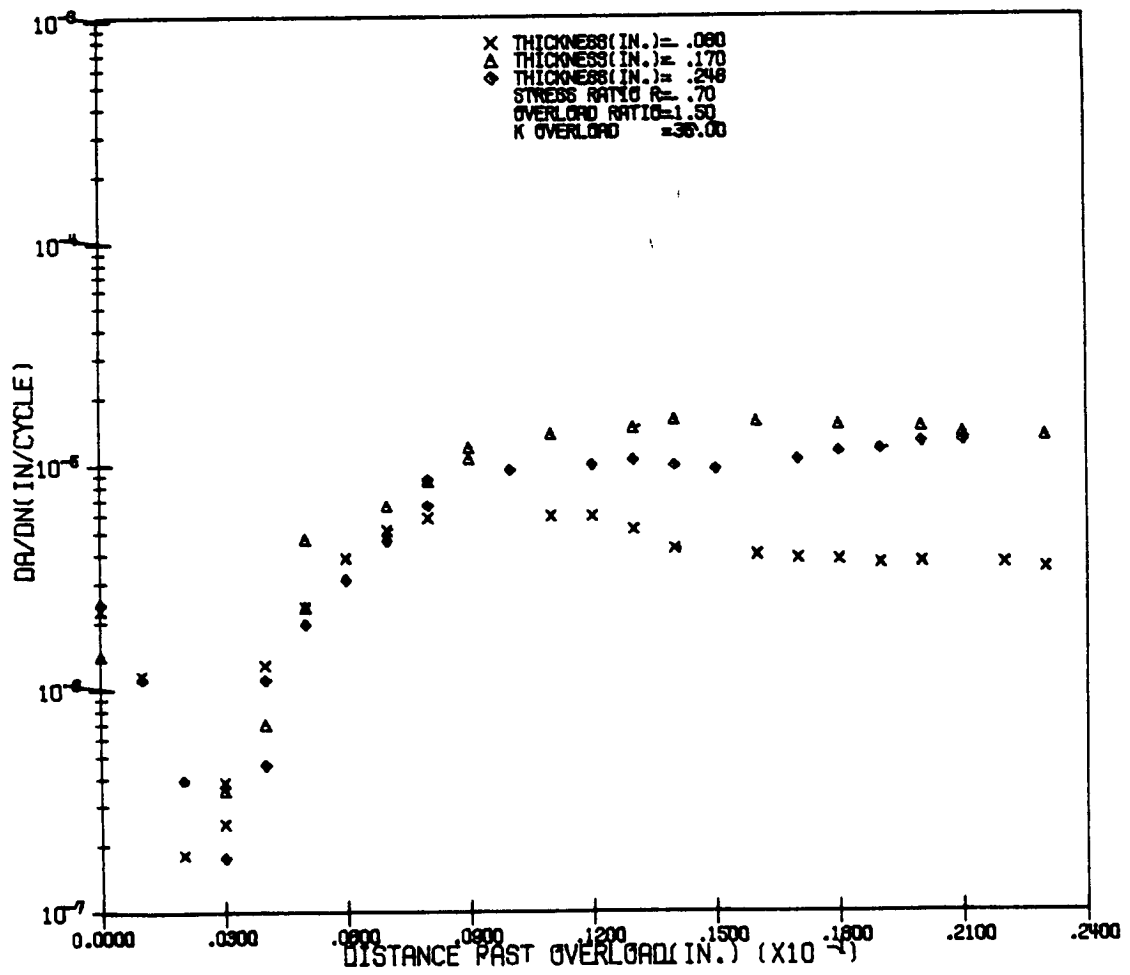


Figure 7.25 Variation of FCP rate after overload for tests at $R=0.70$, $K_{O1}=35.00$.

Comparison of Tests at $R=0.05$ and $R=0.70$

Comparison of the retardation characteristics exhibited at these two stress ratios shows that they are different. The a versus N curves for the tests at $K_{01}=24.75$ at both stress ratios shown in Figure 7.26 illustrate one difference. All tests at $R=0.05$ show a gradual increase in growth rate to the pre-overload value, characteristic of delayed retardation. All tests at $R=0.75$, however, display a period of approximately zero growth followed by a sudden jump to the pre-overload growth rate. The result was larger overload affected zones and higher minimum growth rates in the tests at $R=0.05$, as shown in Figure 7.27, despite the fact that the applied overload K was the same in both tests sets. These differences are further contrasted in Figures 7.28 through 7.30, which show comparisons of the da/dN versus crack growth beyond overload for each thickness. Similar differences were observed between the other two test sets, although the K_{01} was different in each, as shown in Figure 7.31.

Microscopic Behavior

Two specimens were examined using a scanning electron microscope (SEM). One specimen was from a test at $R=0.05$ and the other from a test at $R=0.70$. Both were 0.17 inch thick and the overload stress intensity was $24.75 \text{ ksi}\sqrt{\text{in}}$ in both specimens. Three areas in particular were

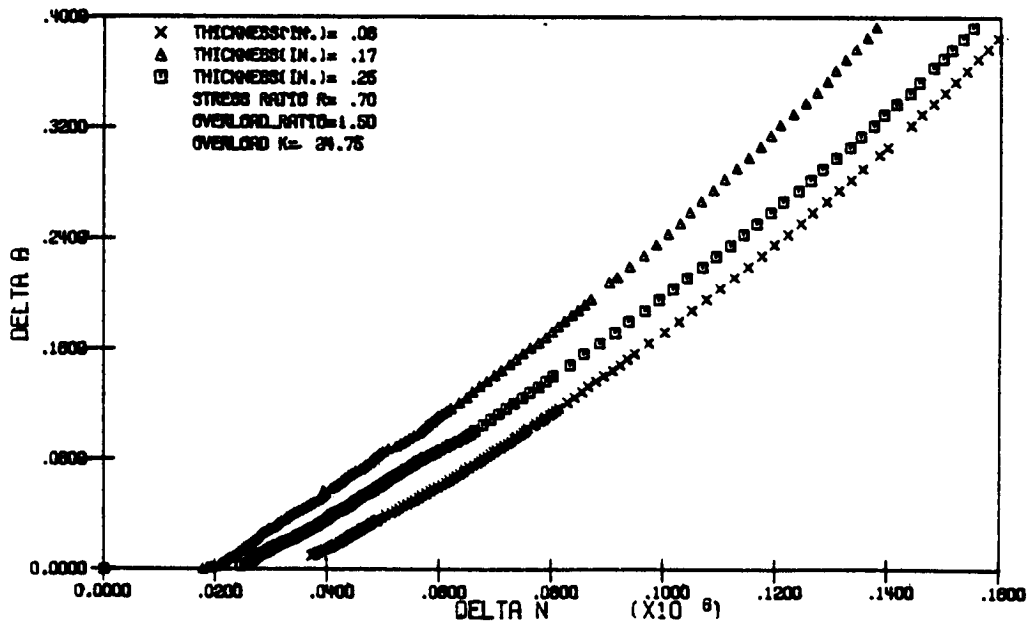
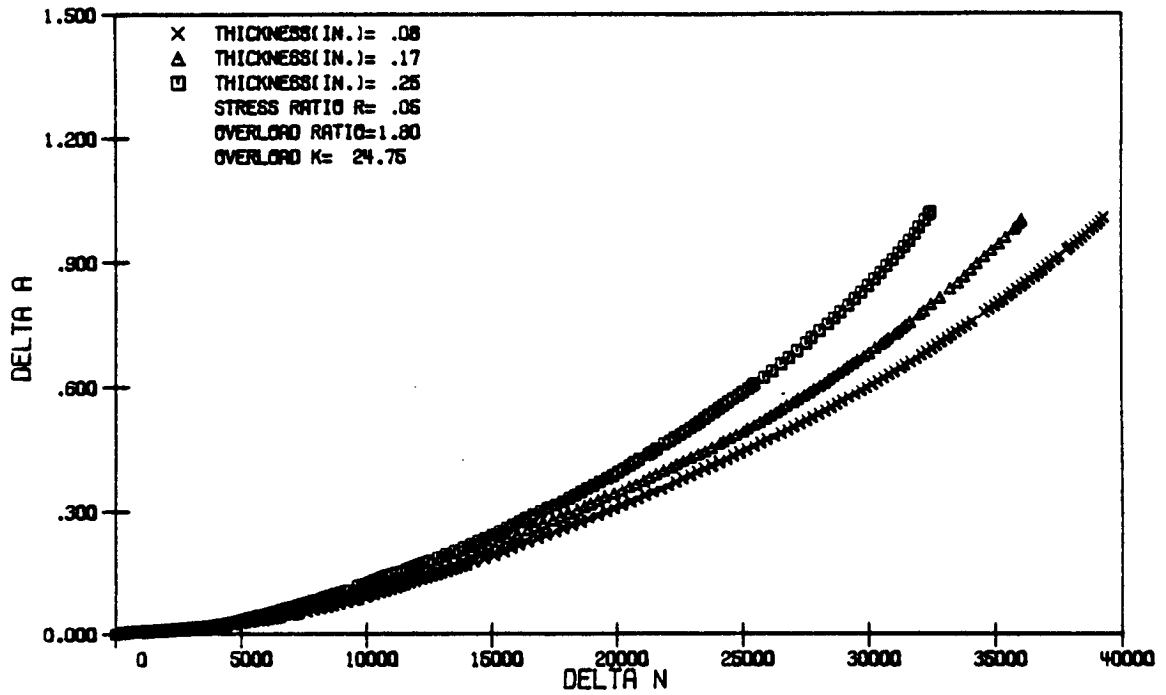


Figure 7.26 Comparison of the nature of a versus N data for tests at $R=0.05$ and $R=0.70$ with $K_{o1}=24.75$.

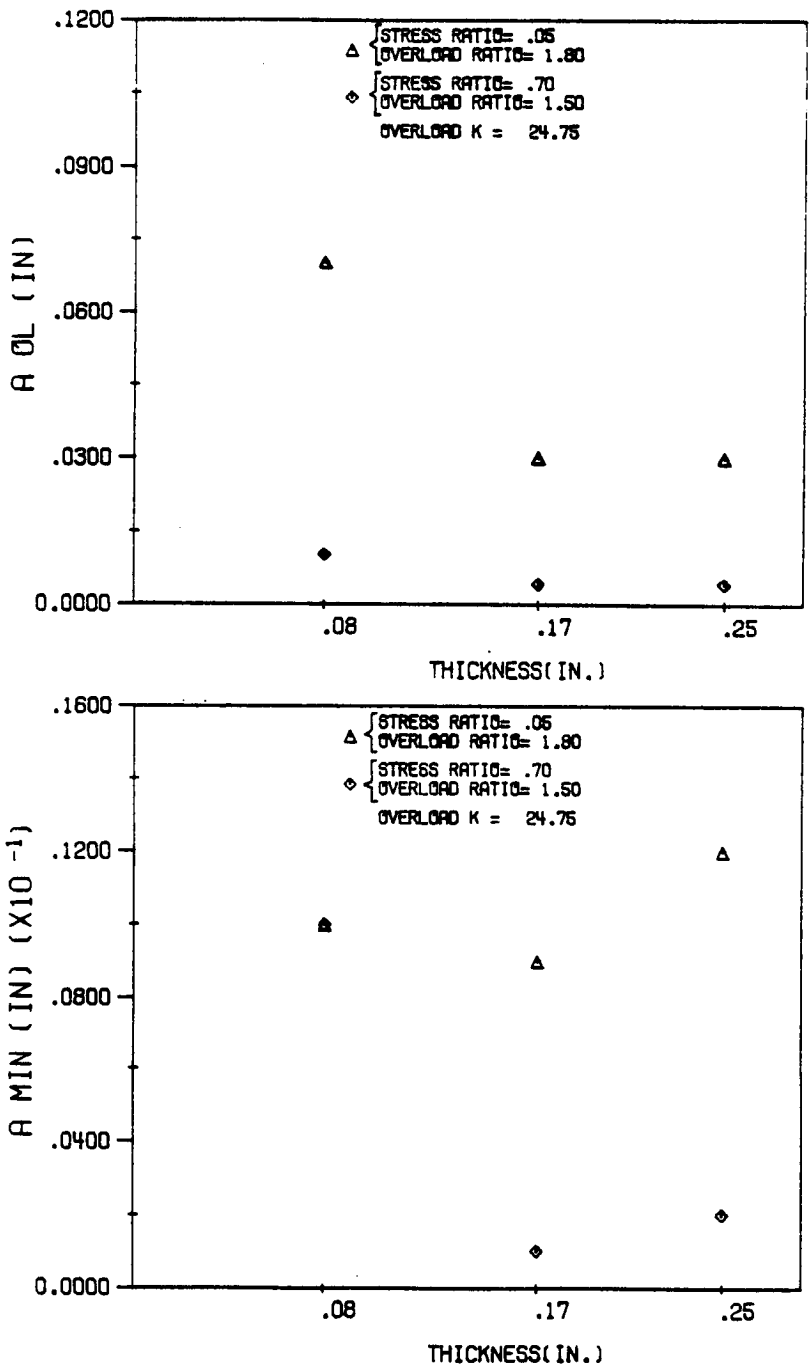


Figure 7.27 Comparison of a_{ol} and a_{min} for tests at $R=0.05$ and $R=0.70$ with $K_{ol}=24.75$.

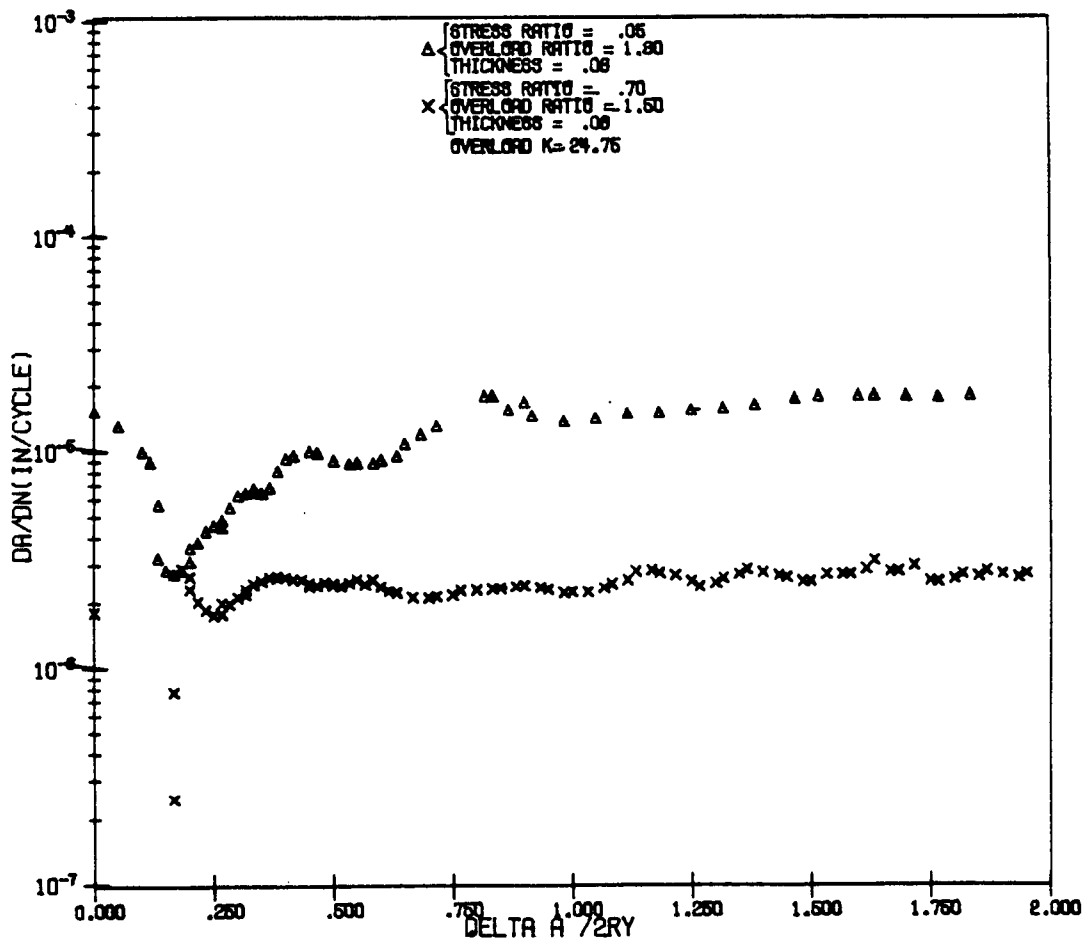


Figure 7.28 Comparison of FCP rate after overload for tests at $R=0.05$ and $R=0.70$ with $K_{o1}=24.75$ and thickness of 0.08 inches.

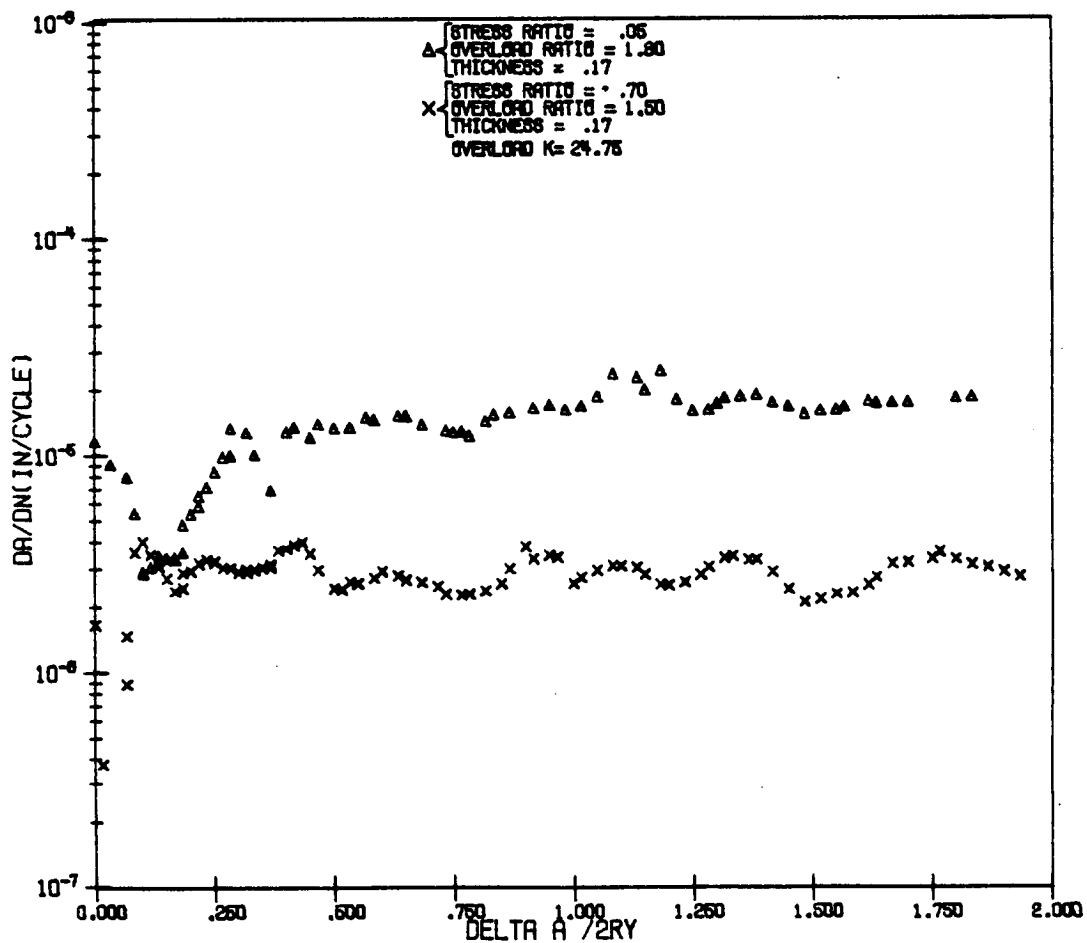


Figure 7.29 Comparison of FCP rate after overload for tests at $R=0.05$ and $R=0.70$ with $K_{o1}=24.75$ and thickness of 0.17 inches.

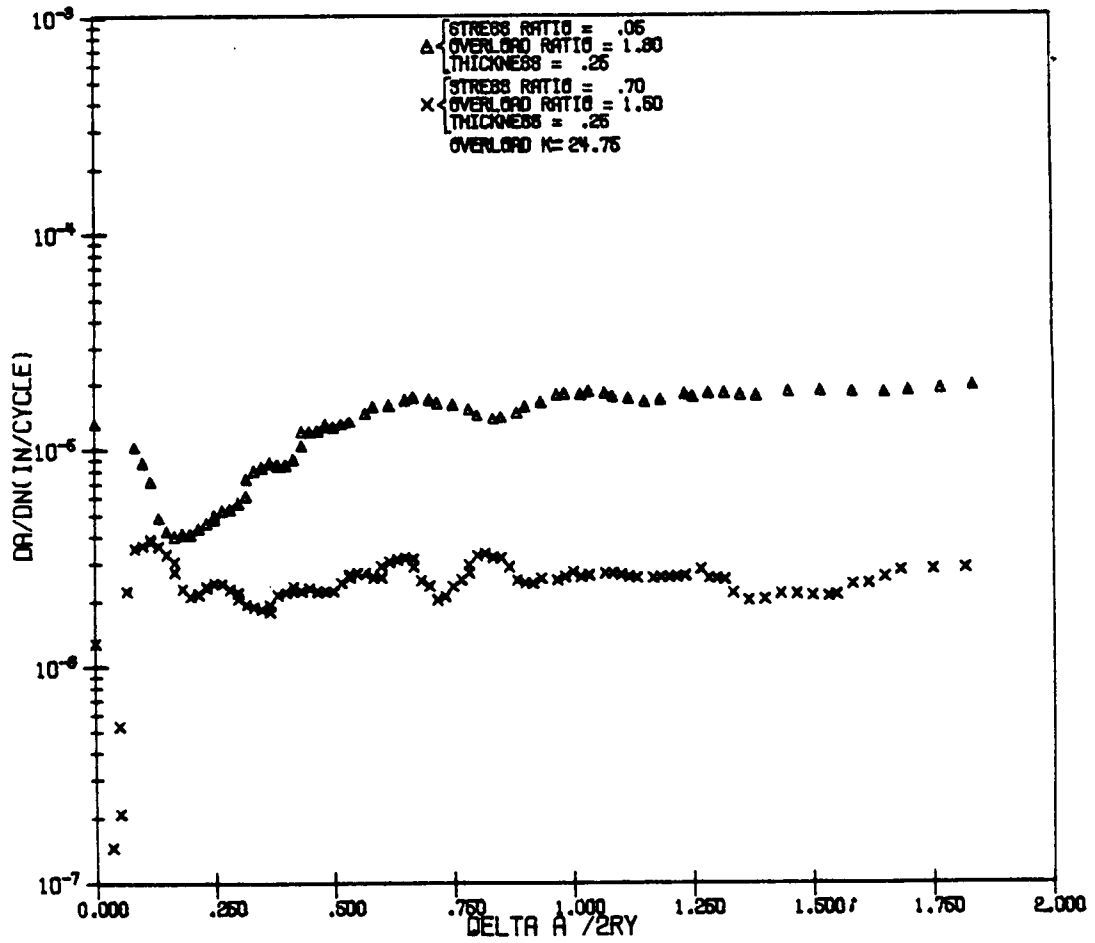


Figure 7.30 Comparison of FCP rate after overload for tests at $R=0.05$ and $R=0.70$ with $K_{o1}=24.75$ and thickness of 0.248 inches.

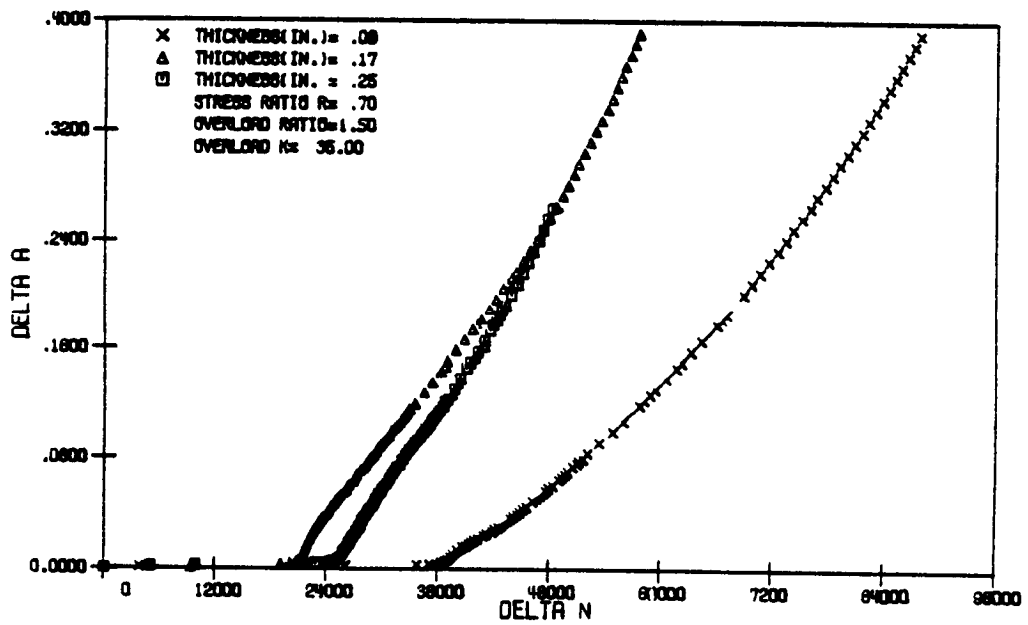
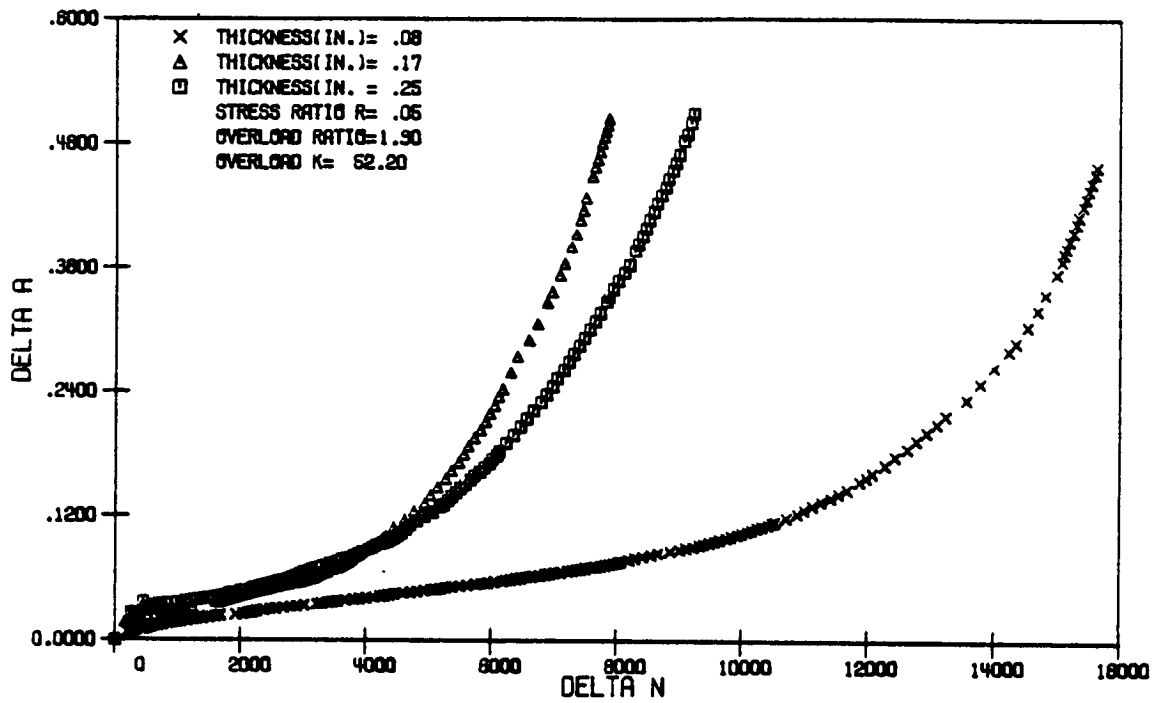


Figure 7.31 Comparison of the nature of a versus N data for tests at $R=0.05, K_{o1}=52.20$, and $R=0.70, K_{o1}=35.00$.

examined: 1) regions ahead of the point of overload; 2) the immediate vicinity of the overload; 3) regions beyond the point of overload. Comparison of the topographical features in these areas provided evidence of a difference in retardation mechanisms active in the tests at the stress ratio of $R=0.05$ and stress ratio of $R=0.70$.

Test at $R=0.05$

The specimen tested at $R=0.05$ showed fatigue striations in regions ahead of the point of overload application, as seen in Figure 7.32. At the point of overload, the fracture surface topography was virtually the same on either side of the overload, also shown in Figure 7.32. However, regions immediately beyond overload showed evidence of abrasion, and fatigue striations were not discernable. Areas well beyond the overload point exhibited features very similar to the areas ahead of overload, as fatigue striations were observable in this region, as shown in Figure 7.33.

Test at $R=0.70$

The specimen tested at $R=0.70$ showed no evidence of fatigue striations ahead of the overload, but rather a dimpled appearance was dominant, as shown in Figure 7.35. Also in Figure 7.34 is a fractograph of of the same area at a higher magnification illustrating the lack of fatigue

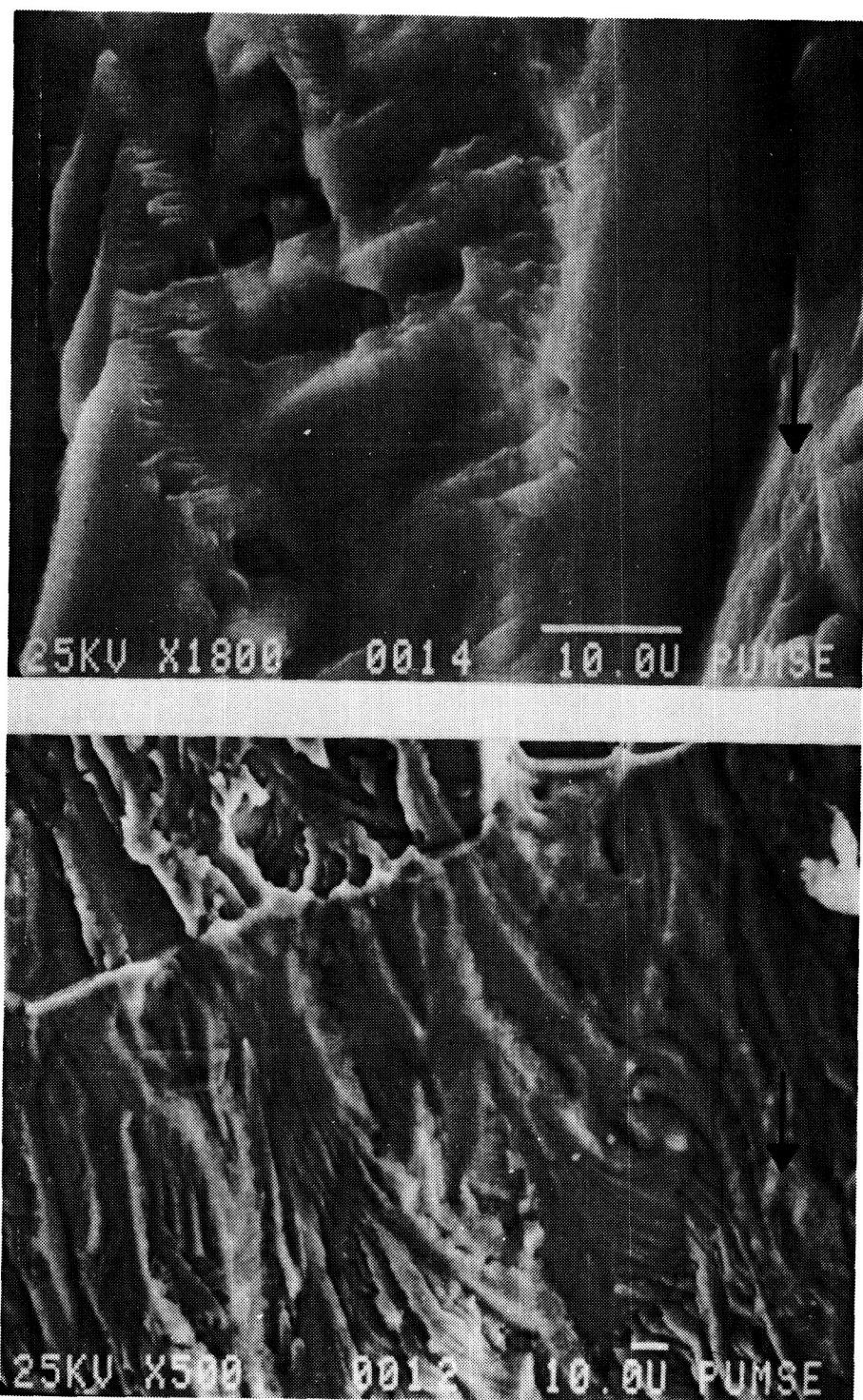


Figure 7.32 Region ahead of overload point (upper photo) and region at overload for test at $R=0.05$, $K_{01}=24.75$. Thickness was 0.17 inch, overload stress state was σ_1 mixed mode, and growth direction is indicated by the arrow.

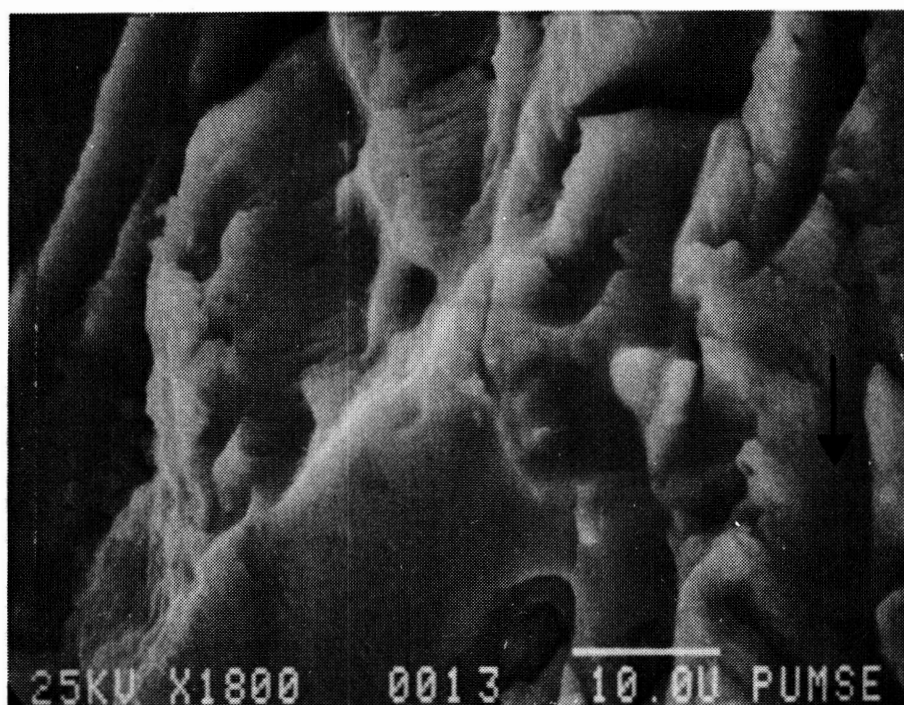


Figure 7.33 Region beyond overload point for test at $R=0.05$, $K_{o1}=24.75$. Thickness was 0.17 inch, overload stress state was mixed mode, and growth direction is indicated by the arrow.

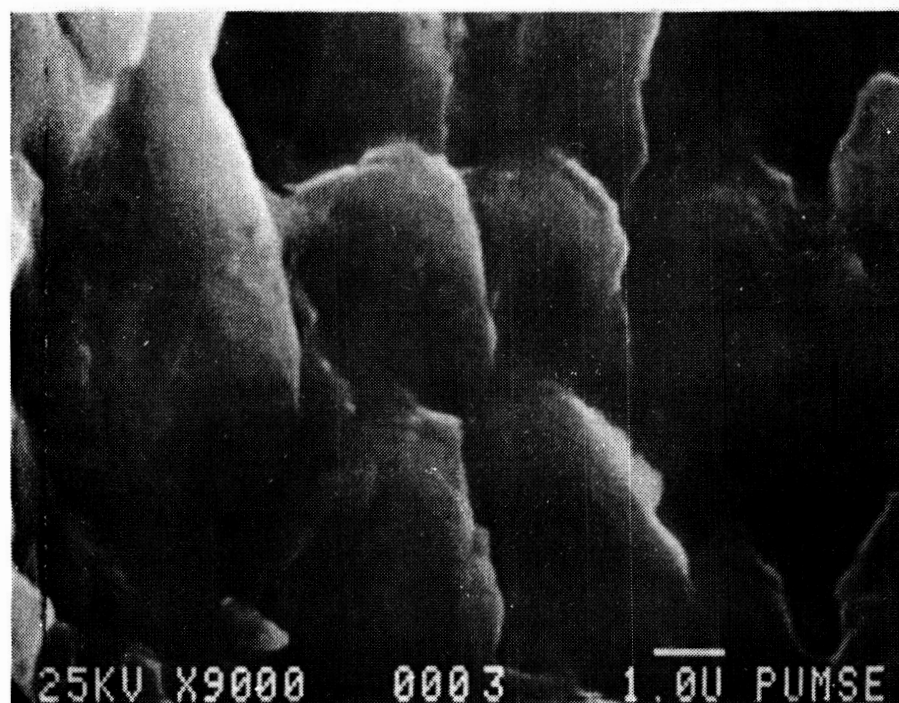
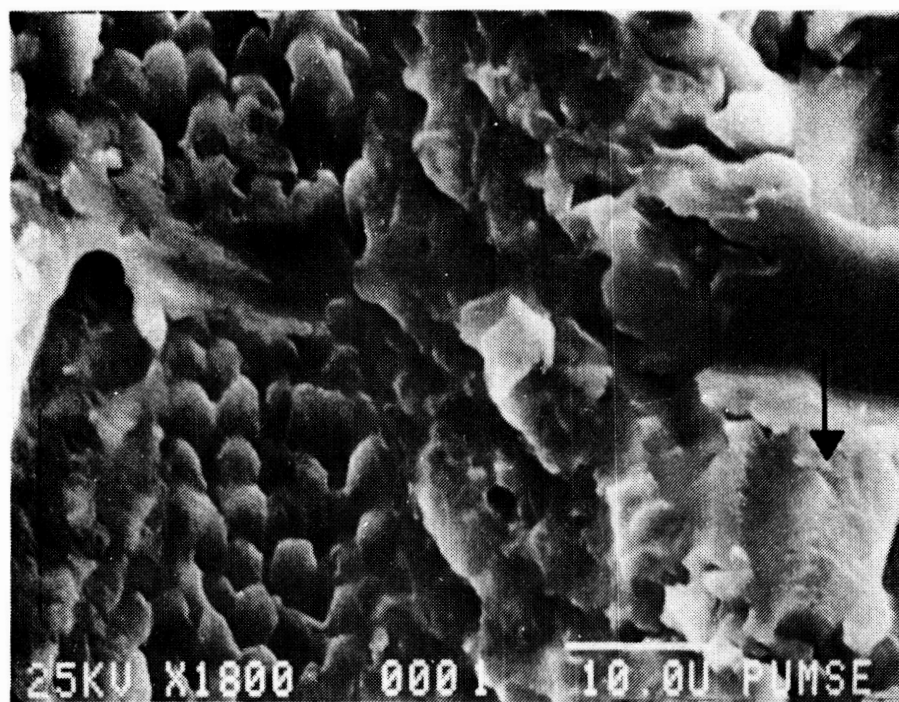


Figure 7.34 Region ahead of overload point (upper photo) and higher magnification of the same region for test at $R=0.70$, $K_{o1}=24.75$. Thickness was 0.17 inch, overload stress state was mixed mode, and growth direction is indicated by the arrow.

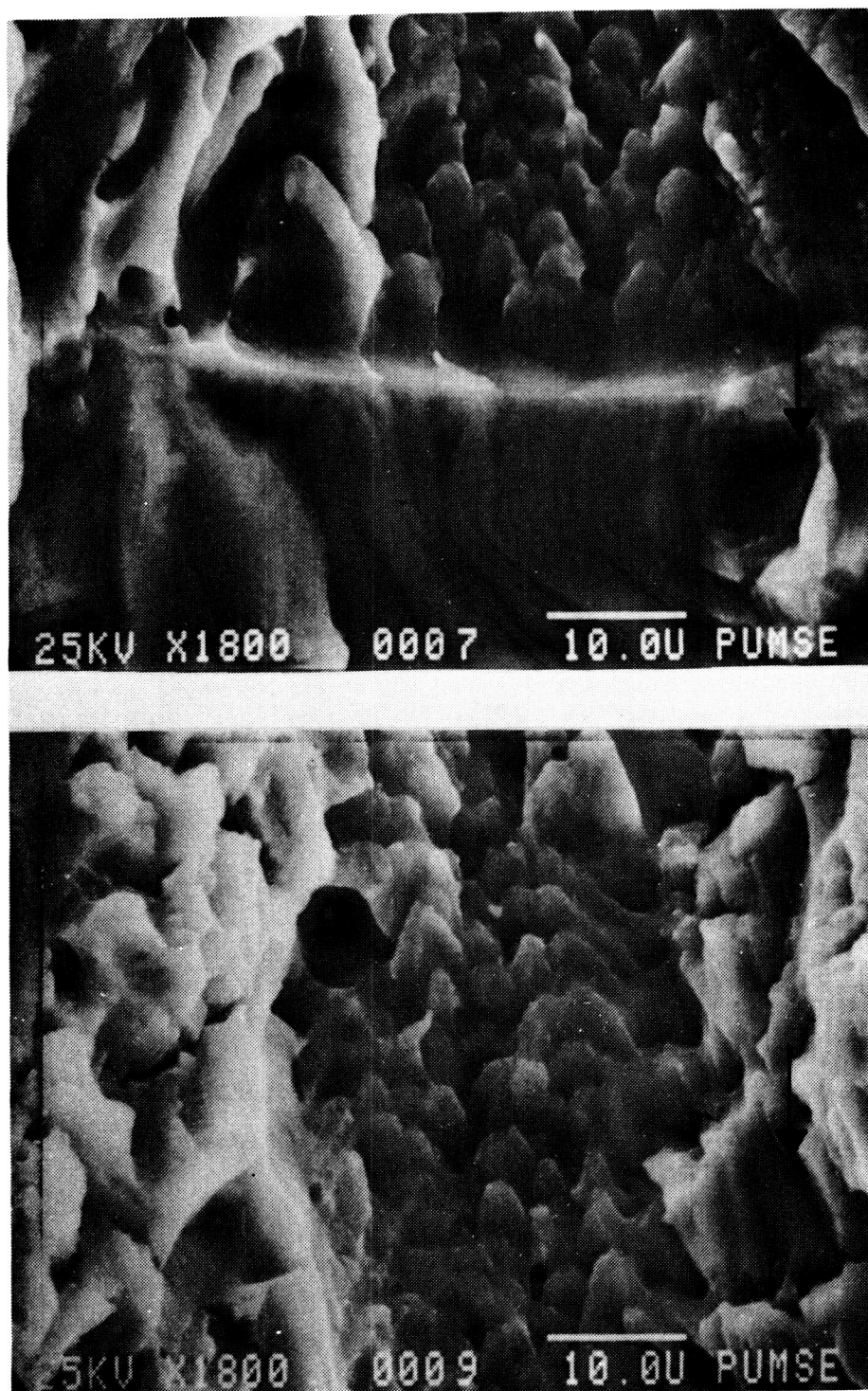


Figure 7.35 Region at overload (upper photo) and beyond overload point for test at $R=0.70$, $K_{ol}=24.75$. Thickness was 0.17 inch, overload stress state was mixed mode, and growth direction is indicated by the arrow.

striations in this region. At overload, there was a sharp contrast between the topography immediately before and after the overload, as shown in Figure 7.35. The dimpled surface changes to a smoother surface with striation-like ridges. Also, the region just beyond overload appears to be a plateau raised above the region ahead of the overload point. At a distance beyond overload, the surface features again had a dimpled appearance with no evidence of fatigue striations, also shown in Figure 7.35, like the regions ahead of the overload point.

CHAPTER 8 - DISCUSSION OF RESULTS AND CONCLUSIONS

Thickness Effects Under Constant Amplitude Loading

The results of the constant amplitude loading tests clearly showed an effect of thickness on fatigue crack propagation at both stress ratios when the growth rate data was correlated with ΔK_I . Specifically, FCP rate increased with increasing specimen thickness, but only in the middle region of the ΔK range. The difference in FCP rate appeared only after a change in slope of the da/dN versus ΔK curve, which occurred at higher values of ΔK and da/dN with increasing thickness. After the change in slope of the curves, higher growth rates occurred in thicker specimens, until once again the slopes of the curves changed. After the second slope change, FCP was again independent of thickness.

The variation of crack closure with thickness due to stress state transition did not explain the thickness effects in these data. A major hypothesis of the crack closure argument is that the stress state transitions occur at constant values of T , the ratio of plastic zone size to specimen thickness, and that differences in growth

rate between thicknesses are delineated at these points. However, the results of these tests did not bear this out. The slope transitions of the da/dN versus ΔK curves did not occur at constant values of T at either stress ratio. As a consequence, the thickness effects could not be directly attributed to the transition from plane strain to plane stress. Furthermore, in the tests conducted at $R=0.75$ where crack closure did not occur, a thickness effect was still present in the data, indicating that some other mechanism was active in the thickness effects observed.

The fracture mode transition from tensile mode to shear mode proved useful in explaining the thickness effects at the stress ratio of $R=0.05$. The points at which tensile mode ended and shear mode began, as determined from the specimen fracture surfaces, corresponded with the points of slope transition of the da/dN versus ΔK curves. The strain energy release rate model, which was developed to account for the slanting of the crack during mode transition, successfully correlated the thickness effects which existed in the original data.

Several significant points were revealed by the strain energy density and strain energy release rate analyses. The strain energy density model was developed to account for the presence of both mode I and mode III when

the crack was slanted through the thickness by combining them into one parameter, S . The resulting correlation with ΔS showed a more pronounced thickness effect than the original correlation with ΔK_I . This indicated that perhaps the magnitude of ΔK_{III} did not reflect how much mode III actually contributed to crack advance, i.e. $(\Delta K_{III})_{eff}$ is negligible. The strain energy release rate model considered only the portion of G produced by crack surface displacement normal to the crack plane. The successful correlation of the data using the strain energy release rate model may substantiate the assertion that $(\Delta K_{III})_{eff}$ was nearly zero.

The second significant point was that the apparent thickness effects in the data may have been a manifestation of the inadequacy of the stress intensity factor to correlate three-dimensional phenomena. Under identical conditions, a thin specimen and a thick specimen should exhibit the same growth rates. However, since shear lip development begins at longer crack lengths in thicker specimens, a thick specimen and a thin specimen are not under identical conditions in the mixed mode region even though the calculated ΔK_I is the same in both, because the cracks will be slanted at different angles. Therefore, this difference may be delineated as a "thickness effect" when the growth rate data is correlated with ΔK_I .

The results of the tests at $R=0.75$ could not be explained by fracture mode transition. Although the data showed slope transitions similar to those observed in the $R=0.05$ data, none of the specimens made a complete transition to shear mode. The values of ΔK at which tensile mode ended on the specimen surfaces were much larger than the ΔK at the first slope transition of the FCP rate data. Apparently, the crack slant argument can not explain the thickness effects in these data, and indicates it is the result of another mechanism which is not yet apparent.

The major conclusions from the constant amplitude loading results can be summarized as follows:

1. Crack growth rates were higher in thicker specimens.
2. The thickness effects could not be explained by crack closure concepts for tests at $R=0.05$ or $R=0.75$.
3. The thickness effects in the $R=0.05$ data could be attributed to the transition from tensile mode to shear mode.
4. The thickness effects in the $R=0.75$ data could not be attributed to fracture mode transition because it did not occur. Another mechanism(s) appears to be active which could not be determined in this investigation.

Thickness Effects Following a Single-Peak Overload

The two sets of tests at $R=0.05$ showed a consistent effect of thickness on retardation following a single-peak overload. Delayed retardation occurred in all tests at this stress ratio, as evidenced by the gradual drop in growth rate to a minimum, followed by a gradual increase to the pre-overload rate. The number of delay cycles decreased as the specimen thickness increased. The overload affected zone increased with decreasing specimen thickness, and it varied in size between the calculated plane stress and plane strain plastic zone sizes, depending on the state of stress attained during the overload. The minimum growth rate attained following overload decreased with decreasing specimen thickness. The distance beyond overload at which the minimum growth rate occurred was relatively invariant with thickness, and it varied in size between the calculated plane stress and plane strain cyclic plastic zone sizes.

These observations are consistent with other investigations in which crack closure was found to be the principle retardation mechanism. When crack closure caused retardation, the thickness effect was determined to be caused by constraint at the crack tip. Although the stress intensity at overload may be the same in each thickness, the stress state may be different in each thickness.

Constraint is larger in thicker specimens, and restricts the inward flow of plasticity, resulting in smaller plastic zones in thicker specimens. The degree of crack closure decreases with decreasing plastic zone size, therefore less closure and less retardation occurs in the thicker specimens. Furthermore, the retardation parameters would show a consistent variation with thickness. Specifically, the size of the overload affected zone would decrease with increasing thickness, the minimum FCP rate would increase with increasing thickness, and the number of delay cycles would decrease with increasing thickness. Therefore, the macroscopic results of the tests at $R=0.05$ indicate that when crack closure is the primary retardation mechanism, the thickness effect on retardation is due to constraint. Constraint is greater in thicker specimens, resulting in less retardation as specimen thickness increases.

The major result of the fractographic analysis of the specimen tested at $R=0.05$ was that retardation appeared to be due to crack closure, which is consistent with the macroscopic observations. The surface topography immediately after overload was similar to that ahead of the overload point, which may be indicative that no change in the FCP mechanism occurred after the overload. Furthermore, evidence of abrasion immediately beyond the overload point and no evidence of abrasion well beyond the overload

point indicates that crack closure caused the retardation. This microscopic behavior supports the delayed retardation behavior observed macroscopically.

The tests at the stress ratio of 0.70 did not show a consistent effect of thickness on retardation. The number of delay cycles was always greatest in the 0.08 inch specimen, while always the least in the 0.17 inch specimens. The retardation did not appear to be delayed in any of the tests, but rather a sudden drop in growth rate occurred after the overload, followed by an abrupt reestablishment of the pre-overload growth rate after the period of retardation. The overload affected zone showed no apparent trends with thickness, and were significantly smaller than the calculated plane stress and plane strain overload plastic zone sizes. The minimum growth rate also showed no apparent trend with thickness.

The macroscopic characteristics of the retardation for tests at $R=0.70$ were different from those at $R=0.05$. This indicates that crack closure was not the principle retardation mechanism in these tests, as was the case in the tests at $R=0.05$. This assertion is further substantiated by calculations based on results by Reuping [26] which showed that no crack closure should have occurred following overload in the tests at $R=0.70$. The retardation behavior at $R=0.70$ appears to be consistent with what

would be expected if crack tip blunting were the retardation mechanism. If crack tip blunting had occurred in the absence of crack closure, no delayed retardation would have been expected. Rather, a sudden drop in growth rate following overload should occur, followed by a period of nearly zero crack growth, and then an abrupt rise of growth rate to the pre-overload value. The overload affected zone would be very small, equal to the size required to initiate the crack from a short to a long crack. The results of the tests at $R=0.70$ are very similar to what would be expected if crack tip blunting were the retardation mechanism in these tests.

Fractographic examination of the specimen tested at $R=0.70$ revealed a distinct difference in surface topography between regions ahead of the overload and just beyond the overload. Regions ahead of the overload had a dimpled appearance, which changed to a smoother surface with striations just beyond the overload. This may be evidence of a change in FCP mechanism due to the overload application. Considering the macroscopically observed growth rates after overload and the increment of crack growth over which these very low growth rates were observed, this contrast in surface topography before and after overload may have been due to a transition from stage II to stage I crack growth due to the overload. Further microscopic evidence of stage I crack growth (crack reinitiation)

following overload was provided by what appeared to be a plateau after the overload. Such a feature may be expected if the crack had reinitiated from the notch formed at the crack tip during the overload application.

If crack tip blunting were the principle retardation mechanism in the tests at $R=0.70$, as appears to be the case, the retardation would be expected to be influenced by specimen thickness. This is because the retardation would be due primarily to the reinitiation of the crack at the notch formed after the overload application, and the initiation life is known to be dependent upon the state of stress. Jack and Price [11] found that the number of cycles for crack initiation from a notch in a sheet specimen was dependent on stress state. Specifically, initiation life was found to be shorter under plane stress conditions than plane strain conditions. If this is the case, then the opposite effect on retardation than that observed in $R=0.05$ overload tests would be expected, i.e. greater retardation would occur in thicker specimens. The results of the tests showed that the thinnest specimen still showed the greatest amount of retardation, while the 0.17 inch specimen had the least amount of retardation. This is not consistent with the observations of Jack and Price. It does seem plausible, though that the initiation lives may be susceptible to scatter, and the trends of the thickness effects on retardation observed in these tests may be a

result of this scatter in the initiation lives.

The information provided by the fractographic observations alone do not provide definitive proof that retardation was caused by crack closure in the tests at $R=0.05$ and by crack tip blunting in the tests at $R=0.70$. However, they do provide microscopic verification of the differences in the retardation characteristics between tests at $R=0.05$ and $R=0.70$ which were observed macroscopically, thereby indicating that different retardation mechanisms were active at these two stress ratios. It therefore seems apparent that the effect of thickness on retardation is not always the same, but rather is dependent on the retardation mechanism.

The major conclusions from the overload test results can be summarized as follows:

1. When crack closure was the retardation mechanism, greater retardation occurred in thinner specimens. The thickness effect was attributed to the difference in through the thickness constraint at the crack tip in different thickness specimens.
2. Crack tip blunting appeared to be the retardation mechanism in tests at the stress ratio of 0.70. In these tests, the greatest retardation occurred in the

thinnest specimens, and the least amount occurred in the intermediate thickness specimens.

LIST OF REFERENCES

LIST OF REFERENCES

- [1] Frost, N.E., Denton, K., "Effect of Sheet Thickness on the Rate of Growth of Fatigue Cracks in Mild Steel", *Journal of Mechanical Engineering Science*, Vol 3, No. 4, 1961.
- [2] Hertzberg, R.W., Paris, P.C., "Application of Electron Fractography and Fracture Mechanics to Fatigue Crack Propagation", *Proceedings: International Conference on Fracture*, Sendai, Japan, 1965.
- [3] Griffiths, J.R., Richards, C.E., "The Influence of Thickness on Fatigue Crack Propagation Rates in a Low Alloy Steel Weld Metal Above and Below General Yield", *Materials Science and Engineering*, Vol 11, 1973.
- [4] Hahn, G.T., Hoagland, R.G., Rosenfield, A.R., "Local Yielding Attending Fatigue Crack Growth", *Metallurgical Transactions*, Vol 3, 1972.
- [5] Clark, W.G., Jr., "Effect of Temperature and Section Size on Fatigue Crack Growth in Pressure Vessel Steel", *Journal of Materials*, Vol 6, No. 1, March 1971.
- [6] Clark, W.G., Jr., "Subcritical Crack Growth and its Effects Upon the Fatigue Characteristics of Structural Alloys", *Engineering Fracture Mechanics*, Vol 1, 1968.
- [7] Bathias, C., "Application of Fracture Mechanics to Aluminum Alloys Selection", *Engineering Fracture Mechanics*, Vol 10, 1978.
- [8] Dowling, N.E., "Fatigue-Crack Growth Rate Testing at High Stress Intensities", Flaw Growth and Fracture, ASTM STP 631, American Society for Testing and Materials, 1977.
- [9] Liu, H.W., "Fatigue Crack Propagation and the Stresses and Strains in the Vicinity of a crack", *Applied Materials Research*, Oct. 1964.

- [10] Wilhem, D.P., "Investigation of Cyclic Crack Growth Transitional Behavior", Fatigue Crack Propagation, ASTM 415, American Society for Testing and Materials, 1967.
- [11] Jack, A.R., Price, A.T., "Effects of Thickness on Fatigue Crack Initiation and Growth in Notched Mild Steel Specimens", *Acta Metallurgica*, Vol 20, July 1972.
- [12] Frost, N.E., Marsh, Pook, Metal Fatigue, Oxford University Press, 1974.
- [13] Hagiwara, Y., Yoshino, T., Kuno, T., "A Method for Estimating Fatigue Crack Propagation in Pre-Strained and Mean Stressed Specimens", *Fatigue of Engineering Materials and Structures*, Vol 1, 1979.
- [14] Broek, D., Schijve, J., "The Effect of Thickness on the Fatigue Crack Propagation in 2024-T3 Alclad Sheet Material", NLR-TR M.2129, National Aero and Astronautical Research Institute, Amsterdam, Jan. 1965.
- [15] Swanson, S.R., Cicci, F., Hoppe, W., "Crack Propagation in Clad 7079-T6 Aluminum Alloy Sheet Under Constant and Random Amplitude Fatigue Loading", Fatigue Crack Propagation, ASTM 415, American Society for Testing and Materials, 1967.
- [16] Heiser, F.A., Mortimer, W., "Effect of Thickness and Orientation on Fatigue Crack Growth Rate in 4340 Steel", *Metallurgical Transactions*, Vol 3, 1972.
- [17] McGowan, J.J., Liu, H.W., "The Role of Three-Dimensional Effects in Constant Amplitude Fatigue Crack Growth Testing", *Journal of Engineering Materials and Technology*, Vol 102, October 1980.
- [18] Sharpe, W.N., Jr., Grandt, A.F., Jr., Mechanics of Crack Growth, ASTM STP 590, American Society for Testing and Materials, Vol 6, 1971.
- [19] Elber, W., "The Significance of Fatigue Crack Closure", Damage Tolerance in Aircraft Structures, ASTM STP 486, American Society for Testing and Materials, 1970.
- [20] Shin, T.T., Wei, R.P., "Effect of Specimen Thickness on Delay in Fatigue Crack Growth", *Journal of Testing and Evaluation*, JTEVA, Vol 3, No. 1, January 1975.

- [21] Chanani, G.R., "Effect of Thickness on Retardation Behavior of 7075 and 2024 Aluminum Alloys", Flaw Growth and Fracture, ASTM STP 631, American Society for Testing and Materials, 1977.
- [22] Mills, W.J., Hertzberg, R.W., "The Effect of Sheet Thickness on Fatigue Crack Retardation in 2024-T3 Aluminum Alloy", Engineering Fracture Mechanics, Vol 7, 1975.
- [23] Wei, R.P., Finelli, N., Unangst, K.D., Shih, T.T., "Fatigue Crack Growth Response Following a High-Load Excursion in 2219-T851 Aluminum Alloy", Journal of Engineering Materials and Technology, Vol 102, 1980.
- [24] Matsuoka, S., Tanaka, K., "The Influence of Sheet Thickness on Delayed Retardation Phenomena in Fatigue Crack Growth in HT80 and A5083 Aluminum Alloy", Engineering Fracture Mechanics, Vol 13, 1980.
- [25] Sharpe, W.N., Jr., Corbly, D.M., Grandt, A.F., Jr., "Effect of Rest Time on Fatigue Crack Retardation and Observations of Crack Closure", Fatigue Crack Growth Under Spectrum Loads, ASTM STP 595, American Society for Testing and Materials, 1976.
- [26] Himmelein, M.K., "The Effect of Stress Ratio and Overload Ratio on Fatigue Crack Delay and Arrest Behavior Due to Single-Peak Overloads", M.S. Thesis, Purdue University, May 1974.
- [27] Reuping, J.E., "Fatigue Crack Closure Behavior: A Comparative Study", M.S. Thesis, Purdue University, August 1976.
- [28] Mehr, P.L., "ALCOA 7475 Sheet and Plate", Aluminum Company of America Aerospace, Ordnance and Marine Market, Alcoa Center, Pa., 1978.
- [29] 1981 Annual Book of ASTM Standards, Part 10, Metals-Mechanical, Fracture, and Corrosion Testing; Fatigue: Erosion and Wear; Effect of Temperature, ASTM, Philadelphia, 1981.
- [30] Sih, G.C., Cha, B.C.K., "A Fracture Criterion for Three-Dimensional Crack Problems", Engineering Fracture Mechanics, Vol 6, 1974.
- [31] Badaliance, R., "Application of Strain Energy Density Factor to Fatigue Crack Growth Analysis", Engineering Fracture Mechanics, Vol 13, 1980.

- [32] Sih, G.C., "Application of Strain Energy Density Theory to Fundamental Fracture Problems", Recent Advances in Engineering Science, Vol 6, 1976.
- [33] Tada, H., Paris, P., Irwin, G., The Stress Analysis of Cracks Handbook, DEL Research Corporation, Hellertown, Pa., 1973.
- [34] Hurd, N.J., Irving, P.E., "Factors Influencing Propagation of Mode III Fatigue Cracks Under Torsional Loading", Design of Fatigue and Fracture Resistant Structures, ASTM 761, American Society for Testing and Materials, 1982.
- [35] Tschegg, E.K., Ritchie, R.O., McClintock, F.A., "On the Influence of Rubbing Fracture Surfaces on Fatigue Crack Propagation in Mode III", International Journal of Fatigue, January 1983.

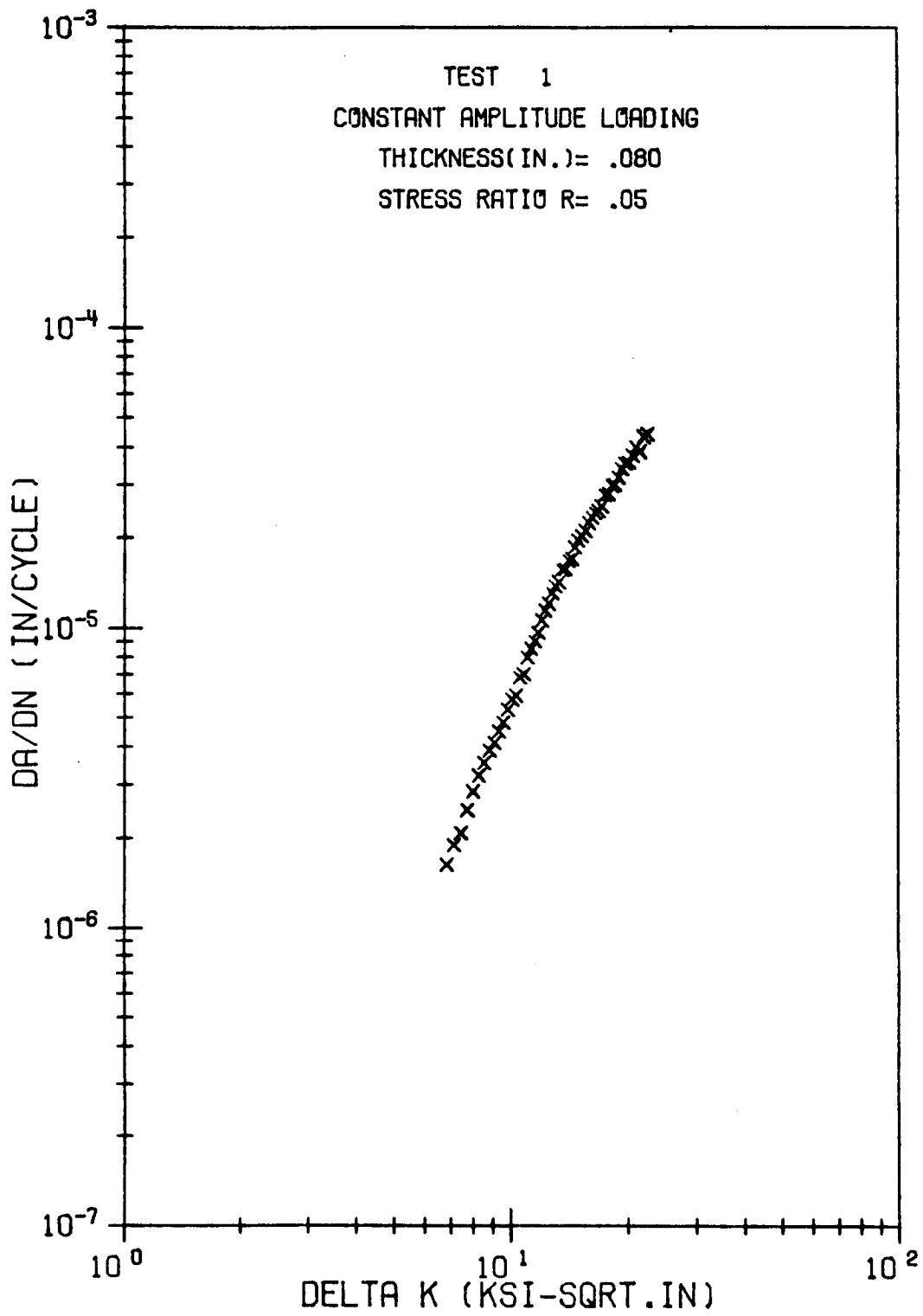


Figure A1. FCP rate data from Test 1.

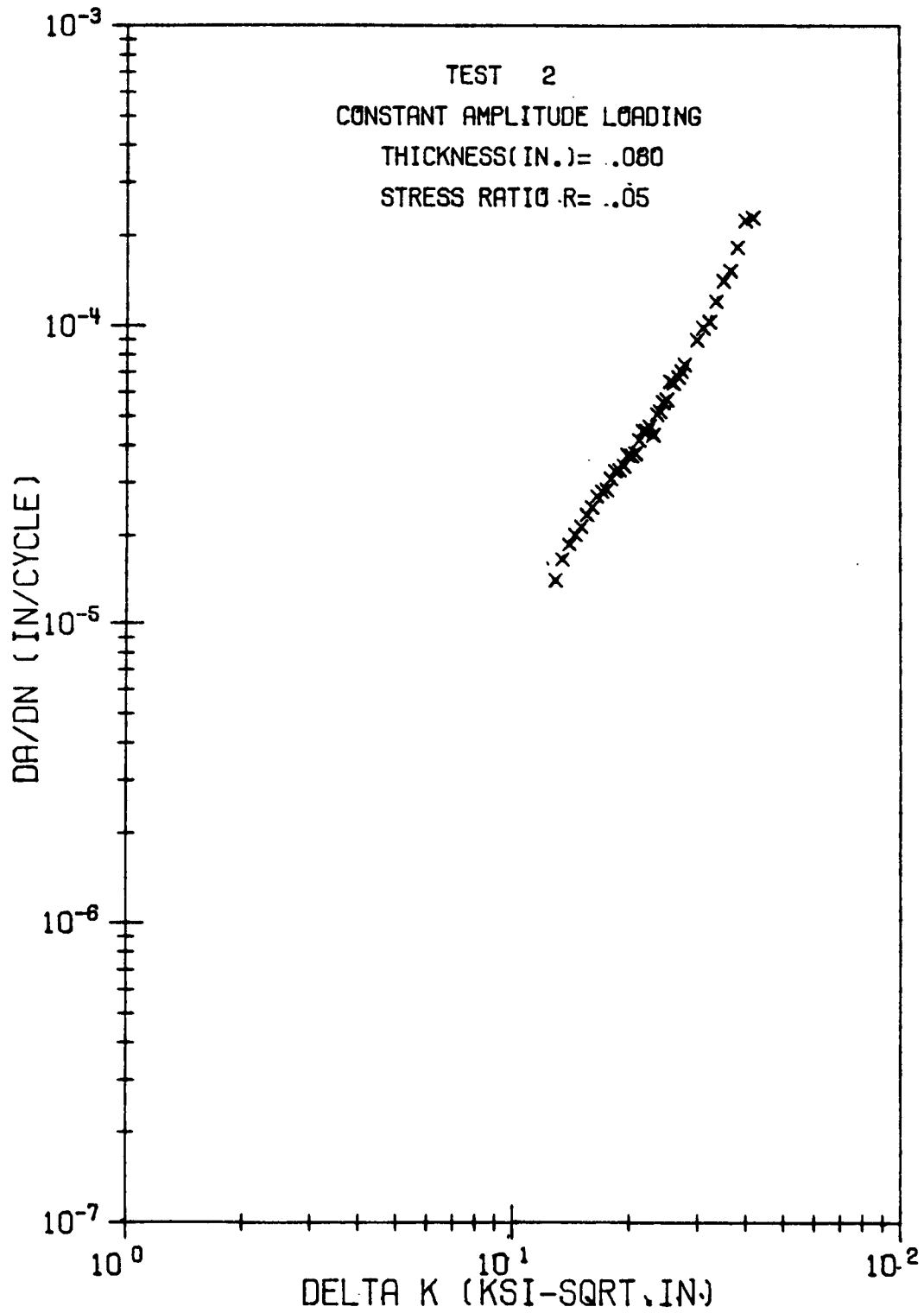


Figure A2. FCP rate data from Test 2.

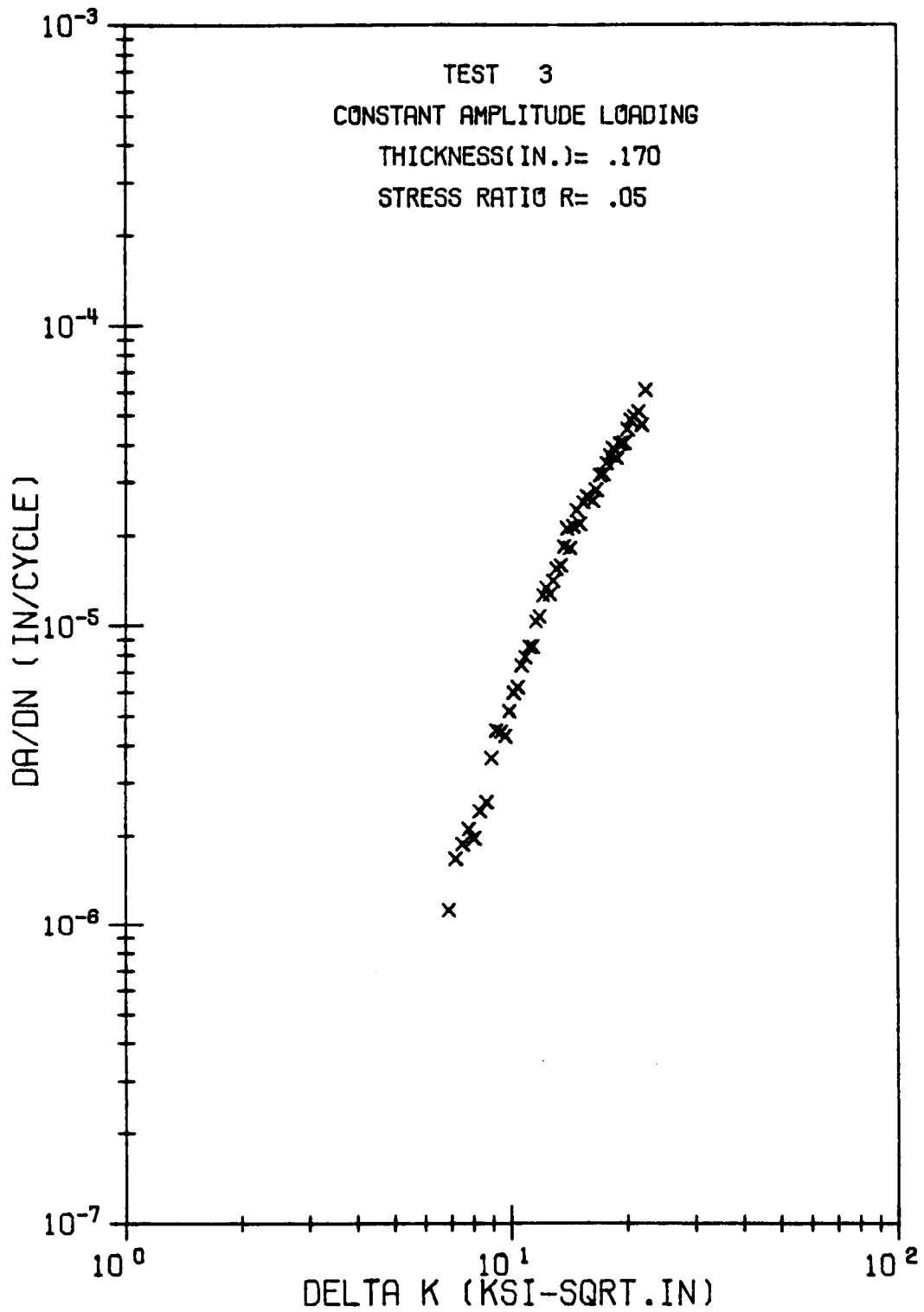


Figure A3. FCP rate data from Test 3.

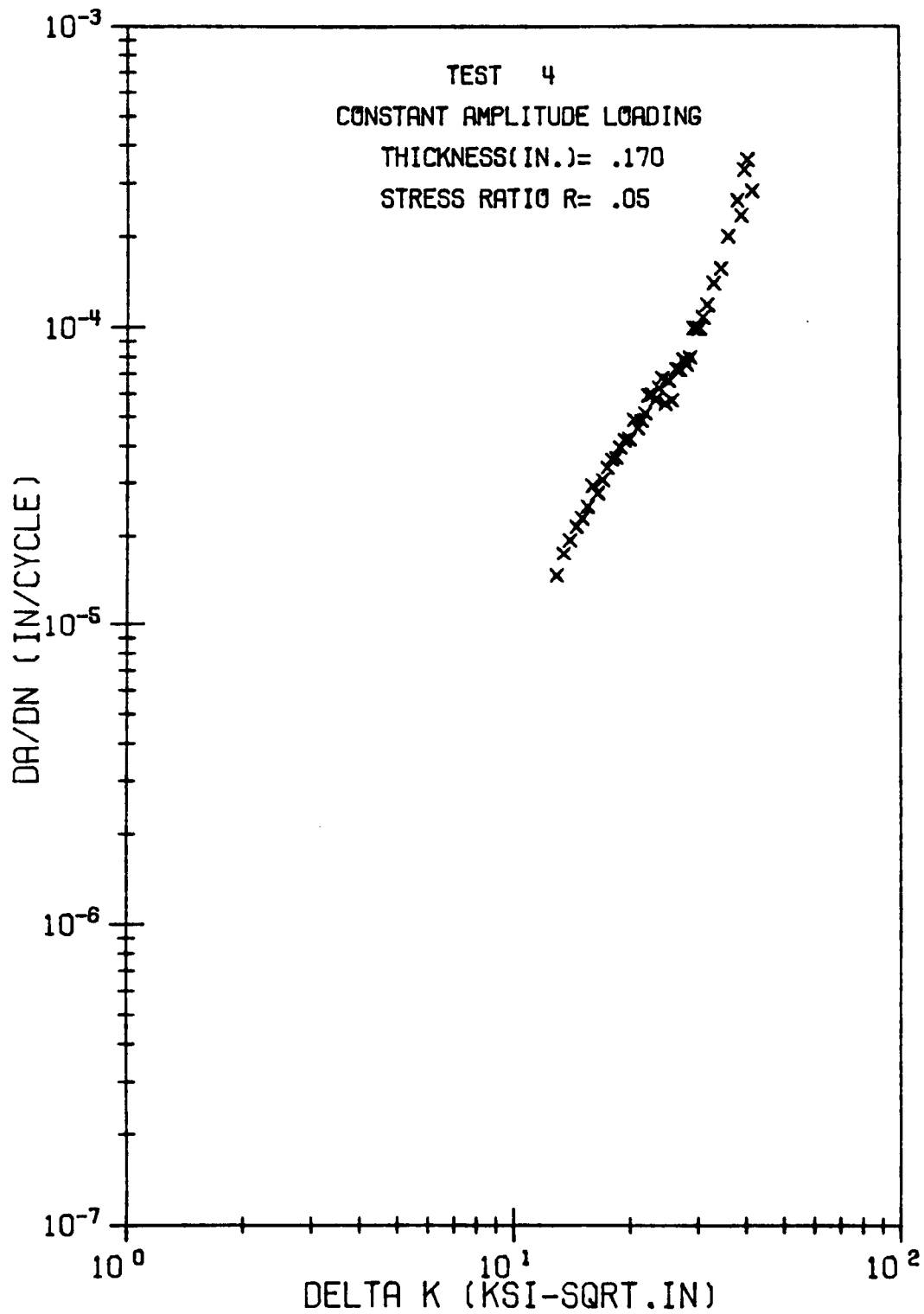


Figure A4. FCP rate data from Test 4.

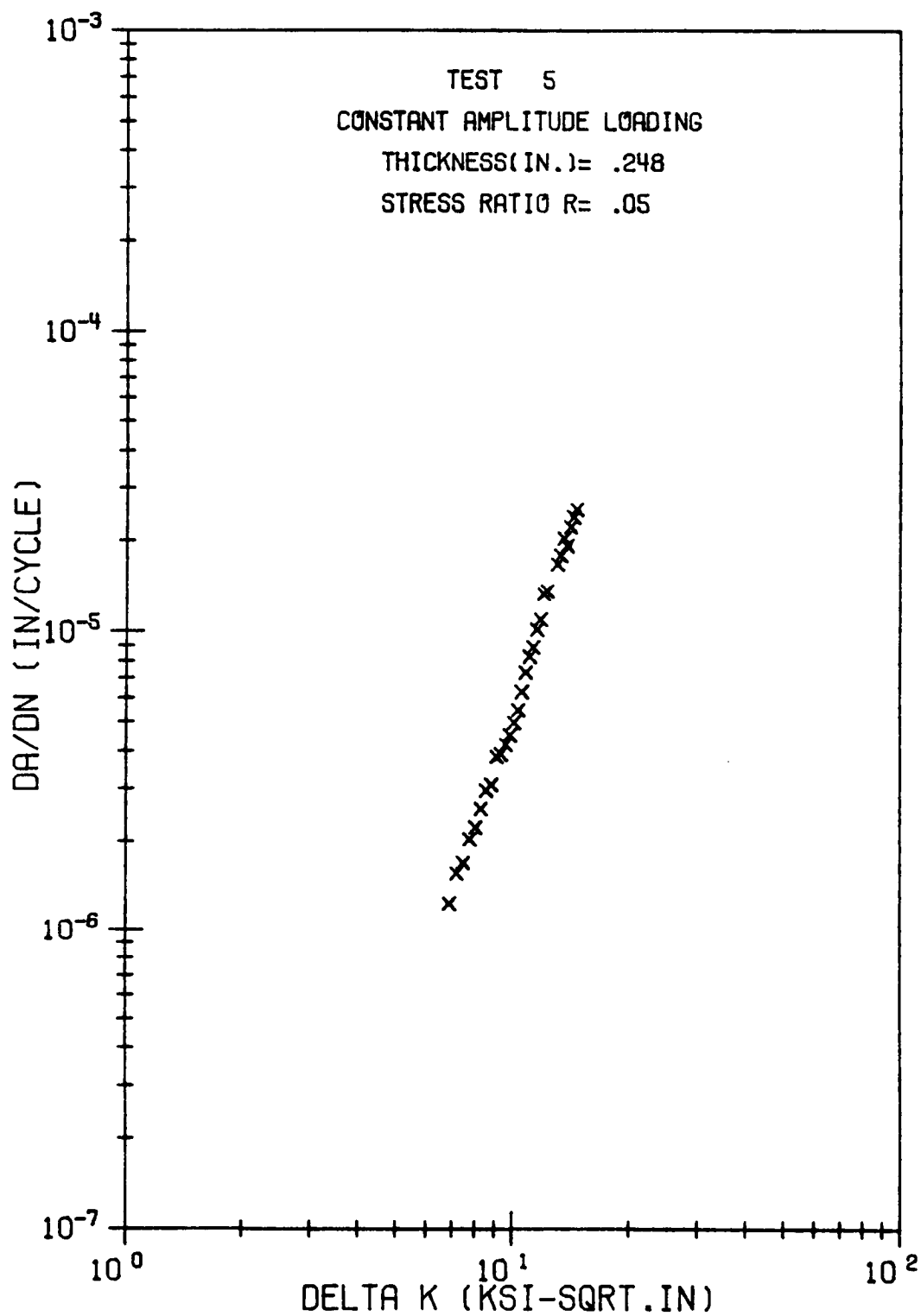


Figure A5. FCP rate data from Test 5.

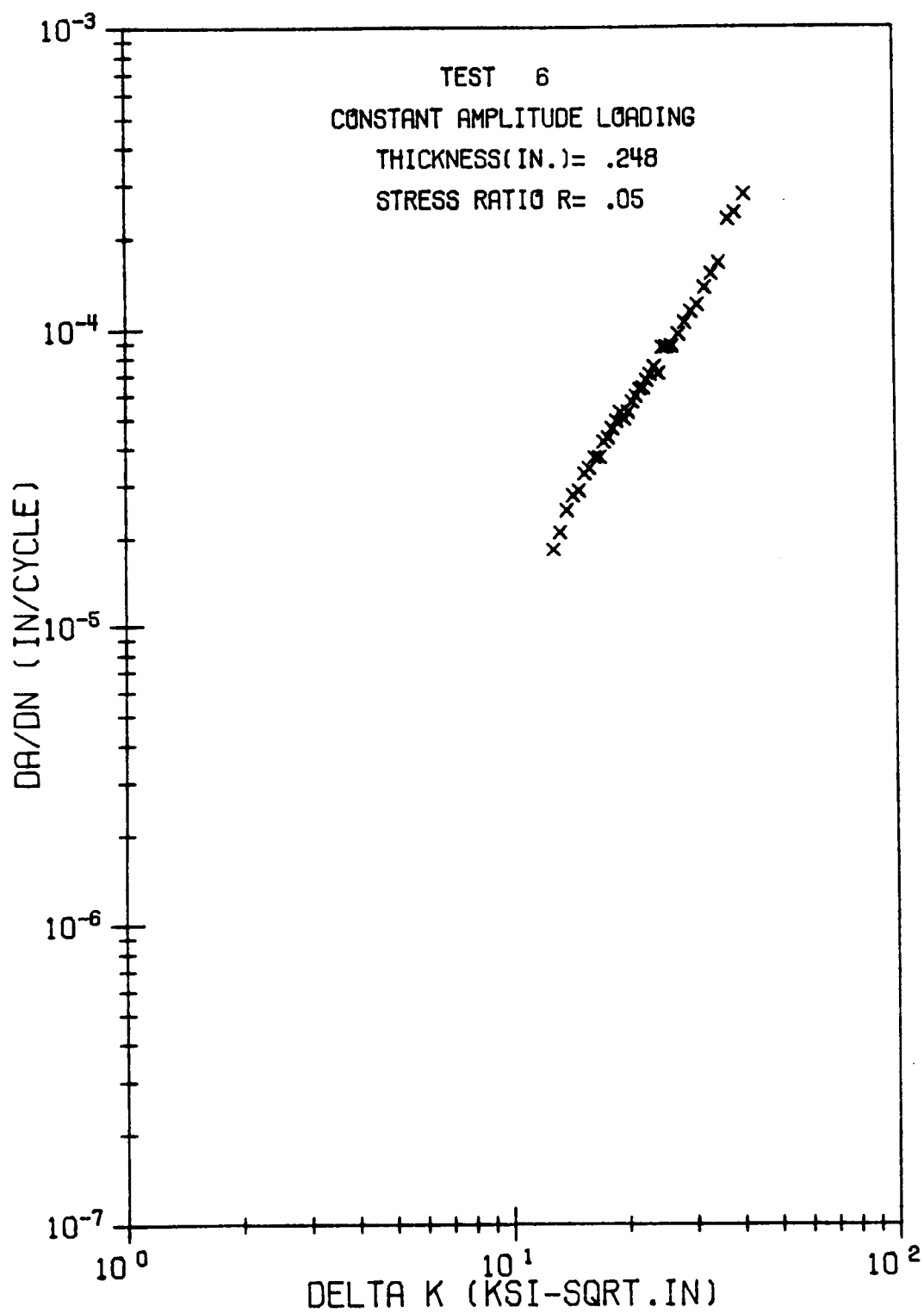


Figure A6. FCP rate data from Test 6.

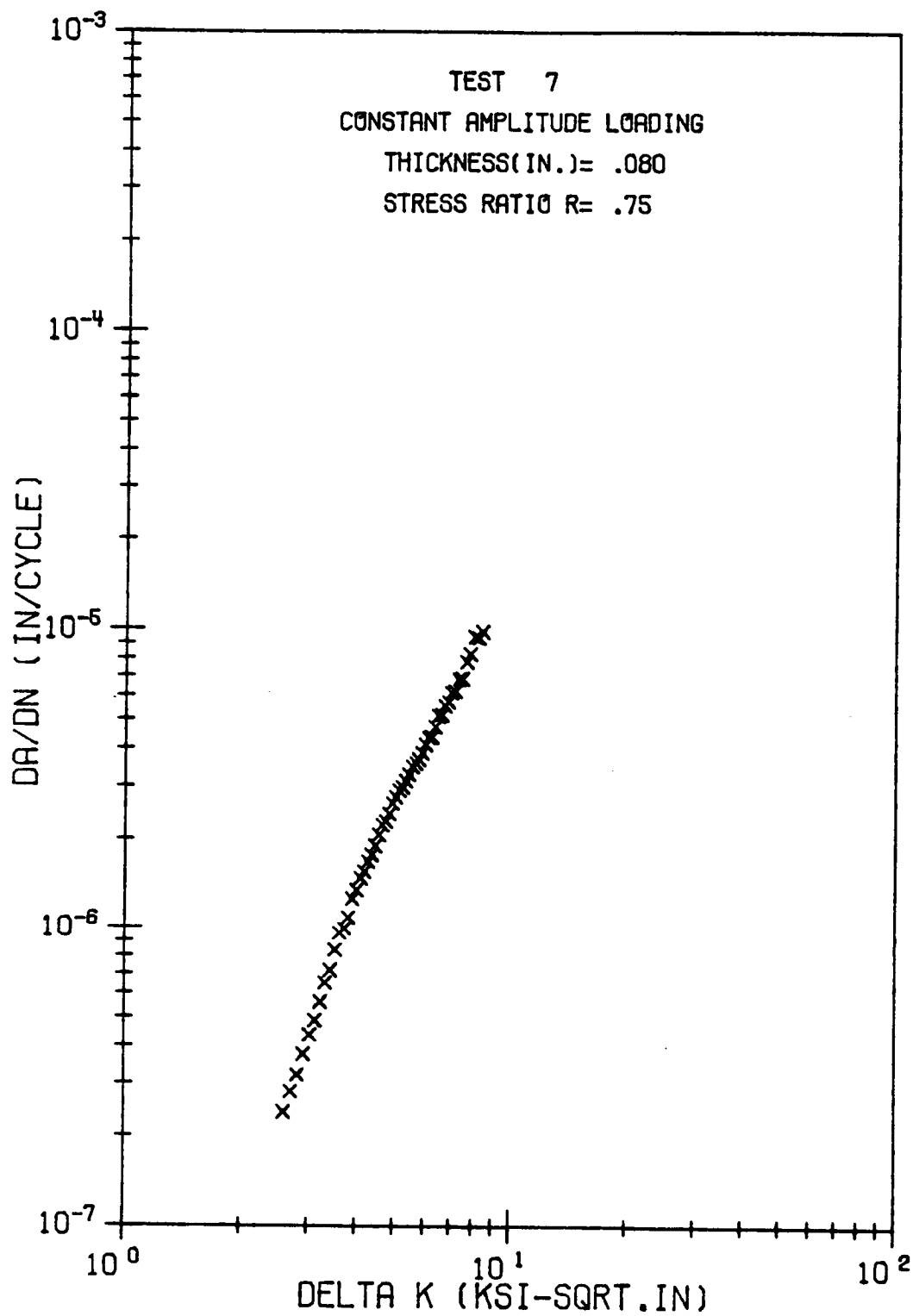


Figure A7. FCP rate data from Test 7.

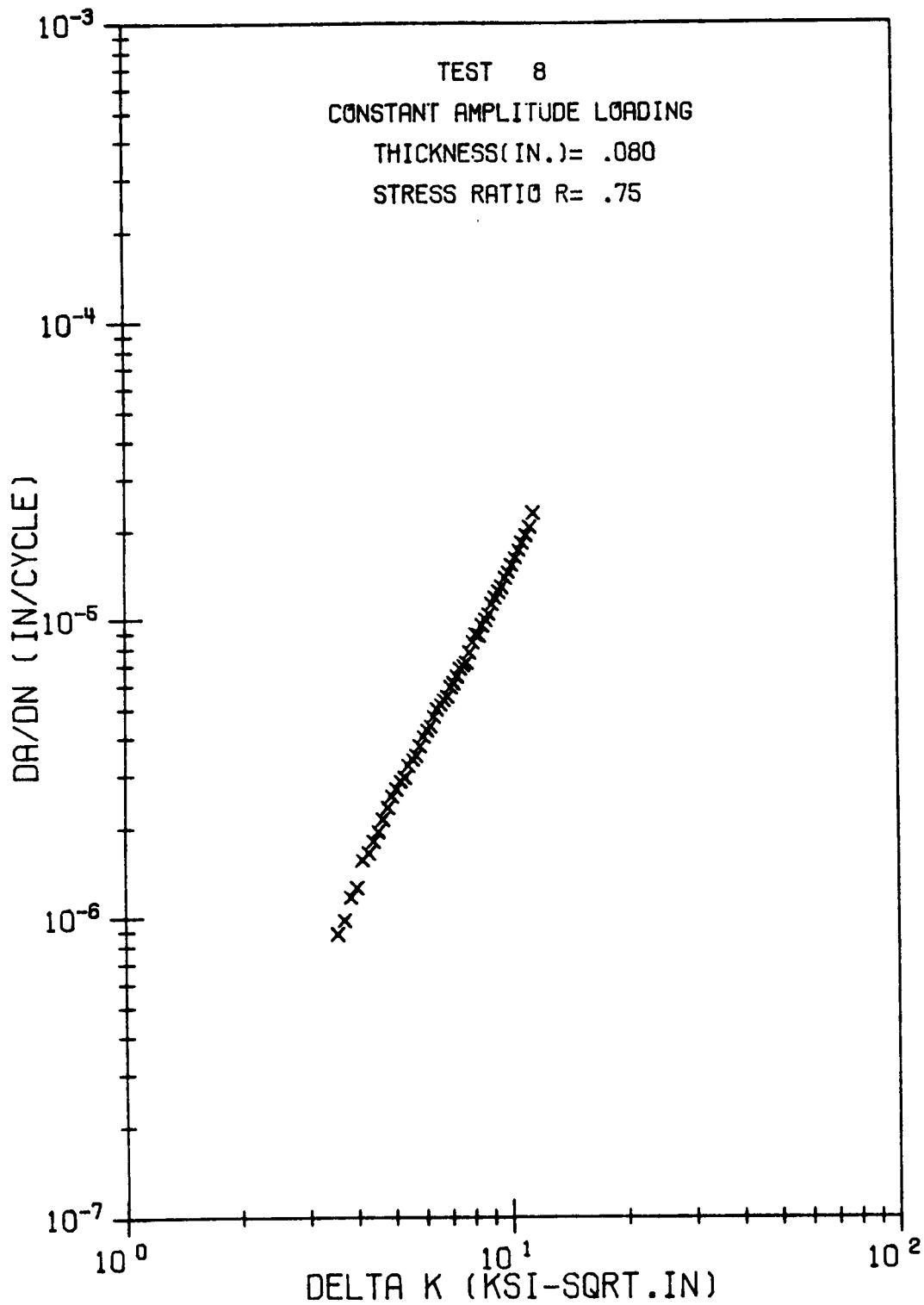


Figure A8. FCP rate data from Test 8.

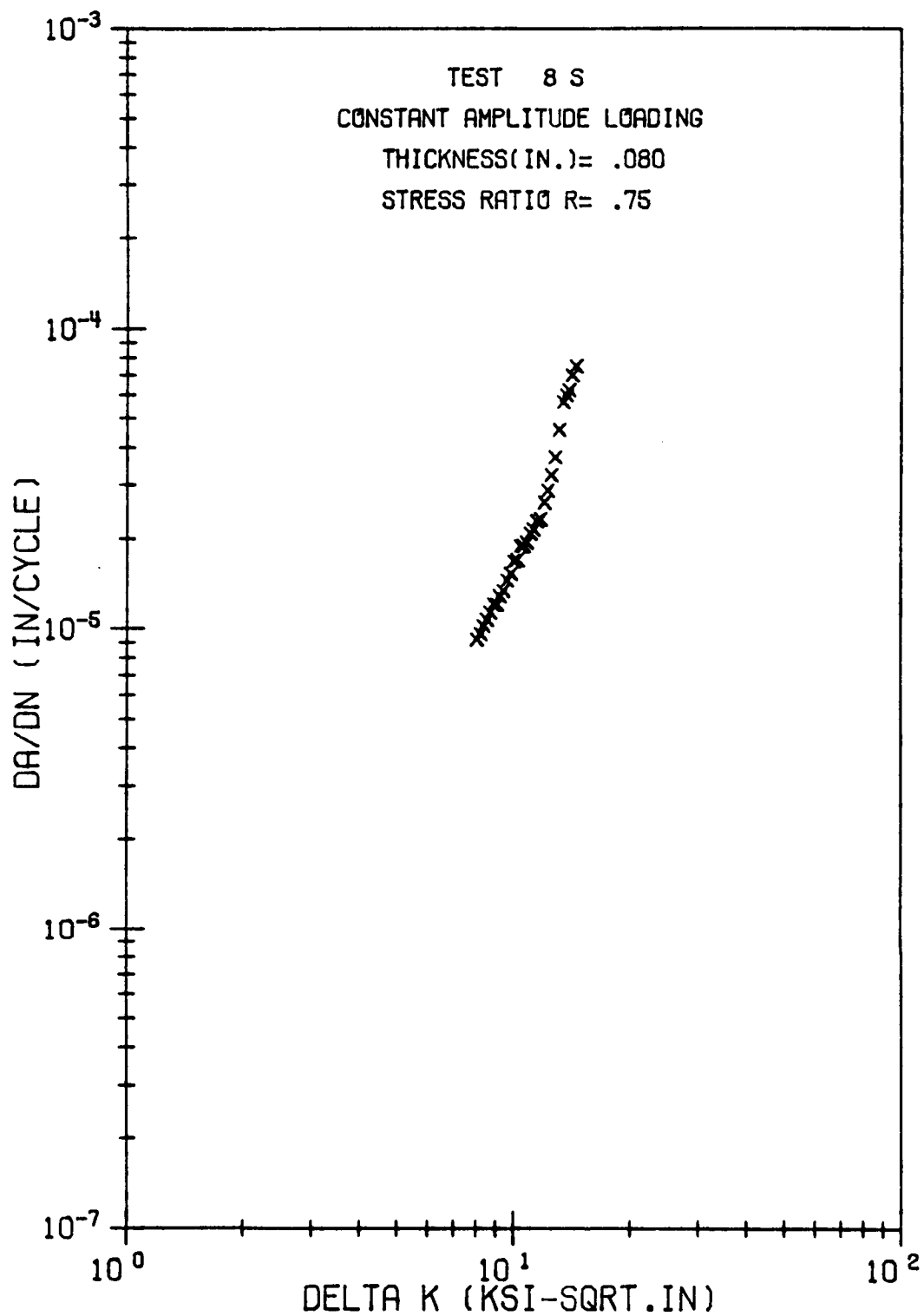


Figure A9. FCP rate data from Test 8S.

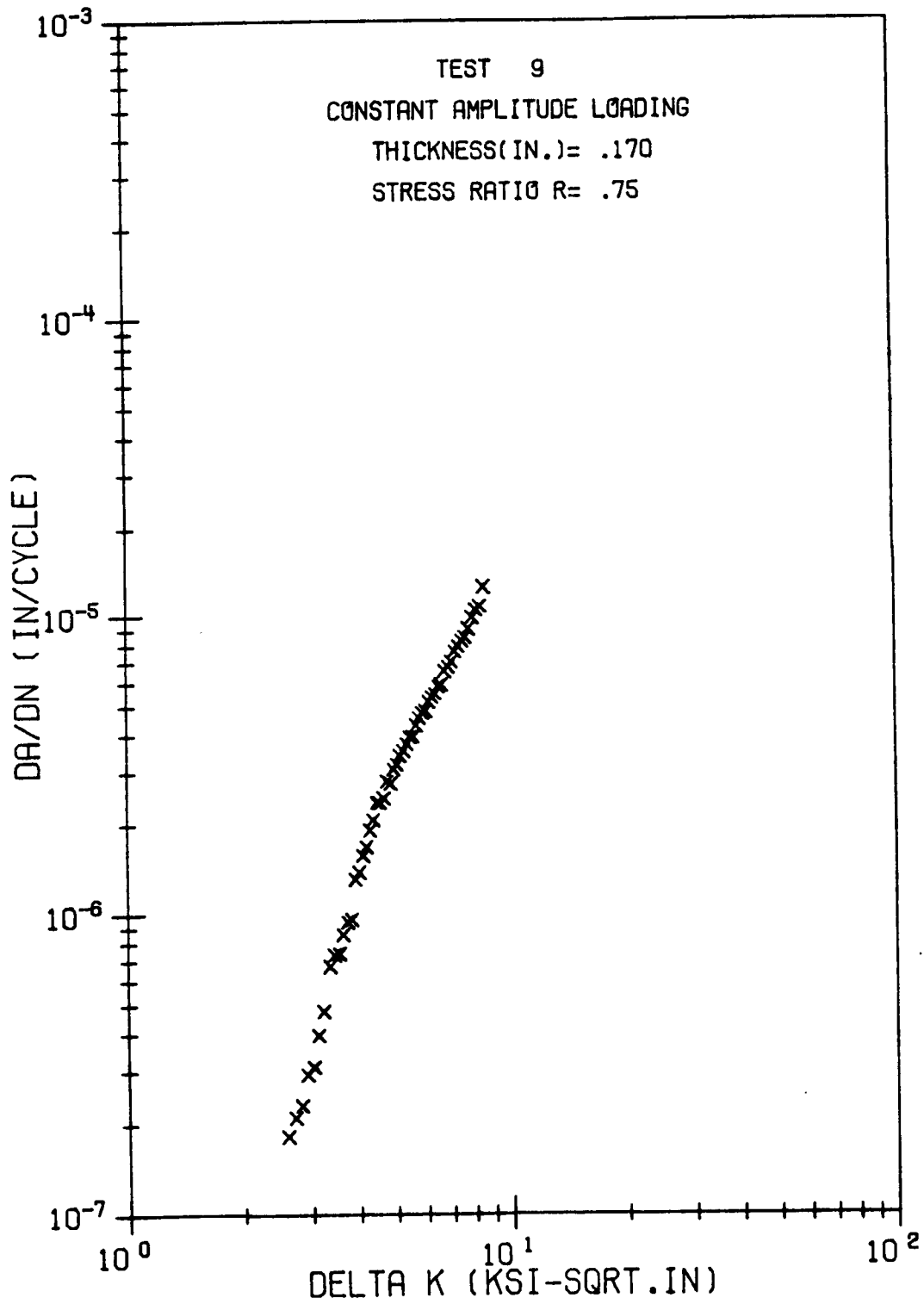


Figure A10. FCP rate data from Test 9.

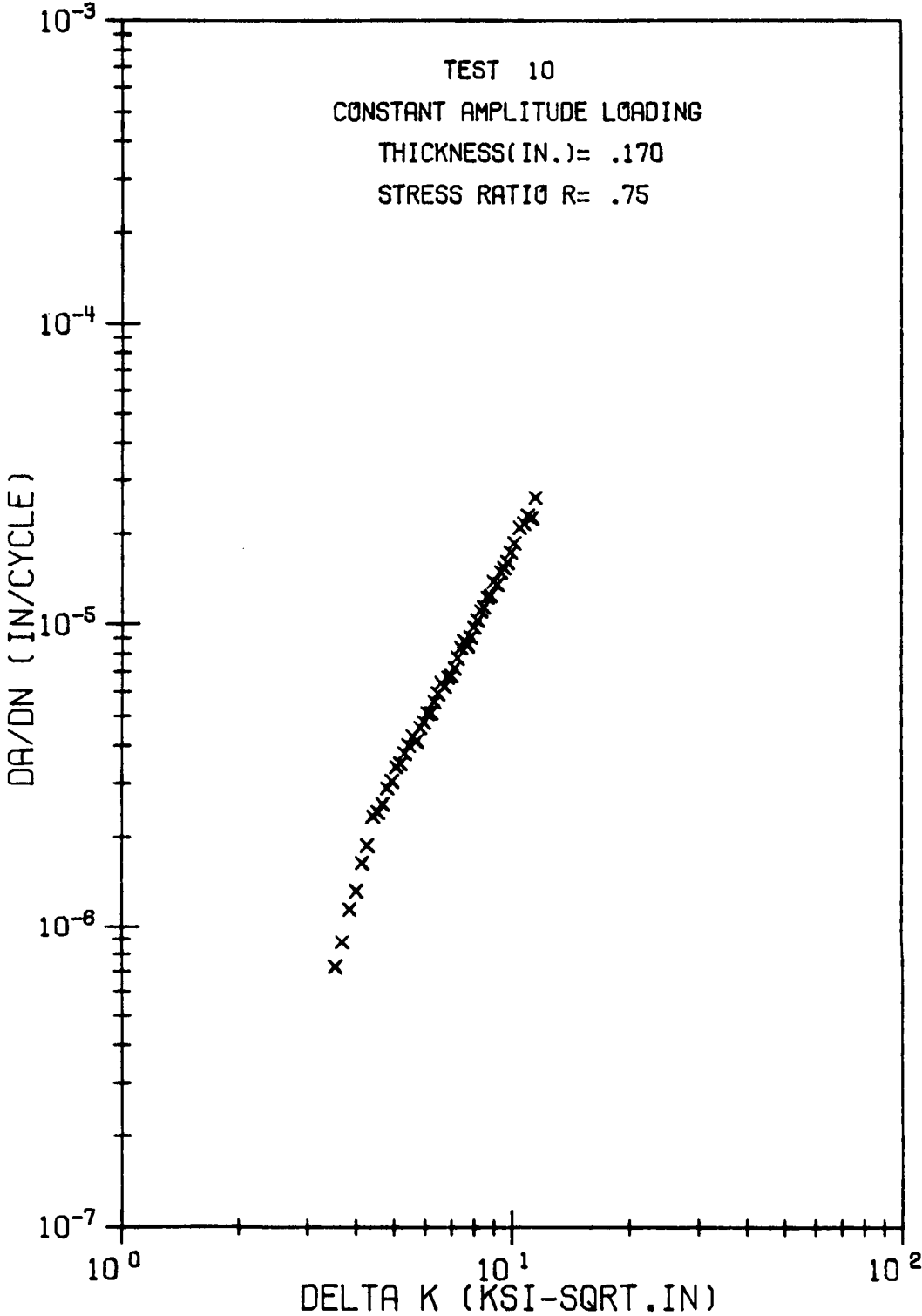


Figure A11. FCP rate data from Test 10.

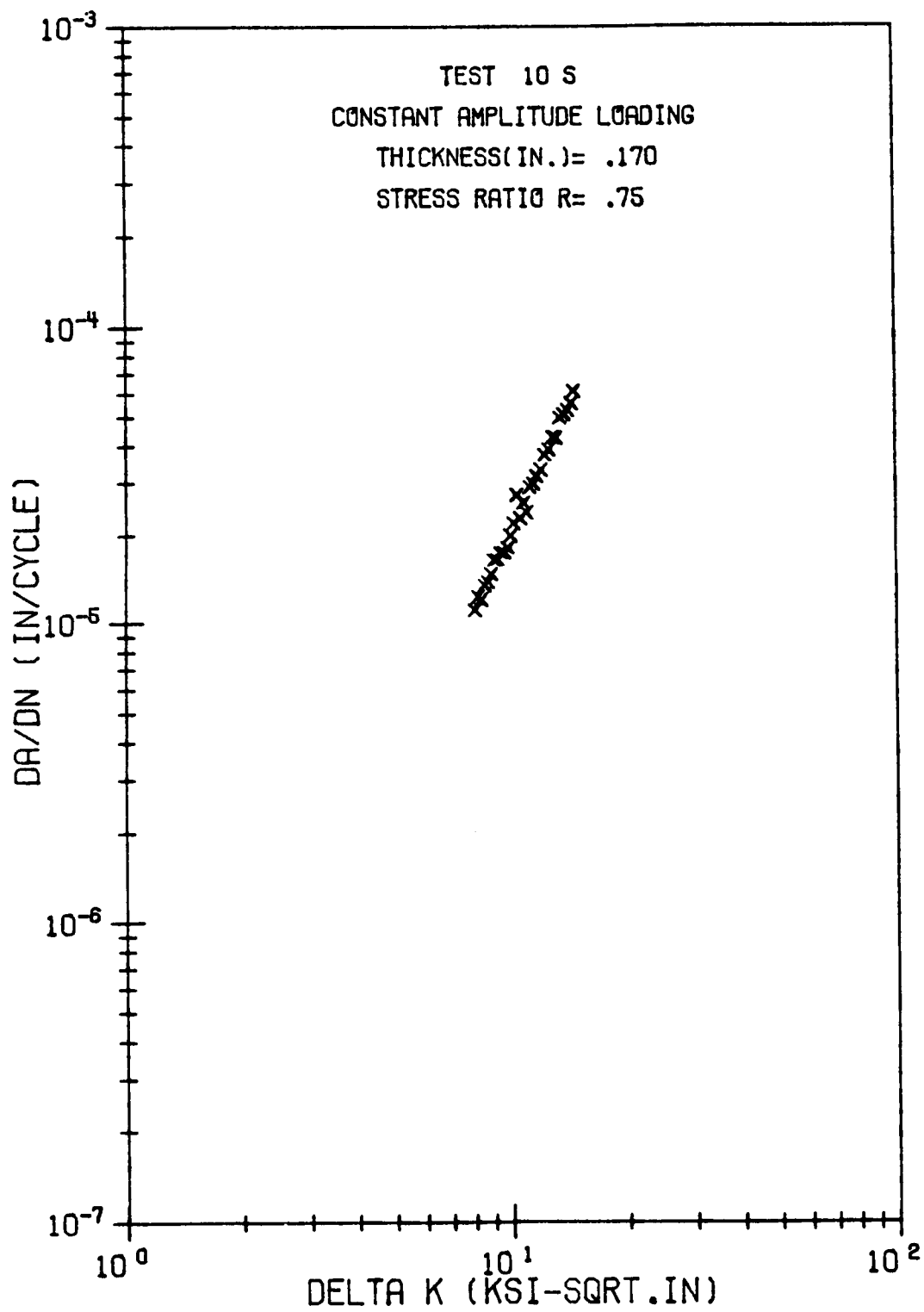


Figure A12. FCP rate data from Test 10S.

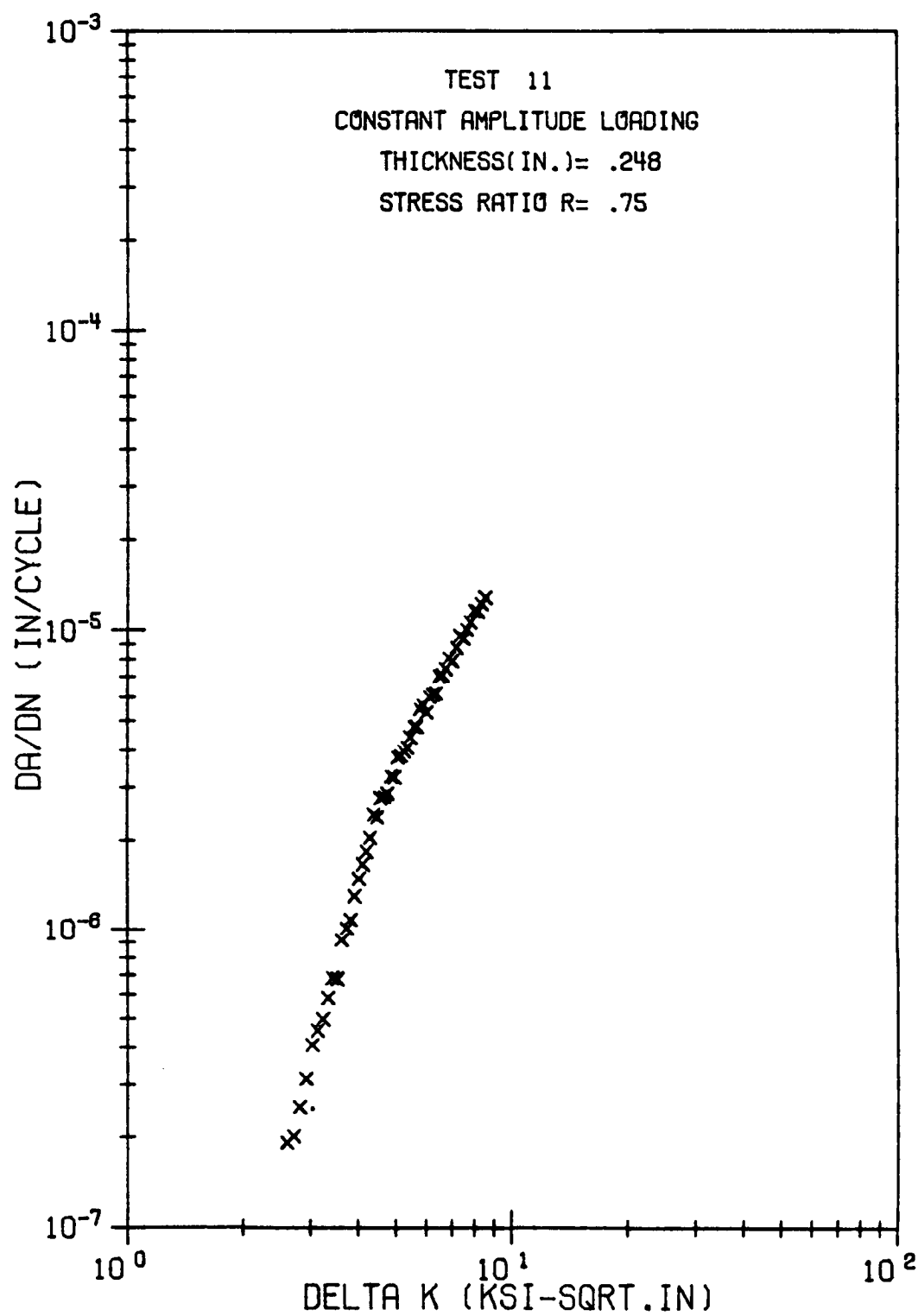


Figure A13. FCP rate data from Test 11.

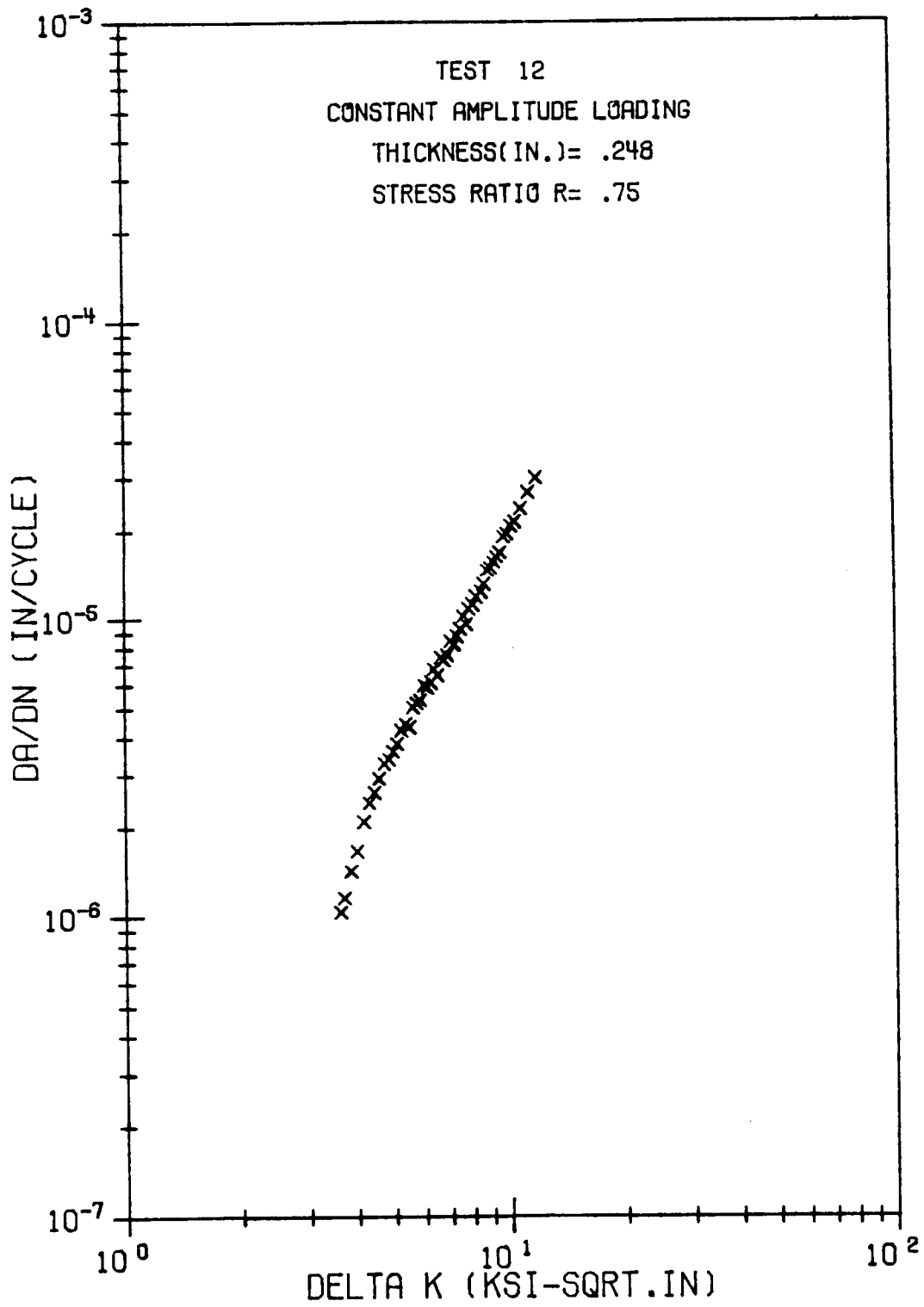


Figure A14. FCP rate data from Test 12.

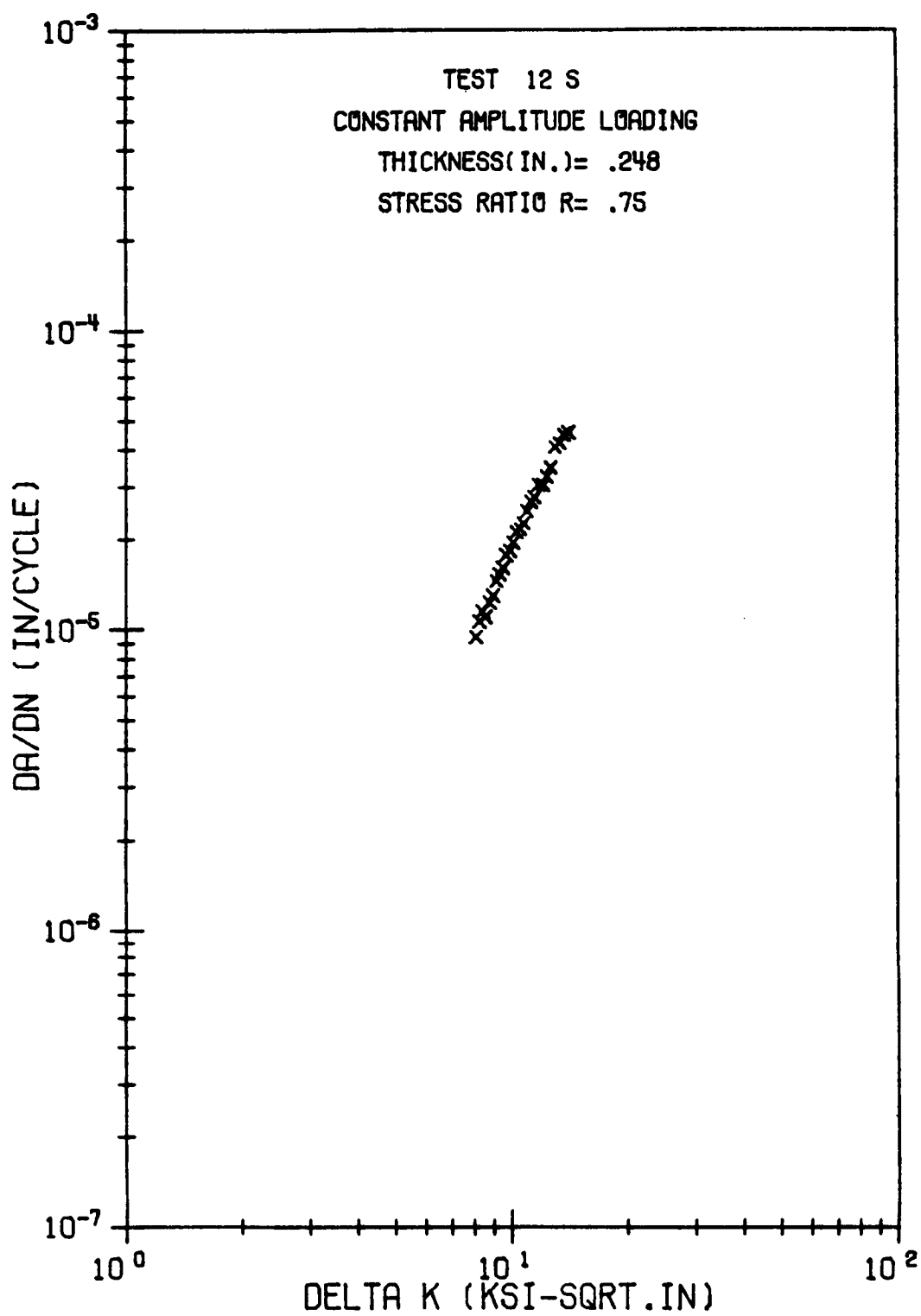


Figure A15. FCP rate data from Test 13.

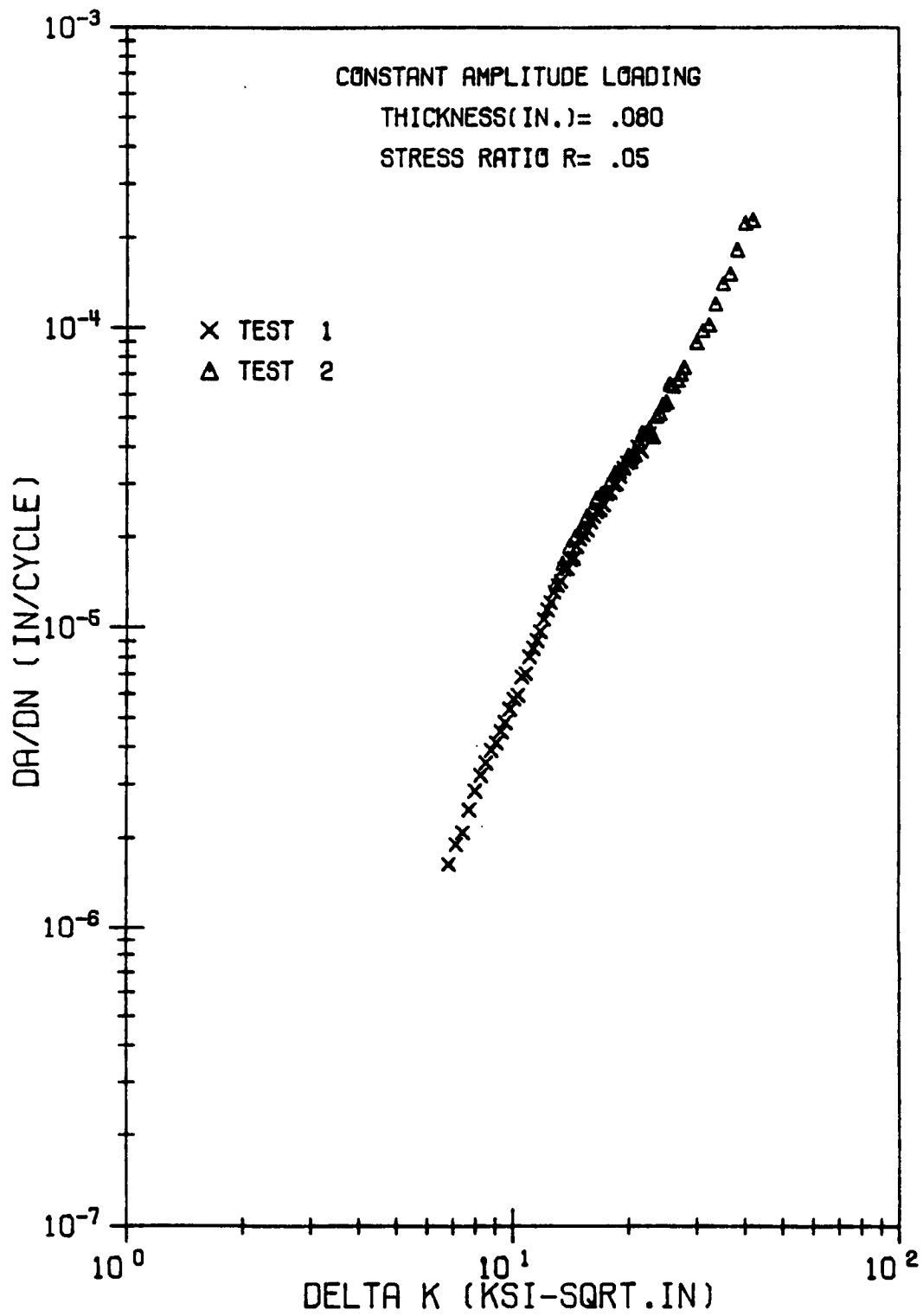
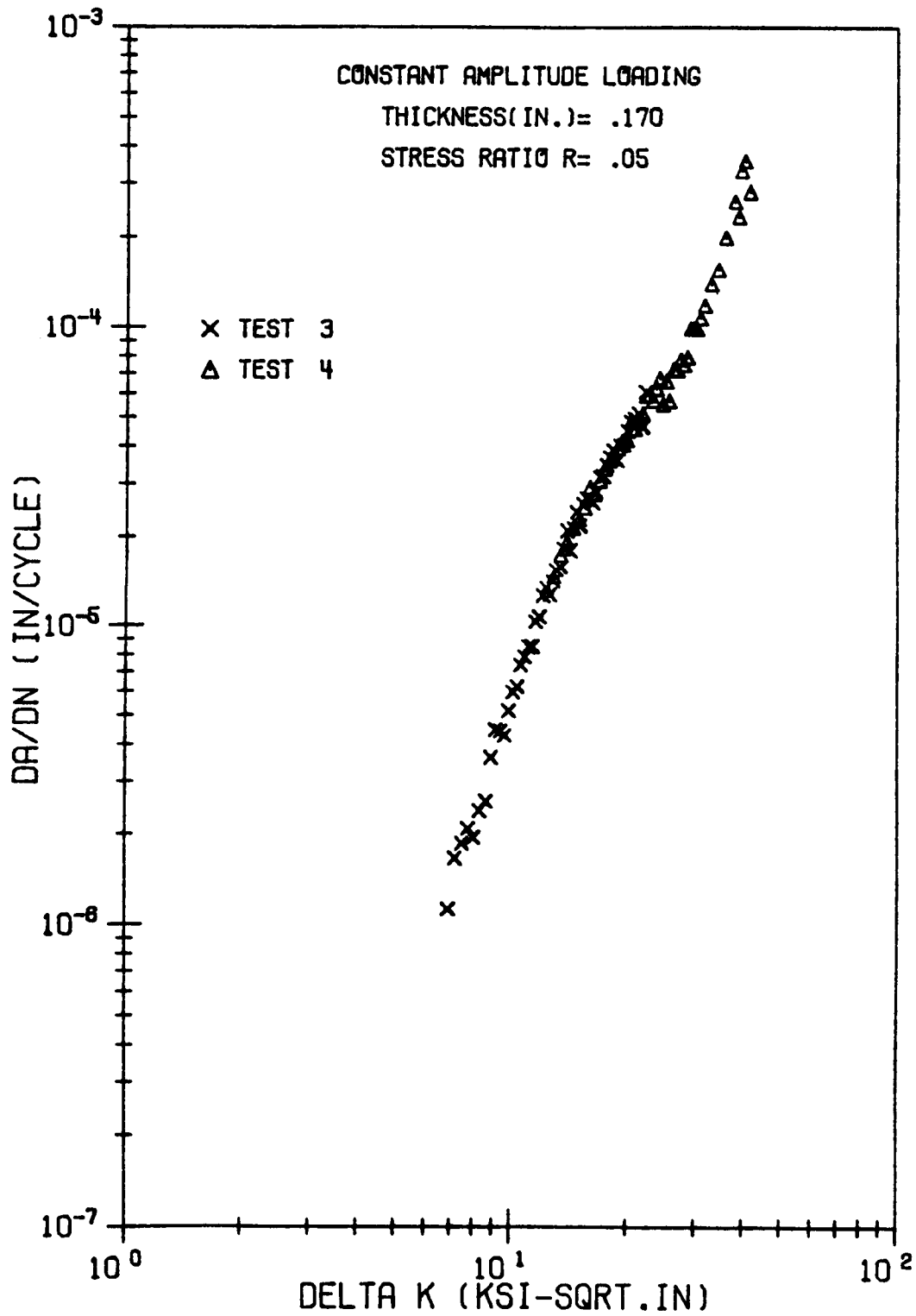
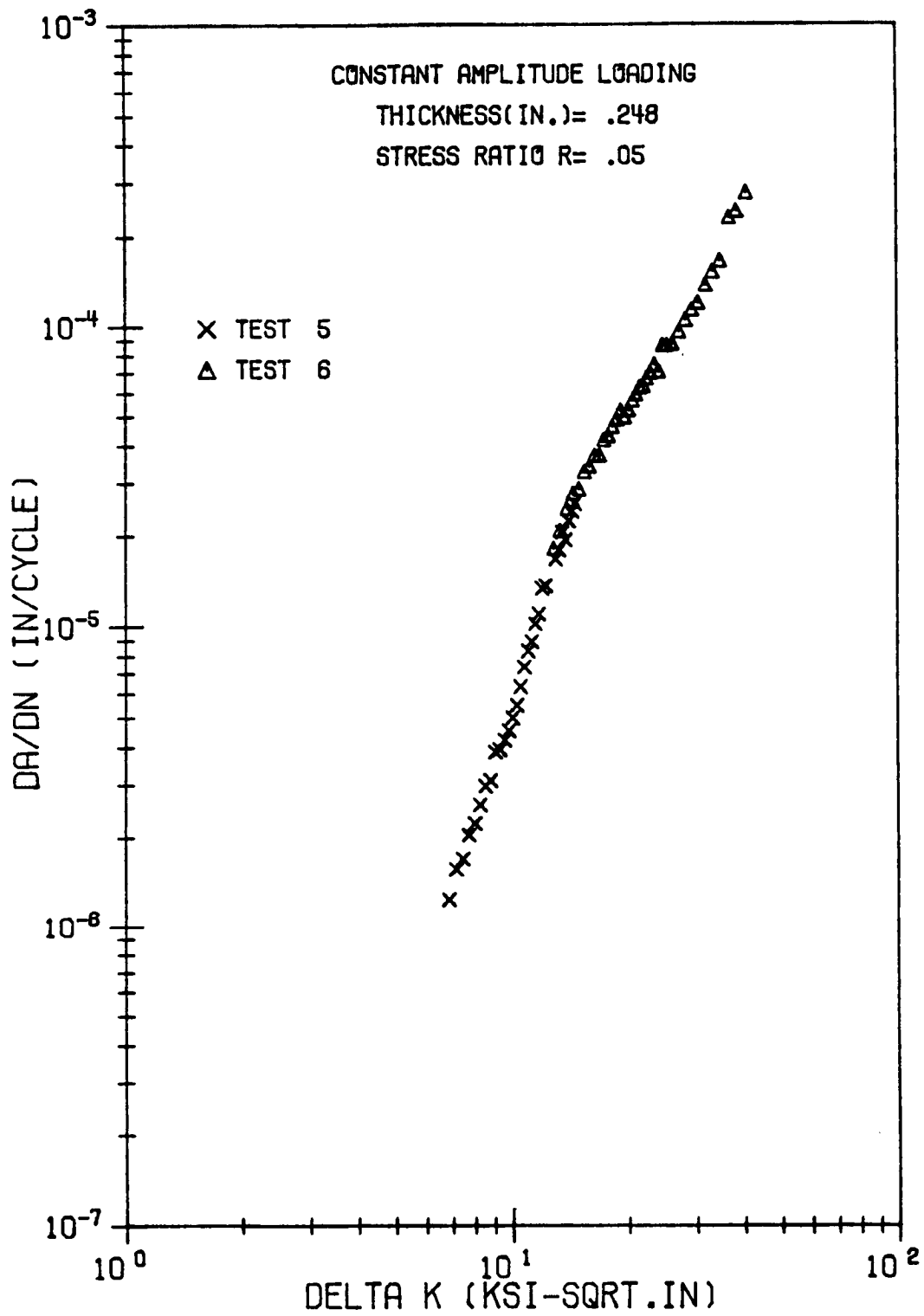


Figure B1. Comparison of FCP rate data from Test 1 and Test 2.





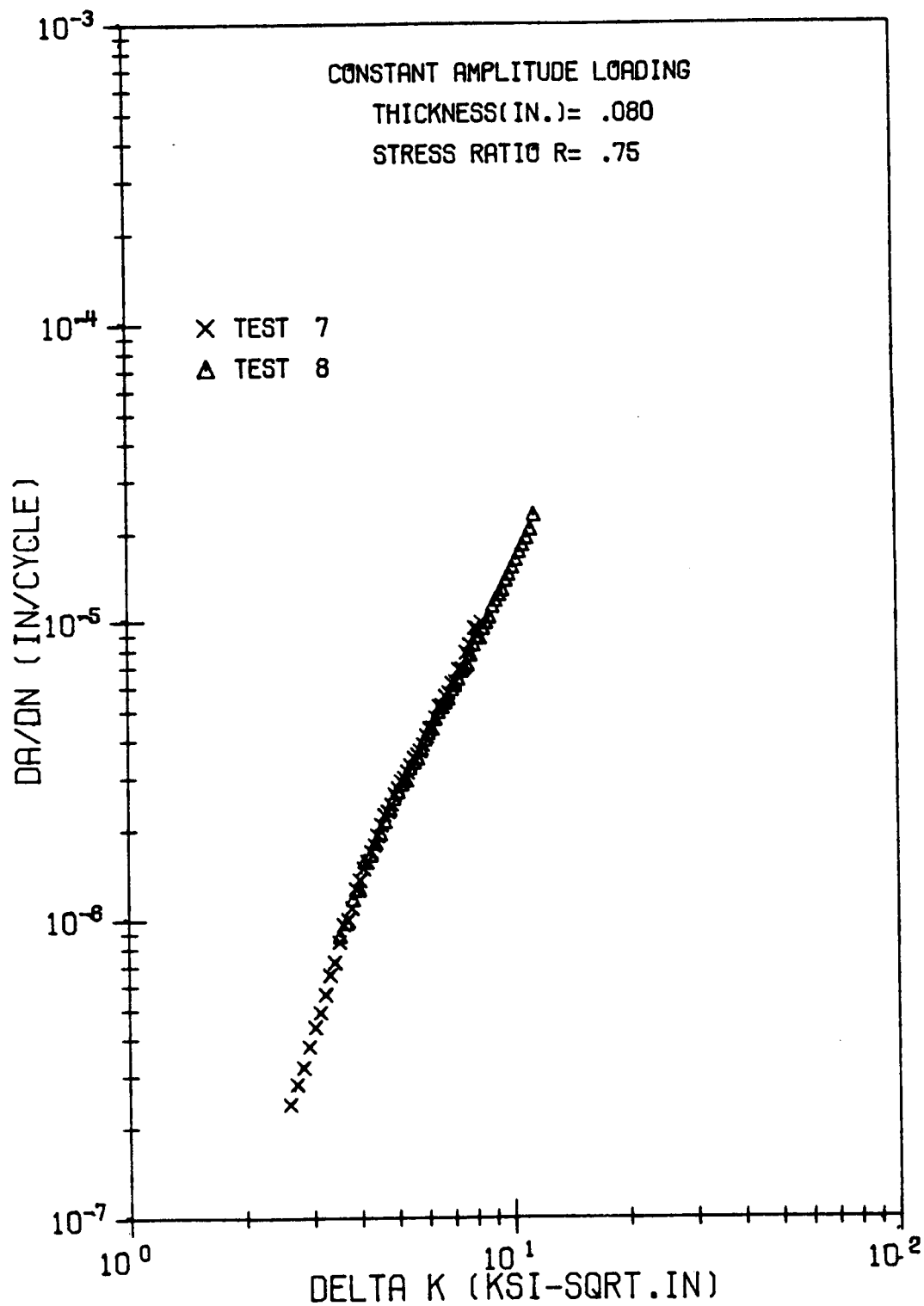


Figure B4. Comparison of FCP rate data from Test 7 and Test 8.

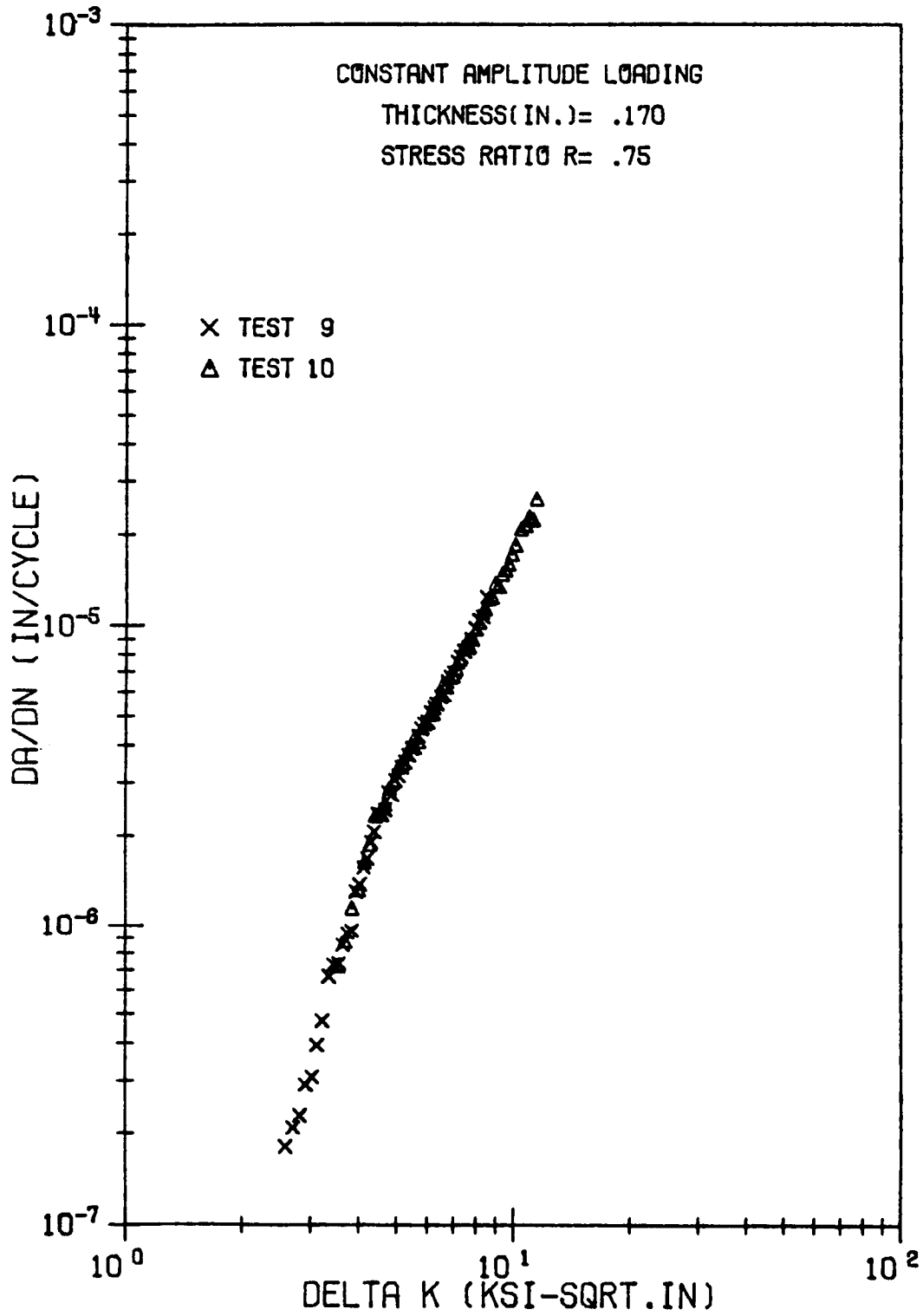
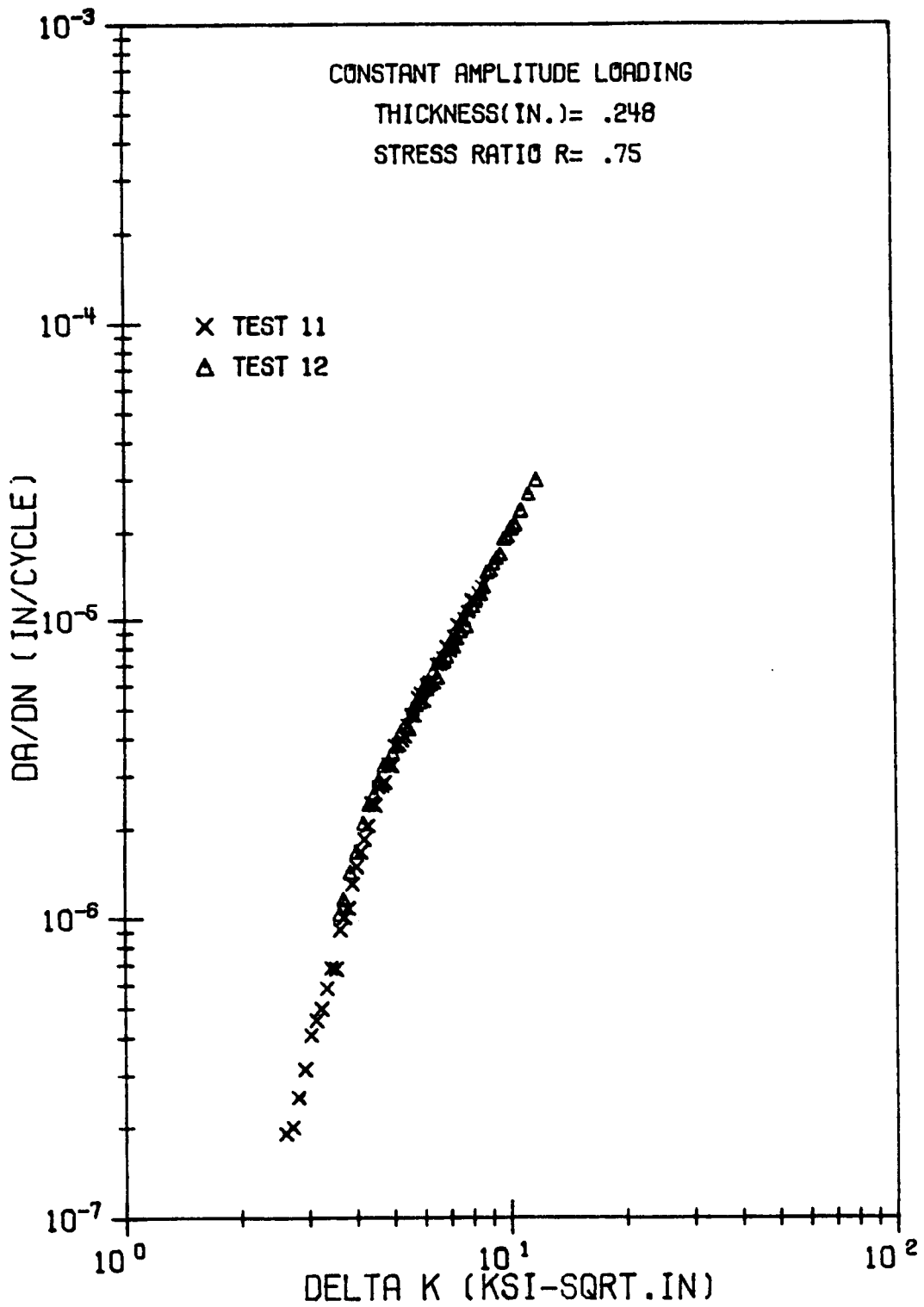


Figure B5. Comparison of FCP rate data from Test 9 and Test 10.



APPENDIX C

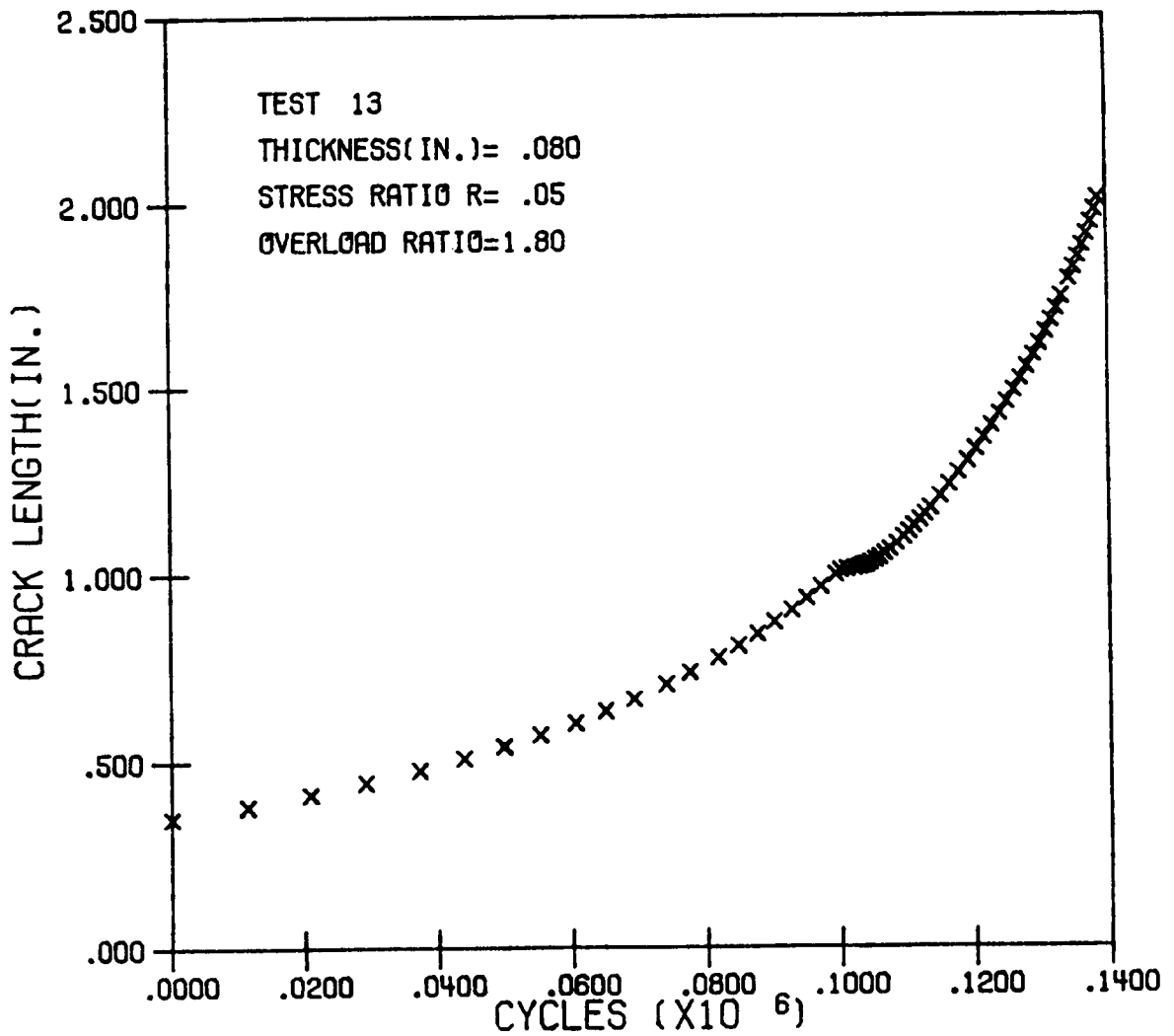


Figure C1. a versus N data from Test 13.

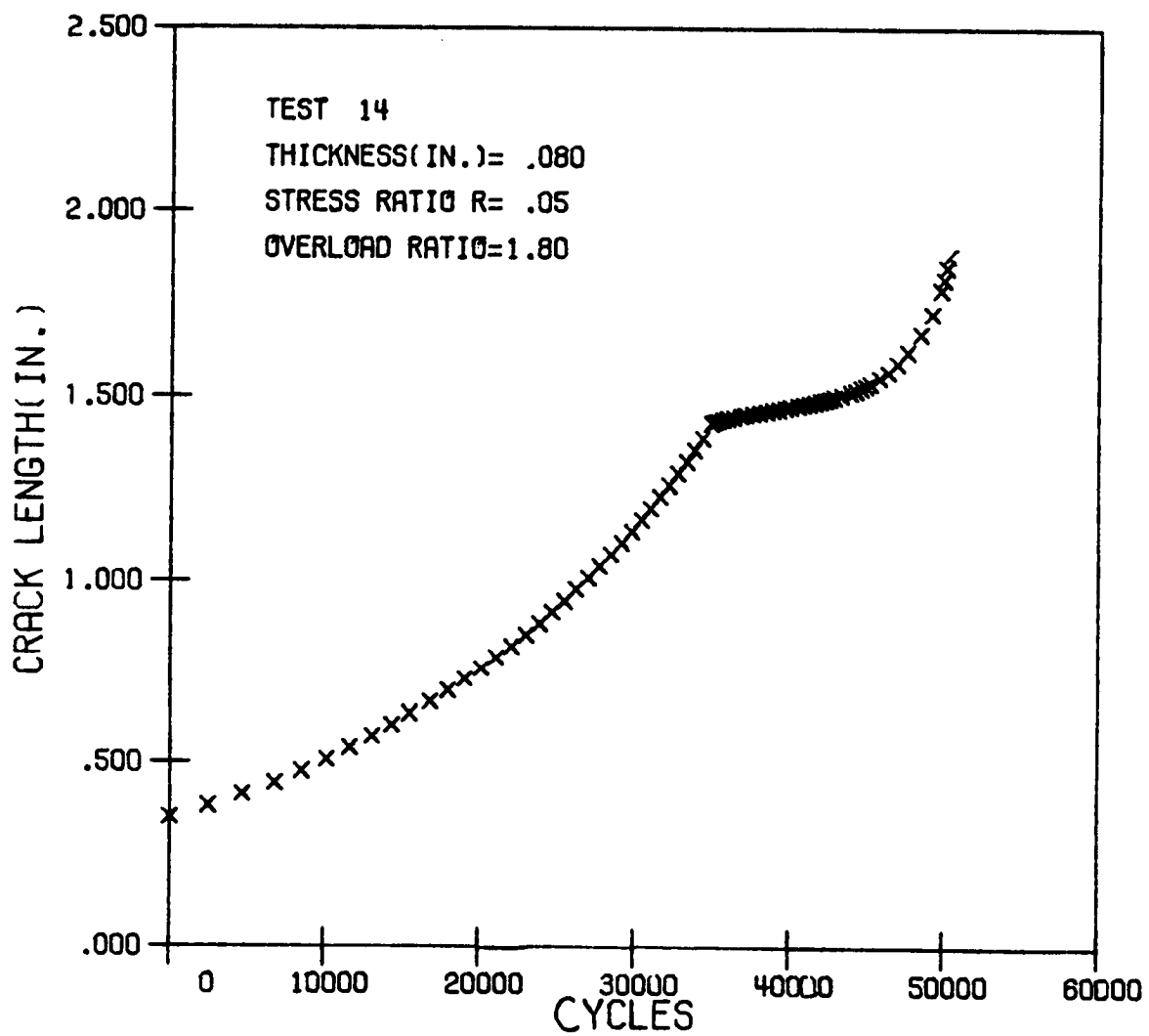


Figure C2. a versus N data from Test 14.

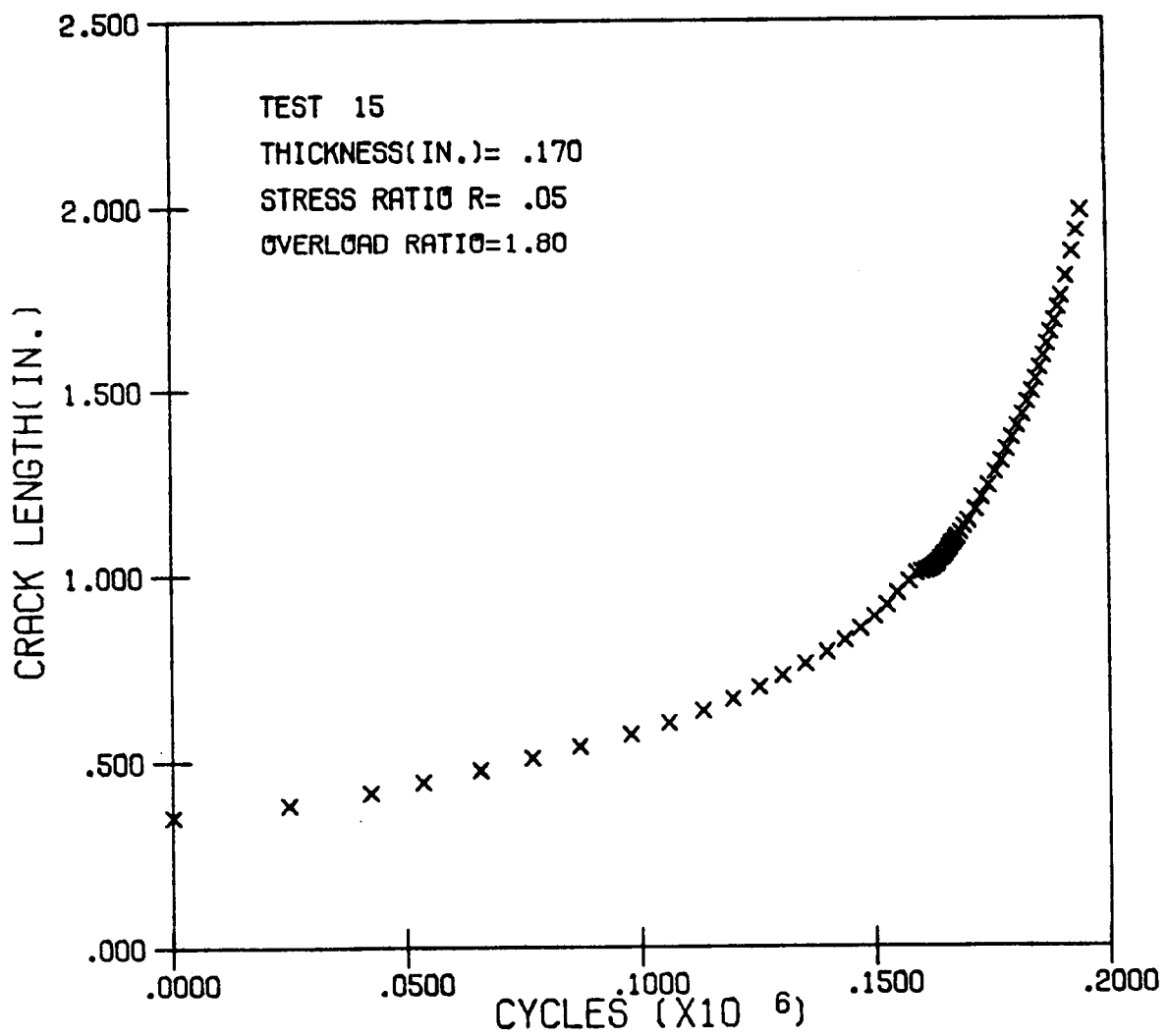


Figure C3. a versus N data from Test 15.

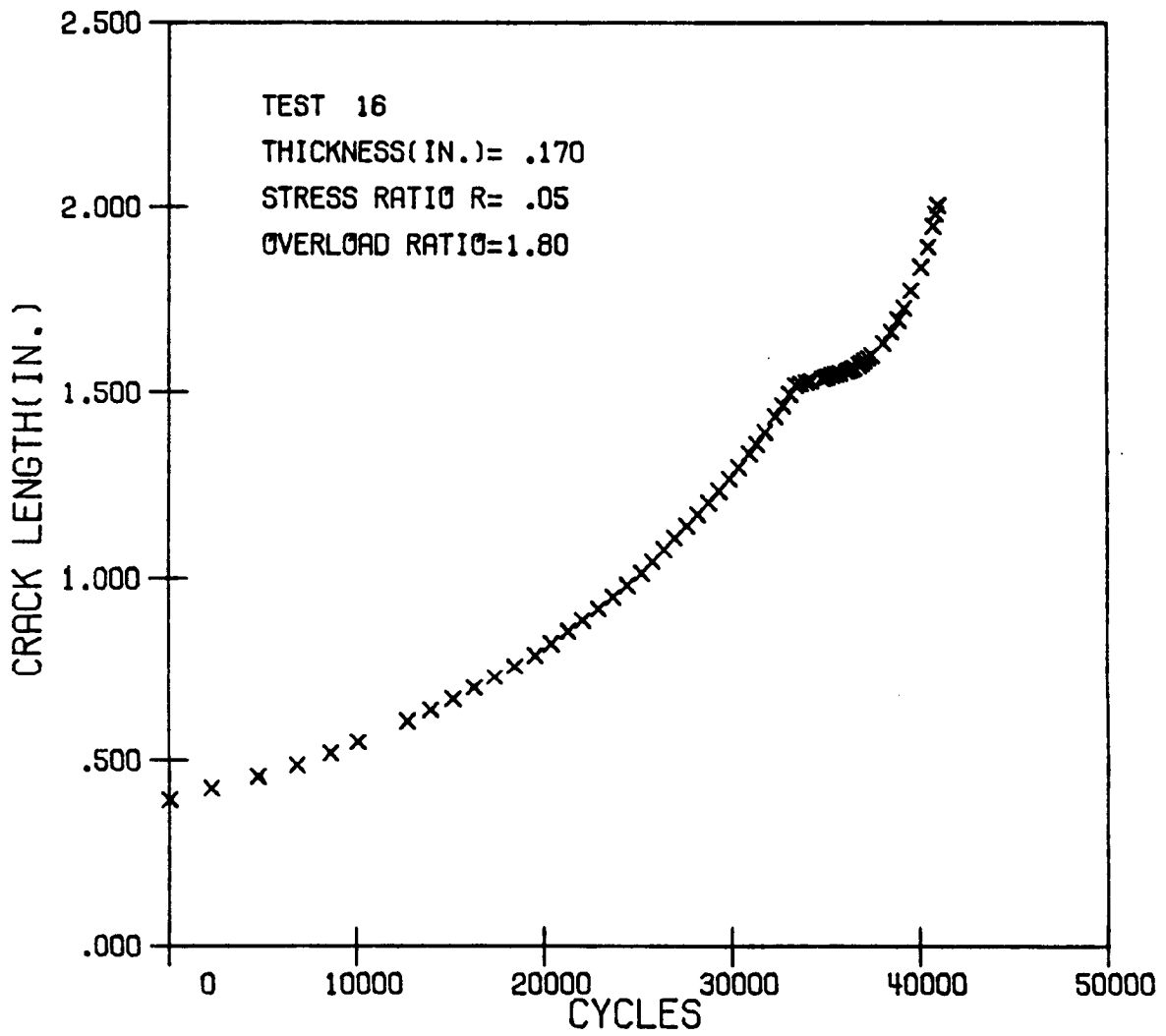


Figure C4. a versus N data from Test 16.

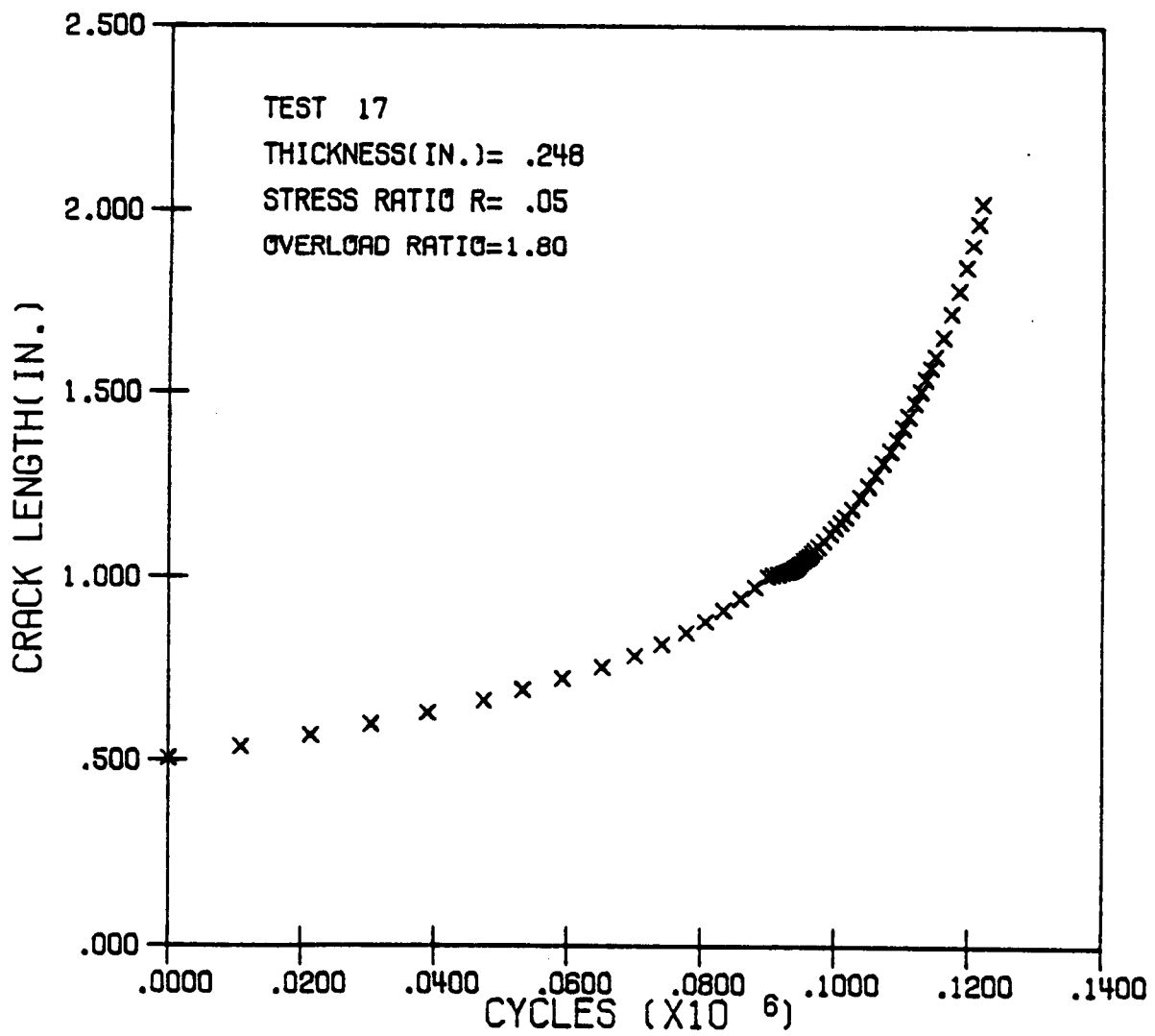


Figure C5. a versus N data from Test 17.

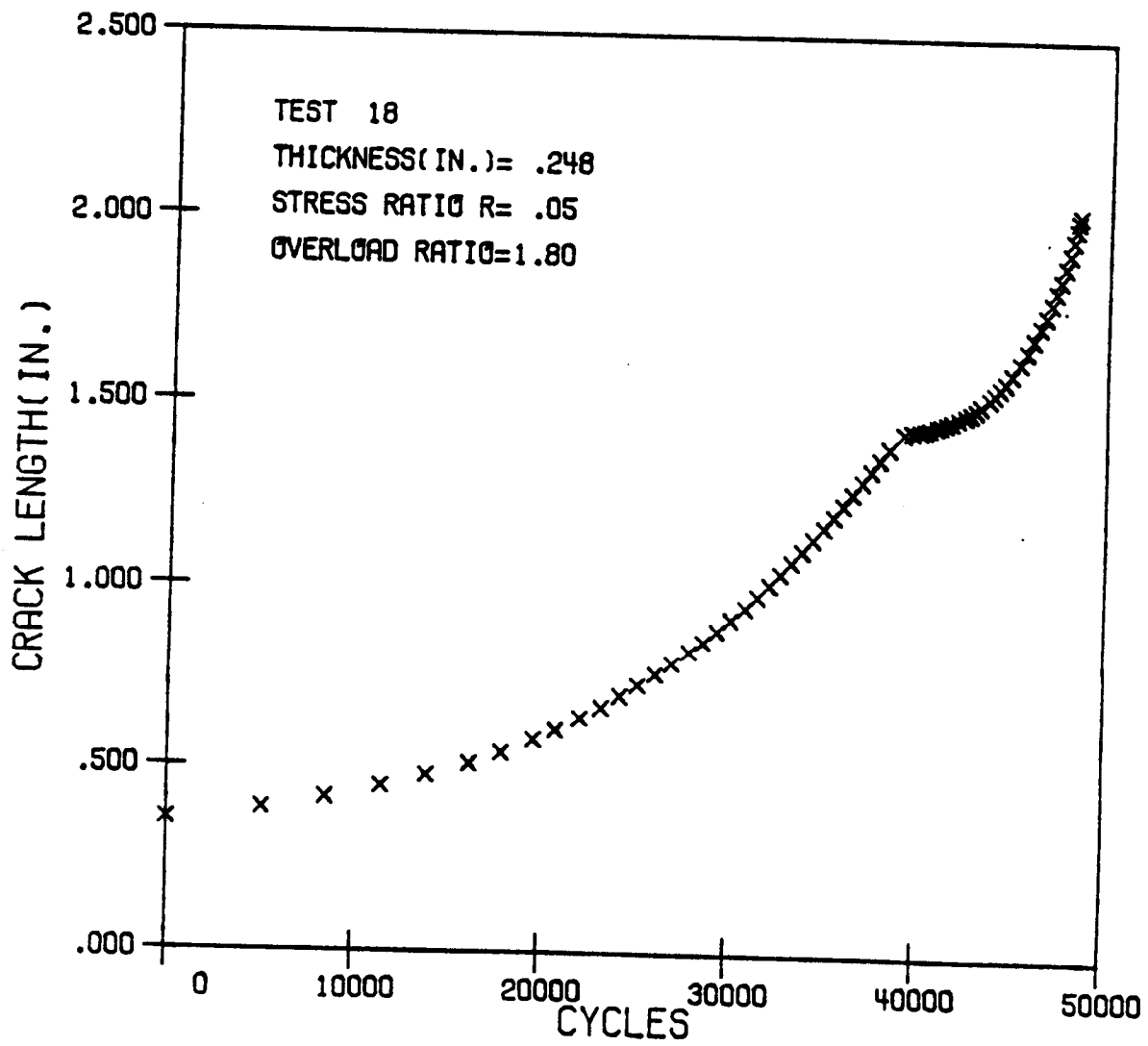


Figure C6. a versus N data from Test 18.

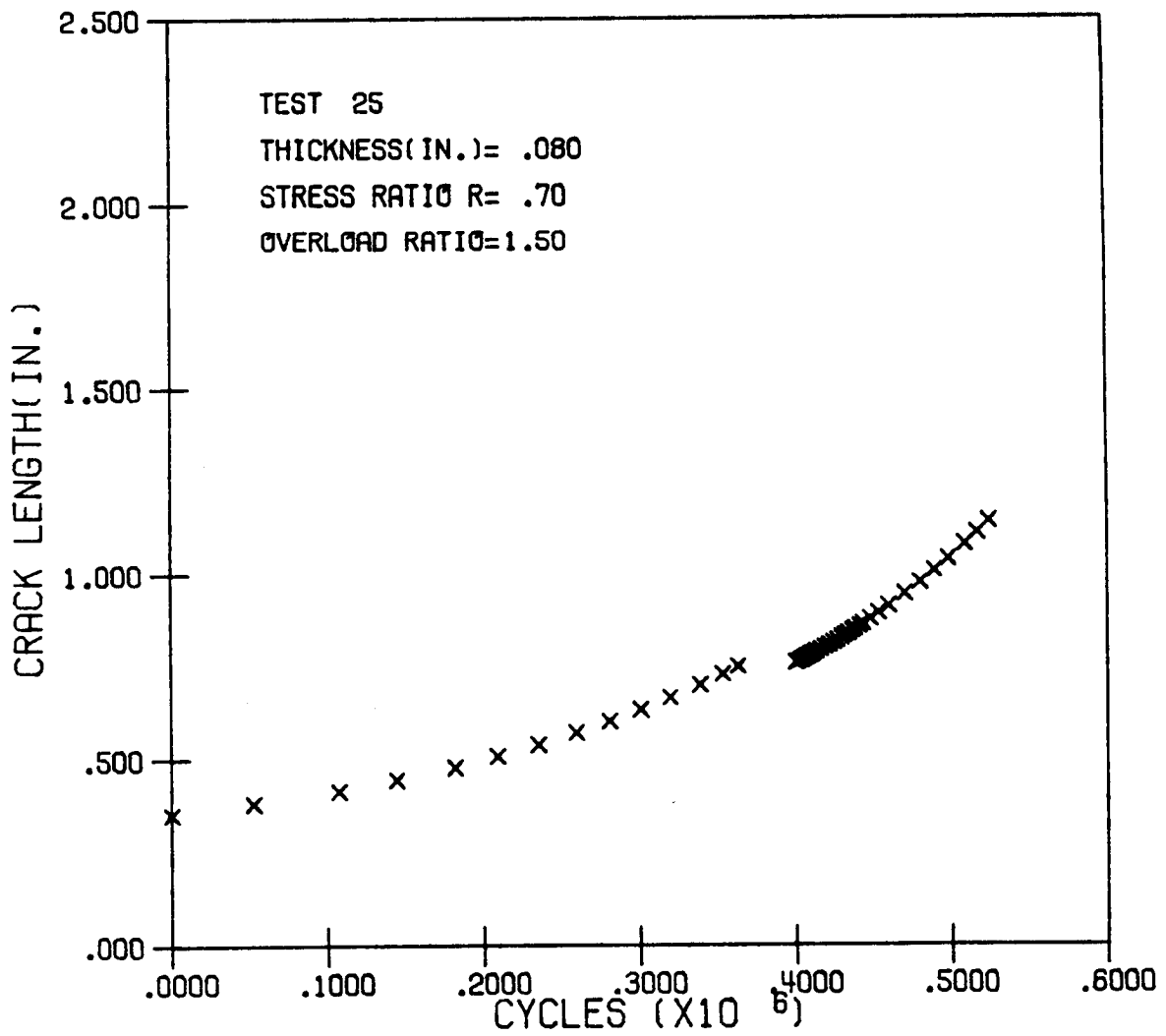


Figure C7. a versus N data from Test 25.

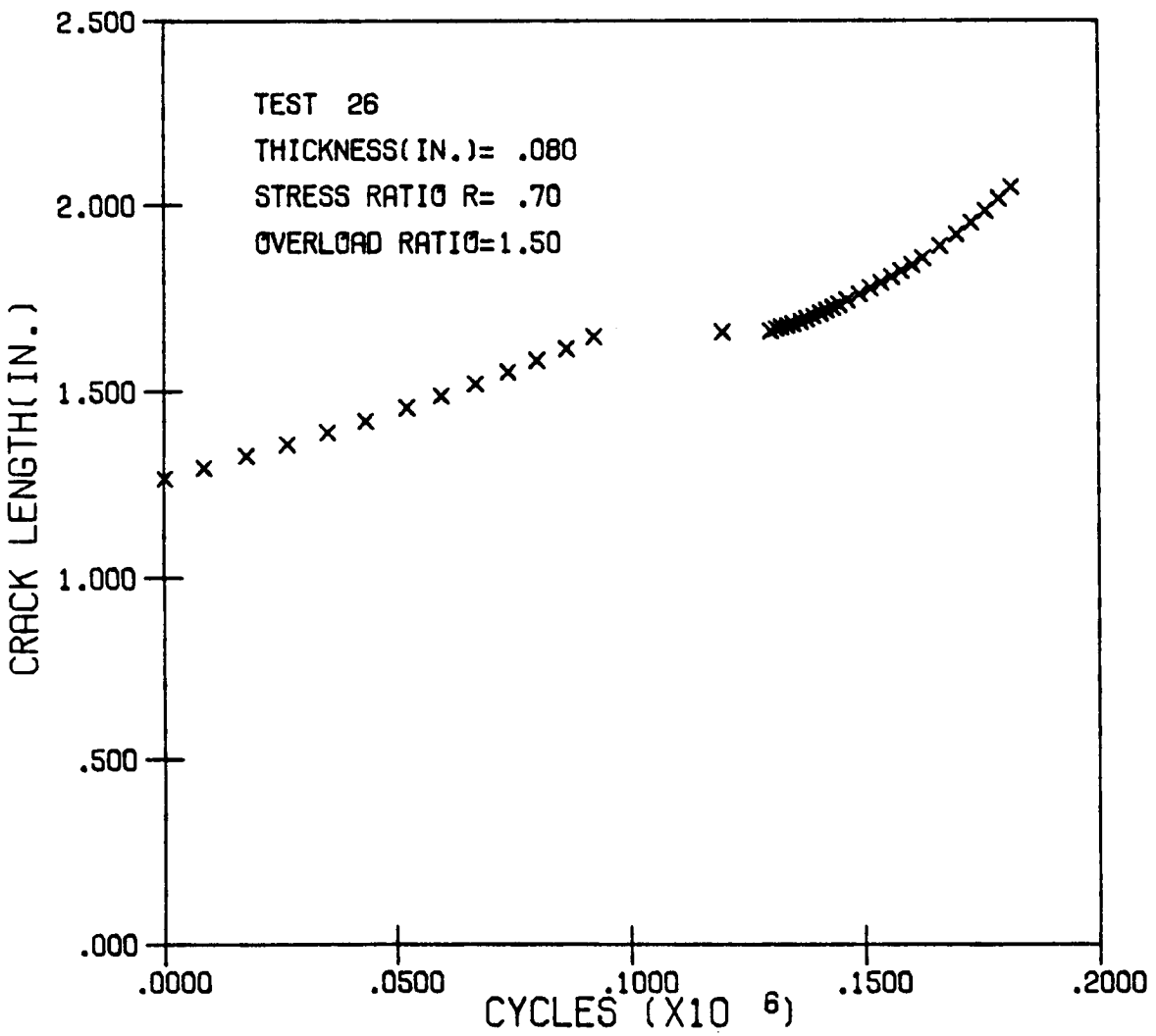


Figure CB. a versus N data from Test 26.

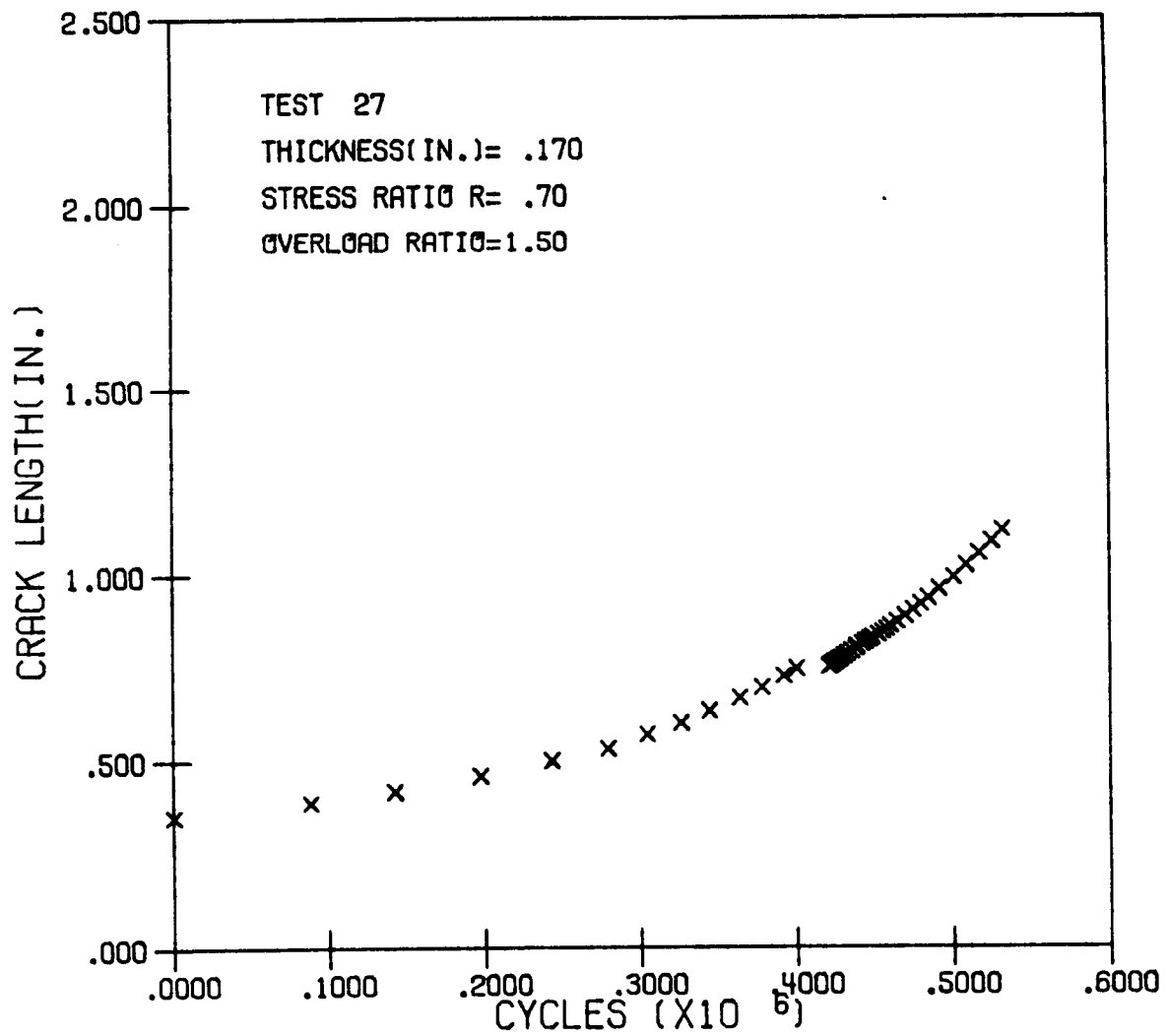


Figure C9. a versus N data from Test 27.

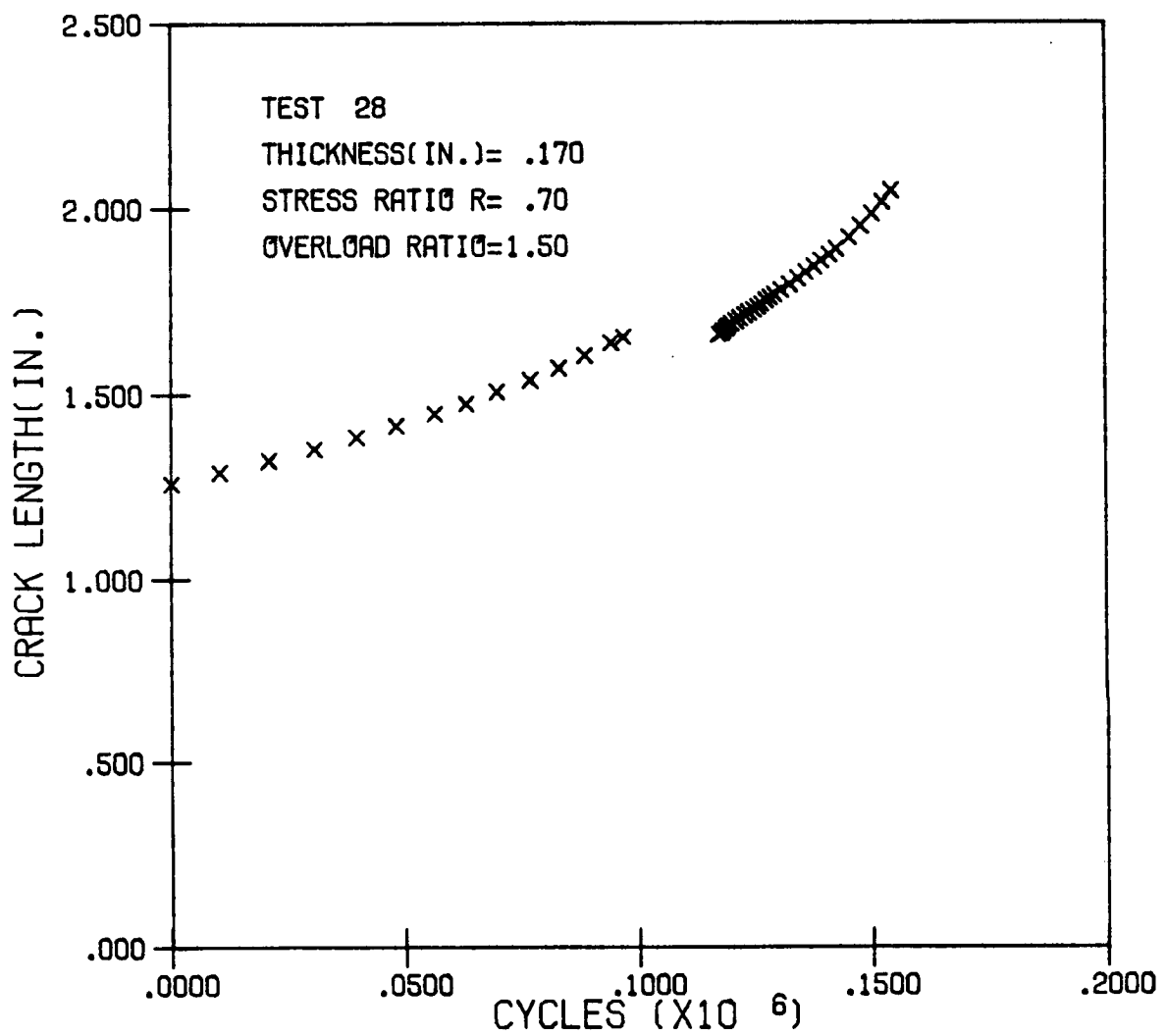


Figure C10. a versus N data from Test 28.

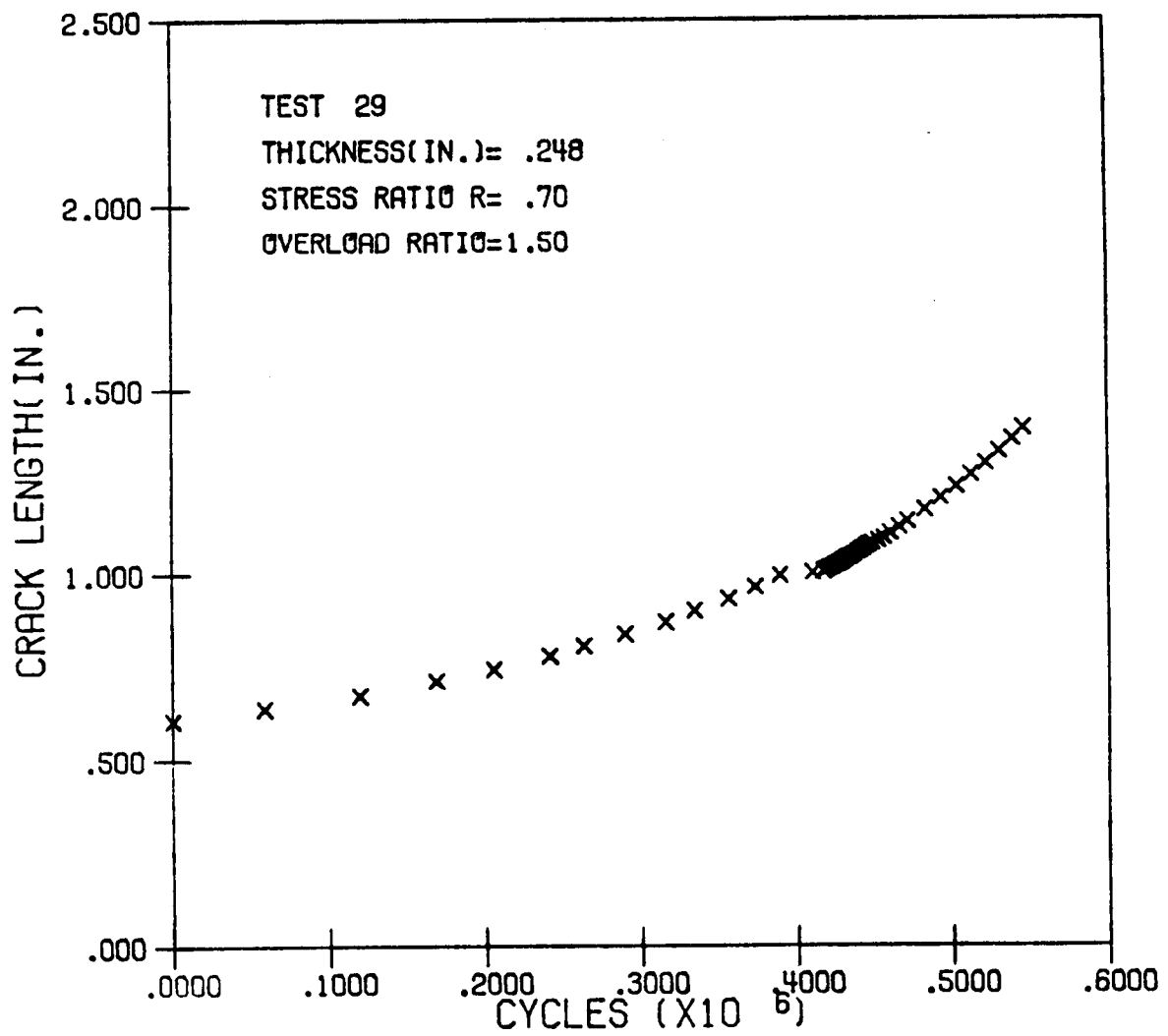


Figure C11. a versus N data from Test 29.

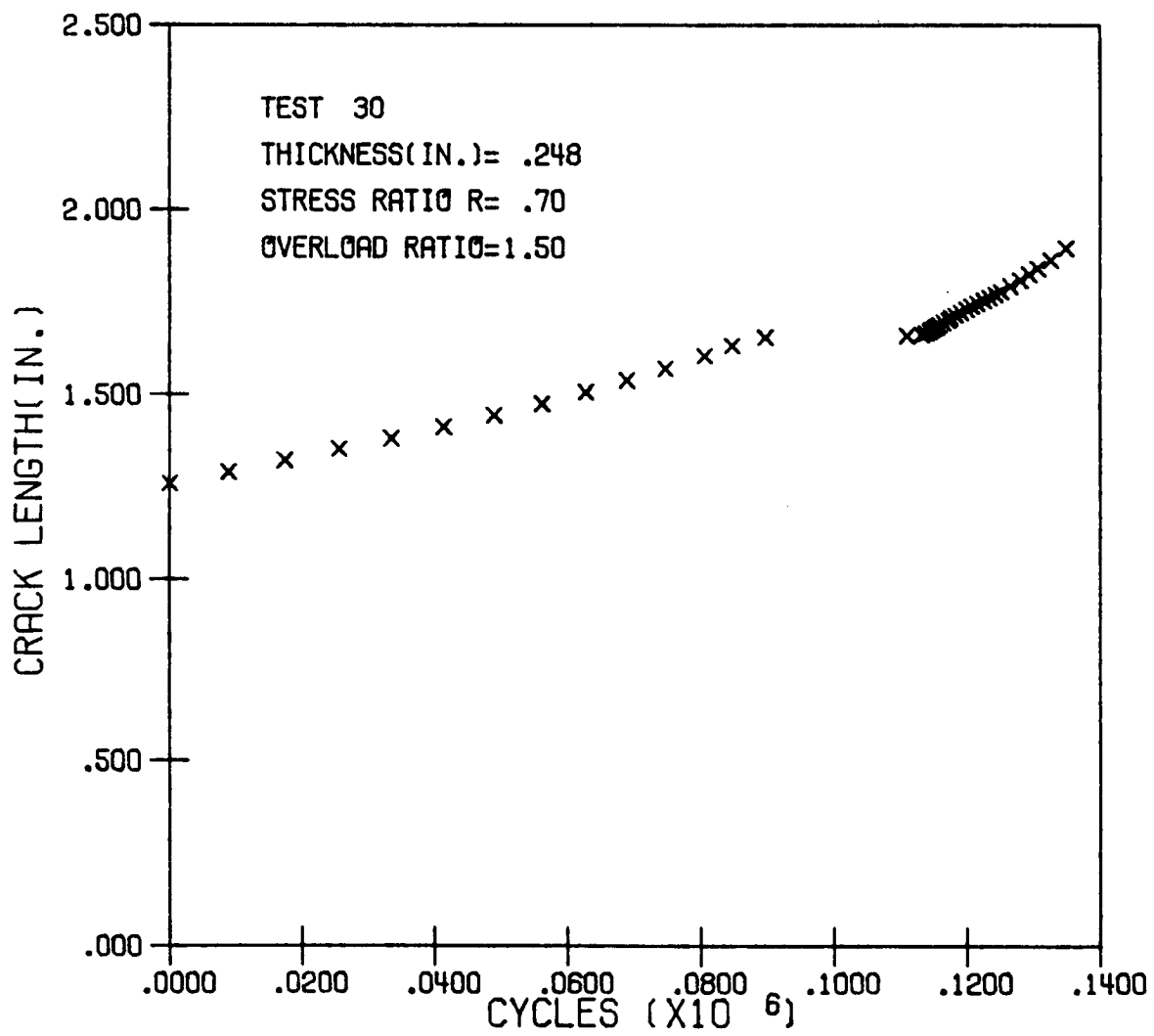


Figure C12. a versus N data from Test 30.

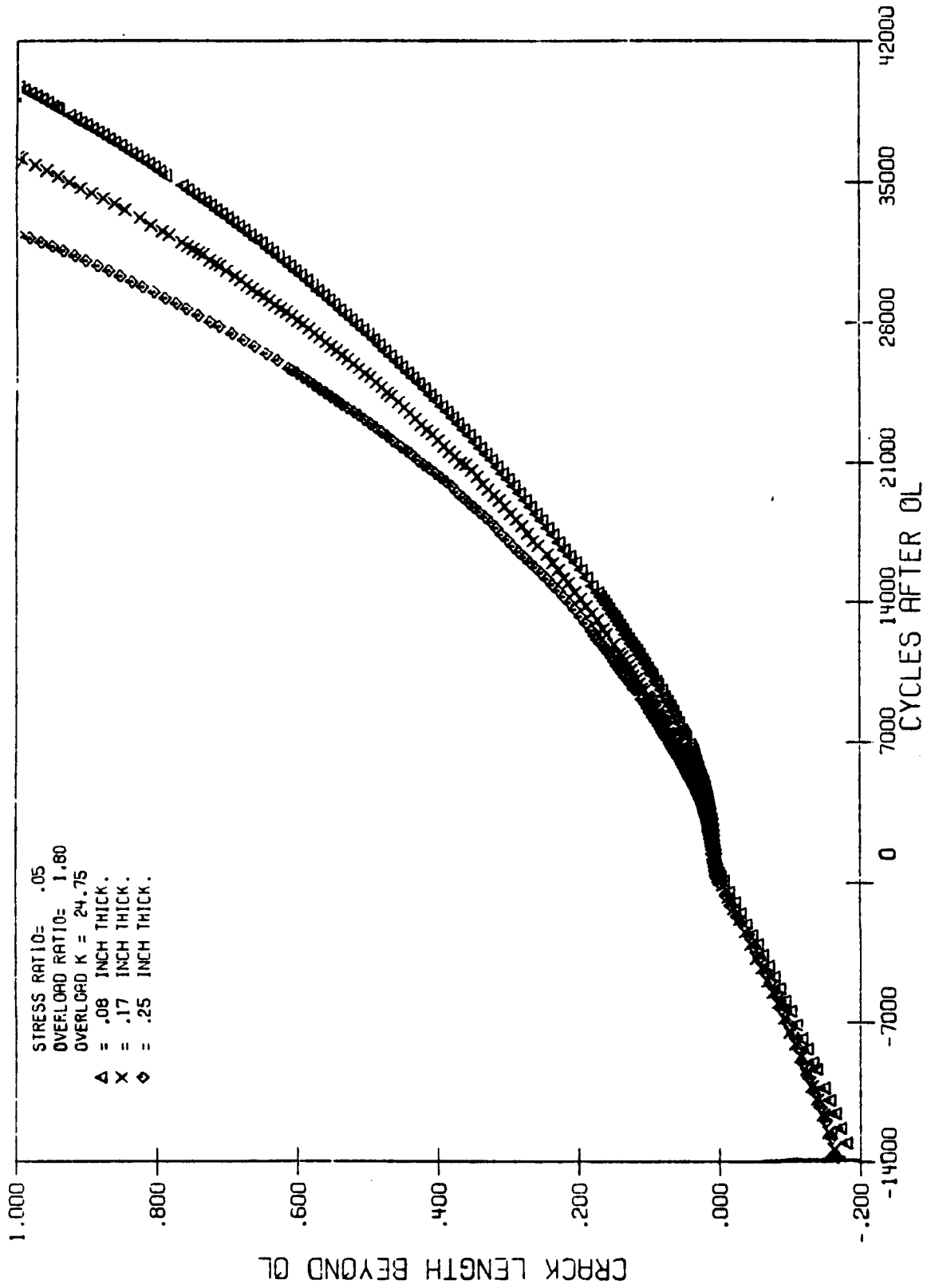


Figure D1. a versus N data after overload from Tests 13, 15 and 17.

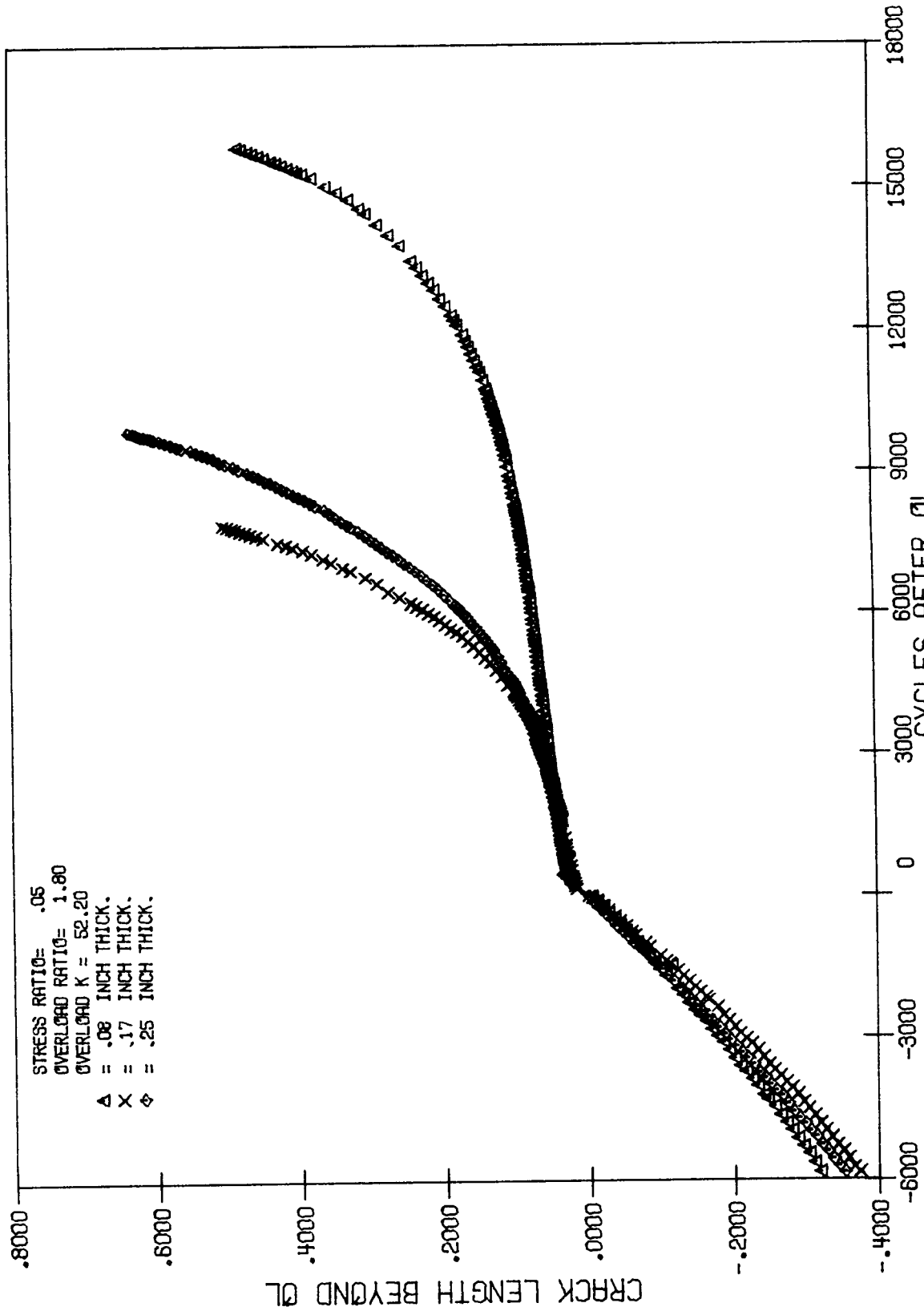


Figure D2. a versus N data after overload from Tests 14, 16 and 18.

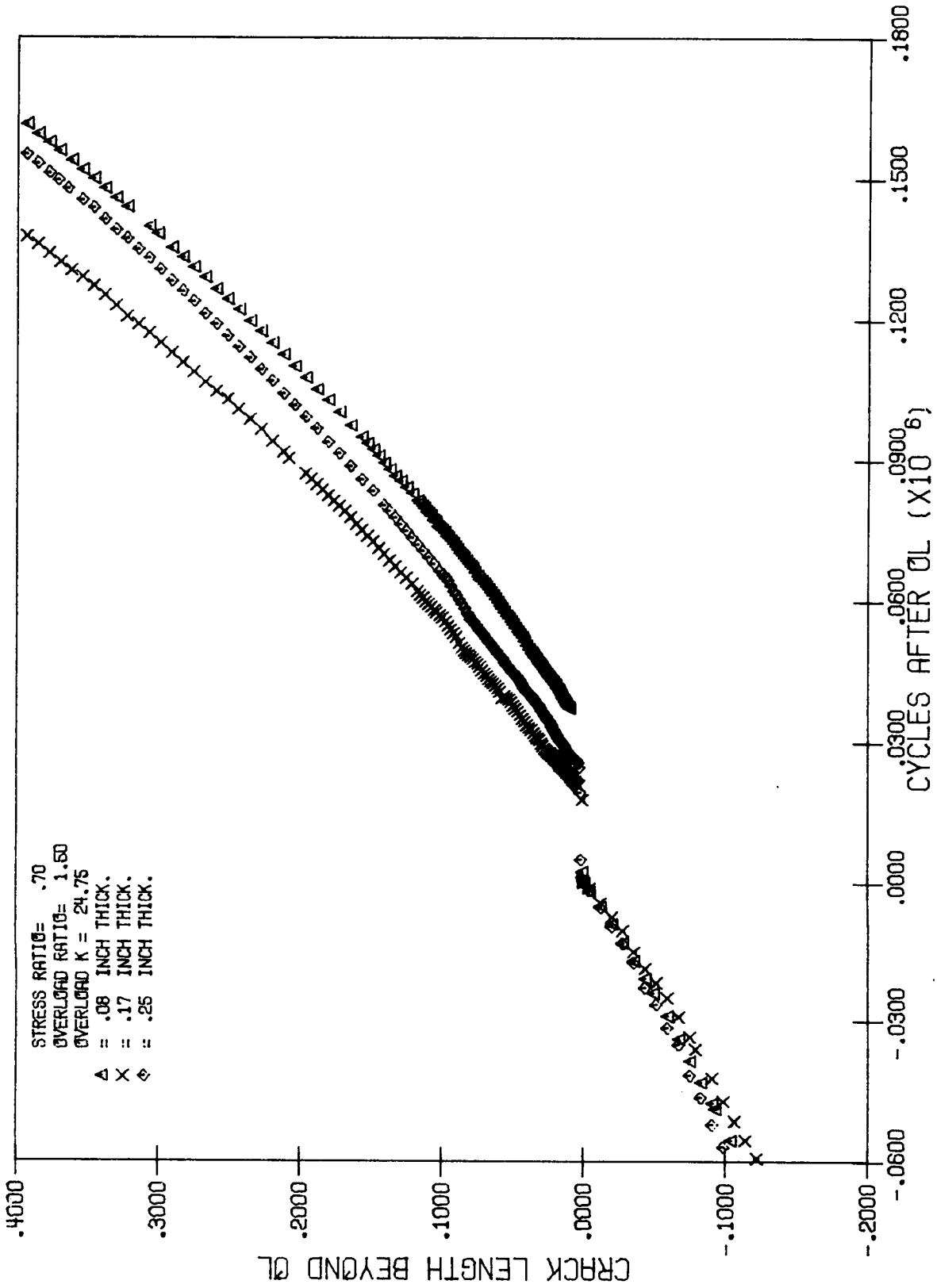


Figure D3. a versus N data after overload from Tests 25, 27 and 29.

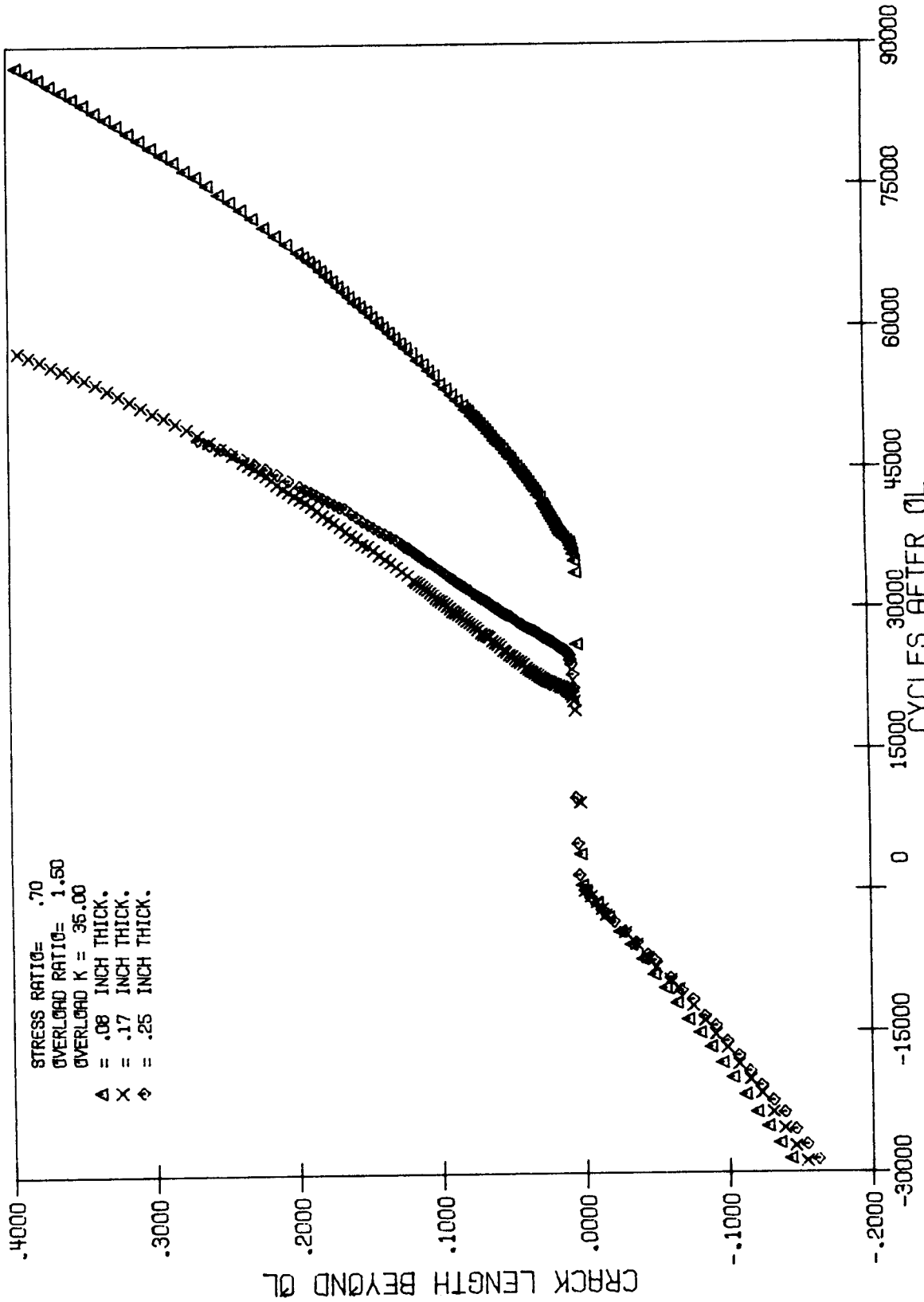


Figure D4. a versus N data after overload from Tests 26, 28 and 30.

APPENDIX E

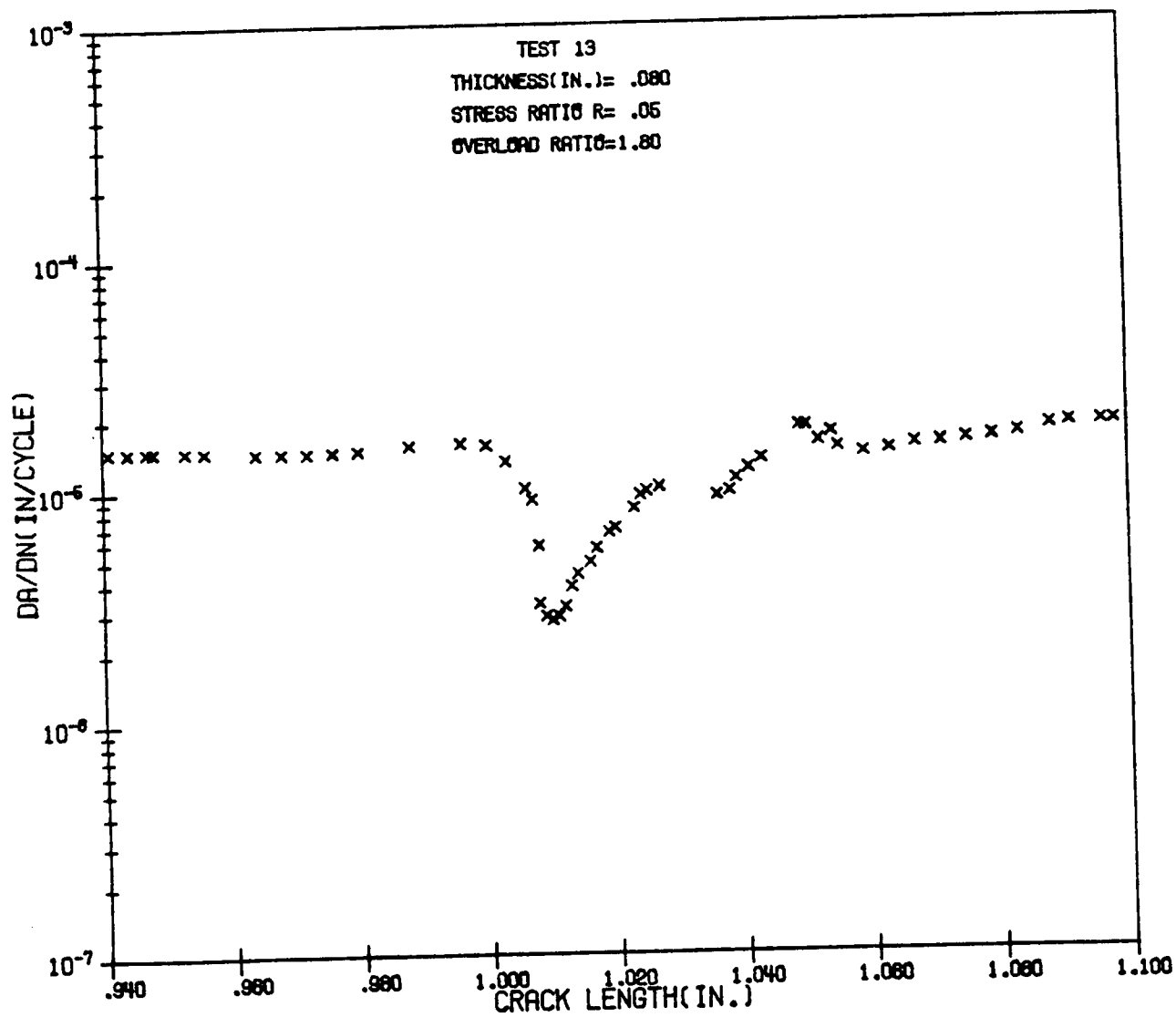


Figure E1. FCP rate data after overload for Test 13.

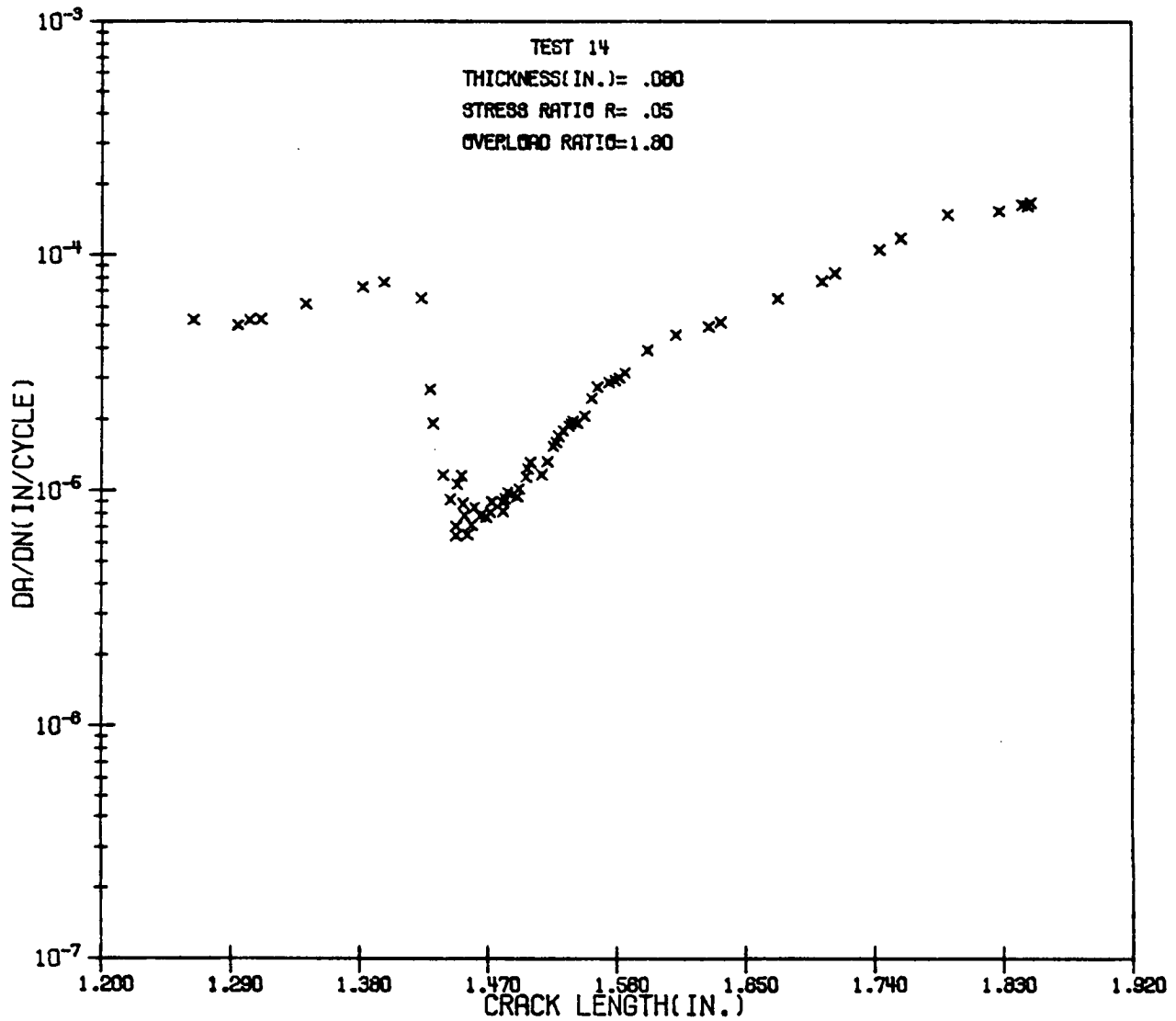


Figure E2. FCP rate data after overload for Test 14.

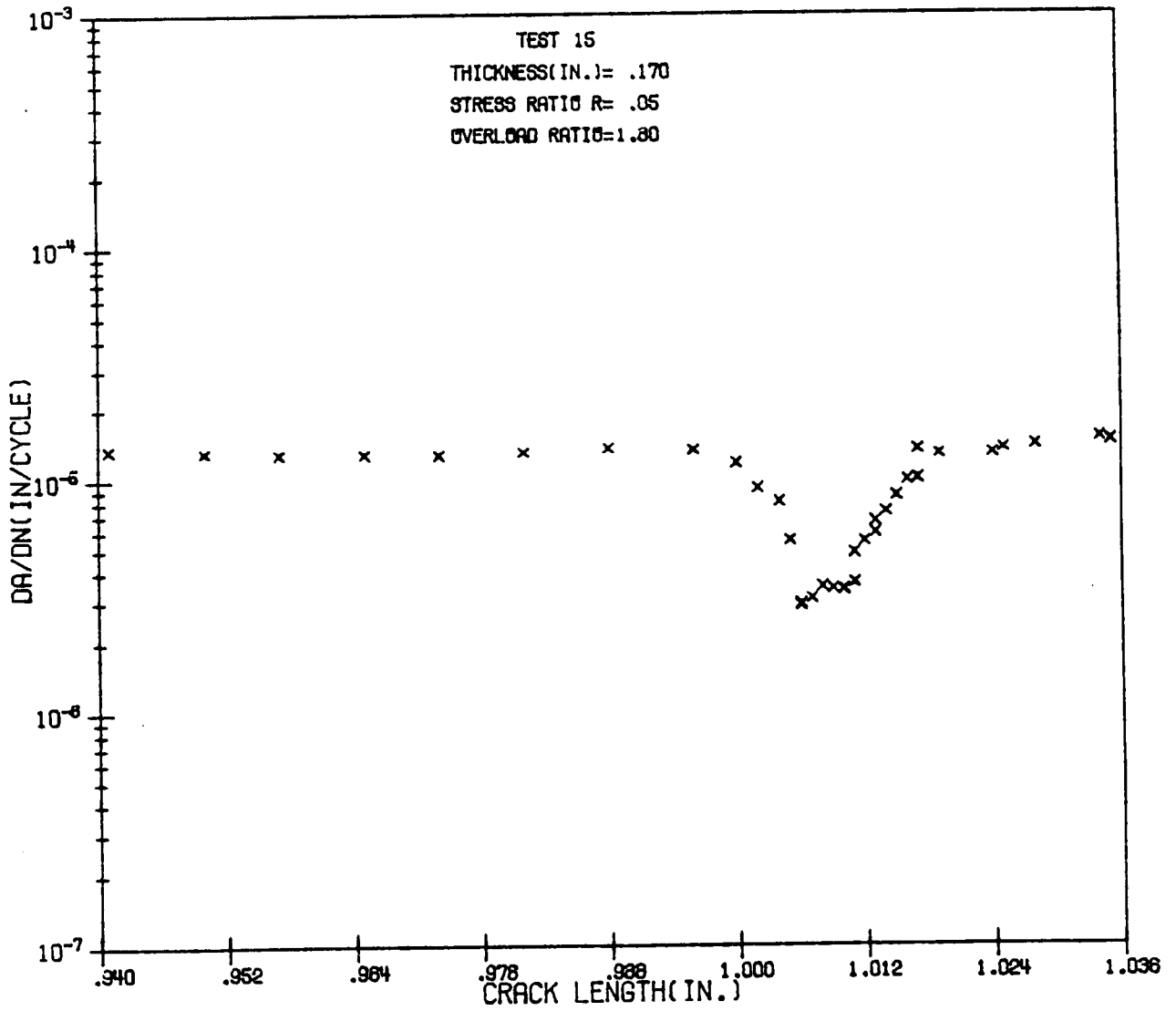


Figure E3. FCP rate data after overload for Test 15.

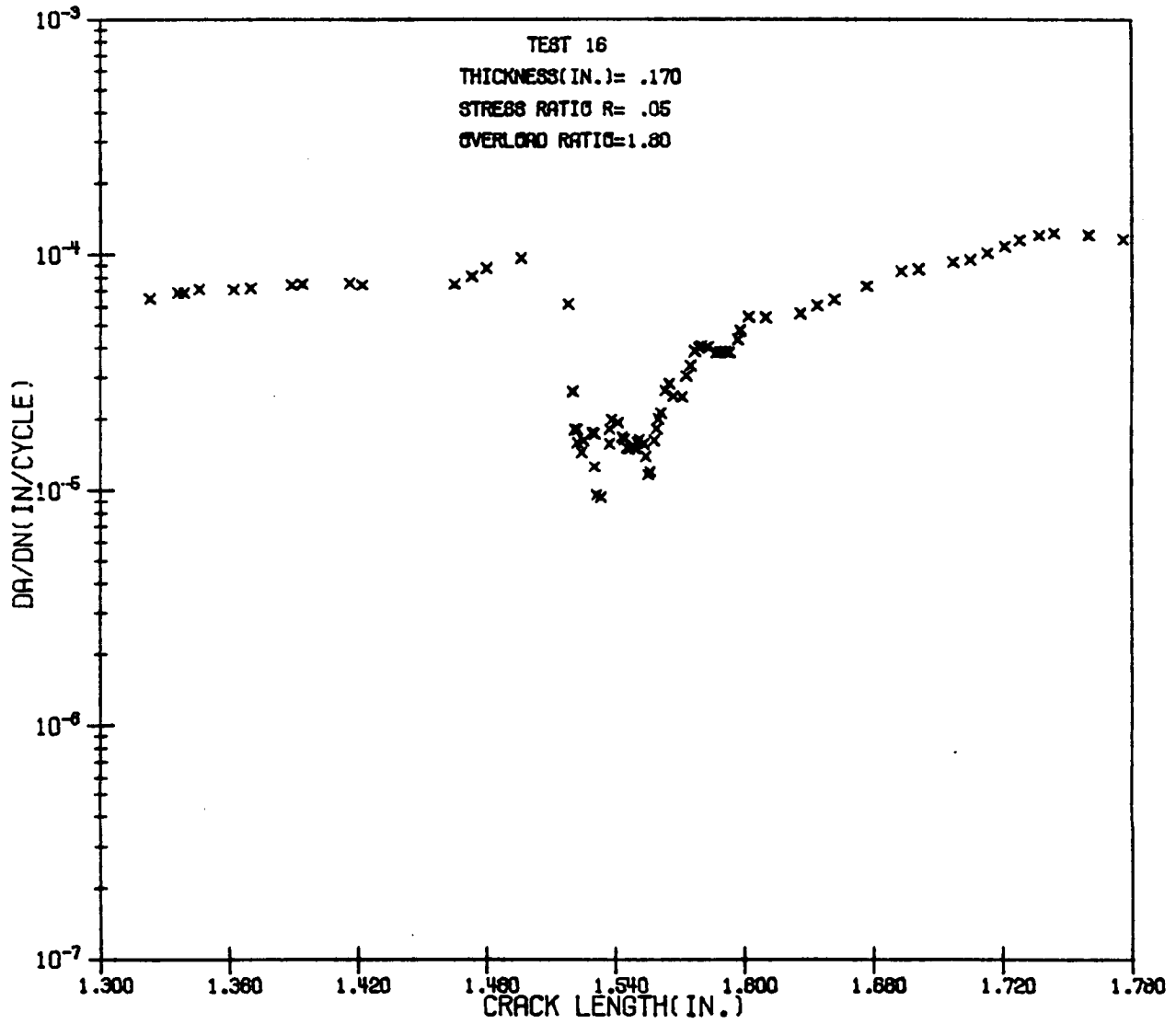


Figure E4. FCP rate data after overload for Test 16.

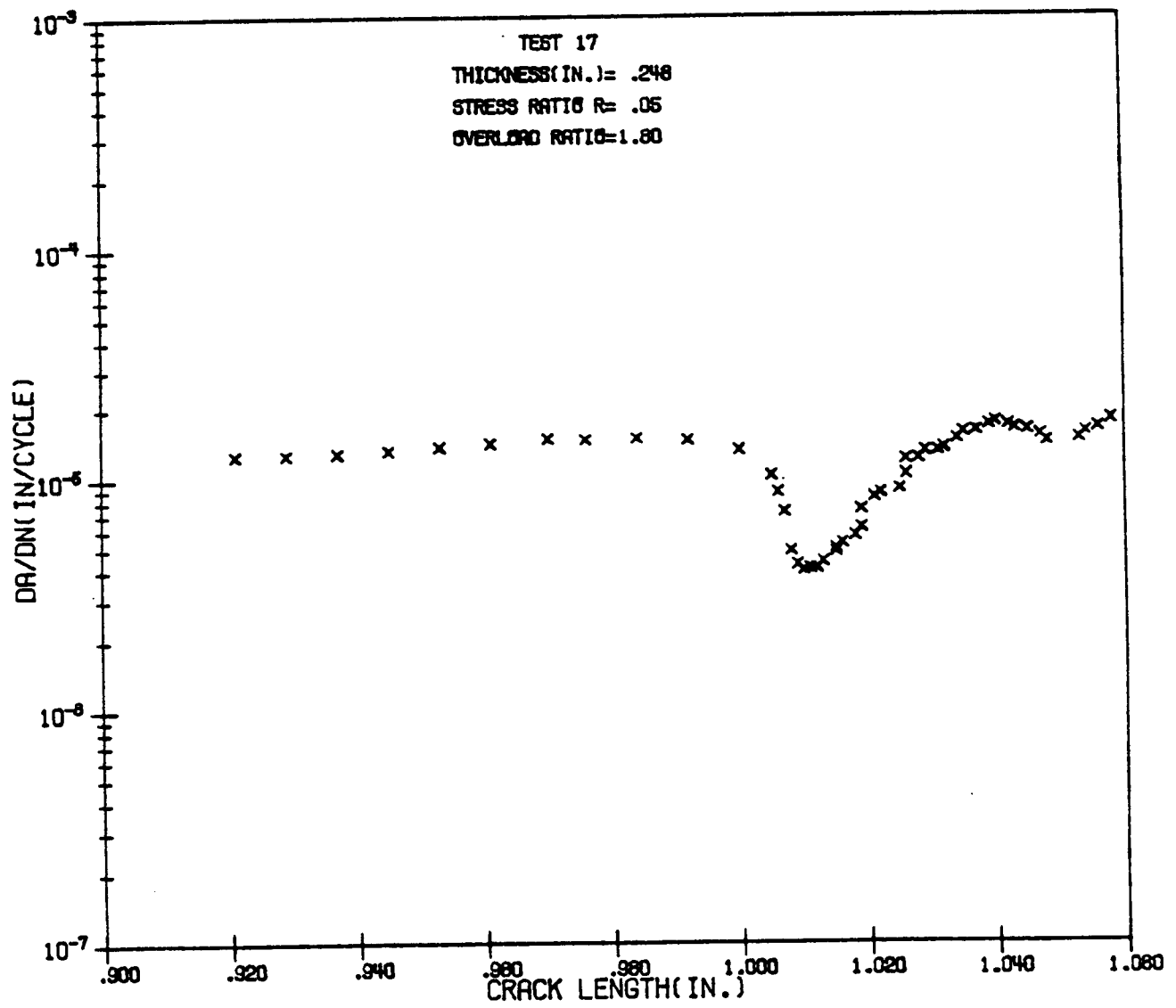


Figure E5. FCP rate data after overload for Test 17.

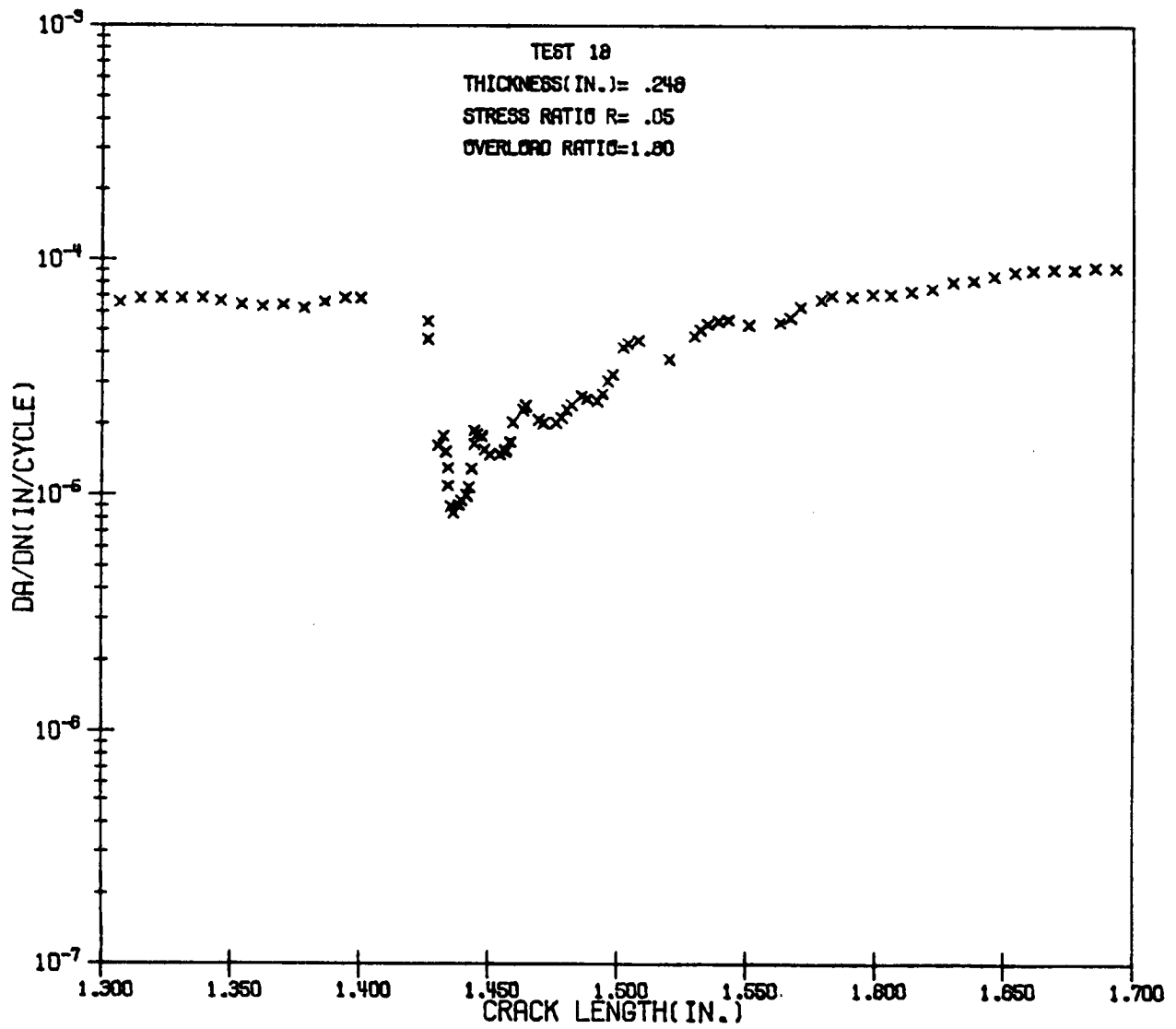


Figure E6. FCP rate data after overload for Test 18.

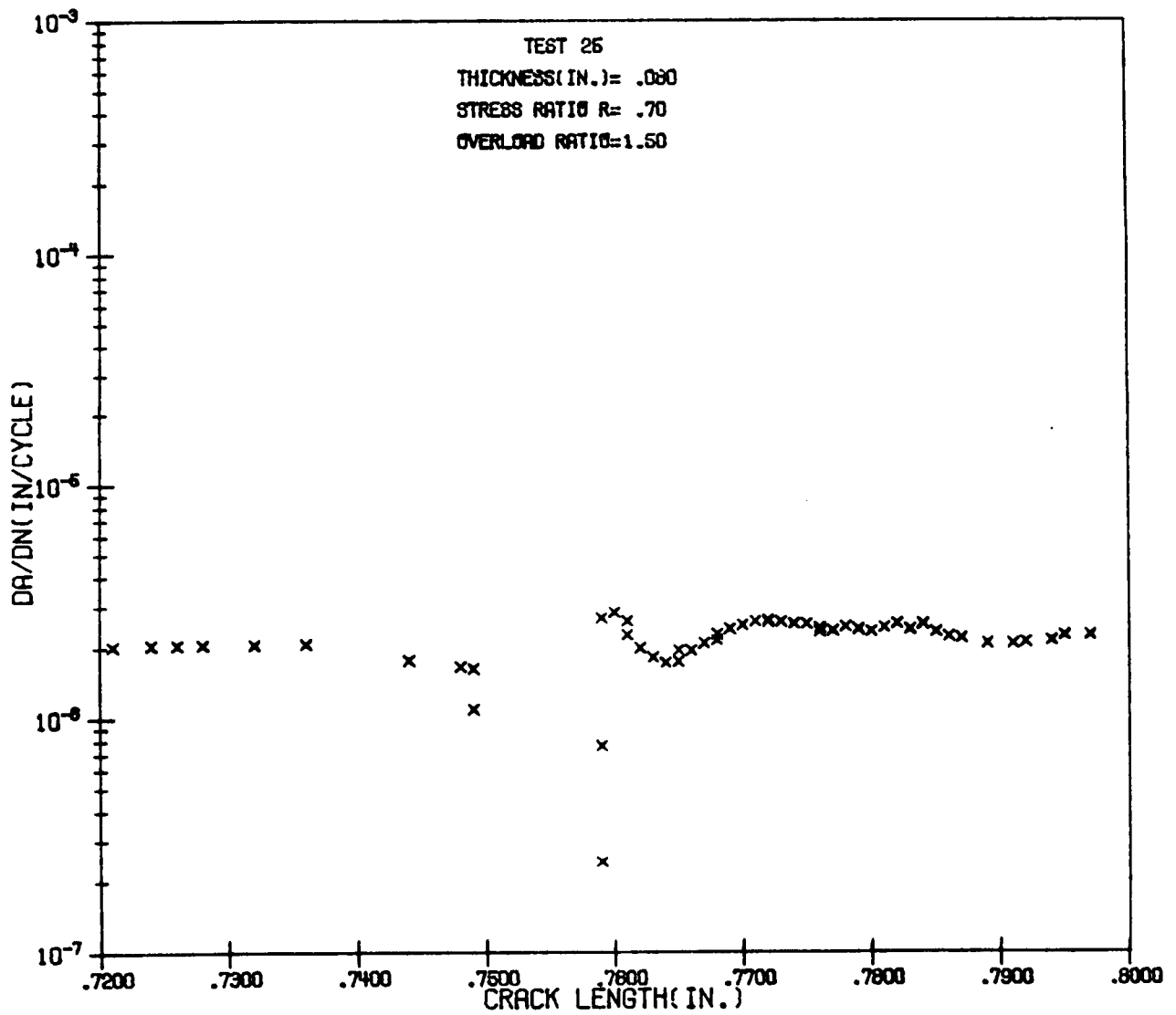


Figure E7. FCP rate data after overload for Test 25.

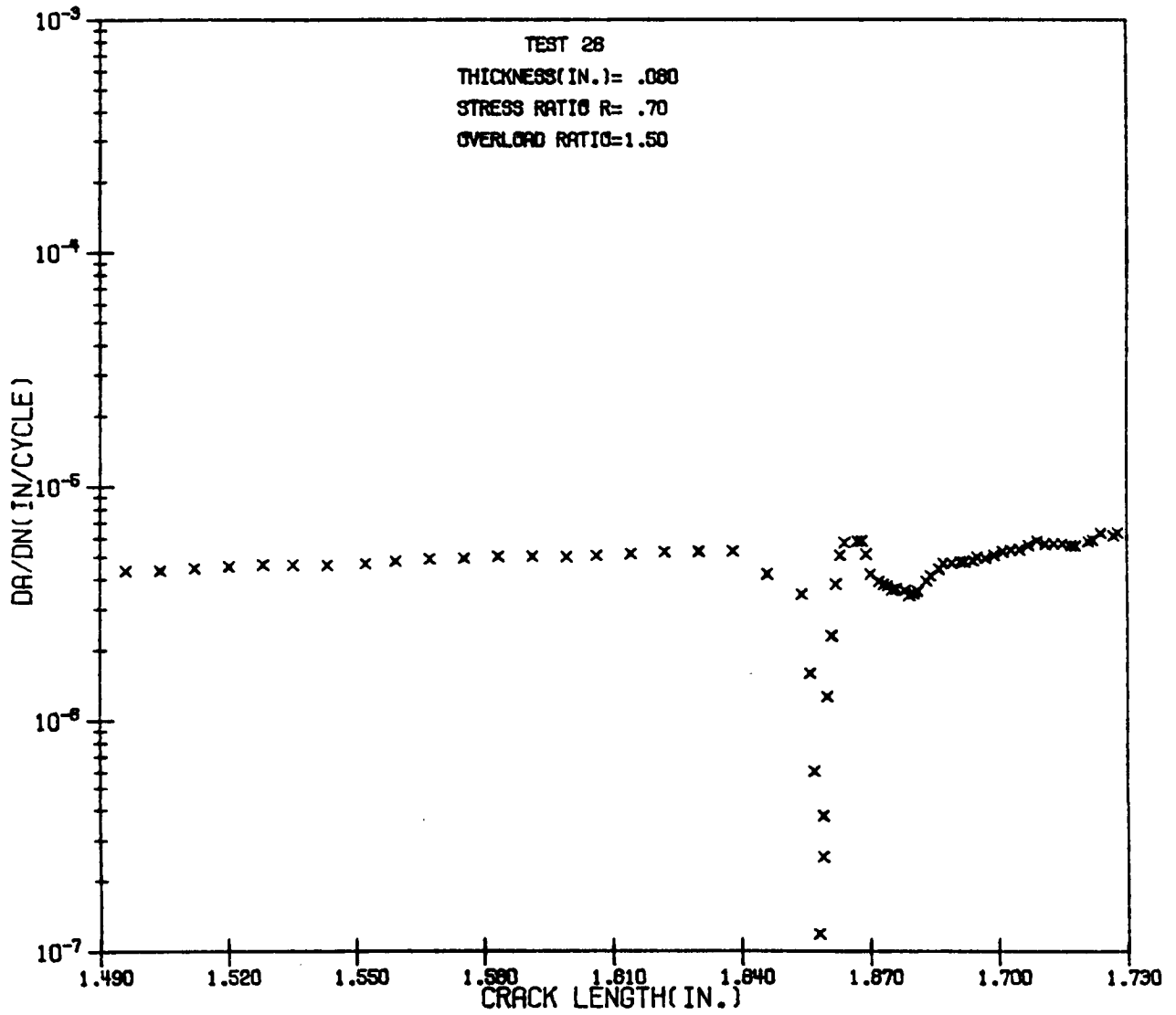


Figure EB. FCP rate data after overload for Test 26.

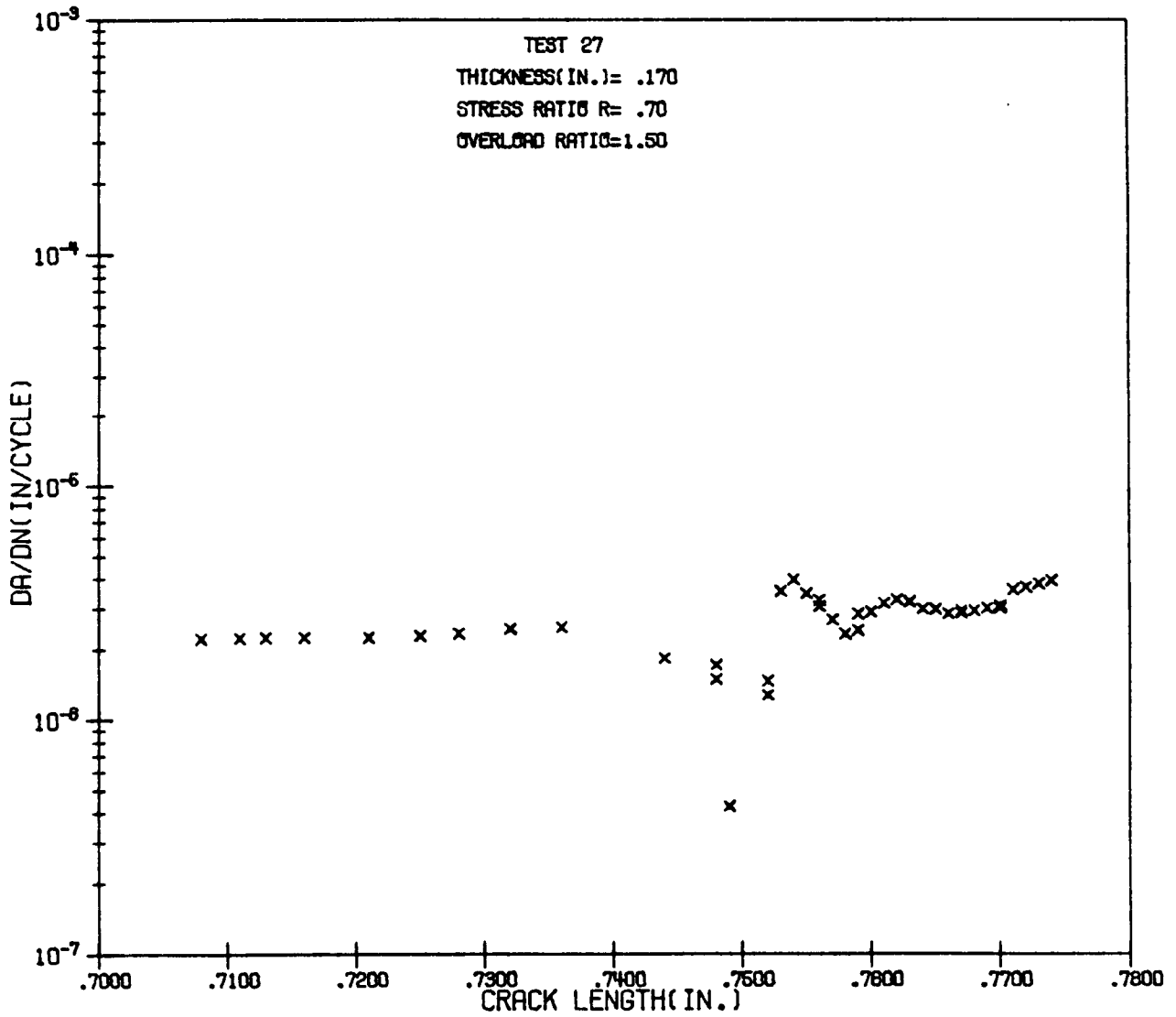


Figure E9. FCP rate data after overload for Test 27.

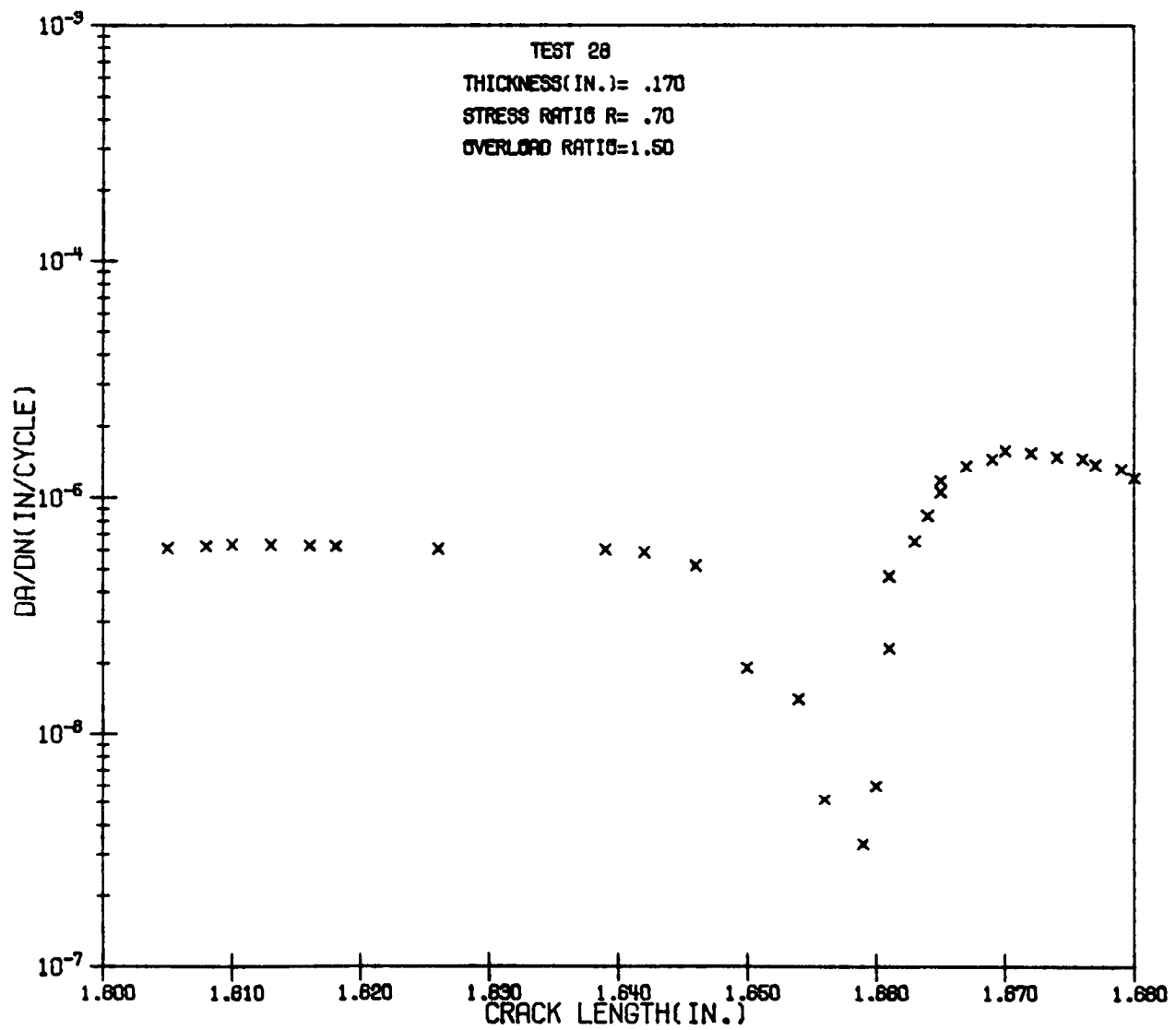


Figure E10. FCP rate data after overload for Test 28.

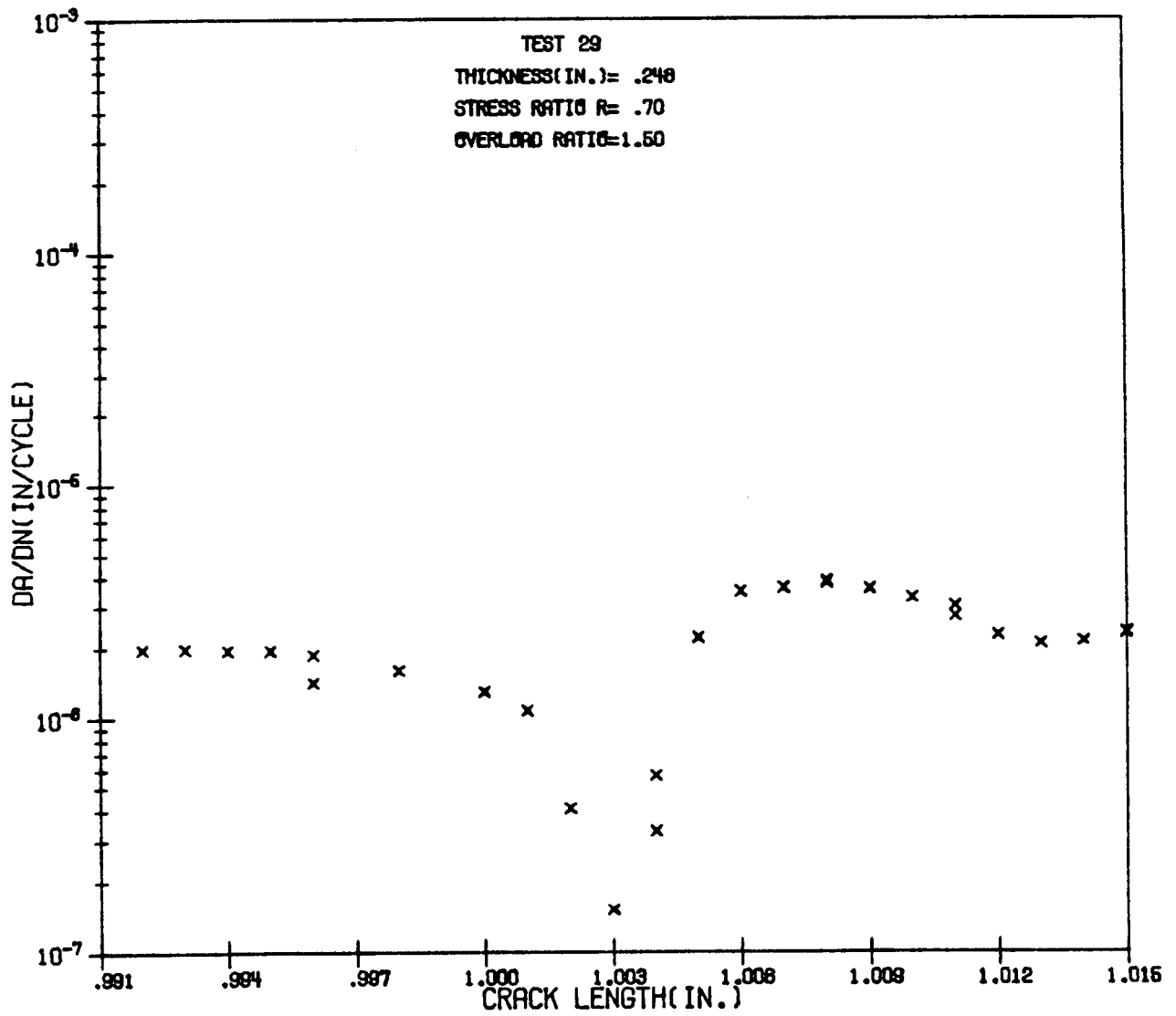


Figure E11. FCP rate data after overload for Test 29.

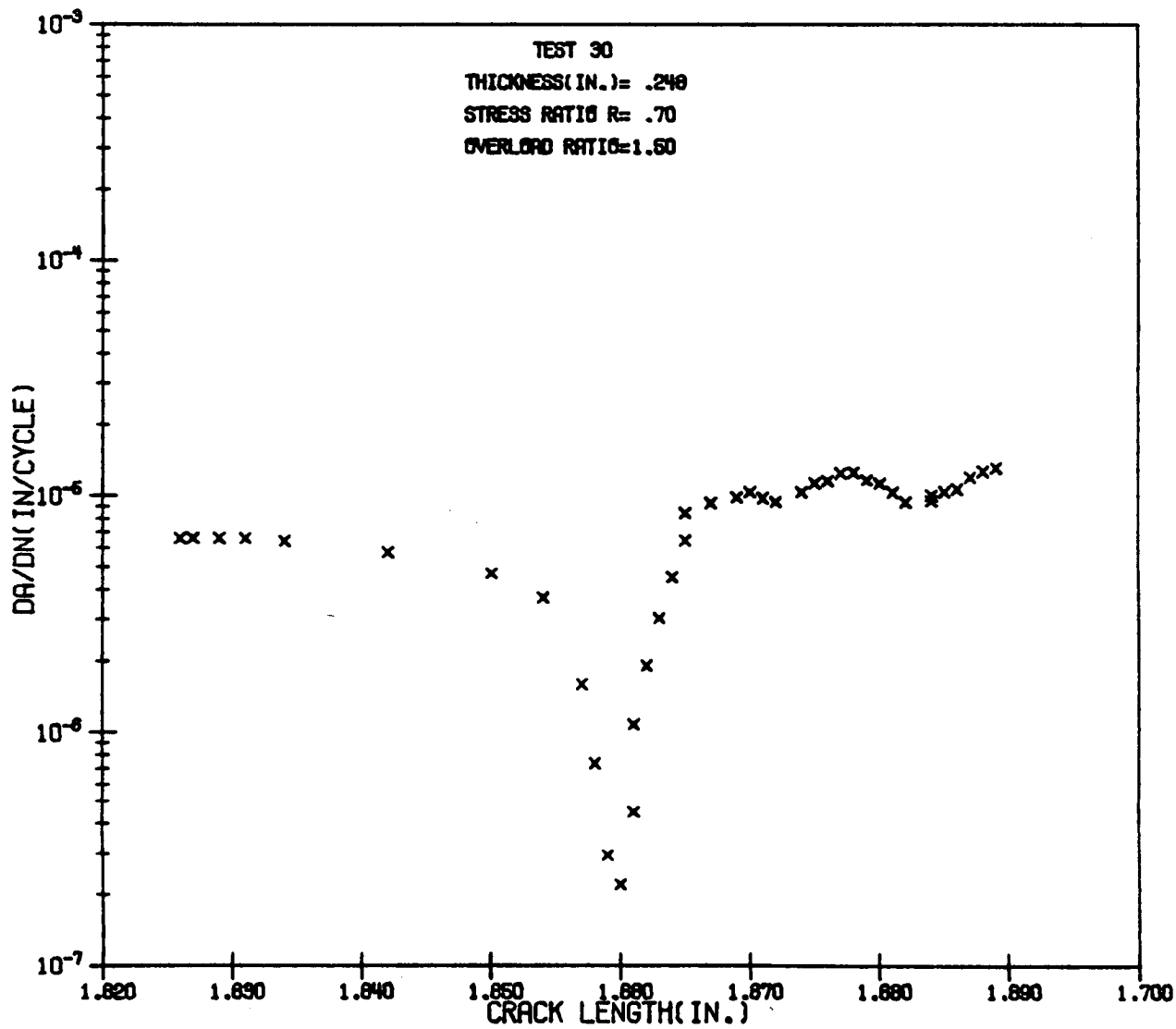


Figure E12. FCP rate data after overload for Test 30.

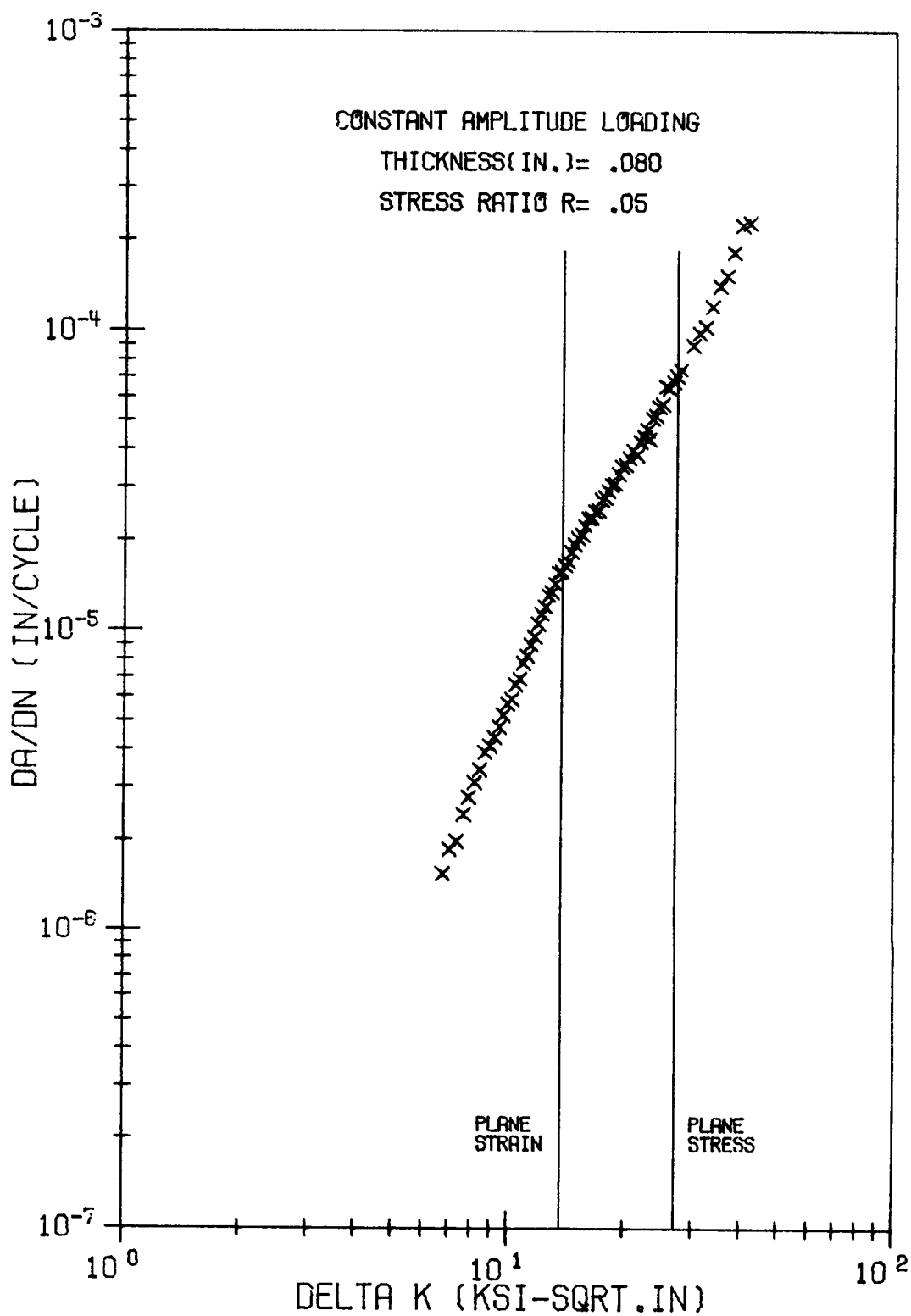


Figure F1. Comparison of theoretical transition estimations with the actual data for R=0.05, t=0.08.

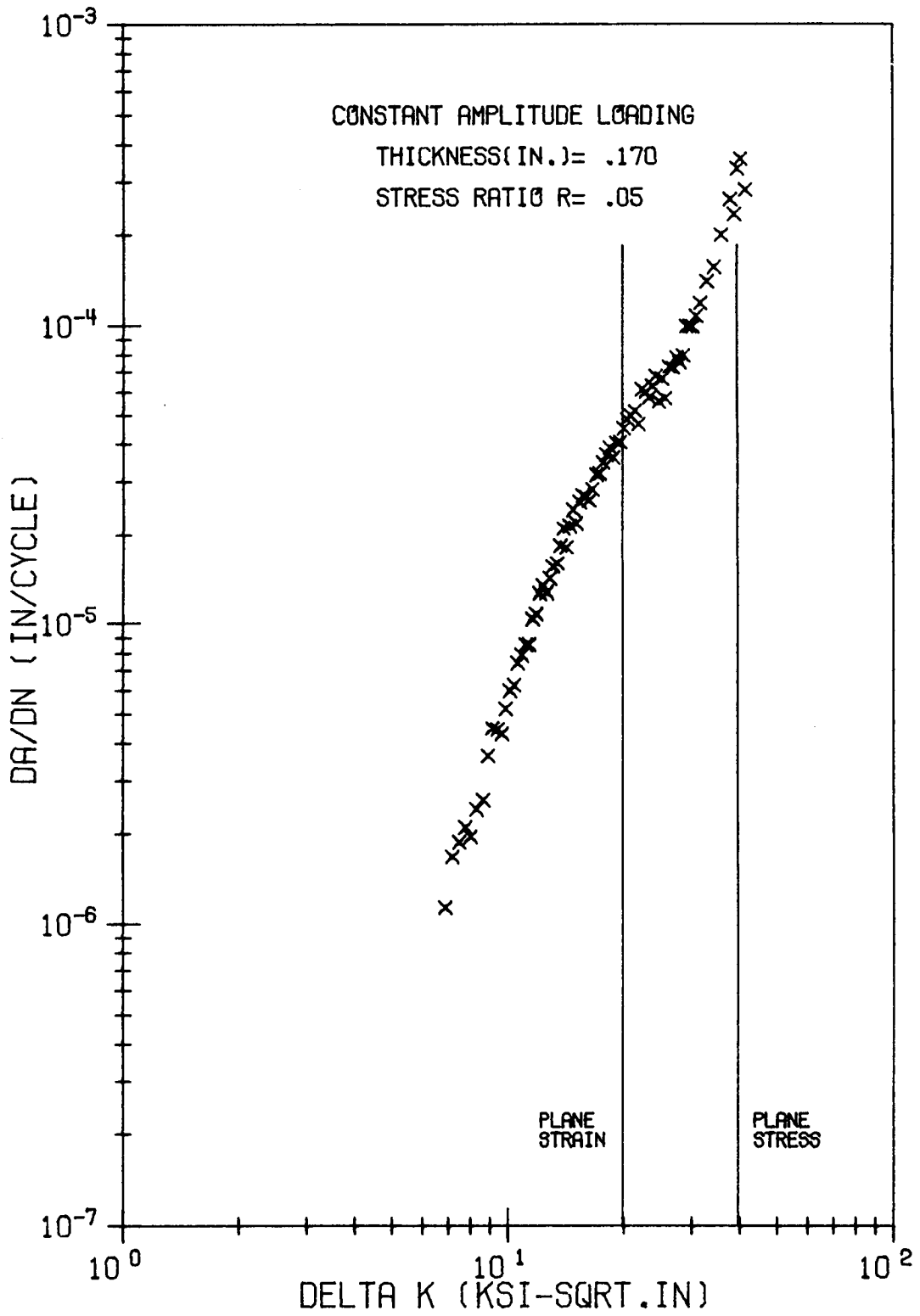


Figure F2. Comparison of theoretical transition estimations with the actual data for R=0.05, t=0.17.

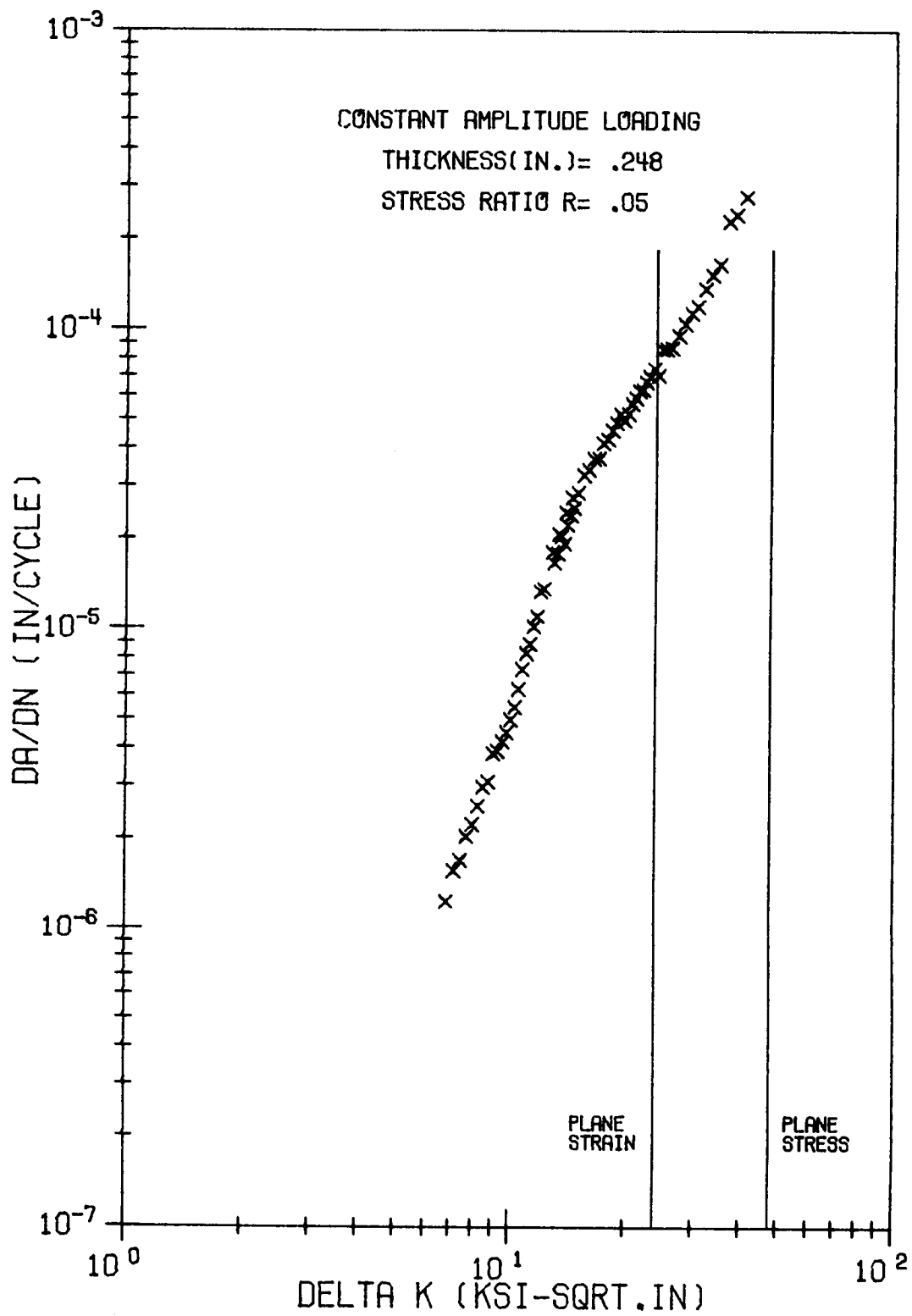


Figure F3. Comparison of theoretical transition estimations with the actual data for R=0.05, t=0.248.

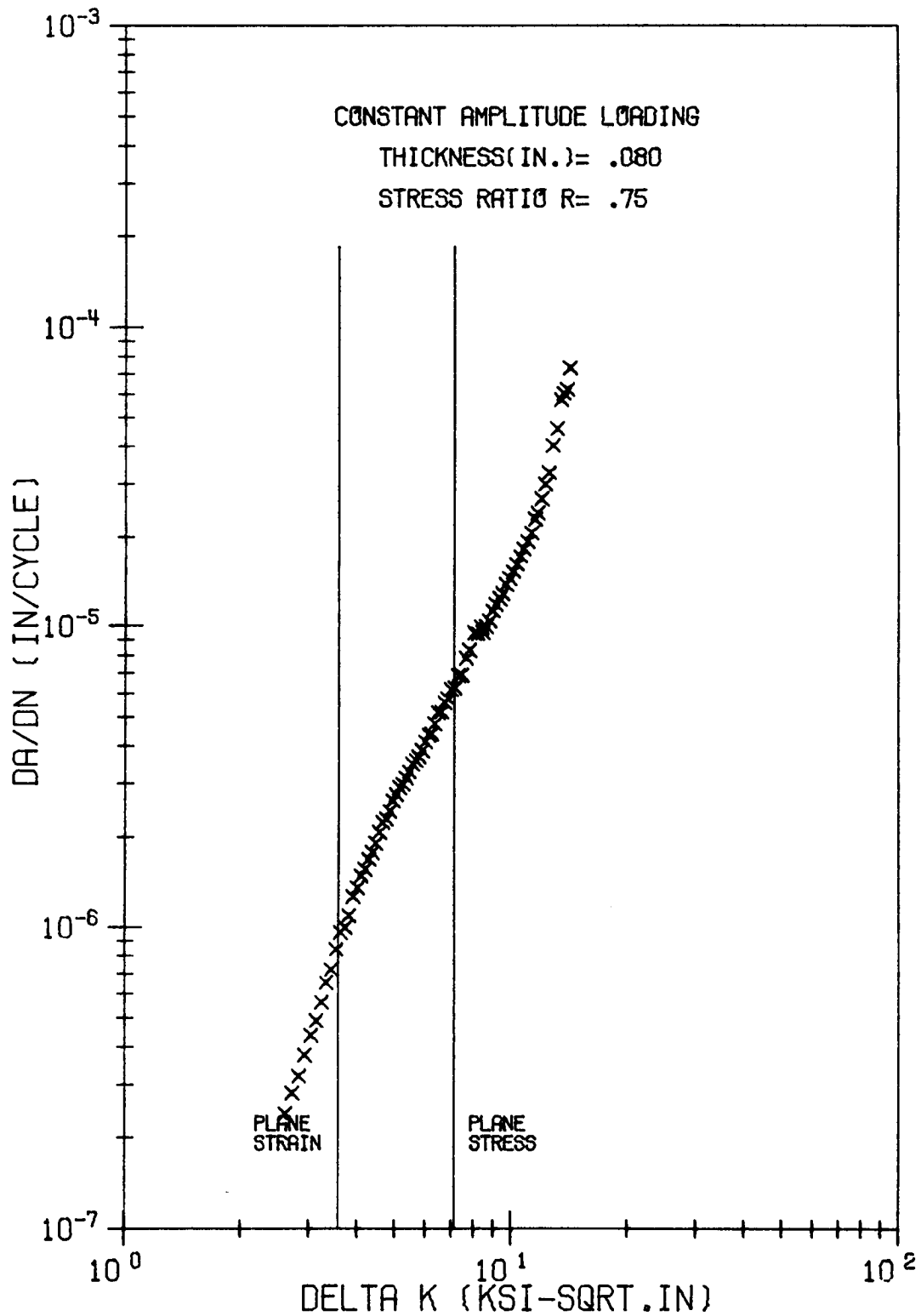


Figure F4. Comparison of theoretical transition estimations with the actual data for $R=0.75$, $t=0.08$.

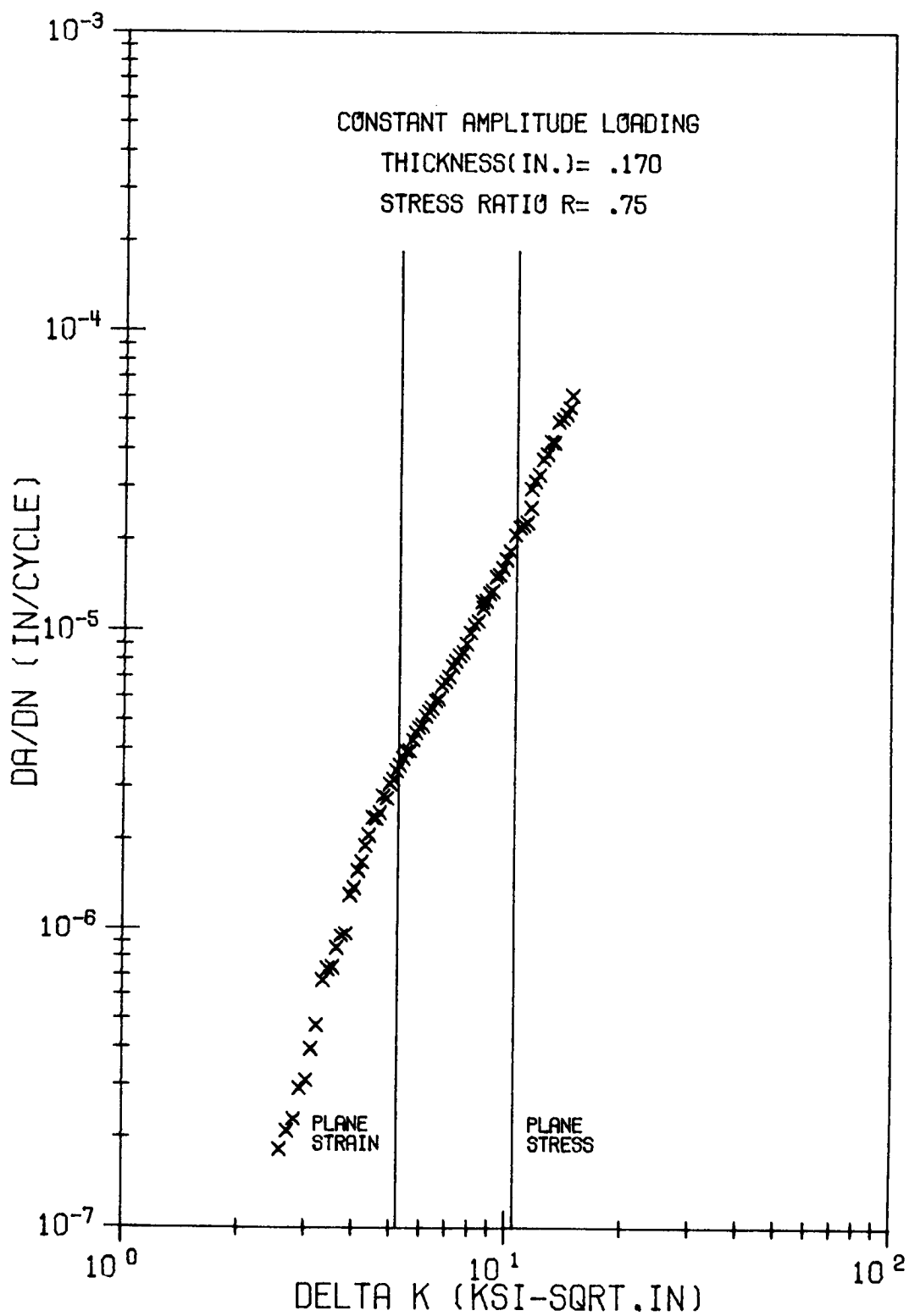


Figure F5. Comparison of theoretical transition estimations with the actual data for $R=0.75$, $t=0.17$.

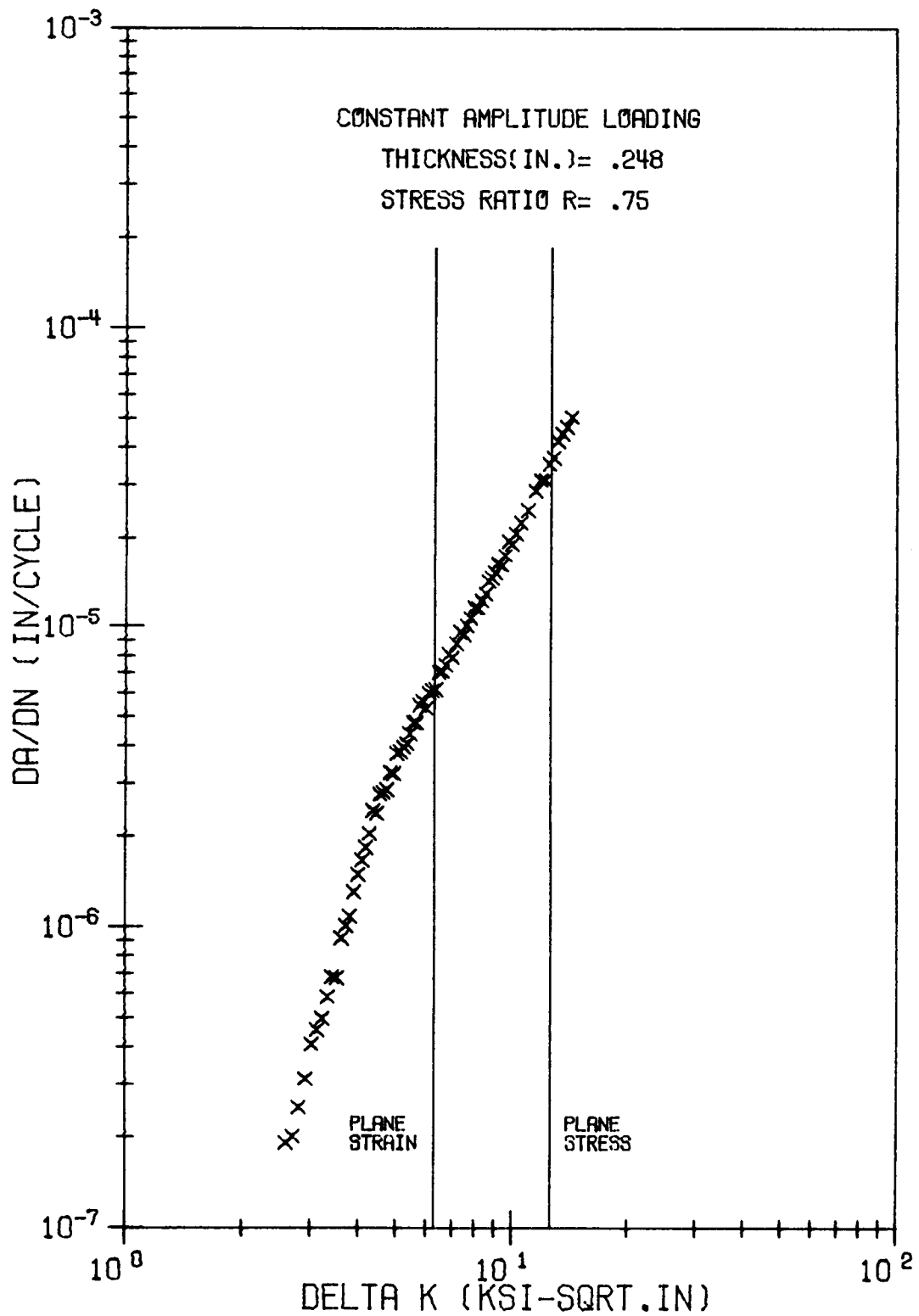


Figure F6. Comparison of theoretical transition estimations with the actual data for $R=0.75$, $t=0.248$.

APPENDIX G

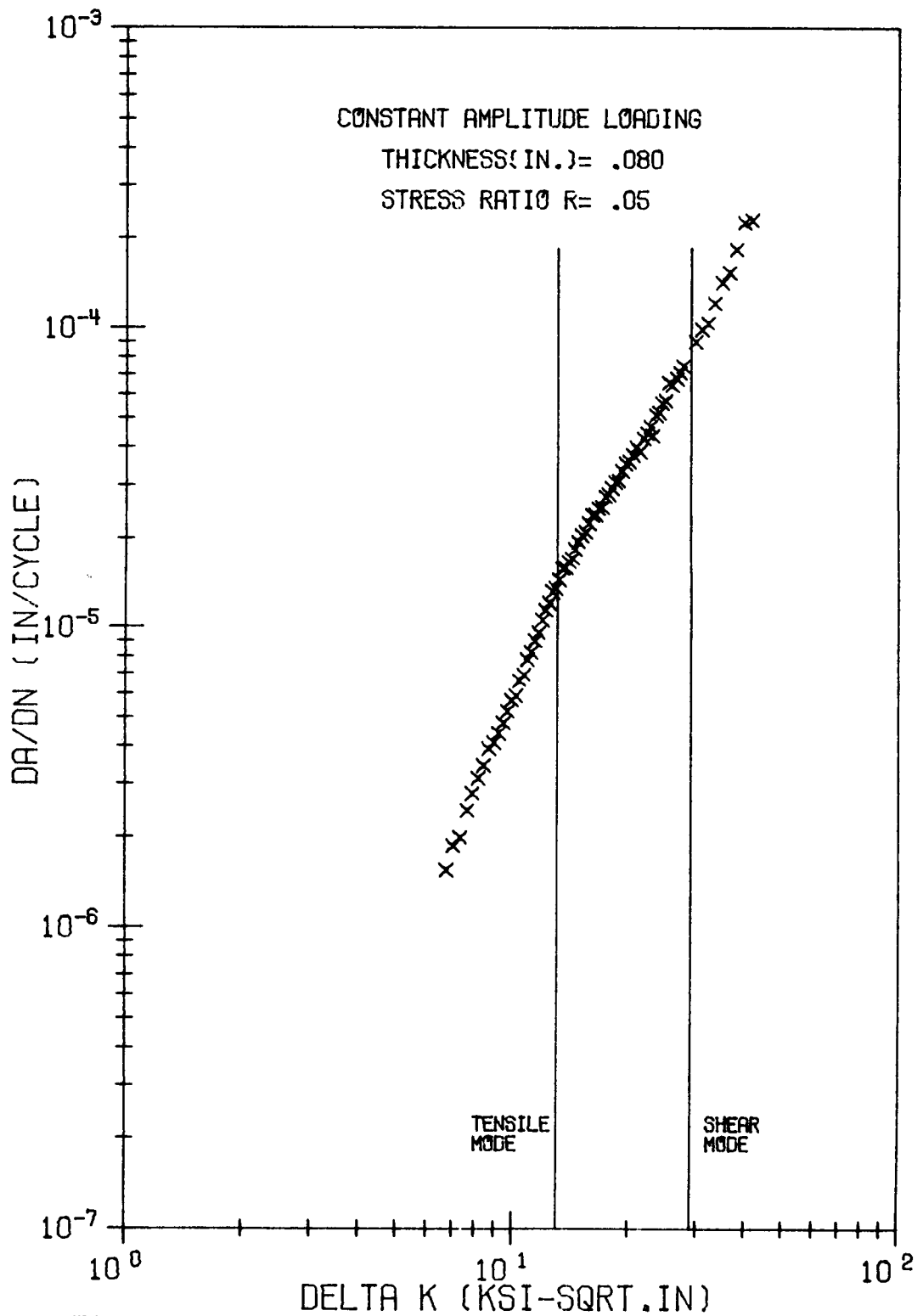


Figure Q1. Comparison of transition based on fracture mode transition with the actual data for $R=0.05$, $t=0.08$.

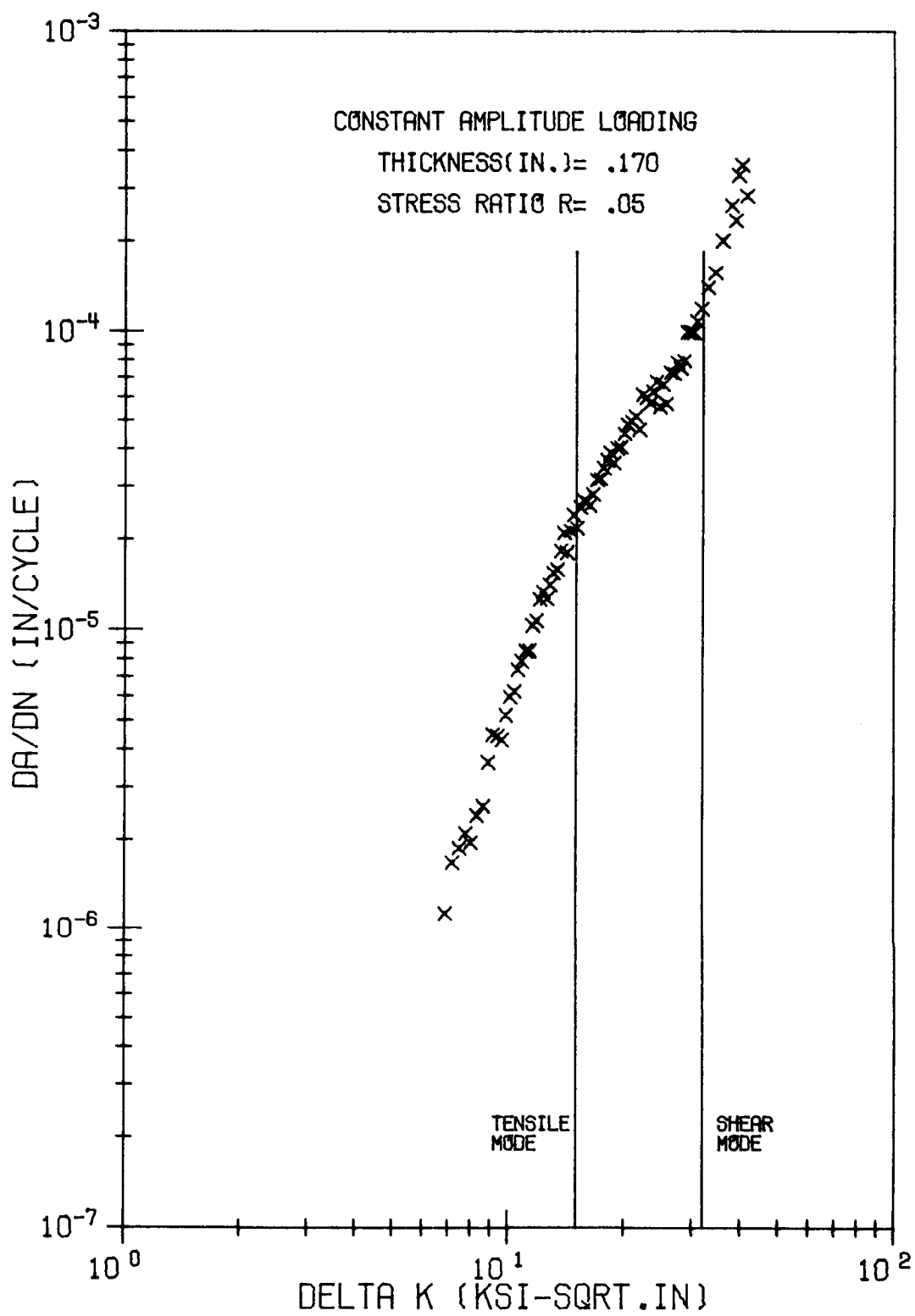


Figure G2. Comparison of transition based on fracture mode transition with the actual data for $R=0.05$, $t=0.17$.

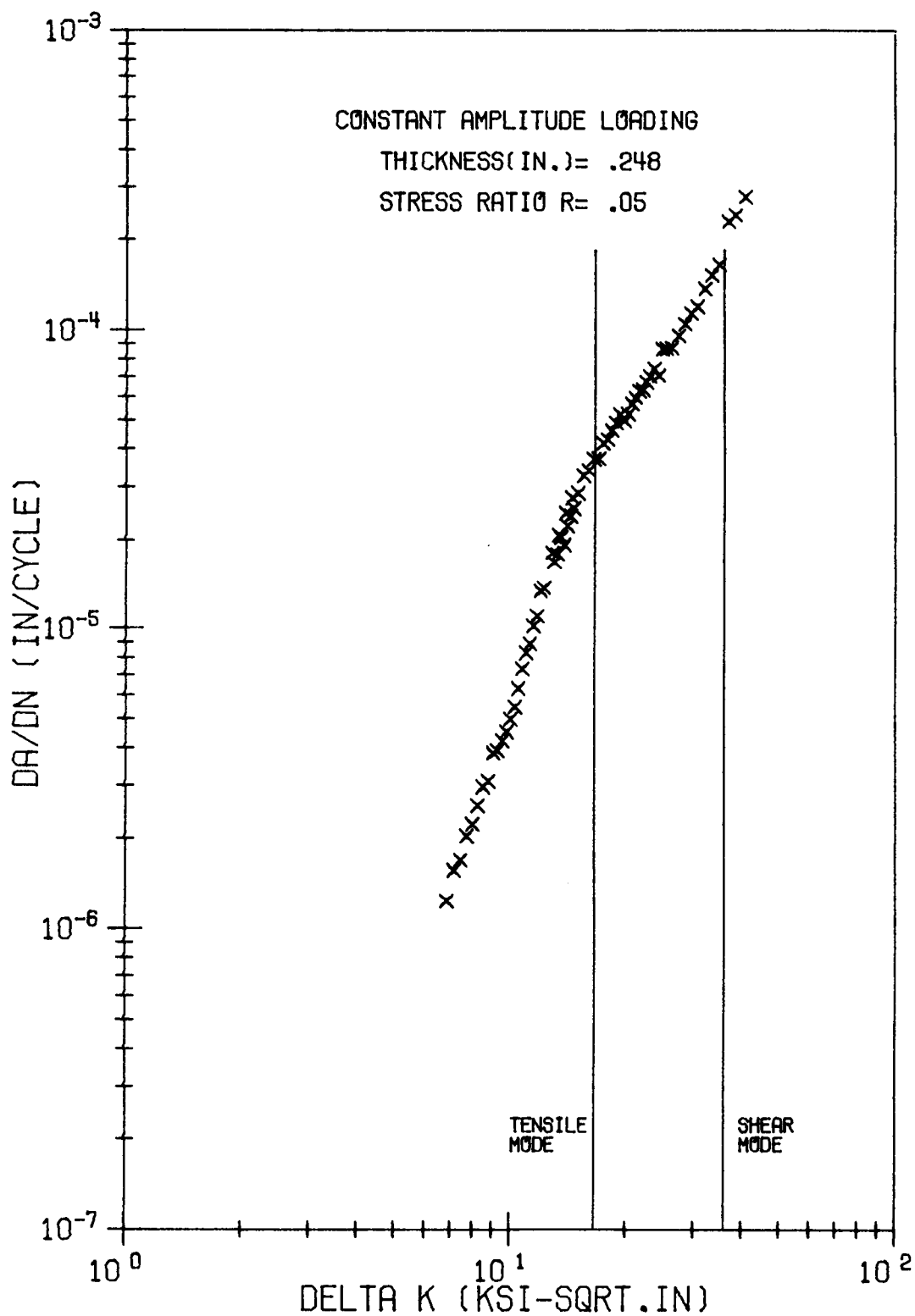


Figure G3. Comparison of transition based on fracture mode transition with the actual data for R=0.05, t=0.248.

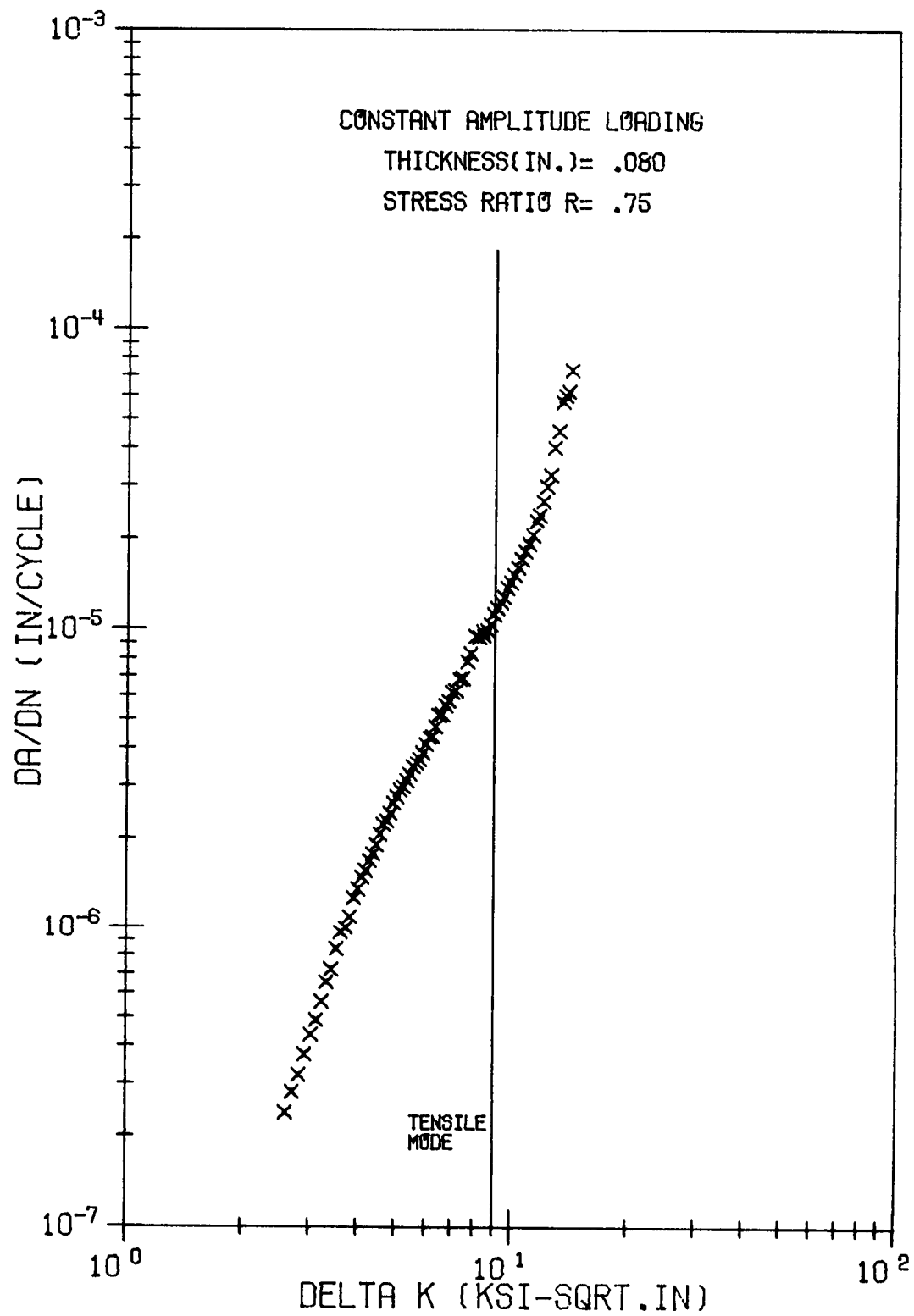


Figure G4. Comparison of transition based on fracture mode transition with the actual data for R=0.75, t=0.08.

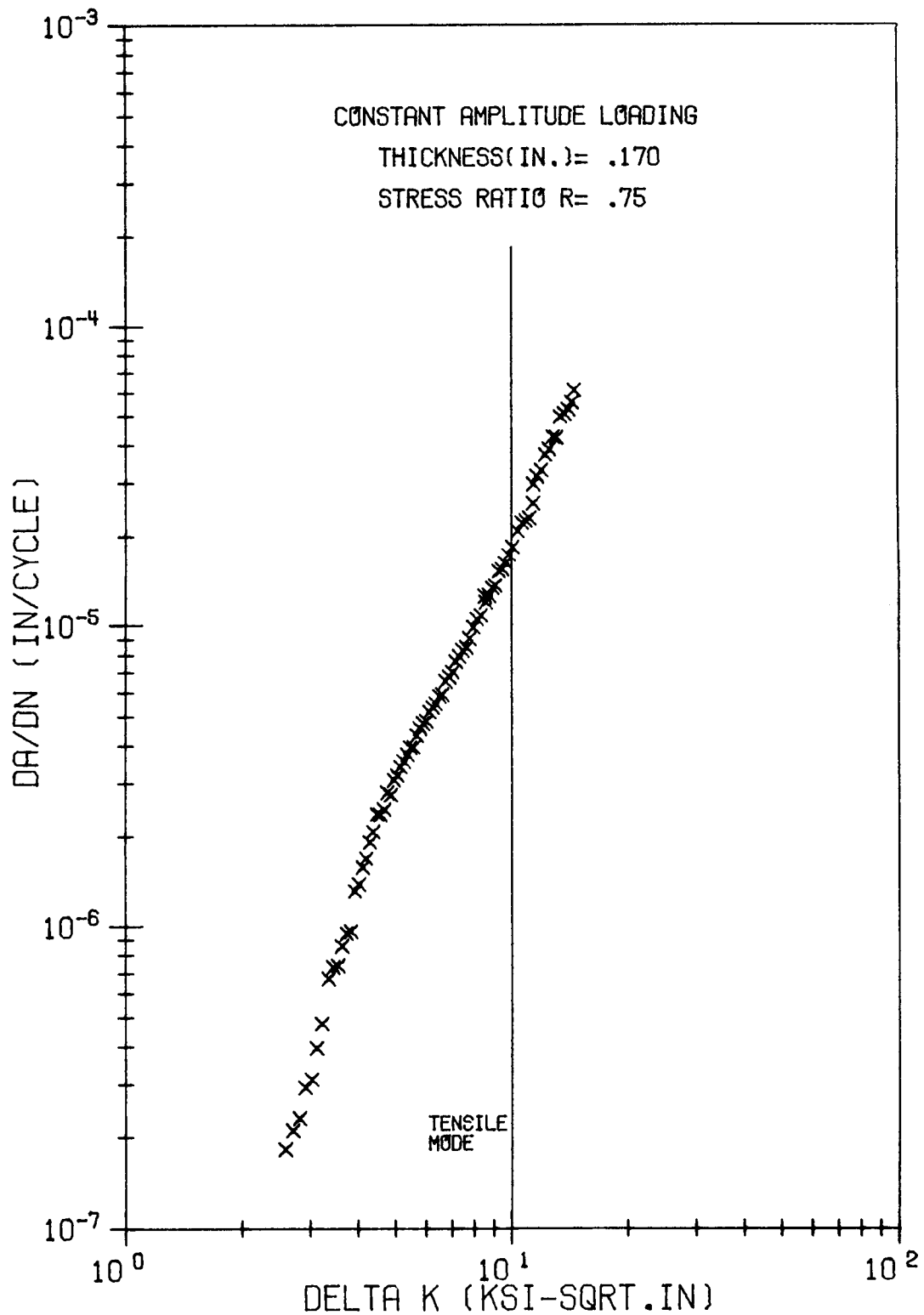


Figure G5. Comparison of transition based on fracture mode transition with the actual data for R=0.75, t=0.17.

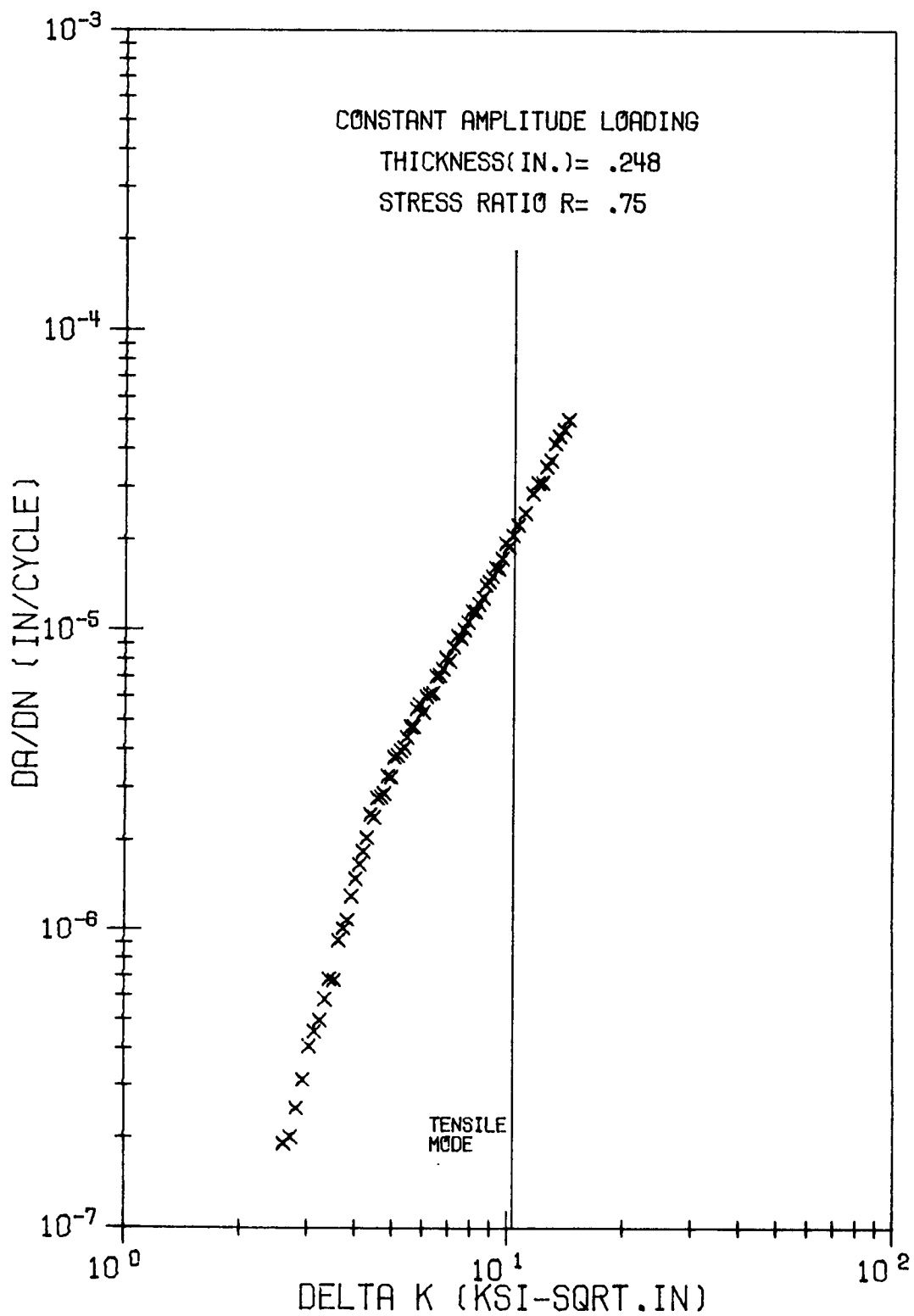


Figure G6. Comparison of transition based on fracture mode transition with the actual data for R=0.75, t=0.248.

1. Report No. NASA CR-172367		2. Government Accession No.		3. Recipient's Catalog No.	
4. Title and Subtitle The Effect of Thickness on Fatigue Crack Propagation in 7475-T731 Aluminum Alloy Sheet				5. Report Date June 1984	
				6. Performing Organization Code	
7. Author(s) R. A. Daiuto and B. M. Hillberry				8. Performing Organization Report No.	
9. Performing Organization Name and Address Purdue University School of Mechanical Engineering West Lafayette, IN 47907				10. Work Unit No.	
				11. Contract or Grant No. NAG1-231	
12. Sponsoring Agency Name and Address National Aeronautics and Space Administration Washington, DC 20546				13. Type of Report and Period Covered Contractor Report	
				14. Sponsoring Agency Code 505-33-23-02	
15. Supplementary Notes Langley Technical Monitor: Dr. W. S. Johnson					
16. Abstract <p>Tests were conducted on three thicknesses of 7475-T731 aluminum alloy sheet to investigate the effect of thickness on fatigue crack propagation under constant amplitude loading conditions and on retardation following a single-peak overload.</p> <p>Constant amplitude loading tests were performed at stress ratios of 0.05 and 0.75 to obtain data for conditions with crack closure and without crack closure, respectively. At both stress ratios a thickness effect was clearly evident, with thicker specimens exhibiting higher growth rates in the transition from plane strain to plane stress region. The effect of thickness for a stress ratio of 0.05 corresponded well with the fracture mode transitions observed on the specimens. A model based on the strain energy release rate which accounted for the fracture mode transition was found to correlate the thickness effects well. The specimens tested at the stress ratio of 0.75 did not make the transition from tensile mode to shear mode, indicating that another mechanism besides crack closure or fracture mode transition was active.</p> <p>Single-peak overload tests were conducted at baseline stress ratios of 0.05 and 0.70 to determine the effect of thickness on retardation for conditions with crack closure and without crack closure. At both stress ratios a thickness effect on retardation was observed. The tests at a stress ratio of 0.05 showed a consistent thickness effect, with thicker specimens exhibiting less retardation. The tests at the stress ratio of 0.70, in which no crack closure occurred following overload, did not show a consistent effect of thickness on retardation. The characteristics of the retardation were different from those observed at the stress ratio of 0.05, and were consistent with those which would be expected if crack tip blunting were the retardation mechanism.</p>					
17. Key Words (Suggested by Author(s)) thickness effects plane strain crack propagation overload retardation crack closure aluminum strain energy release rate plane stress			18. Distribution Statement Unclassified - Unlimited Subject Category 39		
19. Security Classif. (of this report) Unclassified		20. Security Classif. (of this page) Unclassified		21. No. of Pages 212	22. Price A10